AWARD NUMBER: W81XWH-14-1-0232

TITLE:
Epigenetic Therapy of Hematopoietic Malignancies: Novel Approaches for Tissue-Specific and Global Inhibition of EZH2 Enzymatic Activities

PRINCIPAL INVESTIGATOR: Gang (Greg) Wang

CONTRACTING ORGANIZATION:
University of North Carolina at Chapel Hill
Chapel Hill, NC 27599-7295

REPORT DATE: October 2017

TYPE OF REPORT: Final

PREPARED FOR: U.S. Army Medical Research and Materiel Command
Fort Detrick, Maryland 21702-5012

REPORT DOCUMENTATION PAGE

Form Approved
OMB No. 0704-0188

1. REPORT DATE	2. REPORT TYPE	3. DATES COVERED
October 2017	Final	15 Jul 2014 - 14 Jul 2017

4. TITLE AND SUBTITLE

Epigenetic Therapy of Hematopoietic Malignancies: Novel Approaches for Tissue-Specific and Global Inhibition of EZH2 Enzymatic Activities

5a. CONTRACT NUMBER

5b. GRANT NUMBER
W81XWH-14-1-0232

5c. PROGRAM ELEMENT NUMBER

6. AUTHOR(S)
Gang (Greg) Wang, PHD

E-Mail: greg_wang@med.unc.edu

5d. PROJECT NUMBER

5e. TASK NUMBER

5f. WORK UNIT NUMBER

7. PERFORMING ORGANIZATION NAME(S) AND ADDRESS(ES)

University of North Carolina at Chapel Hill
Lineberger Comprehensive Cancer Center
450 West Drive, CB 7295
Chapel Hill, NC 27599-7295

8. PERFORMING ORGANIZATION REPORT NUMBER

9. SPONSORING / MONITORING AGENCY NAME(S) AND ADDRESS(ES)

U.S. Army Medical Research and Materiel Command
Fort Detrick, Maryland 21702-5012

10. SPONSOR/MONITOR'S ACRONYM(S)

11. SPONSOR/MONITOR'S REPORT NUMBER(S)

12. DISTRIBUTION / AVAILABILITY STATEMENT

Approved for Public Release; Distribution Unlimited

13. SUPPLEMENTARY NOTES

14. ABSTRACT

Direct sequencing of hematopoietic cancers identified gain-of-function mutations of EZH2, the gene encoding the enzymatic subunit of *Polycomb Repressive Complex-2* (*PRC*2), among ~10% germ-center B-cell lymphomas. EZH2 silences gene expression through catalysis of methylation of histone H3 lysine 27. However, the currently available EZH2-specific inhibitors are ineffective for treating EZH2-wildtype lymphomas. Novel therapeutics needs to be developed. We found overexpression of PHF19, a PRC2-associated cofactor, is common among B-cell derived malignancies. During this funding period, we have made significant progress in testing our central hypothesis is that, overexpression of PHF19 confers oncogenicity to lymphoma by either enhancing enzymatic activities or chromatin association of PRC2 complexes; in addition, we have evaluated the pan PRC2 inhibitor as a novel means for blockade of unwanted PRC2 hyperactivities among blood cancers including B-cell malignancies.

15. SUBJECT TERMS
hematopoietic cancer, PRC2, inhibitor, histone methylation

16. SECURITY CLASSIFICATION OF:			17. LIMITATION OF ABSTRACT	18. NUMBER OF PAGES	19a. NAME OF RESPONSIBLE PERSON
a. REPORT	b. ABSTRACT	c. THIS PAGE			USAMRMC
Unclassified	Unclassified	Unclassified	Unclassified	125	19b. TELEPHONE NUMBER *(include area code)*

Table of Contents

Page

Progress Report (final -revised) Date: Nov 2017

Project information
Title: Epigenetic Therapy of Hematopoietic Malignancies: Novel Approaches for Tissue-Specific and Global Inhibition of EZH2 Enzymatic Activities
Principal Investigator: Gang (Greg) Wang
Performing Organization: North Carolina, University of, Chapel Hill
Contracting Organization: North Carolina, University of, Chapel Hill

Topic Area: Blood Cancer

1. INTRODUCTION:

EZH2 (enhancer of zeste homolog 2, also known as KMT6A (lysine methyltransferase 6A)) or EZH1 (enhancer of zeste homolog 1, also known as KMT6B) is the catalytic subunit of the polycomb repressive complex 2 (PRC2) that catalyzes methylation of histone H3 lysine 27 (H3K27)(Cao et al., 2002; Kuzmichev et al., 2002; Margueron et al., 2008; Shen et al., 2008). EZH2 and EZH1 are highly homologous (**Fig. 1**; sharing 96% sequence identity in their catalytic domains(McCabe et al., 2012)). The trimethylation of H3K27 (H3K27me3) catalyzed by PRC2 is a transcriptionally repressive epigenetic mark that regulates gene expression, differentiation and development(Margueron and Reinberg, 2011).

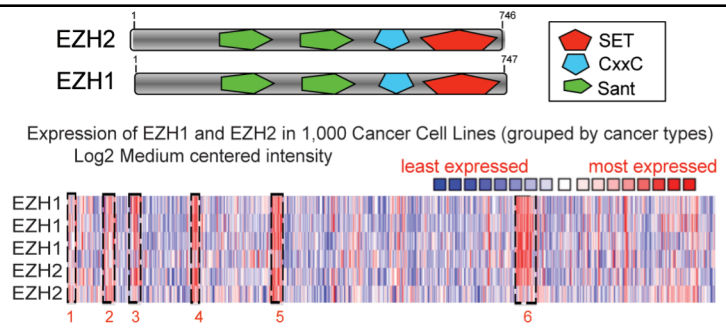

Fig. 1. Domain structures of EZH2 and EZH1 (top). Bottom panel shows co-upregulation (shown in red) of both *EZH1* and *EZH2* as a common feature to various blood cancers. Expression levels of *EZH1* and *EZH2* are extracted from the 'Barretina' dataset of 1,000 cancer cell lines (Broad Institute). Cancer subgroups labeled by numbers 1-6 at the bottom are: 1. acute myeloid leukemia; 2. B-cell lymphoblastic leukemia; 3. chronic myeloid leukemia; 4. Burkitt's lymphoma; 5. diffuse large B-cell lymphoma; 6. multiple myeloma.

EZH2 overexpression and/or gain-of-function mutations occur frequently in human B cell malignancies including germinal center B-cell lymphomas and multiple myeloma, a plasma B cell tumor. However, the currently strategy for suppressing oncogenic functions of PRC2 are ineffective especially for those PRC2-wildtype B cell tumors. We aim to develop new therapeutic approaches for targeting PRC2. Recently, we have found that overexpression of EZH1, an EZH2-ralated enzyme (**Fig. 1**, bottom), and/or PHF19, an EZH2/EZH1-associated cofactor, are common among the human B-cell derived malignancies. This finding led us to hypothesize that, **overexpression of EZH1 and/or PHF19 confers oncogenicity to lymphoma by either enhancing enzymatic activities or chromatin association of PRC2 complexes**, and that **targeting EZH1 or PHF19 provides a novel means for of blockade of unwanted PRC2 hyperactivities**.

The proposed experiments are organized along the following Specific Aims:

Aim 1: to develop and evaluate the pan EZH2 and EZH1 inhibitor for treating blood cancer.
Aim 2: to investigate PHF19 overexpression in conferring EZH2 and EZH1 hyperactivity to B cell tumors to promote oncogenesis.

Aim 3: to map the differential binding of EZH2 in B- versus T- cell lineages, and to identify the responsible tissue-specific recruiters.

2. KEYWORDS:

Hematopoietic cancer, Lymphoma, PRC2, inhibitor, histone methylation, EZH2, PHF19, EZH1

3. ACCOMPLISHMENTS:

In the funding period, our lab and collaborators have made significant progress, and have published 6 manuscripts in total including Mol Cell, Blood, and ACS Chem biol. This funding also allows our lab to secure a NIH/NCI funded R01 grant.

- **What were the major goals of the project?**

Below list the major goals of the project as stated in the approved SOW, as well as the actual completion dates or the percentage of completion.

Major Task 1: To Treat blood cancer cell lines with our pan EZH2 and EZH1 inhibitor in vitro

Subtask 1- To assess the effect of our pan EZH2 and EZH1 inhibitor on tumor cell proliferation in ~30 human cell lines

- completed

Subtask 2-To dissect the effect of our pan EZH2 and EZH1 inhibitor on cell cycle progression, tumor cell differentiation, and/or apoptosis

- completed

Subtask 3 – To identify a common "core signature" associated with cellular treatment of our EZH2 and EZH1 inhibitor

- completed

Summary of Major Task 1-

- completed

Major Task 2: To treat human cancer cell xenograft animal models in vivo with the pan EZH2/EZH1 inhibitor

Subtask 4- perform the pharmacokinetic assay and toxicity evaluation of the pan EZH2/EZH1 inhibitor in animals using different compound administration methods

- completed

Subtask 5- establish tumor xenograft models using human cell lines of myeloma.

- completed

Summary of Major Task 2

- completed

Major Task 3 – to dissect the role of PHF19 overexpression using human B-cell derived multiple myeloma tumor lines

Subtask 6- perform gene knockdown of PHF19 followed by assays for tumor cell proliferation using >10 different B-cell derived malignant cell lines

- completed

Subtask 7 –assess the effect of knockdown of PHF19 on cell cycle, tumor cell differentiation, and apoptosis

- completed

Summary of Major Task 3

- completed

Major Task 4 – to dissect the role of PHF19 overexpression using xenograft models of multiple myeloma

Subtask 8- to establish tumor xenograft models using human B-cell derived malignant cell lines
- completed

Major Task 5 - to investigate the role of PHF19's Tudor motif in regulation of PRC2 and H3K27me3 hyperactivity

Subtask 9- perform gene knockdown of PHF19 followed by quantitative mass spec of histone modifications and western blots
- completed in multiple myeloma

Subtask 10 – perform gene knockdown of PHF19 followed by rescue with shRNA-resistant PHF19 (wildtype or Tudor mutant forms) and RNA-Seq to identify PHF19-regulated downstream targets
- completed in multiple myeloma

Subtask 13 – perform knockdown of PHF19 followed by ChIP-Seq of EZH2 and H3K27me3, in order to dissect the role of PHF19 in regulating EZH2's chromatin association and/or enzymatic activities
- completed in multiple myeloma

Major Task 6- to use genomic approaches to map EZH2's binding sites among B-cell lymphoma versus T-cell leukemia lines

Subtask 11- identify EZH2's binding sites by ChIP-seq among B-cell versus T-cell derived malignant cells
- completed

- **What was accomplished under these goals?**
- *For this reporting period describe: 1) major activities; 2) specific objectives; 3) significant results or key outcomes, including major findings, developments, or conclusions (both positive and negative); and/or 4) other achievements. Include a discussion of stated goals not met. Description shall include pertinent data and graphs in sufficient detail to explain any significant results achieved. A succinct description of the methodology used shall be provided. As the project progresses to completion, the emphasis in reporting in this section should shift from reporting activities to reporting accomplishments.*

(1) Major activities

Within the broadly proposed research areas, we have chosen to focus two main topics during the funding years:

(1) For aim 1: we treated AML, a common and aggressive blood cancer, with our newly developed EZH2 and EZH1 inhibitors in cell lines and in vivo models.

(2) For aim 2: our studies mainly focused on the plasma B-cell tumor, ie. multiple myeloma. Multiple myeloma (MM) is a malignancy of plasma cells, the terminally differentiated B lymphocytes that generate and secrete antibodies. MM represents the 2nd most common hematological cancer, with about 30,330 new cases and 12,650 expected death in U.S. in 2016. It is believed that MM experiences a step-wise progression from a clinically insidious stage, such as monoclonal gammopathy of uncertain significance (MGUS), and acquires both genetic and epigenetic alterations that promote MM development. Unlike most of malignancies, the malignant MM cells are characterized by

an extraordinary low mitotic rate, which possibly contributes to the almost universal resistance to chemotherapeutics. Despite recent FDA-approved proteomsome inhibitors for MM treatment, new targeted therapeutics need to be developed to further improve clinical outcomes for this fatal disease, especially for those refractory cases. In Figure 1 (bottom), we have shown that EZH2 and/or EZH1 are both up-regulated in MM, which indicates targeting EZH2/1 as an attractive way for the treatment of MM.

We summarized our new progress and results in sections below.

This current progress report covers the following aims as originally proposed:

Aim 1: to develop and evaluate the pan EZH2 and EZH1 inhibitor for treating blood cancers.

Major activity 1- To assess the effect of our pan EZH2 and EZH1 inhibitor on tumor cell proliferation in various human tumor cell lines

Major activity 2-To dissect the effect of our pan EZH2 and EZH1 inhibitor on cell cycle progression, tumor cell differentiation, and/or apoptosis

Major activity 3 – To identify a common "core signature" associated with cellular treatment of our EZH2 and EZH1 inhibitor

Aim 2: to investigate PHF19 overexpression in conferring EZH2/1 hyperactivity to multiple myeloma to promote oncogenesis.

The major activities include:

Major activity 5- establish tumor xenograft models using human cell lines of myeloma.

Major activity 6- perform gene knockdown of PHF19 followed by assays for tumor cell proliferation using myeloma cell lines

Major activity 7 assess the effect of knockdown of PHF19 on cell cycle, tumor cell differentiation, and apoptosis

Major activity 8- establish tumor xenograft models using human myeloma cell lines, and study the requirement of PHF19 in tumor development

(2) Specific objectives

2.1- to demonstrate that the pan EZH2 and EZH1 inhibitor represents a new means for achieving complete inhibition of EZH family enzymes in treating blood cancers.

2.2- to establish PHF19 as a new drug target of myeloma.

(3) Significant results or key outcomes, including major findings, developments, or conclusions (both positive and negative);

(3.1) Related to Major activity 1- To assess the effect of our pan EZH2 and EZH1 inhibitor on tumor cell proliferation in various human tumor cell lines

We have identified a set of small-molecule inhibitors for specific targeting of both EZH2 and EZH1, including UNC1999, an EZH2 and EZH1 dual inhibitor, and UNC2400, an inactive analog compound useful for assessment of off-target effect (Figure 2 and also see report from year 1). The discovery of compounds was made with a structure based chemical compound design in a close collaboration with UNC Center for Drug Discovery and Chemical Biology.

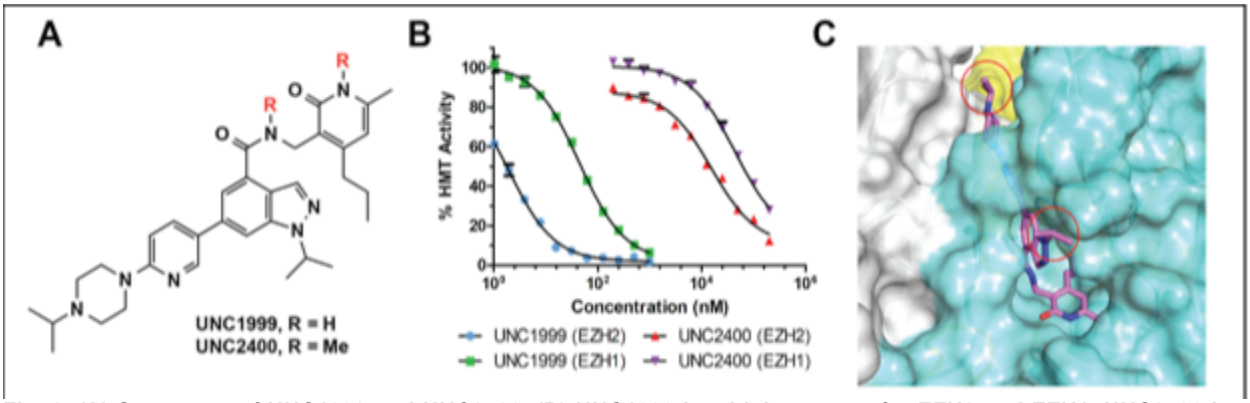

Fig. 2. (A) Structures of UNC1999 and UNC2400. (B) UNC1999 has high potency for EZH2 and EZH1. UNC2400 is > 1,000-fold less potent than UNC1999. (C) Docked pose of UNC1999 in human PRC2 complex. Red rings mark the solvent-exposed moieties.

We characterized molecular effects by these translational tools and aim to establish novel therapeutics for cancer cells. Specifically we show that UNC1999, and not UNC2400, specifically suppressed H3K27me3/2, the enzymatic product of EZH2/1 (Fig 2; our published paper of Xu B et al Blood 2015). We also have shown that UNC1999 concurrently elevated the cellular level of H3K27ac, while having negligible effects on other histone methylations (Fig 3).

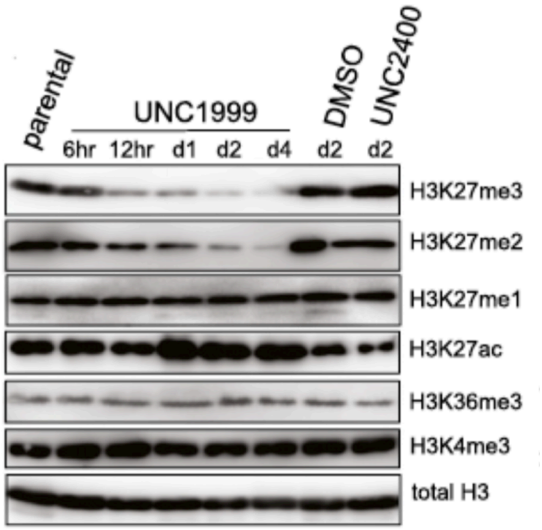

Fig 3. Immunoblot of the indicated histone modifications after treatment with DMSO, or 3 μM UNC1999 or UNC2400.

Next we characterized cellular effects by these translational tools and aim to establish novel therapeutics for cancer cells. We have applied UNC1999 to a larger panel of blood cell lines, such as myeloma (Fig 4) and AML (Fig 5) cell lines. Many showed sensitivity to UNC1999 (Figure 4-5).

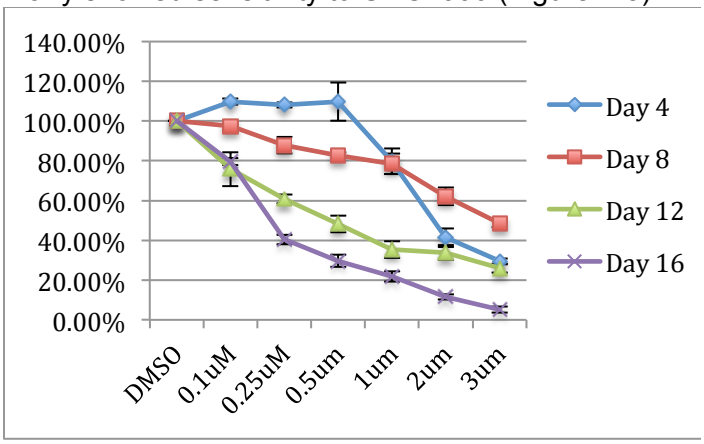

Fig 4. Relative proliferation of a panel of myeloma cell lines treated with various concentrations of UNC1999 for the indicated days (left panel). Y-axis, presented as the mean of triplicates 6 SD, represents the relative percentage of accumulative cell numbers after normalization to DMSO treatment.

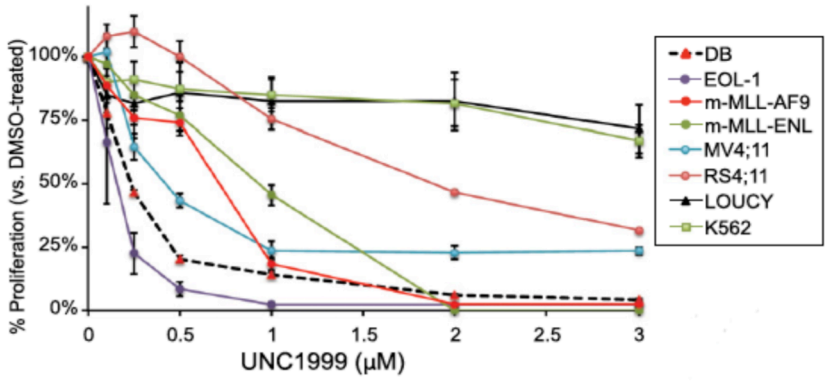

Cell Line	EC50 (μM)	Known Genetic Mutation
DB	0.227	*EZH2 Y641N*
EOL-1	0.1019	*MLL-PTD; FIP1L1-PDGFRA*
K562	N/A (>250)	*BCR-ABL*
LOUCY	N/A (>200)	*EZH2 deleted*
m-MLL-AF9 (4 lines)	0.404~0.621	*MLL-AF9*
m-MLL-ENL (2 lines)	0.547~0.836	*MLL-ENL*
MV4;11	0.5248	*MLL-AF4*
OCI-AML2	1.5	*MLL-AF9*
RS4;11	1.956	*MLL-AF4*

Fig 5. Relative proliferation of a panel of leukemia or lymphoma cell lines treated with various concentrations of UNC1999 for 16 days (left panel). Y-axis, presented as the mean of triplicates 6 SD, represents the relative percentage of accumulative cell numbers after normalization to DMSO treatment. Shown as a dashed line is DB, an EZH2-mutated (Y641N) lymphoma line known to be sensitive to EZH2 inhibition. Right panels show summary of EC50 of a panel of cell lines in response to UNC1999.

Major findings & conclusion

We found that

(1) - UNC1999 induces potent and selective suppression of H3K27me3/2, whereas UNC2400 does not, highlighting them as a pair of compounds useful to manipulate both PRC2-EZH2 and PRC2-EZH1.

(2)- UNC1999, an EZH2 and EZH1 dual inhibitor, efficiently suppresses proliferation of AML and myeloma cells that co-express EZH2 and EZH1.

(3.2) Related to Major activity 2-To dissect the effect of our pan EZH2 and EZH1 inhibitor on cell cycle progression, tumor cell differentiation, and/or apoptosis

- We have also studied the effect of our pan EZH2 and EZH1 inhibitor on cancer cell apoptosis (Figure 6). We found a time- and concentration dependent induction of apoptosis and cell viability after treatment with UNC1999.

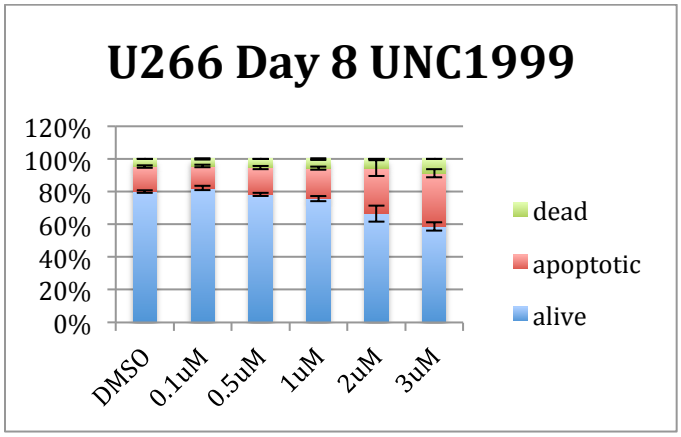

Fig 6. A summary of effect of UNC1999 on apoptosis and cell viability of U266, a myeloma cell line.

We have also shown that UNC1999 induced cell-cycle arrest at the G1-to-S transition of AML cells (Figure 7, right; also refer to our paper of Xu B et al Blood 2015). In contrast, UNC2400 did not alter cell-cycle progression (Figure 4, middle vs. left). By using EOL1 cells as a working model, we have also studied the effect of our pan EZH2 and EZH1 inhibitor on cancer cell apoptosis

In AML cell treatment studies, we further found a time- and concentration dependent induction of apoptosis and cell viability after treatment with UNC1999, and not UNC2400 (Figure 8).

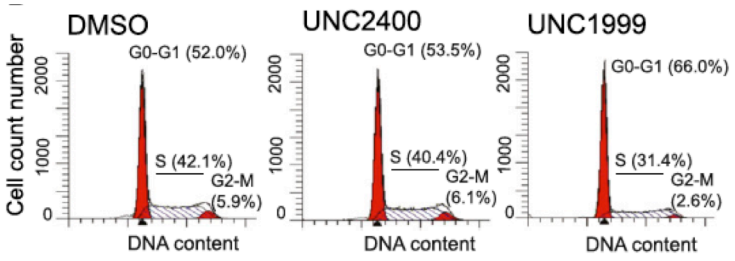

Fig 7. Representative histograms showing DNA contents measured by PI staining of leukemia cells after treatment with 3 μM of compounds for 2 days.

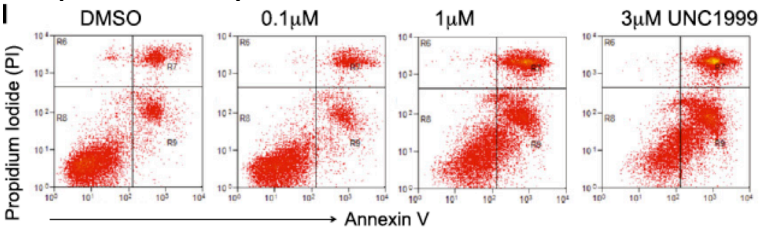

Fig 8. Typical profiles of staining with PI and annexin V after treatment of EOL-1 cells with DMSO or the indicated concentration of UNC1999 for 6 days. PI, propidium iodide.

Major findings & conclusion-

- UNC1999 suppresses growth of two common blood cancer types (ie. malignant multiple myeloma in Fig 6 and AML in Fig 7-8) by inhibiting cell cycle progression and/or promoting apoptosis.

(3.3) Related to Major activity 3 – To identify a common "core signature" associated with cellular treatment of our EZH2 and EZH1 inhibitor

- To dissect the underlying mechanisms for the UNC1999-induced anti-cancer effect, we have carried out gene transcriptome profilings by RNA-seq and aimed to identifying a common "core signature" associated with cellular treatment of our EZH2 and EZH1 inhibitor. These analyses were carried out in UNC genomic core using an Affymetrix gene-array platform.

Effects of UNC1999 on histone modifications and gene expression was carried in an AML model with the common *MLL*-rearranged gene abnormality (Fig 9). We employed proteomics and genomics approaches to dissect the molecular mechanisms that underlie the anti-leukemia effect of UNC1999(Xu et al., 2015). We found that UNC1999 selectively reduced H3K27me2/3 and concurrently increased H3K27ac (H3K27 acetylation) by mass spectrometry profiling of histones (for details, see our paper(Xu et al., 2015)) and by western blots (**Fig. 9A**). The gene-array analysis (**Fig. 9B-C**) further revealed that UNC1999 induced drastic up-regulation of the genes featured with those known to regulate proliferation (*Cdkn2a*), lineage development (*Tet1*), and cell differentiation (*Epx*) (for details, see our paper(Xu et al., 2015)). UNC1999–induced transcriptome alterations overlap with those following knockdown of EED (a common component of PRC2 complexes), again demonstrating the on-target activity of UNC1999(Xu et al., 2015). Mechanistically, UNC1999 preferentially affects distal regulatory elements such as enhancers, leading to gene de-repression(Xu et al., 2015). The gene de-repression correlates with a decrease in H3K27me3 and concurrent gain in H3K27ac at the affected genes (**Fig. 9D**). Collectively, these studies provide a detailed molecular dissection

about how UNC1999 reprograms both epigenetic and genetic features of *MLL*-rearranged leukemias, leading to their differentiation, decelerated proliferation, and, ultimately, tumor regression.

Major findings & conclusion-

Taken together, these results have demonstrated that UNC1999 is an excellent tool

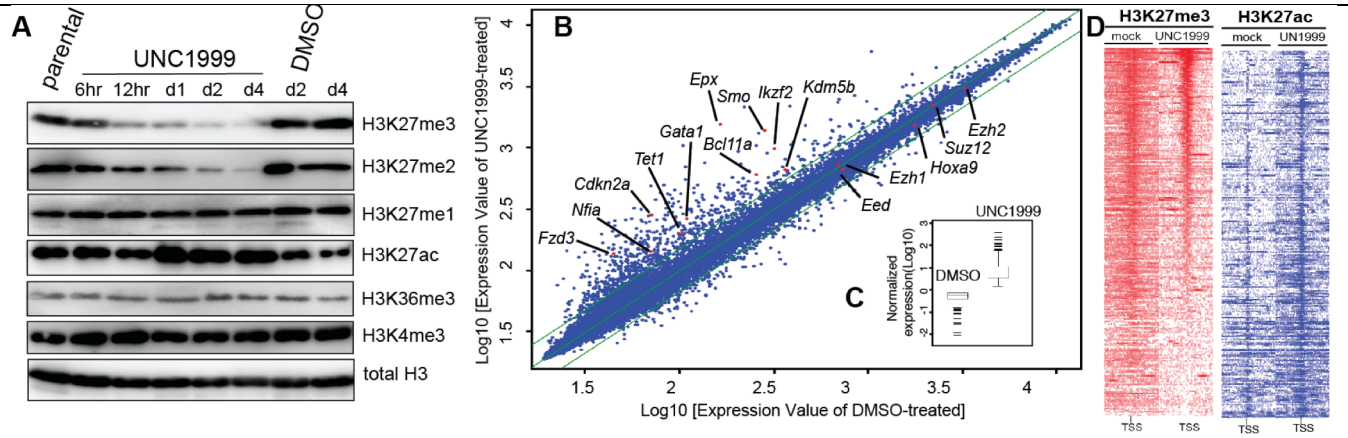

Fig. 9. (A) Immunoblot shows a time-dependent reduction of H3K27me3/2 and concurrent increase of H3K27ac in *MLL-AF9*–transformed leukemia progenitors after treatment with 3 μM UNC1999. (B) Scatter plot to compare the global gene expression pattern in *MLL-AF9*–transformed leukemia cells following DMSO (x-axis) versus UNC1999 treatment (y-axis). Plotted are Log10 values of the signal intensities of all transcripts on gene microarrays after normalization. The flanking lines in green indicate 1.5-fold change in gene expression. (C) Boxplots showing the expression levels (Log10 value in Y-axis) of upregulated transcripts in the UNC1999 versus DMSO-treated samples. (D) Heatmap showing the ChIP-Seq read densities of H3K27me3 (red) and H3K27ac (blue) across the transcription start site (TSS) of up-regulated genes following UNC1999 versus mock treatment. Following UNC1999 treatment, H3K27me3 peaks become narrower and sharper. For detailed results, please see our paper[8].

compound (for details, please see our paper(Xu et al., 2015)).

(3.4) Related to Major activity 4 – We have performed the pharmacokinetic assay and toxicity evaluation of the pan EZH2/EZH1 inhibitor in animals using different compound administration methods (Fig 10);

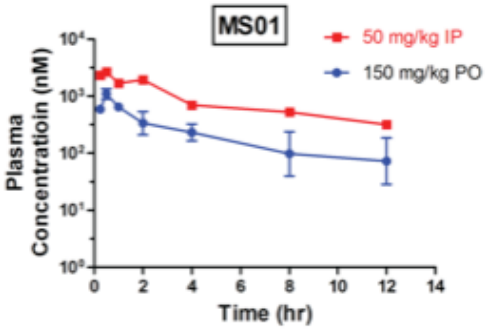

Figure 10. Plasma concentrations of MS01, a new EZH2/1 inhibitor, following a single IP injection (50 mg/kg) or PO dose (150 mg/kg) in mice (average values of 4 mice (2 male and 2 female) per time point).

(3.4) Related to Major activity 5

To treat tumor in vivo models with inhibitor:

For this aim, we have used two blood cancer models, with one published at Blood (2015) and the 2nd study under manuscript preparation.

Tumor suppression by UNC1999 in an *in vivo* AML model of *MLL*-rearranged leukemias. We next performed *in vivo* mouse studies(Xu et al., 2015). In comparison to vehicle, oral administration of UNC1999 (50 mg/kg, twice daily) prolonged the survival of mice bearing *MLL-AF9*-induced AML (**Fig. 11**, p = 0.0033)(Xu et al., 2015). In UNC1999-treated leukemic mice, significant reduction in leukemia burden was observed (for details, please see our paper(Xu et al., 2015)). Notably, UNC1999 treatments did not cause general toxicity in mice(Xu et al., 2015), which is in agreement with little or mild phenotypes seen in mice with complete *Ezh2* or *Ezh1* knockout in their hematopoietic system(Danis et al., 2016; Hidalgo et al., 2012; Mochizuki-Kashio et al., 2015; Mochizuki-Kashio et al., 2011).

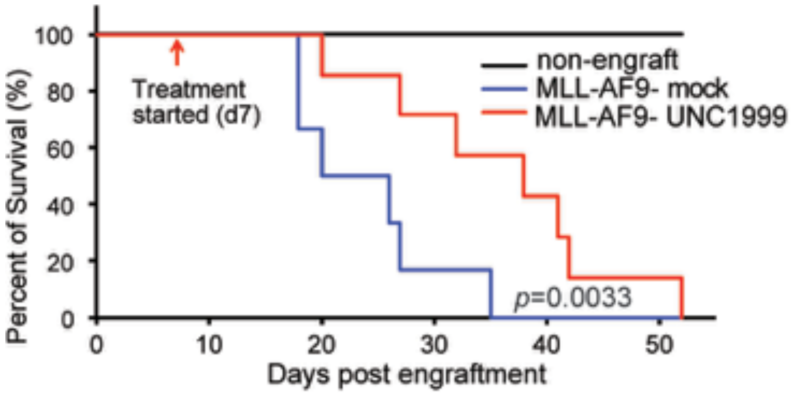

Fig 11. Kaplan-Meier curve showing leukemia kinetics after transplantation of *MLL-AF9*–induced primary murine leukemia into syngeneic mice. Mice received either vehicle (blue) or UNC1999 (red, 50 mg/kg twice daily PO dosing). Cohort size: 7 mice. For details, please see our paper[8].

Tumor suppression by UNC1999 in in vivo models of multiple myeloma.

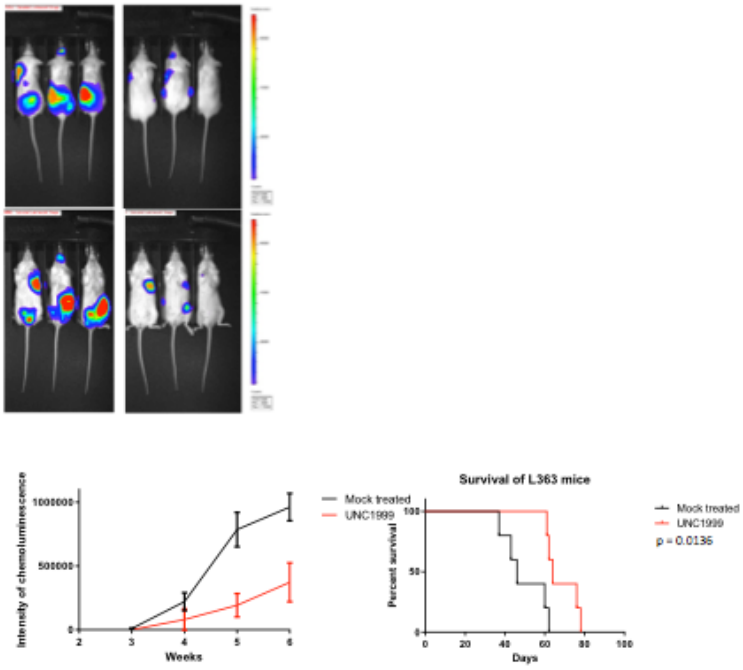

Fig 12. Images of the xenografted tumors in the vehicle- (upper, left) and UNC1999-treated (upper, right) mice. The bottom panels shows summary of growth of xenografted tumors and Kaplan-Meier curve showing cancer development kinetics.

To examine the effect of UNC1999 on myeloma in vivo, we used the same treatment regimen

as above. We show that UNC1999 delayed myeloma development and progression (Fig 12A, red versus black lines).

Major findings & conclusion-

Collectively, these above data show that

- Our established protocol for oral administration of UNC1999 does not cause obvious toxicity in tested animals;
- Oral delivery of UNC1999 delays cancer development and progression in vivo and our EZH2 and EZH1 dual inhibitor provides a new therapeutics for AML and multiple myeloma.

(3.5) Related to Major activity 6 to 8 -

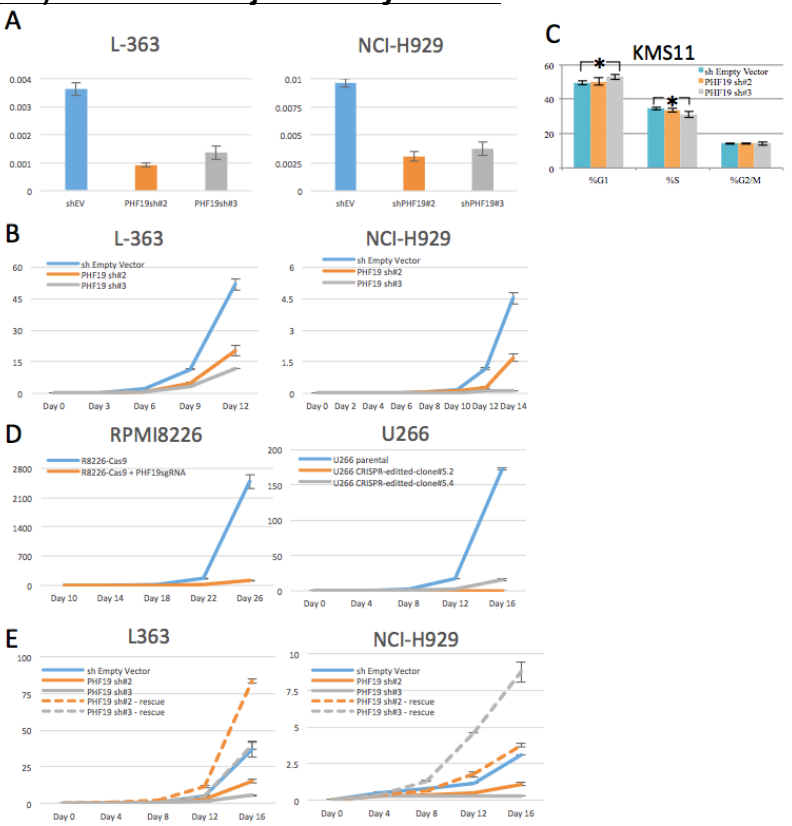

Fig 13. Effect of PHF19 expression in multiple myeloma growth in vitro.

We have successfully carried out Knockdown (KD) of *PHF19* in multiple multiple myeloma tumor lines (Fig 13A-B). We found that *PHF19* is required for *in vitro* tumor growth (Fig. 13B-E).

-

we have used the SCID-NOD-gamma (SNG) mice which were xenografted intravenously with human multiple myeloma cell lines (Fig 14); we found that knockdown (KD) of *PHF19* delays the xenografted tumor formation *in vivo* (Fig. 14). The *in vivo* phenotypes of *PHF19* KD can be rescued by re-introduction of *PHF19* (Fig 14; bottom panels, red).

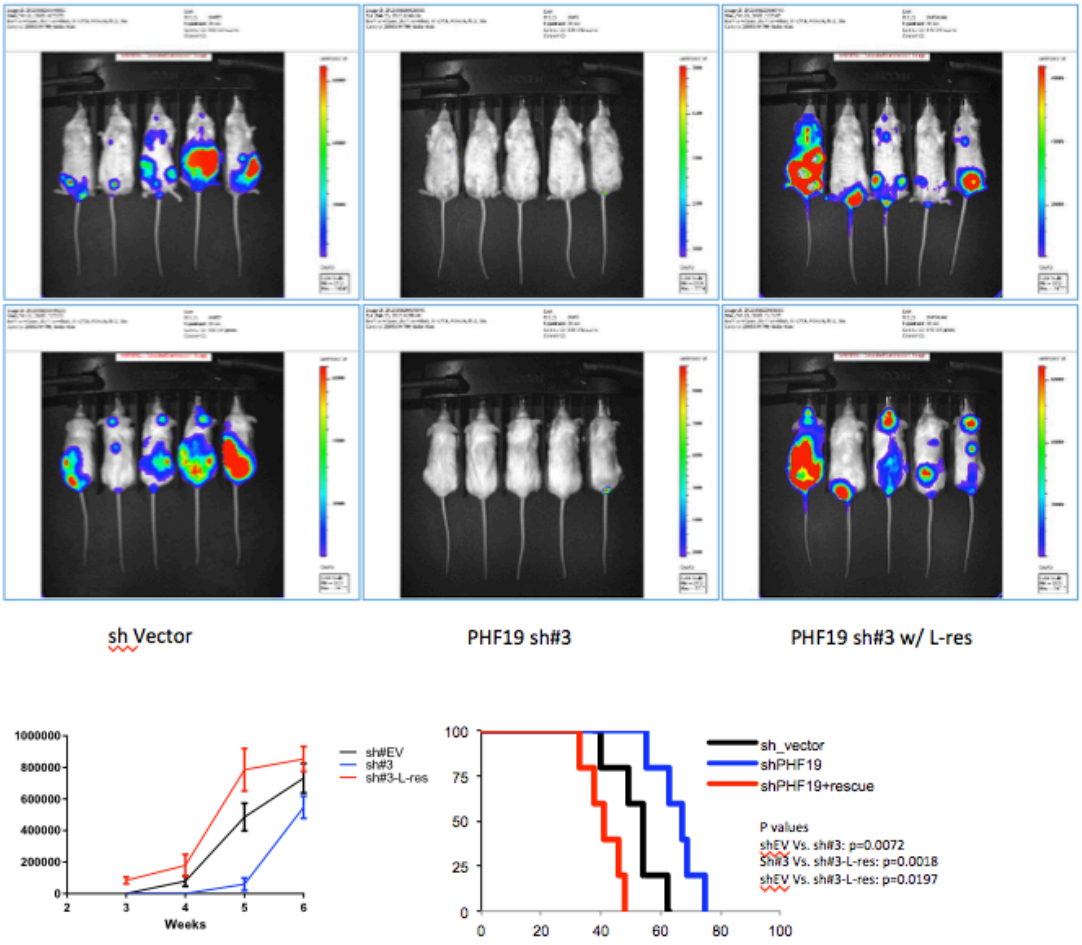

Fig 14. Effect of PHF19 expression in multiple myeloma growth in vivo.

Major findings & conclusion-

-- We found that PHF19 is among the top overexpressed genes in multiple myeloma (MM). In addition, there is a steady increased expression level of PHF19 mRNA among multiple myeloma (MM) and plasma cell leukemia (PCL), in comparison to normal plasma cells.

- PHF19 is crucial for tumor cell proliferation in tested B-cell derived malignant cell lines
- we have established the tumor xenograft models (Fig 8) using human B-cell derived malignant cell lines
- we have shown a requirement of PHF19 for tumor xenograft growth in vivo (Fig 8)

(4) other achievements-

n/a

- **What opportunities for training and professional development has the project provided?**

Training and professional development provided to Dr. Zhihong Ren MD/PHD, who worked on the project as a postdoc researcher-

"Training" activities:

-ChIP, qRT-PCR, western blot

- xenograft studies with human cell lines and SCID nude mice models

- live imaging
- in-house postdoc seminar (weekly)

- **How were the results disseminated to communities of interest?**

(1) our lab has published 6 manuscripts in total including Mol Cell, Blood, and ACS Chem biol. (2) This funding also allows our lab to secure a NIH/NCI funded R01 grant to study the role for PHF19 in multiple myeloma.
Our research is well received and highly cited. As evidence, our Blood (2015) and ACS Chem biol (2014) papers have been cited over 60 and 150 times, respectively, in less than 2-3 years.

What do you plan to do during the next reporting period to accomplish the goals?
n/a

4. IMPACT:

- **What was the impact on the development of the principal discipline(s) of the project?**

The findings and research results are likely to make an impact on blood cancer research and therapies in the following ways:
  - Define a set of new 'Achilles' heels' of blood cell derived malignancies.
  - Targeting these new drug targets with inhibitors we develop shall provide novel therapeutic interventions.

- **What was the impact on other disciplines?**

Nothing to Report.

- **What was the impact on technology transfer?**

Nothing to Report.

- **What was the impact on society beyond science and technology?**

Nothing to Report.

5. CHANGES/PROBLEMS:

- **Changes in approach and reasons for change**

Nothing to Report.

- **Actual or anticipated problems or delays and actions or plans to resolve them**

n/a

- **Changes that had a significant impact on expenditures**

Nothing to Report.

- **Significant changes in use or care of human subjects, vertebrate animals, biohazards, and/or select agents**

Nothing to Report.

6. PRODUCTS:

- **Publications, conference papers, and presentations**

Journal publications – see attached PDFs in the end of this report.

1. Lu R, Wang P, Parton T, Zhou Y, Chrysovergis K, Rockowitz S, Chen WY, Abdel-Wahab O, Wade PA, Zheng D, **Wang GG**. Epigenetic perturbations by Arg882-mutated DNMT3A potentiate aberrant stem cell gene expression program and acute leukemia development. *Cancer Cell* 2016 July 11;30(1):92-107. *
   * Cover image story with News & Views at:

Cancer Cell July 11;30(1):9-10; *Cancer Discovery* July 08, 2016 DOI: 10.1158/2159-8290.CD-RW2016-126

2. Zhou Y, Wang L, Vaseghi HR, Liu Z, Lu R, Alimohamadi S, Yin C, Fu JD, **Wang GG**, Liu J, Qian L. Bmi1 Is a Key Epigenetic Barrier to Direct Cardiac Reprogramming. *Cell Stem Cell*. 2016 Mar 3;18(3):382-95.

3. Zhang ZM, Rothbart SB, Allison DF, Cai Q, Harrison JS, Li L, Wang Y, Strahl BD, **Wang GG**, Song J. An Allosteric Interaction Links USP7 to Deubiquitination and Chromatin Targeting of UHRF1. *Cell Rep*. 2015 Sep 1;12(9):1400-6. PMID: 26299963

4. Li Z, Chen P, Su R, Hu C, Li Y, Elkahloun AG, Zuo Z, Gurbuxani S, Arnovitz S, Weng H, Wang Y, Li S, Huang H, Neilly MB, **Wang GG**, Jiang X, Liu PP, Jin J, Chen J. PBX3 and MEIS1 Cooperate in Hematopoietic Cells to Drive Acute Myeloid Leukemias Characterized by a Core Transcriptome of the MLL-Rearranged Disease. *Cancer Res*. 2016 Feb 1;76(3):619-29. PMID: 26747896

5. Xu B, On DM, Ma A, Parton T, Konze KD, Pattenden SG, Allison DF, Cai L, Rockowitz S, Liu S, Liu Y, Li F, Vedadi M, Frye SV, Garcia BA, Zheng D, Jin J, **Wang GG**. Selective inhibition of EZH2 and EZH1 enzymatic activity by a small molecule suppresses MLL-rearranged leukemia. Blood. 2015 Jan 8; 125(2):346-57. PMCID: PMC4287641.

6. **Wang GG**, Konze KD, Tao J. Polycomb genes, miRNA, and their deregulation in B-cell malignancies. Blood. 2015 Feb 19;125(8):1217-1225. PMCID: PMC4335077.

7. Xu B, Konze KD, Jin J, **Wang GG**. Targeting EZH2 and PRC2 dependence as novel anti-cancer therapy. Exp Hematol. 2015 May 28. pii: S0301-472X(15)00163-0. doi:10.1016/j.exphem.2015.05.001. [Epub ahead of print]

8. Konze KD, Ma A, Li F, Barsyte-Lovejoy D, Parton T, Macnevin CJ, Liu F, Gao C, Huang XP, Kuznetsova E, Rougie M, Jiang A, Pattenden SG, Norris JL, James LI, Roth BL, Brown PJ, Frye SV, Arrowsmith CH, Hahn KM, **Wang GG**, Vedadi M, Jin J#. An Orally Bioavailable Chemical Probe of the Lysine Methyltransferases EZH2 and EZH1. ACS Chem Biol. 2013; 8(6):1324-34.

Books or other non-periodical, one-time publications.

Nothing to Report.

Other publications, conference papers, and presentations.

Nothing to Report.

Website(s) or other Internet site(s)

Nothing to Report

Technologies or techniques

Nothing to Report

Inventions, patent applications, and/or licenses

Nothing to Report

Other Products

Nothing to Report

7. PARTICIPANTS & OTHER COLLABORATING ORGANIZATIONS

What individuals have worked on the project?

Name:	*Gang (Greg) Wang, PHD & Assistant Professor*
Project Role:	*PI*
Researcher Identifier (e.g. ORCID ID):	**orcid.org/0000-0002-7210-9940**
Nearest person month worked:	*5*
Contribution to Project:	*Dr. Wang has served as team leader performing experimental design, guidance and data review/interpretation.*
Funding Support:	*NIH, Kimmel Foundation*

▪

Name:	*Zhihong Ren, PHD/MD (postdoc trainee)*
Project Role:	*postdoc*
Researcher Identifier (e.g. ORCID ID):	**n/a**
Nearest person month worked:	*12*
Contribution to Project:	*Dr. Ren has served as postdoc research performing in vitro and in vivo experiments as proposed; he also carried out data review/interpretation.*
Funding Support:	*n/a*

▪

Has there been a change in the active other support of the PD/PI(s) or senior/key personnel since the last reporting period?

Nothing to Report

What other organizations were involved as partners?

Nothing to Report

8. SPECIAL REPORTING REQUIREMENTS

N/A

9. APPENDICES –n/a.

Reference:

Cao, R., Wang, L., Wang, H., Xia, L., Erdjument-Bromage, H., Tempst, P., Jones, R.S., and Zhang, Y. (2002). Role of histone H3 lysine 27 methylation in Polycomb-group silencing. Science (New York, NY *298*, 1039-1043.

Danis, E., Yamauchi, T., Echanique, K., Zhang, X., Haladyna, J.N., Riedel, S.S., Zhu, N., Xie, H., Orkin, S.H., Armstrong, S.A*., et al.* (2016). Ezh2 Controls an Early Hematopoietic Program and Growth and Survival Signaling in Early T Cell Precursor Acute Lymphoblastic Leukemia. Cell Rep *14*, 1953-1965.

Hidalgo, I., Herrera-Merchan, A., Ligos, J.M., Carramolino, L., Nunez, J., Martinez, F., Dominguez, O., Torres, M., and Gonzalez, S. (2012). Ezh1 is required for hematopoietic stem cell maintenance and prevents senescence-like cell cycle arrest. Cell stem cell *11*, 649-662.

Kuzmichev, A., Nishioka, K., Erdjument-Bromage, H., Tempst, P., and Reinberg, D. (2002). Histone methyltransferase activity associated with a human multiprotein complex containing the Enhancer of Zeste protein. Genes & development *16*, 2893-2905.

Margueron, R., Li, G., Sarma, K., Blais, A., Zavadil, J., Woodcock, C.L., Dynlacht, B.D., and Reinberg, D. (2008). Ezh1 and Ezh2 Maintain Repressive Chromatin through Different Mechanisms. Mol Cell *32*, 503-518.

Margueron, R., and Reinberg, D. (2011). The Polycomb complex PRC2 and its mark in life. Nature *469*, 343-349.

McCabe, M.T., Ott, H.M., Ganji, G., Korenchuk, S., Thompson, C., Van Aller, G.S., Liu, Y., Graves, A.P., Iii, A.D., Diaz, E*., et al.* (2012). EZH2 inhibition as a therapeutic strategy for lymphoma with EZH2-activating mutations. Nature *492*, 108-112.

Mochizuki-Kashio, M., Aoyama, K., Sashida, G., Oshima, M., Tomioka, T., Muto, T., Wang, C., and Iwama, A. (2015). Ezh2 loss in hematopoietic stem cells predisposes mice to develop heterogeneous malignancies in an Ezh1-dependent manner. Blood *126*, 1172-1183.

Mochizuki-Kashio, M., Mishima, Y., Miyagi, S., Negishi, M., Saraya, A., Konuma, T., Shinga, J., Koseki, H., and Iwama, A. (2011). Dependency on the polycomb gene Ezh2 distinguishes fetal from adult hematopoietic stem cells. Blood *118*, 6553-6561.

Shen, X., Liu, Y., Hsu, Y.-J., Fujiwara, Y., Kim, J., Mao, X., Yuan, G.-C., and Orkin, S.H. (2008). EZH1 Mediates Methylation on Histone H3 Lysine 27 and Complements EZH2 in Maintaining Stem Cell Identity and Executing Pluripotency. Mol Cell *32*, 491-502.

Xu, B., On, D.M., Ma, A., Parton, T., Konze, K.D., Pattenden, S.G., Allison, D.F., Cai, L., Rockowitz, S., Liu, S*., et al.* (2015). Selective inhibition of EZH2 and EZH1 enzymatic activity by a small molecule suppresses MLL-rearranged leukemia. Blood *125*, 346-357.

10.

Article

Cancer Cell

Epigenetic Perturbations by Arg882-Mutated DNMT3A Potentiate Aberrant Stem Cell Gene-Expression Program and Acute Leukemia Development

Graphical Abstract

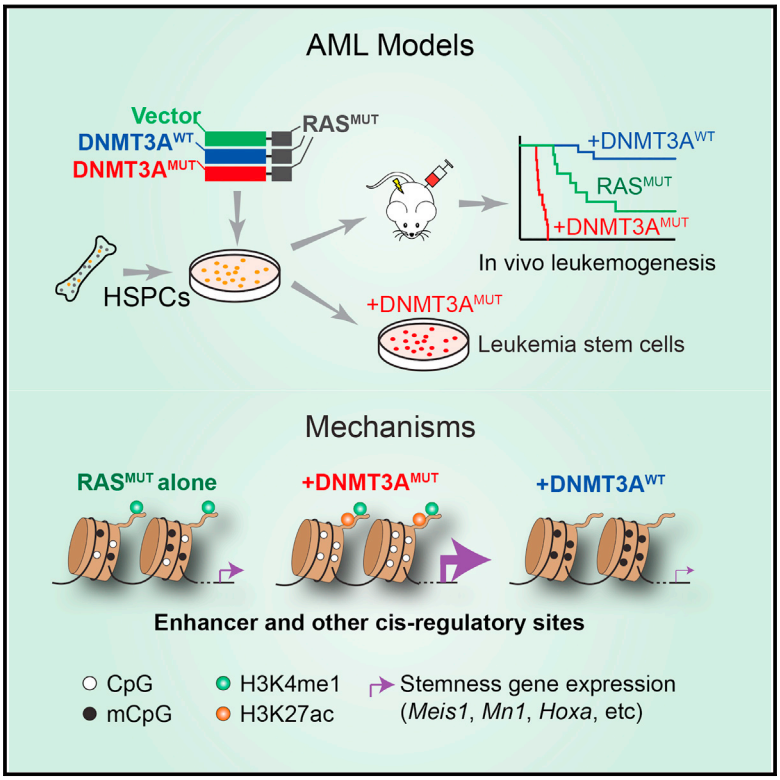

Highlights

- DNMT3A^{R882H} promotes acute leukemogenicity in the presence of mutant NRAS
- DNMT3A^{R882H} induces focal DNA hypomethylation at *cis* elements of key stemness genes
- DNMT3A^{R882H} potentiates stemness gene expression via enhancer/promoter activation
- DNMT3A^{R882H}-induced gene activation programs are sensitive to Dot1l blockade

Authors

Rui Lu, Ping Wang, Trevor Parton, ..., Paul A. Wade, Deyou Zheng, Gang Greg Wang

Correspondence

deyou.zheng@einstein.yu.edu (D.Z.), greg_wang@med.unc.edu (G.G.W.)

In Brief

Lu et al. establish that Arg882-mutated DNMT3A contributes to acute myeloid leukemia (AML) pathogenesis through epigenetic activation of leukemia-related genes. Inhibition of Dot1l reverses mutant DNMT3A-induced gene expression, indicating a potential therapeutic strategy for AMLs harboring this mutation.

Accession Numbers

GSE71475

Lu et al., 2016, Cancer Cell *30*, 1–16
July 11, 2016
http://dx.doi.org/10.1016/j.ccell.2016.05.008

CellPress

Please cite this article in press as: Lu et al., Epigenetic Perturbations by Arg882-Mutated DNMT3A Potentiate Aberrant Stem Cell Gene-Expression Program and Acute Leukemia Development, Cancer Cell (2016), http://dx.doi.org/10.1016/j.ccell.2016.05.008

Cancer Cell
Article

Epigenetic Perturbations by Arg882-Mutated DNMT3A Potentiate Aberrant Stem Cell Gene-Expression Program and Acute Leukemia Development

Rui Lu,[1,2] Ping Wang,[3] Trevor Parton,[1] Yang Zhou,[4] Kaliopi Chrysovergis,[5] Shira Rockowitz,[6] Wei-Yi Chen,[7] Omar Abdel-Wahab,[8] Paul A. Wade,[5] Deyou Zheng,[3,6,*] and Gang Greg Wang[1,2,9,*]
[1]Lineberger Comprehensive Cancer Center
[2]Department of Biochemistry and Biophysics
University of North Carolina School of Medicine, Chapel Hill, NC 27599, USA
[3]Department of Neurology, Albert Einstein College of Medicine, Bronx, NY 10461, USA
[4]Department of Pathology and Laboratory Medicine, McAllister Heart Institute, University of North Carolina School of Medicine, Chapel Hill, NC 27599, USA
[5]Laboratory of Molecular Carcinogenesis, National Institute of Environmental Health Sciences, National Institute of Health, Research Triangle Park, NC 27709, USA
[6]Departments of Genetics and Neuroscience, Albert Einstein College of Medicine, Bronx, NY 10461, USA
[7]Institute of Biochemistry and Molecular Biology, National Yang-Ming University, Taipei 11221, Taiwan
[8]Human Oncology and Pathogenesis Program, Memorial Sloan-Kettering Cancer Center, New York, NY 10065, USA
[9]Curriculum in Genetics and Molecular Biology, University of North Carolina at Chapel Hill, Chapel Hill, NC 27599, USA
*Correspondence: deyou.zheng@einstein.yu.edu (D.Z.), greg_wang@med.unc.edu (G.G.W.)
http://dx.doi.org/10.1016/j.ccell.2016.05.008

SUMMARY

DNA methyltransferase 3A (*DNMT3A*) is frequently mutated in hematological cancers; however, the underlying oncogenic mechanism remains elusive. Here, we report that the *DNMT3A* mutational hotspot at Arg882 (*DNMT3A*^{R882H}) cooperates with *NRAS* mutation to transform hematopoietic stem/progenitor cells and induce acute leukemia development. Mechanistically, DNMT3A^{R882H} directly binds to and potentiates transactivation of stemness genes critical for leukemogenicity including *Meis1*, *Mn1*, and *Hoxa* gene cluster. DNMT3A^{R882H} induces focal epigenetic alterations, including CpG hypomethylation and concurrent gain of active histone modifications, at *cis*-regulatory elements such as enhancers to facilitate gene transcription. CRISPR/Cas9-mediated ablation of a putative *Meis1* enhancer carrying DNMT3A^{R882H}-induced DNA hypomethylation impairs *Meis1* expression. Importantly, DNMT3A^{R882H}-induced gene-expression programs can be repressed through Dot1l inhibition, providing an attractive therapeutic strategy for *DNMT3A*-mutated leukemias.

INTRODUCTION

DNA methylation provides a critical epigenetic means for defining cellular identity and regulating functional output of gene-regulatory elements such as promoters and enhancers (Jones, 2012; Schubeler, 2015). Recently, DNA methyltransferase 3A (*DNMT3A*), a de novo DNA methyltransferase gene, was found mutated in ~20%–30% of human acute myeloid leukemias (AMLs) and ~10%–20% of various other hematological cancers (Cancer Genome Atlas Research Network, 2013; Ley et al., 2010; Patel et al., 2012; Yan et al., 2011; Yang et al., 2015). *DNMT3A* mutations also associate well with clonally

Significance

Recurrent *DNMT3A* mutations at Arg882 are found in hematological malignancies and disorders; however, due to a lack of relevant disease models, molecular mechanisms by which *DNMT3A* mutations influence leukemogenesis remain largely undefined. Through establishment and characterization of murine leukemia and leukemia stem cell models, we show that *DNMT3A*^{R882H} mutation potentiates transactivation of stemness genes required for acute leukemogenicity. Integrated epigenomic profiling of murine models further reveals the underlying epigenetic alterations induced by DNMT3A^{R882H}, which are enriched at gene-regulatory sites and resemble those seen in human patients. Pharmacological inhibition of Dot1l suppresses DNMT3A^{R882H}-associated gene activation and acute leukemogenesis. Our findings not only promote mechanistic understandings of *DNMT3A* mutation-associated clonal and malignant hematopoiesis but also provide a therapeutic avenue for *DNMT3A*-mutated leukemias.

derived hematopoiesis at premalignant stages (Genovese et al., 2014; Jaiswal et al., 2014; Shlush et al., 2014; Xie et al., 2014) and often coexist with a secondary lesion that "hits" either the FLT3-RAS kinase pathway, an epigenetic regulator (*IDH1/2*, *TET2*), or *NPM1* in AML patients (Cancer Genome Atlas Research Network, 2013; Ley et al., 2010; Patel et al., 2012; Yang et al., 2015). These clinical findings suggest that *DNMT3A* mutation acts as a founder lesion and requires an additional genetic event to induce malignant development. Consistently, mice with *Dnmt3a* knockout in the bone marrow produced phenotypically normal hematopoietic stem cells (HSCs); only after rounds of transplantation did *Dnmt3a*-null HSCs display self-renewal advantages (Challen et al., 2012). Mice with *Dnmt3a* mutation alone did not develop frank AML but showed increased susceptibility to malignant development upon acquisition of additional mutations (Celik et al., 2015; Chang et al., 2015; Mayle et al., 2015; Xu et al., 2014).

Mutational hotspot at Arg882 (R882), a residue located within the homodimerization interface of DNMT3A, accounts for the majority (~60%) of *DNMT3A* mutations found in AMLs (Ley et al., 2010; Yang et al., 2015). Due to a primarily heterozygous nature of *DNMT3A* R882 mutation, it was thought to act in a dominant-negative and/or haploinsufficient manner (Holz-Schietinger et al., 2012; Kim et al., 2013; Russler-Germain et al., 2014). Clinical evidence supports this notion, as AML patients with *DNMT3A* R882 mutation exhibited focal DNA hypomethylation (Russler-Germain et al., 2014). Despite these advances, there is a lack of relevant AML animal models for studying *DNMT3A* R882 mutation. Molecular pathways and mechanisms by which *DNMT3A* mutation contributes to AML pathogenesis remain undefined. Targeted approaches for the treatment of *DNMT3A*-mutated AMLs remain to be developed.

RESULTS

DNMT3A Hotspot Mutation Enhances Sensitivity of Hematopoietic Stem/Progenitor Cells to Transformation In Vitro

Previous reports indicate that hotspot mutations of *DNMT3A* such as *DNMT3A*^{R882H} act in a dominant-negative manner by disrupting formation of a DNMT3A-associated tetramer complex required for efficient DNA methylation (Holz-Schietinger et al., 2012; Kim et al., 2013; Russler-Germain et al., 2014). These studies prompted us to ask whether ectopic expression of human DNMT3A^{R882H} in murine hematopoietic stem/progenitor cells (HSPCs) could establish a transformation phenotype in a colony-forming unit (CFU) and replating assay (Figure S1A). Initially, we found a lack of CFU-promoting effect by DNMT3A^{R882H} alone (Figures 1A–1C). We then asked whether DNMT3A^{R882H} could enhance sensitivity of HSPCs to transformation in the presence of a second oncogenic lesion. Toward this end, we used a bicistronic retroviral system to coexpress either wild-type (WT) or R882H-mutant (RH) DNMT3A, together with other mutations known to coexist with *DNMT3A* mutation in human AMLs: NRAS (NRAS^{G12D}), NPM1 (NPM1c), or IDH1 (IDH1^{R132H}) (Figure S1A) (Ley et al., 2010; Patel et al., 2012; Shih et al., 2012). Following viral transduction and drug selection, we obtained highly pure HSPCs with comparable levels of oncogene expression for CFU assays (Figures 1C, S1B, and S1C). We did not observe a CFU-promoting effect of DNMT3A^{R882H} in the presence of NPM1c or IDH1^{R132H} (Figure S1D). However, a significant increase in CFUs was seen after replating of HSPCs co-expressing DNMT3A^{R882H} and NRAS^{G12D} (hereafter referred to as "RH-RAS"), relative to those with either oncogene alone (Figures 1A and 1B). In contrast to DNMT3A^{R882H}, DNMT3A^{WT} did not promote colony formation (Figures 1A and 1B). Post replating, HSPCs expressing NRAS^{G12D} alone produced tiny and diffuse colonies of differentiated cells whereas those with RH-RAS gave rise to large, compact colonies that mainly comprised undifferentiated progenitors (Figures 1A [inset], 1B, S1E, and S1F). Importantly, cells expressing RH-RAS as derived from serially replated colonies were able to propagate and maintain their immature progenitor status in long-term liquid culture (Figures 1D and S1G), suggesting acquisition of indefinite self-renewal capability by these cells. These data have shown that, in contrast to DNMT3A^{WT}, R882-mutated DNMT3A promotes aberrant self-renewal of HSPCs and enhances their sensitivity to transformation in vitro. In addition, *NRAS*^{G12D} genetic background provides a useful platform for dissecting the role of *DNMT3A* mutation in AML development.

DNMT3A^{R882H} Acts in Concert with Activated RAS to Induce Murine AMLs In Vivo

The observed in vitro effect of DNMT3A^{R882H} on aberrant HSPC self-renewal and immortalization indicates that it could cooperate with NRAS^{G12D} to cause malignant transformation in vivo. Thus, we transplanted murine HSPCs freshly transduced with DNMT3A (either WT or RH) and/or NRAS^{G12D} to syngeneic mice. NRAS^{G12D} alone induced a myeloproliferative disease with incomplete penetrance (Figures 1E and S1H). DNMT3A^{R882H} alone did not cause detectable diseases over a 12-month monitoring period; however, in the presence of NRAS^{G12D}, it significantly accelerated development of leukemia with a shorter latency phenotype and full penetrance (Figure 1E). RH-RAS-induced leukemia was also characterized by hepatosplenomegaly (Figures 1F, 1G, and S1I), leukemic infiltration to bone marrow, spleen, and liver (Figures 1H and S1J), and elevated counts of peripheral white blood cells and blasts (Figures 1I and S1K–S1O; Table S1). Leukemia induced by RH-RAS expressed virally transduced genes at a level comparable with progenitors immortalized by RH-RAS in vitro (Figure 1J) and displayed an immature myeloid (AML) immunophenotype (Mac-1^{+}/c-Kit^{low}/Cd34^{low}/Gr1^{-}/Cd3e^{-}/Cd19^{-}/Ter119^{-}; Figures 1K, S1P, and S1Q; Table S1). Whole-exome sequencing of three independent murine AMLs identified no recurrent mutation of additional genes (Figure S1R), suggesting that DNMT3A^{R882H} and NRAS^{G12D} are sufficient to drive AML development. Interestingly, unlike DNMT3A^{R882H}, DNMT3A^{WT} suppressed leukemogenesis in vivo (Figure 1E), suggesting that normal DNMT3A activities oppose AML pathogenesis.

DNMT3A Hotspot Mutation Produces Leukemia-Initiating Stem Cells Ex Vivo in the Presence of NRAS^{G12D}

To further verify the cell transformation effect of RH-RAS, we used a previously described liquid cultivation system (Wang et al., 2007, 2009) and were able to recapitulate HSPC immortalization with RH-RAS only, and not either oncogene alone or

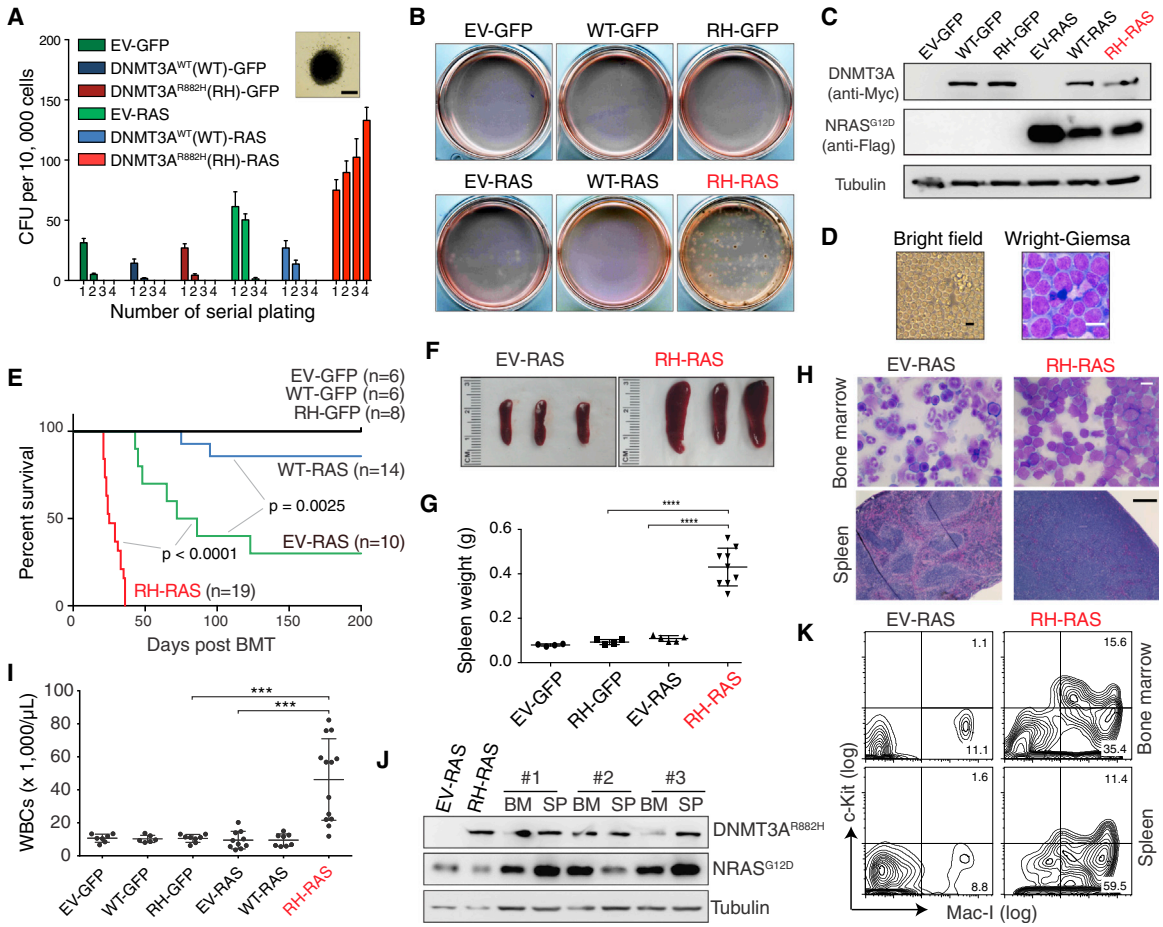

Figure 1. DNMT3A^{R882H} Acts in Concert with Mutant RAS to Transform Murine HSPCs Ex Vivo and Induce AMLs In Vivo

(A) Colony-forming unit (CFU) assay using murine HSPCs expressing empty control (EV), wild-type (WT), or R882H mutant (RH) DNMT3A in combination with GFP or NRAS^{G12D} (RAS). Inset shows a typical colony expressing RH-RAS at the fourth replating. Scale bar, 1 mm.

(B) Images of CFU assay at the fourth replating.

(C) Immunoblot of DNMT3A (Myc-tagged) and NRAS (Flag-tagged) in HSPCs after infection.

(D) Microscopic image and Wright-Giemsa staining of RH-RAS-coexpressing cells derived from the fourth replating after long-term culture with the SCF cytokine in vitro. Scale bars, 10 μm.

(E) Kaplan-Meier survival curve of mice after bone marrow transplantation (BMT) of HSPCs freshly transduced with indicated genes. The p values were calculated by log-rank test.

(F and G) Spleen size (F, n = 3) and weight (G, n = 4–9) of indicated cohorts 3–4 weeks post BMT. The p values were calculated by Student's t test.

(H) Wright-Giemsa staining of bone marrow (upper) and H&E staining of spleen (bottom) of indicated cohorts 4 weeks post BMT. Scale bar, 10 μm (upper) and 200 μm (bottom).

(I) White blood cell (WBC) counts in peripheral blood of indicated cohorts (n = 6–13) 4 weeks post BMT. The p values were calculated by Student's t test.

(J) Immunoblot of DNMT3A (Myc) and NRAS (Flag) proteins in bone marrow (BM) and spleen (SP) cells from mice with leukemia induced by RH-RAS coexpression. The first two lanes were loaded with samples of in vitro infected HSPCs.

(K) Fluorescence-activated cell sorting (FACS) analysis of Mac-1 and c-Kit with bone marrow and spleen cells of indicated cohorts 4 weeks post BMT.

Error bar denotes ±SD; ***p < 0.001, ****p < 0.0001. See also Figure S1 and Table S1.

coexpression of DNMT3A^{WT} with NRAS^{G12D} (Figure S2A). Similarly to those derived from CFU assays, RH-RAS-immortalized progenitors stably maintained their progenitor identity in vitro in the presence of SCF or Flt3 ligand, and presented with expression of immature myeloid (c-Kit^{+}/Mac-1^{low}/Gr1^{-}) and stem cell antigens (Cd34^{low}/Flt3^{+}/Sca1$^{low/-}$) as well as a lack of other lineage markers (Figures 2A, 2B, S2B, and S2C). Exposure of these progenitors to myeloid-promoting cytokines decreased cell proliferation (Figure S1G) and induced terminal myeloid differentiation (c-Kit^{-}/Mac-1^{high}/F4-80^{high}; Figures 2B and S2D), demonstrating their myeloid differentiation capability. Engraftment with each of three independent RH-RAS-immortalized progenitor lines induced murine AMLs (Figures S2E–S2H) that can be propagated in vivo with sequential transplantation (Figure 2C). Importantly, as few as 50–500 of these cells were sufficient to cause AML (Figure 2D), illustrating their leukemia-initiating stem cell (LSC) characteristic (hereafter called "LSCs$^{RH\text{-}RAS}$"). To further characterize LSCs$^{RH\text{-}RAS}$, we profiled their transcriptome and genome-wide occupancy of H3K4me1, a histone mark demarcating lineage-specific enhancers (Lara-Astiaso

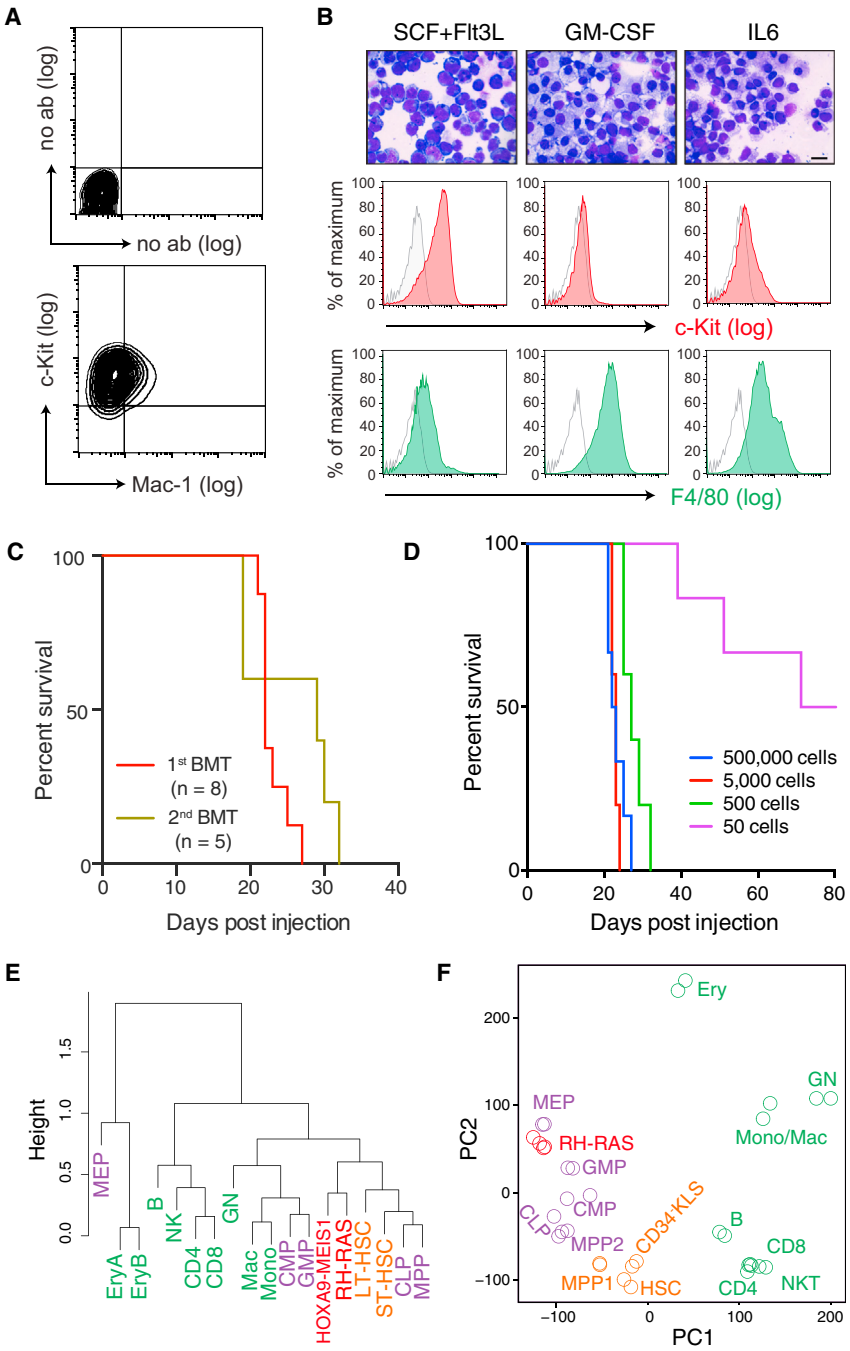

Figure 2. R882-Mutated DNMT3A Establishes Leukemia-Initiating Stem Cells Ex Vivo in the Presence of Activated RAS

(A) FACS analysis of in vitro immortalized progenitors by RH-RAS using a liquid culture system.

(B) Wright-Giemsa staining (upper) and FACS analysis of RH-RAS-immortalized progenitors 14 days after cultivation with indicated cytokines. FACS control, non-specific immunoglobulin G (gray trace). Scale bar, 10 μm.

(C) Kaplan-Meier curve of mice receiving primary or secondary BMT with RH-RAS-induced leukemia.

(D) Kaplan-Meier curve of mice (n = 5–6) receiving BMT of the indicated numbers of RH-RAS immortalized cells.

(E) Hierarchical clustering of genome-wide H3K4me1 profiles of LSCs^{RH-RAS}, AML-causing leukemia-initiating stem cell (LSC) lines produced by overexpressed HOXA9 plus MEIS1 (HOXA9-MEIS1), and various normal blood cell types. LT-HSC, long-term HSC; ST-HSC, short-term HSC; MPP, multipotent progenitor; CMP, common myeloid progenitor; CLP, common lymphoid progenitor; GMP, granulocyte-monocyte progenitor; MEP, megakaryocyte-erythroid progenitor; Mac, macrophage; Mono, monocyte; GN, granulocyte; B, B220$^+$/CD19$^+$ B cell; CD4/8, CD4/8$^+$ T cell; NK, natural killer cell; EryA and EryB, Ter119$^+$/CD71$^+$ erythroid cell with high and low forward scatter, respectively.

(F) Principal component (PC) analysis of transcriptome profiles of LSCs^{RH-RAS} and various normal blood cell types. CD34$^-$KLS, Cd34$^-$/c-Kit$^+$/Lin$^-$/Scal$^+$ HSC; MPP1, Flk2$^-$ multipotent progenitor; MPP2, Flk2$^+$ multipotent progenitor; NKT, natural killer T cell; Ery, erythroid cell. Other abbreviations as in (E).

See also Figure S2.

monality of pathways underlying leukemogenicity by these oncogenes.

R882-Mutated DNMT3A Potentiates Abnormal Transcription of Stem Cell Genes Including a Meis1-Mn1-Hoxa Regulatory Node

Next, we sought to understand the molecular basis underlying indefinite self-renewal shown by LSCs^{RH-RAS}. First, we asked whether they carry self-renewal or stemness gene-expression programs, a known feature of LSCs (Abramovich et al., 2005; et al., 2014). Unsupervised clustering of H3K4me1 profiles of LSCs^{RH-RAS} and various hematopoietic cell lineages revealed a similarity of LSCs^{RH-RAS} to HSPCs such as HSC and myeloid progenitors, when compared with differentiated cell types (Figures 2E and S2I); similar results were found in their transcriptome comparison (Figures 2F and S2J). Notably, a closer similarity was seen when comparing LSCs^{RH-RAS} with leukemic progenitors we and others previously produced using either HOXA9 plus MEIS1 (Wang et al., 2005), MLL translocation (Bernt et al., 2011), NUP98-NSD1 (Wang et al., 2007), or NUP98-JARID1A (Wang et al., 2009) (Figures 2E, S2I, and S2J), implying a common... Eppert et al., 2011; Krivtsov et al., 2006). By transcriptome analysis, we identified 54 genes uniquely expressed in LSCs^{RH-RAS} and primitive HSPCs with self-renewal capabilities, relative to differentiating and mature hematopoietic cell types (Figure 3A and Table S2). The stem cell signature genes expressed in LSCs^{RH-RAS} are only part of HSC stemness gene programs (~10%, Figure S3A); we further verified enrichment of the LSC^{RH-RAS} stemness signature in self-renewing HSCs with independent datasets (Figures S3B and S3C). The top LSC^{RH-RAS} stemness genes included *Hoxa9*, *Mn1*, *Hoxa5*, and *Meis1* (Figure 3A), which encode a set of transcription factors (TFs) and

cofactors crucial for sustaining self-renewal of normal HSCs and leukemic LSCs (Heuser et al., 2011; Huang et al., 2012; Wang et al., 2006; Wong et al., 2007). Gene targets of Meis1-Mn1-Hoxa, *Flt3* and *Sox4* (Heuser et al., 2011; Huang et al., 2012; Wang et al., 2005), were also among top stemness genes identified (Figure 3A), indicating activity of this TF regulatory circuitry in $LSCs^{RH\text{-}RAS}$. Moreover, activation of Meis1 and Hoxa in $LSCs^{RH\text{-}RAS}$ was found to be comparable with that in LSCs defined by other deregulated chromatin factors such as MLL-AF9, NUP98-JARID1A, or NUP98-NSD1, while *Mn1* and *Mycn* showed unique expression in $LSCs^{RH\text{-}RAS}$ (Figures S3D and S3E).

As $LSCs^{RH\text{-}RAS}$ carry both *DNMT3A* and *NRAS* mutations, we next asked which stemness gene signatures are dependent on $DNMT3A^{R882H}$. We performed microarray studies using HSPCs after transduction of $NRAS^{G12D}$ alone or with coexpressed DNMT3A, either WT or R882H mutant (hereafter referred to as EV-RAS, WT-RAS, or RH-RAS). These HSPCs were collected 12 and 16 days after viral transduction when their proliferation rates were comparable (Figure S2A). Among the 54 $LSC^{RH\text{-}RAS}$ stemness genes, nine were found to be upregulated by $DNMT3A^{R882H}$ at both time points, including *Meis1*, *Mn1*, and *Hoxa* (Figures 3B and S3F). Consistently, gene set enrichment analysis (GSEA) found that gene sets associated with AML development, undifferentiated myeloid cells, and NUP98-HOXA9 targets were significantly enriched in HSPCs with RH-RAS (Figure 3C). Conversely, gene sets associated with myeloid differentiation showed reduced expression in HSPCs expressing RH-RAS, relative to EV-RAS (Figure 3D), whereas the same gene sets showed enhanced expression in HSPCs expressing WT-RAS (Figure 3D), thus suggesting opposite effects of WT and R882-mutated DNMT3A on regulating genes crucial for HSPC self-renewal versus differentiation. We verified unique upregulation of *Meis1*, *Hoxa*, and *Mn1* in RH-RAS HSPCs (Figures 3E and S3G) and their induced AMLs (Figures 3F, 3G, and S3H). To functionally assess whether the activated Meis1-Mn1-Hoxa circuitry is essential for RH-RAS-induced AML development, we introduced independent small hairpin RNAs (shRNAs) of *Meis1* or *Mn1* into $LSCs^{RH\text{-}RAS}$ (Figure 3H) and found that knocking down either gene significantly impaired in vitro growth of $LSCs^{RH\text{-}RAS}$ (Figures 3I and S3I) as well as their in vivo leukemogenic function (Figures 3J, S3J, and S3K).

Together, these data reveal a role of R882-mutated *DNMT3A* in potentiating abnormal activation of stemness genes such as *Meis1*, *Mn1*, and *Hoxa*, which are required for mutant DNMT3A-mediated AML progression.

ChIP-Seq Reveals Context-Dependent Targeting of R882-Mutated DNMT3A into the LSC Genome

The $LSC^{RH\text{-}RAS}$ cellular model described above provides an ideal system for dissecting the molecular mechanism underlying $DNMT3A^{R882H}$-mediated oncogenesis. Mutant DNMT3A proteins are exclusively nuclear (Figure S4A); thus, we first mapped their genome-wide occupancy in $LSCs^{RH\text{-}RAS}$ by chromatin immunoprecipitation sequencing (ChIP-seq) using antibodies against the Myc tag fused to $DNMT3A^{R882H}$ (Figure S1A). Myc-$DNMT3A^{R882H}$ ChIP-seq gave robust and specific signals (Figure 4A); as a negative control, Myc ChIP-seq using cells without Myc-$DNMT3A^{R882H}$ expression did not detect any peaks (Figure S4B). We identified 13,705 genomic regions with significant $DNMT3A^{R882H}$ binding (i.e., $DNMT3A^{R882H}$ peaks, Table S3) in $LSCs^{RH\text{-}RAS}$, which spread over promoter and inter- or intragenic regions (Figure S4C). $DNMT3A^{R882H}$ exhibited a broad binding pattern with an average peak size of ~17 kb (Figures S4D and 4B, with an example peak at *Lig1*). Interestingly, $DNMT3A^{R882H}$ binding was stronger at intermediately transcribed genes, relative to lowly or highly expressed genes (Figure 4A), and positively correlated to CpG dinucleotide density except at CpG islands (CGIs) where $DNMT3A^{R882H}$ has a sharp drop in overall binding (Figure 4C). $DNMT3A^{R882H}$ binding regions also showed depletion of H3K4me3 (Figure 4D), a histone modification known to suppress DNMT3A binding due to an intrinsic histone H3 "reader" activity of DNMT3A's ADD domain (Guo et al., 2015; Noh et al., 2015). Intriguingly, 76.1% of $DNMT3A^{R882H}$ peaks were found in close proximity to and significantly overlapped with peaks of H3K4me1, a histone mark demarcating enhancer elements (observed/expected = 10.2, $p < 10^{-300}$; Figure 4E), as exemplified by those identified in an intron region of *Lig1* and an intergenic region of *Vegfa* (Figures 4B [inset] and S4E [boxed areas]). Ontology analysis of $DNMT3A^{R882H}$ peaks revealed their significant enrichment at genes related to normal and malignant hematopoiesis, PML-RARα targets, and *MLL* rearrangement-associated genes (Figures 4F and S4F). Notably, key AML-promoting or stemness genes upregulated by $DNMT3A^{R882H}$ such as *Meis1*, *Mn1*, *Hoxa*, and *Mycn* were all found directly bound by $DNMT3A^{R882H}$ (Figures 4G, 4H, S4G, and S4H). Collectively, our genome-wide profiling of $DNMT3A^{R882H}$ has revealed a CpG content and "histone code"-dependent targeting of R882-mutated DNMT3A into cancer cell genomes; we have also identified a previously unappreciated overlap of $DNMT3A^{R882H}$ with putative enhancer and *cis*-regulatory sites (marked by H3K4me1) at numerous developmental genes including a Meis1-Mn1-Hoxa node.

R882-Mutated DNMT3A Induces Focal Hypomethylation of CpG Sites Enriched with Gene-Regulatory Elements

We next aimed to delineate $DNMT3A^{R882H}$-induced epigenetic perturbations during AML progression. By enhanced reduced representation bisulfite sequencing (eRRBS), we mapped global DNA methylation patterns of murine HSPCs 16 days after transduction of EV-RAS, RH-RAS, or WT-RAS. Analysis of eRRBS data, which had 11–12× coverage for 6.5 million CpGs in all samples, revealed no significant changes in global CpG methylation (Figures S5A–S5C) except a moderate change at CpG shores (Figure S5C). By pairwise comparison of CpG methylation, we identified 12,889 differentially methylated CpG sites (DMCs) in HSPCs expressing RH-RAS relative to EV-RAS, with most DMCs (80.8%) hypomethylated (Figure 5A, left; hereafter termed "$DNMT3A^{R882H}$-associated hypo-DMCs"); in contrast, DMCs associated with $DNMT3A^{WT}$ are largely hypermethylated (hyper-DMCs, 80.6%; Figure 5A, right). $DNMT3A^{R882H}$-associated hypo-DMCs were found mainly in intron, intragenic, and promoter regions, while $DNMT3A^{WT}$-induced hyper-DMCs were enriched in promoters and CGIs (Figures S5D and S5E). Importantly, $DNMT3A^{R882H}$-associated hypo-DMCs were significantly enriched at genomic regions with H3K4me1 (Figure 5B) or with $DNMT3A^{R882H}$ binding (Figures

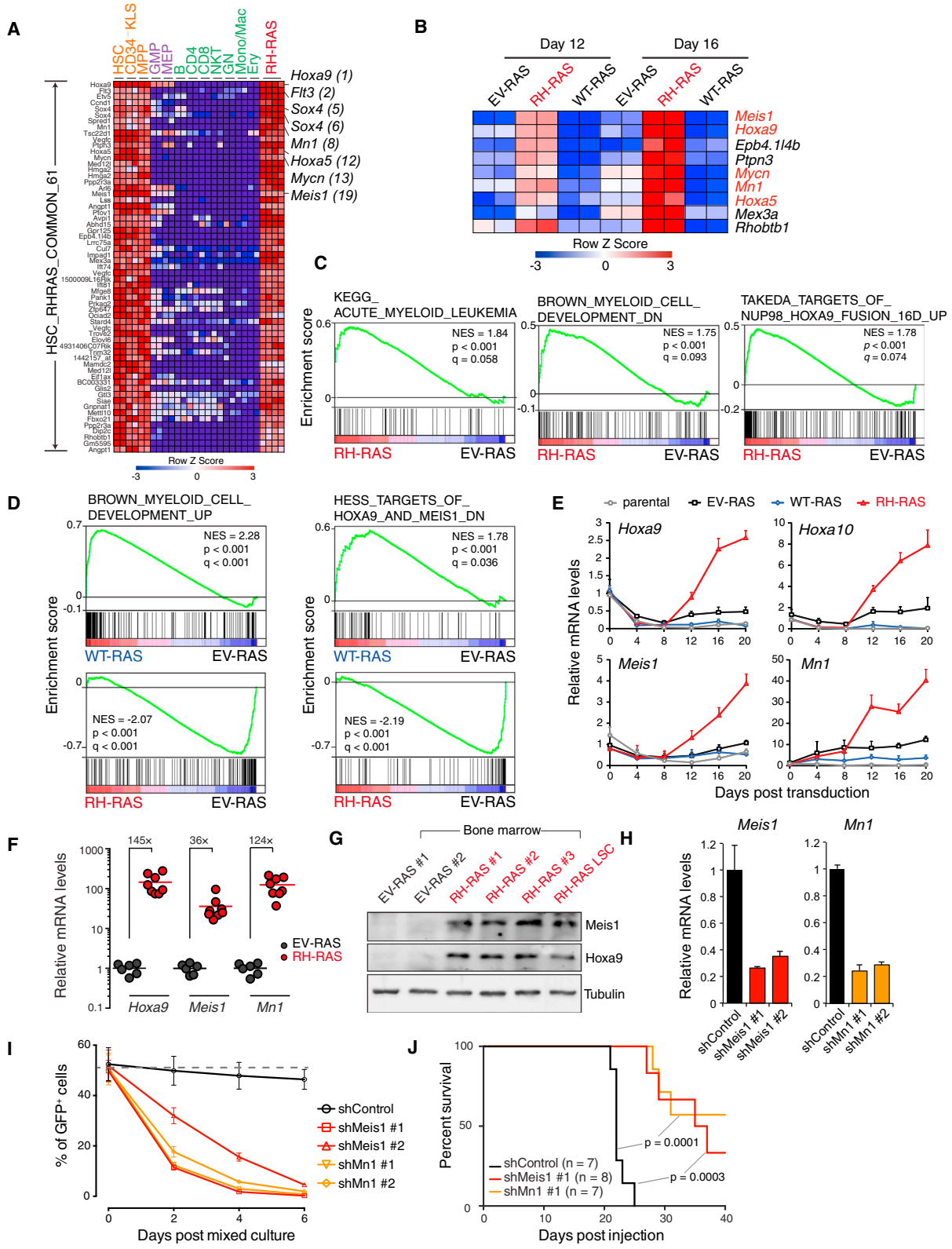

Figure 3. DNMT3A^{R882H} Potentiates Aberrant Activation of Stemness Genes Including a Critical *Meis1-Mn1-Hoxa* Regulatory Node

(A) Heatmap of 61 probes (54 genes) showing unique expression in both self-renewing HSPCs (HSC, Cd34^{-}KLS, and MPP) and LSCs^{RH-RAS} but not in differentiating (purple) or mature (green) blood cell types. Probes are ranked by higher expression in LSCs^{RH-RAS} relative to differentiating and mature cells. Example genes are highlighted along with their respective rankings.

(legend continued on next page)

5B and 5C). DNMT3A^{R882H}-associated hypo-DMCs were also found to be enriched with the binding site of the ETS family of TFs (Erg and Spi1/PU.1) and other hematopoietic TFs (Runx1 and Mycn; Figure 5D). In contrast, DNMT3A^{R882H}-associated hyper-DMCs exhibited none of these features and, instead, correlated negatively to DNMT3A^{R882H} binding (Figures 5B–5D), suggesting that creation of hyper-DMCs is due to an indirect effect of DNMT3A^{R882H}.

Consistent with DMCs, differentially methylated regions (DMRs) identified in HSPCs co-transduced with DNMT3A^{R882H} relative to control were mainly hypomethylated (hereafter called "DNMT3A^{R882H}-associated hypo-DMRs"; Table S4, n = 1,199) while DNMT3A^{WT}-associated DMRs were mainly hypermethylated (hyper-DMRs) (Figures 5E and S5F). These two sets of DMRs showed a significant overlap, including those found at DNMT3A^{R882H}-deregulated stemness genes (*Meis1*, *Mn1*, *Hoxa7*, and *Mycn*), further highlighting that WT and R882-mutated DNMT3A have opposing effects on DNA methylation of crucial AML-promoting genes (Figure 5F). In addition, DNMT3A^{R882H}-associated hypo-DMRs were enriched at genes related to transcriptional regulation, hematopoietic development, and cancer (Figures 5G and S5G). Consistent with results in DMCs, H3K4me1 and DNMT3A^{R882H} binding was significantly enriched at DNMT3A^{R882H}-associated hypo-DMRs (Figures 5H and S5H). Taken together, our results show that R882-mutated DNMT3A is sufficient to induce CpG hypomethylation at putative *cis*-regulatory sites of key stemness genes that we have functionally validated as essential for AML progression in murine models.

DNMT3A^{R882H}-Induced DNA Hypomethylation Identified in Murine Models Mirrors What Was Seen in Human AMLs with *DNMT3A* R882 Mutation

A focal CpG hypomethylation phenotype seen in the above murine model is reminiscent of what was observed in human AMLs with *DNMT3A* mutation (Russler-Germain et al., 2014). To assess whether our murine model mimics human disease, we first identified regions in the human genome that are homologous (i.e., conserved) to DNMT3A^{R882H}-associated hypo-DMRs defined in the murine model. We then found that, relative to randomized control, CpGs located in such conserved human genomic sites showed a significant reduction in their methylation levels among human AML samples with *DNMT3A* R882 mutation, relative to those with normal *DNMT3A* (Figure 5I; $p < 2.2 \times 10^{-16}$). Despite a relatively limited coverage of CpGs by the 450K-array platform used in the human AML study (Russler-Germain et al., 2014), genes with hypo-DMRs identified in AML patients carrying *DNMT3A* R882 mutation also had a significant overlap with those that gain DNMT3A^{R882H}-associated hypo-DMRs in our murine model (Table S5; $p < 0.05$). We identified 119 genes showing CpG hypomethylation in both human AMLs and murine LSC models, which again include stemness and AML-promoting genes *MEIS1*, *HOXA7*, and *MN1* (Figures 5J and S5I). We subsequently verified differential CpG methylation of DMRs at these genes in murine cells by direct bisulfite sequencing (Figures 5K and S5J), and further showed that a consistent hypomethylation pattern exists at conserved DMRs in human AMLs with *DNMT3A* R882 mutation, relative to those with non-R882 mutated or normal *DNMT3A* (Figures 5L and S5K).

Hypo-DMRs Induced by DNMT3A^{R882H} Facilitate Gain of Histone Acetylation at Gene-Regulatory Sites

Because DNMT3A^{R882H} binding and induced hypo-DMRs showed significant overlap with H3K4me1, a histone mark demarcating gene-regulatory regions such as enhancers and proximal elements close to promoters (Rada-Iglesias et al., 2011), we performed ChIP-seq profiling of H3K27ac, a histone modification correlating to enhancer/promoter activity, with the samples we used for eRRBS. Intriguingly, we found that introducing DNMT3A^{R882H} to HSPCs caused an overall gain of H3K27ac at DNMT3A^{R882H}-associated hypo-DMRs (Figure 6A, left) whereas no overall change in H3K4me1 was seen for these hypo-DMRs (Figure 6B, left); in contrast, expression of DNMT3A^{WT} decreased overall H3K27ac and H3K4me1 at these hypo-DMRs (Figures 6A and 6B, left). As a control, DNMT3A^{R882H}-associated hyper-DMRs did not show such changes (Figures 6A and 6B, right). Consistently, similar histone modification changes were seen at regions in close proximity to DNMT3A-associated DMCs (Figures S6A and S6B). Importantly, DMRs at key stemness or AML genes such as *Meis1*, *Mn1*, *Hoxa*, and *Mycn* all exhibited significant gain of H3K27ac in DNMT3A^{R882H}-expressing HSPCs as well as loss of H3K27ac in DNMT3A^{WT}-expressing HSPCs at their putative *cis*-regulatory sites (Figures 6C and S6C–S6H). By ChIP-qPCR, we verified the observed changes of H3K27ac and H3K4me1 at a panel of DMRs after transduction of DNMT3A^{R882H} versus DNMT3A^{WT} into HSPCs (Figures 6D and S6I). Furthermore, expression of DNMT3A^{R882H} enhanced binding of the H3K27 acetyltransferase p300 to hypo-DMRs at stemness genes (Figure 6E), suggesting that CpG hypomethylation facilitates recruitment of H3K27ac

(B) Of the 54 self-renewal genes, genes showing consistently higher expression in HSPCs 12 and 16 days after transduction of RH-RAS relative to EV-RAS.
(C) GSEA shows enrichment of AML-associated genes (left), genes downregulated upon myeloid differentiation (middle), and NUP98-HOXA9 targets (right) in HSPCs with RH-RAS versus EV-RAS.
(D) GSEA shows enrichment of differentiation gene sets in WT-RAS or RH-RAS HSPCs relative to EV-RAS. Left, myeloid differentiation genes; right, genes downregulated upon activation of HOXA9 and MEIS1.
(E) qRT-PCR of indicated genes in murine HSPCs after transduction of EV-RAS, WT-RAS, or RH-RAS.
(F) qRT-PCR of indicated genes in mouse bone marrow 21 days post BMT of HSPCs with EV-RAS (n = 6) or RH-RAS (n = 8).
(G) Immunoblot of Meis1 and Hoxa9 in bone marrow of mice 21 days post BMT of HSPCs with EV-RAS or RH-RAS. The last lane was loaded with LSC^{RH-RAS} samples.
(H) qRT-PCR showing shRNA-mediated *Meis1* or *Mn1* knockdown in LSCs^{RH-RAS}.
(I) Relative proliferation of indicated shRNA-expressing LSCs^{RH-RAS} (GFP$^+$) versus parental cells (GFP$^-$). These GFP$^-$ and GFP$^+$ cells were mixed in a 1:1 ratio at day 0, followed by measurement of percentage of GFP$^+$ cells.
(J) Kaplan-Meier curve of mice engrafted with indicated shRNA-expressing LSCs^{RH-RAS}. The p values were calculated by log-rank test.
Error bars denote ±SD. See also Figure S3 and Table S2.

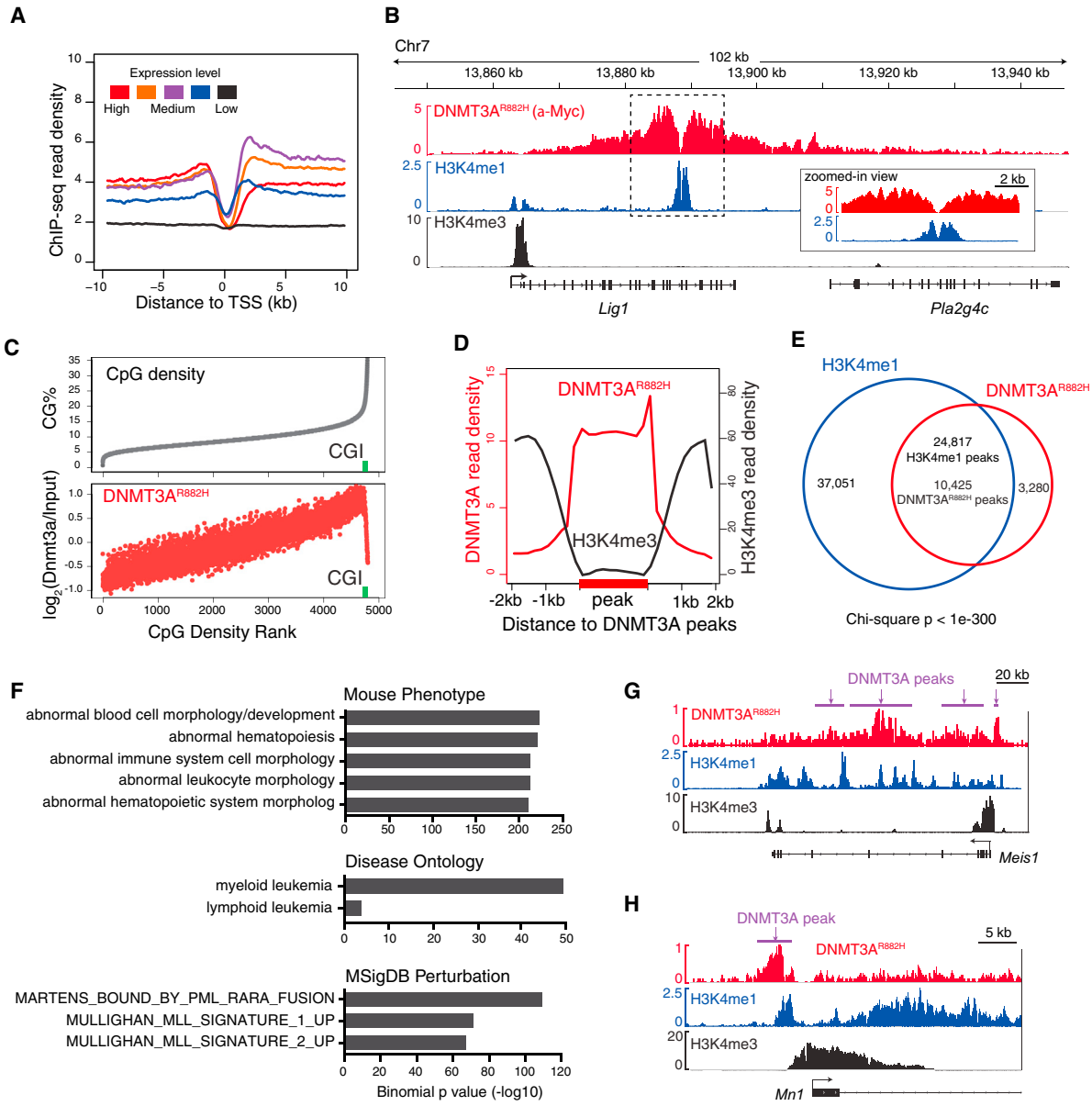

Figure 4. ChIP-Seq Reveals Chromatin Context-Dependent Binding of R882-Mutated DNMT3A to Genomic Regions, Including Stemness Genes such as a *Meis1-Mn1-Hoxa* Node

(A) DNMT3A^{R882H} ChIP-seq profiles across transcription start site (TSS) of genes with different expression levels in LSCs$^{RH\text{-}RAS}$.

(B) Example ChIP-seq profiles for DNMT3A^{R882H}, H3K4me1, and H3K4me3 at the Lig1 gene. Box shows a zoomed-in view of dashed-box region showing overlap of DNMT3A^{R882H} and H3K4me1 peaks.

(C) Correlation of DNMT3A^{R882H} binding and CpG density. Shown is percentage of CpG density (gray) and DNMT3A^{R882H} ChIP-seq reads (red) at 1-kb windows of the entire genome ranked by CpG density. Green square, CpG island (CGI).

(D) Plot of averaged DNMT3A^{R882H} (red) and H3K4me3 (black) ChIP-seq signals at DNMT3A^{R882H} peaks (labeled in bold on x axis) and surrounding regions (±2 kb).

(E) Venn diagram shows significant overlap of DNMT3A^{R882H} and H3K4me1 peaks in LSCs$^{RH\text{-}RAS}$.

(F) Genomic Regions Enrichment of Annotations Tool (GREAT) analysis shows enrichment of indicated gene signatures among DNMT3A^{R882H} peaks.

(G and H) ChIP-seq profiles of DNMT3A^{R882H}, H3K4me1 and H3K4me3 at Meis1 (G) and Mn1 (H). Purple bars, DNMT3A^{R882H} peak calls.

See also Figure S4 and Table S3.

"writers." In addition, overall gain of H3K27ac at hypo-DMRs was found to be significant regardless of expression changes of their associated genes (Figure S6J), indicating that H3K27ac gain at hypo-DMRs is not merely a consequence of gene activation, as exemplified by that found at hypo-DMRs of *Kdm2b*, *Sirt4*, and *Pax5* (Figures S6K–S6M).

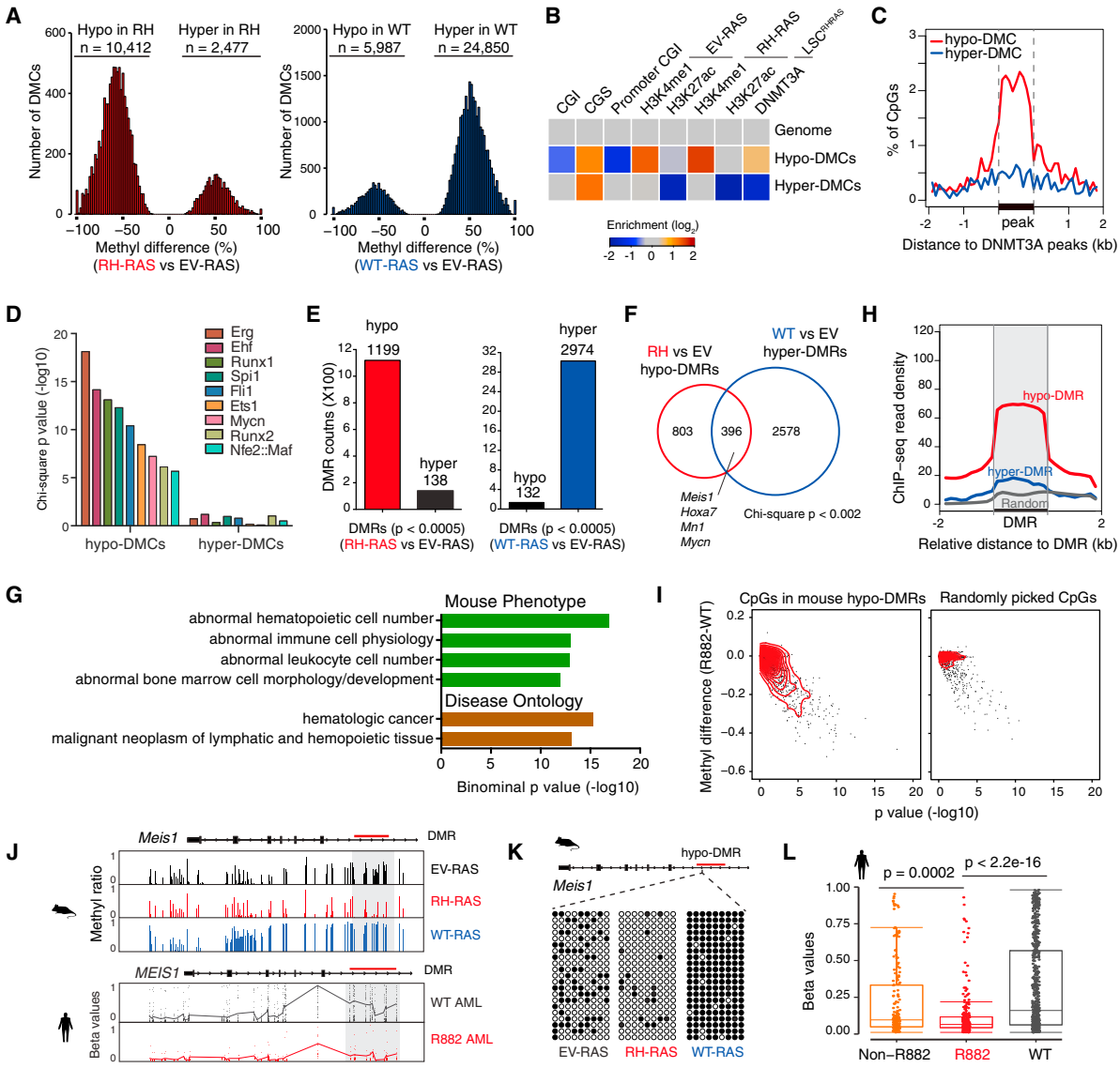

Figure 5. DNMT3A^{R882H} Induces Focal CpG Hypomethylations Enriched at H3K4me1-Demarcated, Gene-Regulatory Sites in HSPCs

(A) Distribution of DMCs (defined by q < 0.05) in the genome of murine HSPCs transduced with RH-RAS or WT-RAS, relative to EV-RAS.

(B) Heatmap showing enrichment of DNMT3A^{R882H}-associated DMCs at indicated genomic regions or ChIP-seq peaks in comparison with genome average. The enrichment value was calculated as $\log_2$(observed/expected) of the DMC numbers. CGI, CpG island; CGS, CpG shore.

(C) Distribution of DNMT3A^{R882H}-associated DMCs across DNMT3A^{R882H} ChIP-seq peaks (shown by a bold bar on x axis). y Axis shows percentage of DMCs located at 100-bp window of genomic regions centered on DNMT3A^{R882H} peaks.

(D) Enrichment of indicated TF binding motifs in DNMT3A^{R882H}-associated hypo-DMCs and hyper-DMCs.

(E) Summary of DMRs identified in the HSPCs with RH-RAS or WT-RAS, relative to EV-RAS.

(F) Venn diagram showing overlap of DNMT3A^{R882H} and DNMT3A^{WT}-associated DMRs.

(G) GREAT annotation of DNMT3A^{R882H}-associated hypo-DMRs.

(H) H3K4me1 profiles at DNMT3A^{R882H}-associated hypo-DMRs, hyper-DMRs, and random control regions. Plotted across DMRs (labeled by a bold line on x axis) were averaged H3K4me1 ChIP-seq read densities in EV-RAS cells.

(I) Scatterplots showing methylation changes of selected CpGs in human AMLs with DNMT3A R882 mutation relative to DNMT3A WT AMLs. Mean methylation differences (y axis) and p value (x axis) for each CpG between two AML patient groups were plotted. Left, CpGs in the human genome homologous to DNMT3A^{R882H}-associated hypo-DMRs identified in murine HSPCs; right, randomly picked CpG controls.

(J) DNA methylation profiles of Meis1 in indicated murine HSPCs and MEIS1 in human AMLs with WT (n = 50) or R882-mutated (n = 20) *DNMT3A*. Faded points show individual CpG methylation β values and connected lines indicate the mean methylation levels at each CpG site. Gray box and red bar represent a hypo-DMR in intron 6.

(K) Bisulfite sequencing of the Meis1 intron 6 DMR in indicated murine HSPC samples.

(legend continued on next page)

Because DNMT3A^{R882H}-induced hypo-DMRs can be found outside of gene-regulatory regions, we focused on those overlapping with a peak of H3K4me1 (a total of 777 DMRs) or H3K27ac (333 DMRs) in at least one cell condition and found that, in either case, 9- to 11-fold more DMRs showed enhanced H3K27ac levels than those with decreased H3K27ac (Figure 6F). These results indicate that DNA hypomethylation facilitates H3K27ac gain at gene-regulatory sites but also acts in a context-dependent manner. Consistently, more hypo-DMRs with gained H3K27ac were observed at regions showing a greater loss of CpG methylation (Figure 6G), supporting the degree of DNA hypomethylation as a contributing factor that fine-tunes functional output of gene-regulatory sites. Moreover, genes with increased H3K27ac at their hypo-DMRs were found to be enriched in HSPCs expressing RH-RAS relative to EV-RAS (Figure 6H), from which we identified 57 genes as both epigenetically altered and transcriptionally activated by DNMT3A^{R882H} (thus hereafter termed "DNMT3A^{R882H} signature genes," Figure 6I and Table S6). Notably, these DNMT3A^{R882H} signature genes included DNMT3A^{R882}-associated stemness genes studied above (a *Meis1-Mn1-Hoxa* node and *Mycn*) as well as other putative AML-promoting genes such as *Id2*, *Bcl2*, and *Runx3* (Figure 6I).

The *Meis1* Intron 6 Enhancer Carrying DNMT3A^{R882H}-Induced CpG Hypomethylation Is Crucial for *Meis1* Gene Activation in LSCs

To demonstrate a causal role of DNMT3A^{R882H}-induced focal DNA hypomethylation in gene-expression regulation, we cloned sequences from a panel of hypo-DMRs into a CpG-free reporter system designed to assess putative gene-regulatory activity and its relationship to CpG methylation (Schmidl et al., 2009). We found that all tested hypo-DMRs possess strong expression-enhancing activity in the absence of their CpG methylation (Figure 6J). CpG methylation of these hypo-DMRs completely abolished their expression-enhancing activities (Figure 6J), demonstrating a hypomethylation-dependent activation of *cis*-regulatory elements harbored within hypo-DMRs. To further verify DMR-associated enhancer activity in LSCs^{RH-RAS}, we closely examined a hypo-DMR located in the intron 6 of *Meis1* (Figure 6C, green bar) because *Meis1* is a critical effector gene for DNMT3A^{R882H}-associated AML progression (Figures 3H–3J) and this hypo-DMR is also found to be conserved in human AMLs with *DNMT3A* R882 mutation (Figures 5J–5L). Notably, this hypo-DMR is positive for H3K4me1 (Figure 6C) and has a significant overlap with a previously reported *MEIS1* enhancer in human cells (Xiang et al., 2014). First, we carried out chromosome conformation capture (3C), a surrogate assay for scoring enhancer usage and promoter association, and indeed detected a long-range looping interaction of the intron 6 hypo-DMR with the *Meis1* promoter in LSCs^{RH-RAS} (Figure 6K). To further determine the role of this putative intron 6 enhancer in DNMT3A^{R882H}-induced *Meis1* gene activation, we employed the CRISPR/Cas9-based genomic editing technology. Cas9 and a pair of single guide RNAs (sgRNA) targeting boundaries of the *Meis1* hypo-DMR were transduced into LSCs^{RH-RAS} (Figure 6L). PCR and direct sequencing confirmed sgRNA-mediated specific deletion of the hypo-DMR in five independent LSC^{RH-RAS} lines (Figures 6M, 6N, and S6N). In all cases, ablation of this putative enhancer significantly reduced *Meis1* expression (Figure 6O). Consistently, among human AMLs with *DNMT3A* R882 mutation, lower DNA methylation at the *MEIS1* intron 6 correlated with higher expression of *MEIS1* (Figure 6P). It is also worth noting that 54.5% (6 of 11) of *DNMT3A* WT AMLs display significant DNA methylation of *MEIS1* intron 6 and yet express *MEIS1* at high levels (Figure 6P), indicating that different gene activation mechanisms exist in these AML cases. Together, using *Meis1* as a paradigm example, we show that focal CpG hypomethylation induced by DNMT3A R882 mutation promotes enhancer activation and expression of key AML genes.

Dot1l Inactivation Suppresses DNMT3A^{R882H}-Associated LSC Properties and Aberrant Activation of Stemness Gene Programs

To explore the potential strategy for reversing DNMT3A^{R882H}-induced gene deregulation and thus treating *DNMT3A*-mutated leukemia, we conducted compound treatment studies with a collection of epigenetic regulator inhibitors and identified that LSCs^{RH-RAS} showed a significantly higher sensitivity to a Dot1l inhibitor, SGC0946, relative to control cells without *DNMT3A* mutation, i.e., LSCs expressing *NRAS^{G12D}* plus oncogenic TFs (Figure S7A). Dot1l, a histone H3 lysine 79 (H3K79) methyltransferase, belongs to a transcription elongation regulatory complex that engages acetylated histones at *cis*-regulatory sites (Li et al., 2014). Genomic profiling of H3K79 dimethylation (H3K79me2) detected its overall elevation at DNMT3A^{R882H}-associated hypo-DMRs in HSPCs (Figure 7A), as exemplified by those at *Meis1*, *Hoxa*, *Mn1*, and *Mycn* (Figures 7B and S7B). We confirmed H3K79me2 gain at these genes by ChIP-qPCR (Figure S7C). Next, we asked whether pharmacological inhibition of Dot1l could reverse DNMT3A^{R882H}-induced gene activation. We first confirmed SGC0946-mediated suppression of H3K79me2 in LSCs^{RH-RAS} (Figure S7D), followed by microarray profiling. Notably, after SGC0946 treatment, we detected significant downregulation of DNMT3A^{R882H} signature genes (Figures 7C and 7D) and concurrent upregulation of myeloid differentiation genes in LSCs^{RH-RAS} (Figures 7D and S7E). Although *Hoxa* and *Meis1* were shown as part of MLL-AF9 target genes that are dependent on Dot1l (Chen et al., 2015), the DNMT3A^{R882H} signature genes displayed a greater sensitivity to Dot1l inhibitors than MLL-AF9 targets in LSCs^{RH-RAS} (Figure 7E); conversely, the DNMT3A^{R882H} signature genes do not show overall response to Dot1l inhibitors in MLL-AF9-transformed AML cells (Figure S7F). These analyses indicate that *DNMT3A* R882 mutation confers a unique dependency on the Dot1l enzymatic activity in AML. We further verified downregulation of DNMT3A^{R882H}-associated

(L) Box plots of methylation β values of all CpGs (shown as dots in box plot) at MEIS1 intron 6 in human AMLs with R882-mutated DNMT3A (n = 20) relative to AMLs with either non-R882 mutated (n = 15) or WT (n = 50) DNMT3A. Horizontal line, median; box, interquartile range; whiskers extend to 1.5× the interquartile range. The p values were calculated by Mann-Whitney U test.
See also Figure S5; Tables S4 and S5.

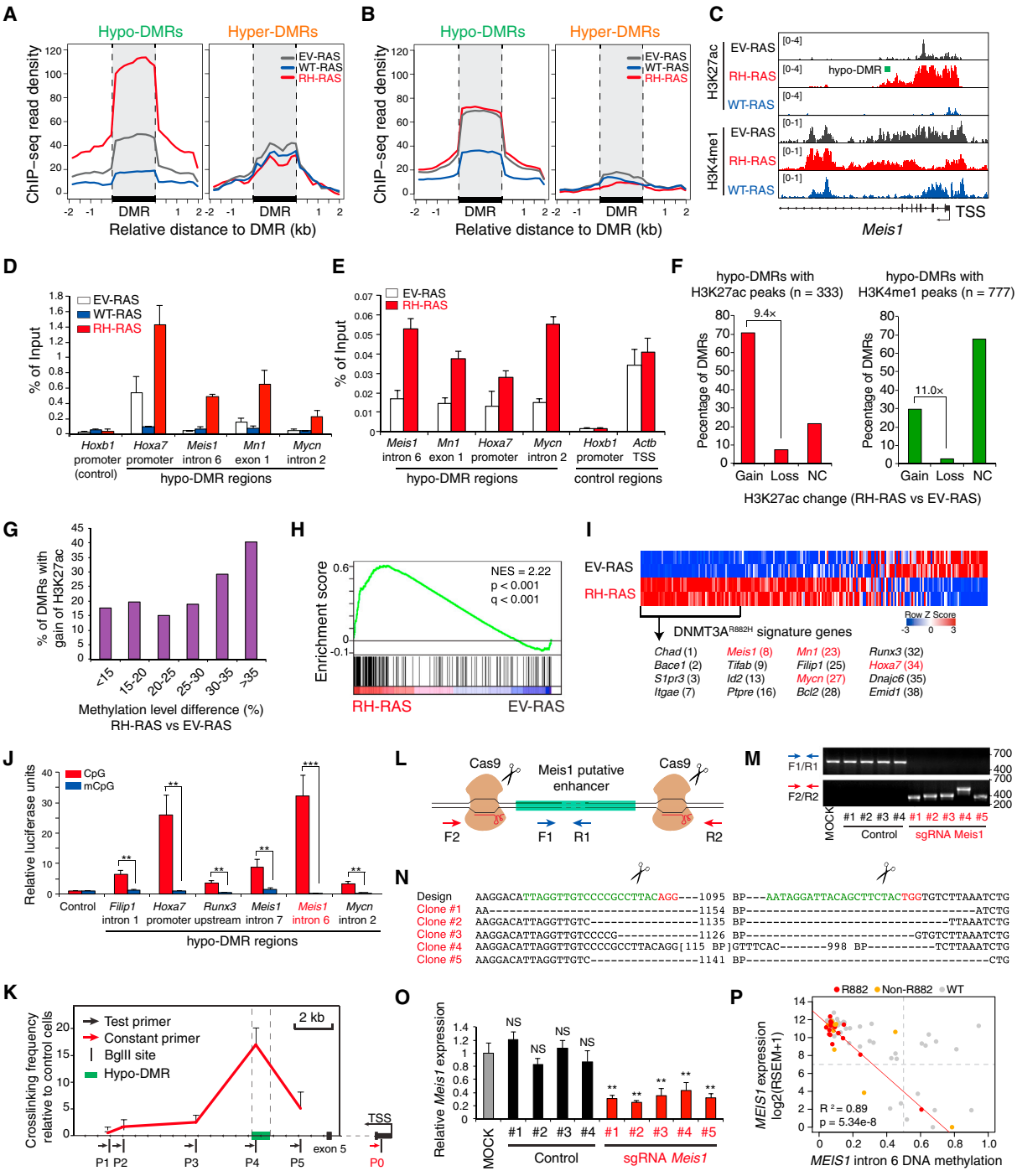

Figure 6. DNMT3A^{R882H}-Associated Hypo-DMRs Gain Epigenetic Alterations Associated with Gene Activation

(A and B) H3K27ac (A) and H3K4me1 (B) profiles at DNMT3A^{R882H}-associated DMRs (bold bar on x axis) and the surrounding regions. Averaged ChIP-seq read densities in HSPCs with EV-RAS, RH-RAS, or WT-RAS were plotted.

(C) H3K27ac and H3K4me1 profiles at *Meis1* intron 6 in indicated HSPCs. Green bar, hypo-DMR.

(D and E) ChIP-qPCR of H3K27ac (D) and p300 binding (E) at hypo-DMRs in indicated HSPCs.

(F) Percentage of DNMT3A^{R882H}-associated hypo-DMRs showing indicated H3K27ac changes in HSPCs with RH-RAS versus EV-RAS. Gain, increased H3K27ac; Loss, reduced H3K27ac; NC, no significant H3K27ac change. The total DMRs used for calculation were hypo-DMRs carrying H3K27ac (left) or H3K4me1 (right) in at least one cell condition.

(G) Percentage of DNMT3A^{R882H}-associated hypo-DMRs (n = 1,199) showing H3K27ac gain in HSPCs with RH-RAS versus EV-RAS, when these hypo-DMRs are divided based on degree of DNA methylation reduction (x axis) shown in the same samples.

(H) GSEA shows that genes with gain of H3K27ac at hypo-DMRs are enriched in HSPCs 16 days after transduction of RH-RAS, relative to EV-RAS.

(legend continued on next page)

stemness genes *Hoxa*, *Meis1*, *Mn1*, and *Mycn* after treatment with SGC0946 (Figures 7F, 7G, and S7G) or knockdown of Dot1l (Figures 7H, S7H, and S7I). In response to Dot1l inactivation, multiple murine and human AML lines bearing *DNMT3A* mutation showed suppressed in vitro growth (Figures 7I, S7J, and S7K) and concurrent cell differentiation (Figures 7J, 7K, and S7L–S7N). *DNMT3A*-mutated human AML lines also had decreased *HOXA* or *MEIS1* expression upon DOT1L blockade (Figures S7O and S7P). In contrast, various murine and human leukemia lines established by oncogenic TFs were all insensitive to Dot1l inhibition (Figures 7I and S7K). Also, enforced expression of HOXA9 plus MEIS1 reversed sensitivity of LSCs$^{RH\text{-}RAS}$ to Dot1l inhibition (Figure 7L), demonstrating a crucial role of these TFs in DNMT3A^{R882H}-mediated oncogenic effects. Importantly, knockdown of Dot1l in LSCs$^{RH\text{-}RAS}$ or their pretreatment with Dot1l inhibitors significantly delayed in vivo AML progression and prolonged the survival of engrafted mice (Figure 7M). Collectively, we show that expression of *DNMT3A*^{R882H} confers Dot1l dependency in AML and that reversing DNMT3A^{R882H}-induced gene activation by Dot1l inhibition may provide a potential therapeutic means for the treatment of AMLs with *DNMT3A* mutation.

DISCUSSION

In this study, we report a set of ex vivo LSC and in vivo murine AML model systems for studying the functionality of *DNMT3A* R882 mutation in AML pathogenesis. Using these human disease-mimicking models, we have (1) defined a causal role of DNMT3A^{R882H} in promoting AML transformation in vitro and in vivo; (2) identified DNMT3A^{R882H}-deregulated gene pathways, including a Meis1-Mn1-Hoxa TF node that we functionally validated as essential for DNMT3A^{R882H}-mediated AML progression; (3) shown that DNMT3A^{R882H} directly binds to gene-regulatory sites, notably enhancers, inducing focal DNA hypomethylation and concurrent gain of histone acetylation; (4) determined a critical role of the epigenetically altered enhancer and *cis*-regulatory elements for DNMT3A^{R882H}-associated gene activation; and (5) demonstrated, importantly, that pharmacological inhibition of Dot1l reverses the mutant DNMT3A-associated gene activation, thus providing a potential therapeutic avenue for the affected AMLs.

The molecular pathways identified in this study help explain several important biological phenomena related to *DNMT3A* mutation and hematological disease. First, as the Meis1-Mn1-Hoxa circuitry is crucial for both normal expansion of HSCs and malignant transformation of LSCs (Argiropoulos and Humphries, 2007; Heuser et al., 2011), deregulation of this TF node by R882-mutated DNMT3A provides a molecular explanation not only for malignant hematopoiesis but also for clonal hematopoiesis, a phenotype strongly associated with *DNMT3A* mutation (Genovese et al., 2014; Jaiswal et al., 2014; Xie et al., 2014). In addition, these findings help explain a mutually exclusive pattern for *DNMT3A* mutation and *MLL* rearrangement in AMLs (Cancer Genome Atlas Research Network, 2013; Patel et al., 2012) because the latter itself is a strong inducer of *Meis1* and *Hoxa* activation (Chi et al., 2010).

Our results also demonstrate the requirement of cooperation between *DNMT3A* mutation and the activated kinase such as RAS for AML induction. RAS mutation alone induces a hyperproliferative phenotype but does not support self-renewal, which is in agreement with previous studies (Zhang et al., 2009); RAS activation was also known to induce cell senescence, a barrier of cancer development (Campisi and d'Adda di Fagagna, 2007). On the other hand, *DNMT3A* mutation confers aberrant HSPC self-renewal, blocks differentiation programs, and yet lacks a pro-proliferation effect; besides a Meis1-Mn1-Hoxa node we have functionally confirmed as essential for DNMT3A^{R882H}-associated AML, other downstream targets of DNMT3A^{R882H}, such as pro-survival (*Bcl2*), anti-differentiation (*Id2*), and stemness (*Mycn*) genes, might be equally crucial for AML progression. These findings suggest that synergy between DNMT3A and kinase mutations is likely due to their differential effects on pathways relating to AML development. However, it is also possible that the two mutations may affect distinctive sets as well as the same sets of downstream effectors via genetic or epigenetic mechanisms. A similar synergy is most likely to exist between *DNMT3A* mutation and the activated FLT3, which acts upstream of RAS and coexists with the former in human AMLs as well.

Our studies clearly show that *DNMT3A* mutation-induced CpG hypomethylations are not random: they are significantly enriched at gene-regulatory sites, notably, putative enhancers marked by H3K4me1 as well as the binding sites of master hematopoietic TFs. Precise mechanisms by which CpG methylation of these *cis*-regulatory sites regulates gene expression remain to be fully studied. For example, despite a large number of DMCs found to be associated with either *DNMT3A* or *TET2* mutation in AML, a relatively small number of genes show changes in their expression (Russler-Germain et al., 2014; Shih et al., 2015). A possible

(I) Heatmap shows expression of genes in (H) ranked by higher expression in HSPCs with RH-RAS, relative to EV-RAS. The significantly upregulated genes in RH-RAS HSPCs are defined as "DNMT3A^{R882H} signature genes" (n = 57), with selected ones listed along with their respective rankings (bottom).

(J) Quantification of expression-enhancing activity of DNMT3A^{R882H}-associated hypo-DMRs with the embedded CpGs either non-methylated (CpG) or methylated (mCpG) using a CpG-free luciferase reporter system. The reporter without any DMR insertion was used as control. The p values were calculated by Student's t test.

(K) 3C assay shows looping interaction of the *Meis1* intron 6 hypo-DMR (P4) to gene promoter (P0), relative to other tested sites.

(L and M) Scheme (L) and PCR validation (M) of CRISPR/Cas9-mediated deletion of the *Meis1* intron 6 DMR. MOCK, parental LSC$^{RH\text{-}RAS}$; Control, no sgRNA; sgMeis1, a pair of sgRNAs that target the DMR boundaries.

(N) Sequencing of the genomic PCR products from F2/R2 primers shows CRISPR/Cas9-induced deletion of the *Meis1* intron 6 DMR.

(O) Expression levels of Meis1 in LSC$^{RH\text{-}RAS}$ lines shown in (M). The p values were calculated by Student's t test by comparing with MOCK.

(P) Impact of DNA methylation levels in *MEIS1* intron 6 in cytogenetically normal human AMLs grouped by *DNMT3A* WT (n = 45), non-R882 (n = 13), and R882 mutations (n = 16). Plotted were mean methylation β values of CpGs at *MEIS1* intron 6 and $\log_2$-transformed expression values of RNA sequencing by expectation maximization (RSEM). R^2 and p values shown were determined with data of R882-mutant AMLs.

Error bar denotes ±SD. **p < 0.01, ***p < 0.001; NS, not significant. See also Figure S6; Tables S4 and S6.

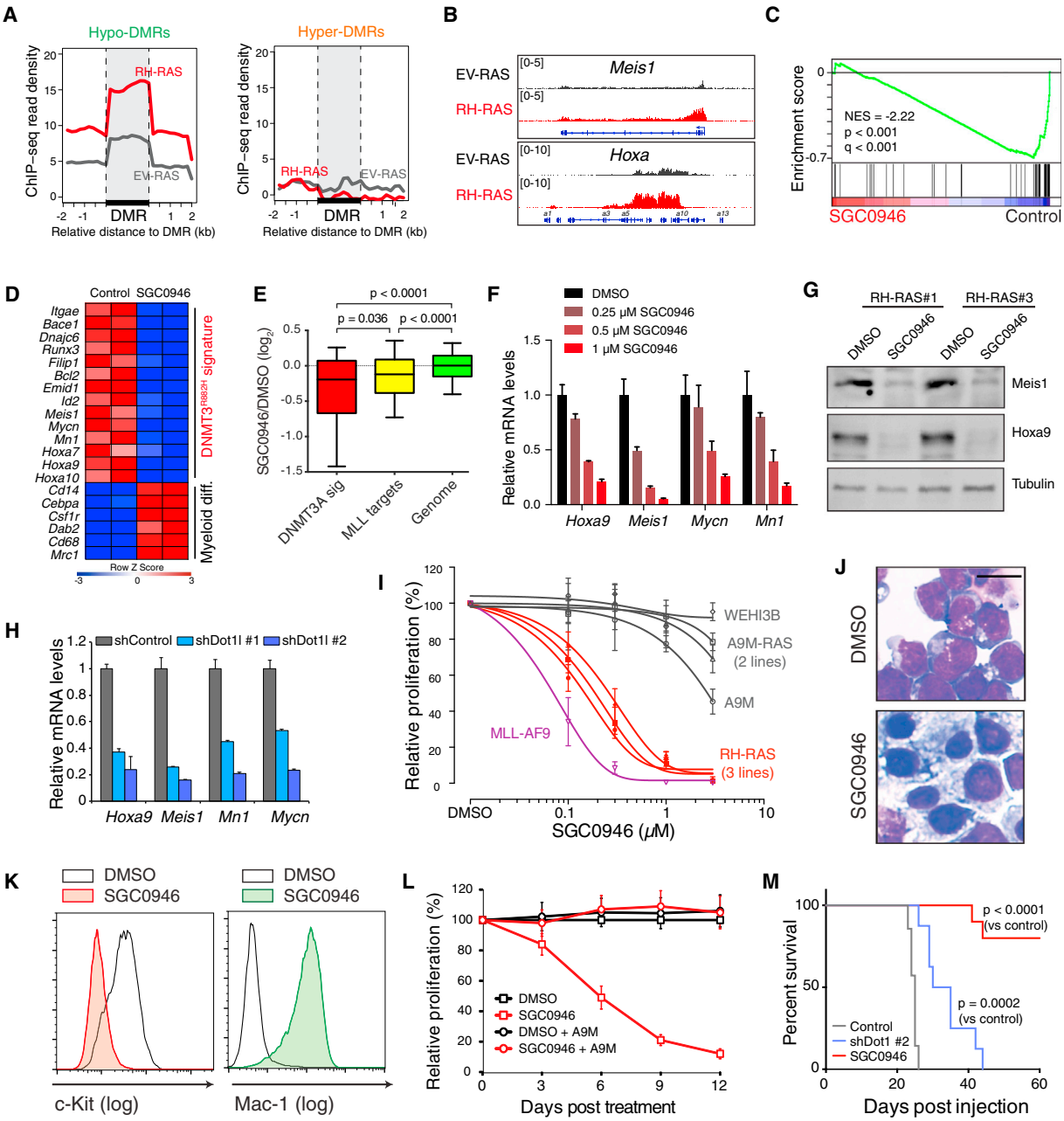

Figure 7. Dot1l Inhibition Reverses DNMT3A^{R882H}-Mediated Aberrant Transactivation of Stem Cell Genes, thereby Suppressing Acute Leukemogenicity

(A) Averaged H3K79me2 ChIP-seq signals at DNMT3A^{R882H}-associated hypo-DMRs and hyper-DMRs in HSPCs with RH-RAS or EV-RAS.

(B) H3K79me2 profiles at Meis1 and *Hoxa* in indicated HSPCs.

(C) GSEA shows downregulation of DNMT3A^{R882H} signature genes in LSCs^{RH-RAS} after treatment with 1 μM SGC0946 for 4 days.

(D) Heatmap shows downregulation of DNMT3A^{R882H} signature genes and upregulation of myeloid differentiation genes in SGC0946-treated LSCs^{RH-RAS} versus mock treatment.

(E) Box plots show relative expression of DNMT3A signature genes (n = 54), MLL-AF9 gene targets (n = 129), and all genes in the genome in SGC0946-treated LSCs^{RH-RAS}, relative to mock treatment. Horizontal line, median; box, interquartile range; whiskers, 10–90 percentiles. The p values were calculated by Mann-Whitney U test.

(F and G) qRT-PCR (F) and immunoblot (G) of indicated genes and proteins in LSCs^{RH-RAS} 6 days after treatment with SGC0946.

(H) Expression of indicated genes in LSCs^{RH-RAS} transduced with *Dot1l* shRNAs or vector control.

(I) Relative growth of LSCs^{RH-RAS} and other AML lines established by MLL-AF9, Hoxa9 plus Meis1 (A9M), A9M plus NRAS^{G12D} (A9M-RAS), and Hoxb8 plus Meis2 (WEHI3B) after a 12-day treatment with SGC0946 versus DMSO.

(J and K) Wright-Giemsa staining (J) and FACS analysis (K) of LSCs^{RH-RAS} 6 days after treatment with DMSO or 1 μM SGC0946. Scale bar, 10 μm.

(legend continued on next page)

explanation is that the effect of CpG methylation on gene expression is context dependent (Baubec and Schubeler, 2014): degree of CpG methylation change, density, or genomic location of CpG, methyl-CpG "readers," and TF binding are all possible factors affecting the ultimate effect of DNA methylation on gene expression. Unlike histone (de)acetylation, CpG (de) methylation at distal *cis*-regulatory sites such as enhancers may act as a permissive mechanism influencing gene expression, rather than a strong and instructive one controlling levels of gene activation and transcription. Nevertheless, using reporter assays and CRISPR/Cas9-mediated enhancer editing, we have determined the role of select hypo-DMRs in the activation of associated target genes such as *Meis1*.

This study also provides useful information on how to treat *DNMT3A*-mutated AMLs. Pharmacological blockade of Dot1l reversed *DNMT3A* mutation-induced gene activation, resulting in an impaired AML pathogenesis. In the future, examination of other "druggable" factors would likely identify additional therapeutic strategies for the treatment of *DNMT3A*-mutated AMLs. Therefore, in addition to elucidating the underlying oncogenic mechanisms, the ex vivo and in vivo model systems presented herein should be useful for exploring AML therapeutics.

EXPERIMENTAL PROCEDURES

The detailed procedures of plasmid construction, cell culture, antibody and immunoblot, flow cytometry, microarray analysis, ChIP-seq, eRRBS, Exome-seq, qRT-PCR, ChIP-qPCR, 3C-qPCR, shRNA-mediated knockdown, luciferase reporter assay, CRISPR/Cas9-mediated genomic editing, as well as the detailed information for computational and statistical analysis of deep sequencing data are described in Supplemental Experimental Procedures.

In Vitro CFU Assay with Serial Replating

Following lineage-negative (Lin^-) enrichment and retroviral transduction, 30,000 infected HSPCs were plated in the semi-solid methylcellulose cultivation system (Methocult; Stem Cell Technologies), followed by CFU counting and replating for every 10–14 days according to the manufacturer's protocol.

Animal Studies and In Vivo Leukemogenic Assay

All animal experiments were approved by and performed in accord with the guidelines of the Institutional Animal Care and Use Committee at the University of North Carolina. Leukemogenic potentials of transduced HSPCs were evaluated by bone marrow transplantation into sublethally irradiated syngeneic mice. In brief, 200,000 of bone marrow-derived Lin^- HSCPs following procedures of cytokine stimulation, retroviral transduction, and drug selection were injected via tail vein to recipient mice as described previously (Wang et al., 2009).

Statistical Analysis

Data are presented as the mean ± SD of three independent experiments unless otherwise noted. Statistical analysis was performed with Student's t test for comparing two sets of data with assumed normal distribution. We used a Mann-Whitney U test for data not showing a normal distribution, chi-square test for categorical variables, and log-rank test for Kaplan-Meier survival curves to determine statistical significance. $p < 0.05$ was considered significant.

ACCESSION NUMBERS

The microarray, eRRBS-seq, and ChIP-seq data reported in this paper have been deposited in the Gene Expression Omnibus with accession number GEO: GSE71475.

SUPPLEMENTAL INFORMATION

Supplemental Information includes Supplemental Experimental Procedures, seven figures, and six tables and can be found with this article online at http://dx.doi.org/10.1016/j.ccell.2016.05.008.

AUTHOR CONTRIBUTIONS

R.L. designed the research, performed experiments and computational analysis, interpreted data, and wrote the manuscript. P.W., S.R., and D.Z. performed computational analysis. T.P., Y.Z., and W.C. helped with animal modeling, viral transduction, and immunostaining studies, respectively. K.C. and P.A.W. participated in DNA methylome studies. O.A. helped with human AML cell studies. D.Z. supervised the computational studies. G.G.W. supervised the work, designed the research, interpreted data, and wrote the manuscript.

ACKNOWLEDGMENTS

We graciously thank Drs. Y. Xiong and K. Humphries for providing constructs, M. Kamps and M. Minden for leukemia lines, M. Torres for Meis1 antibody, D. Bauer and F. Zhang for CRISPR/Cas9 systems, M. Rehli for a CpG-free reporter, and J. Bear for an shRNA vector used in this study. Thanks to Drs. D. Allison and L. Cai and other members of the Wang laboratory for helpful discussion and technical support. We thank UNC's Genomics Core, Animal Studies Core, Flow Core, and HTSF core for their support of this work. This work is supported by NCI K99/R00 grant CA151683 to G.G.W., a DoD grant CA130247 to G.G.W., and grants of Gabrielle's Angel Foundation to O.A. and G.G.W. G.G.W. is an American Society of Hematology Scholar and a Kimmel Scholar. R.L. is a Lymphoma Research Foundation Postdoctorate Fellow. UNC Cores including the flow cytometry facility are supported in part by the North Carolina Biotech Center Institutional Support Grant 2012-IDG-1006 and UNC Cancer Center Core Support Grant P30 CA016086.

Received: July 21, 2015
Revised: March 3, 2016
Accepted: May 19, 2016
Published: June 23, 2016

REFERENCES

Abramovich, C., Pineault, N., Ohta, H., and Humphries, R.K. (2005). Hox genes: from leukemia to hematopoietic stem cell expansion. Ann. N. Y. Acad. Sci. *1044*, 109–116.

Argiropoulos, B., and Humphries, R.K. (2007). Hox genes in hematopoiesis and leukemogenesis. Oncogene *26*, 6766–6776.

Baubec, T., and Schubeler, D. (2014). Genomic patterns and context specific interpretation of DNA methylation. Curr. Opin. Genet. Dev. *25*, 85–92.

Bernt, K.M., Zhu, N., Sinha, A.U., Vempati, S., Faber, J., Krivtsov, A.V., Feng, Z., Punt, N., Daigle, A., Bullinger, L., et al. (2011). MLL-rearranged leukemia is dependent on aberrant H3K79 methylation by DOT1L. Cancer Cell *20*, 66–78.

Campisi, J., and d'Adda di Fagagna, F. (2007). Cellular senescence: when bad things happen to good cells. Nat. Rev. Mol. Cell Biol. *8*, 729–740.

(L) Effect of SGC0946 on growth of $LSCs^{RH\text{-}RAS}$ transduced with vector or Hoxa9 plus Meis1 (A9M). Relative proliferation was normalized to DMSO-treated cells. (M) Survival of mice engrafted with $LSCs^{RH\text{-}RAS}$, either mock-treated, stably transduced with a *Dot1l* shRNA, or pretreated with 1 μM SGC0946 ex vivo for 6 days. The p values were calculated by log-rank test.
Error bars denote ±SD. See also Figure S7 and Table S6.

Cancer Genome Atlas Research Network. (2013). Genomic and epigenomic landscapes of adult de novo acute myeloid leukemia. N. Engl. J. Med. *368*, 2059–2074.

Celik, H., Mallaney, C., Kothari, A., Ostrander, E.L., Eultgen, E., Martens, A., Miller, C.A., Hundal, J., Klco, J.M., and Challen, G.A. (2015). Enforced differentiation of Dnmt3a-null bone marrow leads to failure with c-Kit mutations driving leukemic transformation. Blood *125*, 619–628.

Challen, G.A., Sun, D., Jeong, M., Luo, M., Jelinek, J., Berg, J.S., Bock, C., Vasanthakumar, A., Gu, H., Xi, Y., et al. (2012). Dnmt3a is essential for hematopoietic stem cell differentiation. Nat. Genet. *44*, 23–31.

Chang, Y.I., You, X., Kong, G., Ranheim, E.A., Wang, J., Du, J., Liu, Y., Zhou, Y., Ryu, M.J., and Zhang, J. (2015). Loss of Dnmt3a and endogenous Kras(G12D/+) cooperate to regulate hematopoietic stem and progenitor cell functions in leukemogenesis. Leukemia *29*, 1847–1856.

Chen, C.W., Koche, R.P., Sinha, A.U., Deshpande, A.J., Zhu, N., Eng, R., Doench, J.G., Xu, H., Chu, S.H., Qi, J., et al. (2015). DOT1L inhibits SIRT1-mediated epigenetic silencing to maintain leukemic gene expression in MLL-rearranged leukemia. Nat. Med. *21*, 335–343.

Chi, P., Allis, C.D., and Wang, G.G. (2010). Covalent histone modifications—miswritten, misinterpreted and mis-erased in human cancers. Nat. Rev. Cancer *10*, 457–469.

Eppert, K., Takenaka, K., Lechman, E.R., Waldron, L., Nilsson, B., van Galen, P., Metzeler, K.H., Poeppl, A., Ling, V., Beyene, J., et al. (2011). Stem cell gene expression programs influence clinical outcome in human leukemia. Nat. Med. *17*, 1086–1093.

Genovese, G., Kahler, A.K., Handsaker, R.E., Lindberg, J., Rose, S.A., Bakhoum, S.F., Chambert, K., Mick, E., Neale, B.M., Fromer, M., et al. (2014). Clonal hematopoiesis and blood-cancer risk inferred from blood DNA sequence. N. Engl. J. Med. *371*, 2477–2487.

Guo, X., Wang, L., Li, J., Ding, Z., Xiao, J., Yin, X., He, S., Shi, P., Dong, L., Li, G., et al. (2015). Structural insight into autoinhibition and histone H3-induced activation of DNMT3A. Nature *517*, 640–644.

Heuser, M., Yun, H., Berg, T., Yung, E., Argiropoulos, B., Kuchenbauer, F., Park, G., Hamwi, I., Palmqvist, L., Lai, C.K., et al. (2011). Cell of origin in AML: susceptibility to MN1-induced transformation is regulated by the MEIS1/AbdB-like HOX protein complex. Cancer Cell *20*, 39–52.

Holz-Schietinger, C., Matje, D.M., and Reich, N.O. (2012). Mutations in DNA methyltransferase (DNMT3A) observed in acute myeloid leukemia patients disrupt processive methylation. J. Biol. Chem. *287*, 30941–30951.

Huang, Y., Sitwala, K., Bronstein, J., Sanders, D., Dandekar, M., Collins, C., Robertson, G., MacDonald, J., Cezard, T., Bilenky, M., et al. (2012). Identification and characterization of Hoxa9 binding sites in hematopoietic cells. Blood *119*, 388–398.

Jaiswal, S., Fontanillas, P., Flannick, J., Manning, A., Grauman, P.V., Mar, B.G., Lindsley, R.C., Mermel, C.H., Burtt, N., Chavez, A., et al. (2014). Age-related clonal hematopoiesis associated with adverse outcomes. N. Engl. J. Med. *371*, 2488–2498.

Jones, P.A. (2012). Functions of DNA methylation: islands, start sites, gene bodies and beyond. Nat. Rev. Genet. *13*, 484–492.

Kim, S.J., Zhao, H., Hardikar, S., Singh, A.K., Goodell, M.A., and Chen, T. (2013). A DNMT3A mutation common in AML exhibits dominant-negative effects in murine ES cells. Blood *122*, 4086–4089.

Krivtsov, A.V., Twomey, D., Feng, Z., Stubbs, M.C., Wang, Y., Faber, J., Levine, J.E., Wang, J., Hahn, W.C., Gilliland, D.G., et al. (2006). Transformation from committed progenitor to leukaemia stem cell initiated by MLL-AF9. Nature *442*, 818–822.

Lara-Astiaso, D., Weiner, A., Lorenzo-Vivas, E., Zaretsky, I., Jaitin, D.A., David, E., Keren-Shaul, H., Mildner, A., Winter, D., Jung, S., et al. (2014). Immunogenetics. Chromatin state dynamics during blood formation. Science *345*, 943–949.

Ley, T.J., Ding, L., Walter, M.J., McLellan, M.D., Lamprecht, T., Larson, D.E., Kandoth, C., Payton, J.E., Baty, J., Welch, J., et al. (2010). DNMT3A mutations in acute myeloid leukemia. N. Engl. J. Med. *363*, 2424–2433.

Li, Y., Wen, H., Xi, Y., Tanaka, K., Wang, H., Peng, D., Ren, Y., Jin, Q., Dent, S.Y., Li, W., et al. (2014). AF9 YEATS domain links histone acetylation to DOT1L-mediated H3K79 methylation. Cell *159*, 558–571.

Mayle, A., Yang, L., Rodriguez, B., Zhou, T., Chang, E., Curry, C.V., Challen, G.A., Li, W., Wheeler, D., Rebel, V.I., and Goodell, M.A. (2015). Dnmt3a loss predisposes murine hematopoietic stem cells to malignant transformation. Blood *125*, 629–638.

Noh, K.M., Wang, H., Kim, H.R., Wenderski, W., Fang, F., Li, C.H., Dewell, S., Hughes, S.H., Melnick, A.M., Patel, D.J., et al. (2015). Engineering of a histone-recognition domain in Dnmt3a alters the epigenetic landscape and phenotypic features of mouse ESCs. Mol. Cell *59*, 89–103.

Patel, J.P., Gonen, M., Figueroa, M.E., Fernandez, H., Sun, Z., Racevskis, J., Van Vlierberghe, P., Dolgalev, I., Thomas, S., Aminova, O., et al. (2012). Prognostic relevance of integrated genetic profiling in acute myeloid leukemia. N. Engl. J. Med. *366*, 1079–1089.

Rada-Iglesias, A., Bajpai, R., Swigut, T., Brugmann, S.A., Flynn, R.A., and Wysocka, J. (2011). A unique chromatin signature uncovers early developmental enhancers in humans. Nature *470*, 279–283.

Russler-Germain, D.A., Spencer, D.H., Young, M.A., Lamprecht, T.L., Miller, C.A., Fulton, R., Meyer, M.R., Erdmann-Gilmore, P., Townsend, R.R., Wilson, R.K., and Ley, T.J. (2014). The R882H DNMT3A mutation associated with AML dominantly inhibits wild-type DNMT3A by blocking its ability to form active tetramers. Cancer Cell *25*, 442–454.

Schmidl, C., Klug, M., Boeld, T.J., Andreesen, R., Hoffmann, P., Edinger, M., and Rehli, M. (2009). Lineage-specific DNA methylation in T cells correlates with histone methylation and enhancer activity. Genome Res. *19*, 1165–1174.

Schubeler, D. (2015). Function and information content of DNA methylation. Nature *517*, 321–326.

Shih, A.H., Abdel-Wahab, O., Patel, J.P., and Levine, R.L. (2012). The role of mutations in epigenetic regulators in myeloid malignancies. Nat. Rev. Cancer *12*, 599–612.

Shih, A.H., Jiang, Y., Meydan, C., Shank, K., Pandey, S., Barreyro, L., Antony-Debre, I., Viale, A., Socci, N., Sun, Y., et al. (2015). Mutational cooperativity linked to combinatorial epigenetic gain of function in acute myeloid leukemia. Cancer Cell *27*, 502–515.

Shlush, L.I., Zandi, S., Mitchell, A., Chen, W.C., Brandwein, J.M., Gupta, V., Kennedy, J.A., Schimmer, A.D., Schuh, A.C., Yee, K.W., et al. (2014). Identification of pre-leukaemic haematopoietic stem cells in acute leukaemia. Nature *506*, 328–333.

Wang, G.G., Pasillas, M.P., and Kamps, M.P. (2005). Meis1 programs transcription of FLT3 and cancer stem cell character, using a mechanism that requires interaction with Pbx and a novel function of the Meis1 C-terminus. Blood *106*, 254–264.

Wang, G.G., Pasillas, M.P., and Kamps, M.P. (2006). Persistent transactivation by meis1 replaces hox function in myeloid leukemogenesis models: evidence for co-occupancy of meis1-pbx and hox-pbx complexes on promoters of leukemia-associated genes. Mol. Cell Biol. *26*, 3902–3916.

Wang, G.G., Cai, L., Pasillas, M.P., and Kamps, M.P. (2007). NUP98-NSD1 links H3K36 methylation to Hox-A gene activation and leukaemogenesis. Nat. Cell Biol. *9*, 804–812.

Wang, G.G., Song, J., Wang, Z., Dormann, H.L., Casadio, F., Li, H., Luo, J.L., Patel, D.J., and Allis, C.D. (2009). Haematopoietic malignancies caused by dysregulation of a chromatin-binding PHD finger. Nature *459*, 847–851.

Wong, P., Iwasaki, M., Somervaille, T.C., So, C.W., and Cleary, M.L. (2007). Meis1 is an essential and rate-limiting regulator of MLL leukemia stem cell potential. Genes Dev. *21*, 2762–2774.

Xiang, P., Wei, W., Lo, C., Rosten, P., Hou, J., Hoodless, P.A., Bilenky, M., Bonifer, C., Cockerill, P.N., Kirkpatrick, A., et al. (2014). Delineating MEIS1 cis-regulatory elements active in hematopoietic cells. Leukemia *28*, 433–436.

Xie, M., Lu, C., Wang, J., McLellan, M.D., Johnson, K.J., Wendl, M.C., McMichael, J.F., Schmidt, H.K., Yellapantula, V., Miller, C.A., et al. (2014).

Age-related mutations associated with clonal hematopoietic expansion and malignancies. Nat. Med. *20*, 1472–1478.

Xu, J., Wang, Y.Y., Dai, Y.J., Zhang, W., Zhang, W.N., Xiong, S.M., Gu, Z.H., Wang, K.K., Zeng, R., Chen, Z., and Chen, S.J. (2014). DNMT3A Arg882 mutation drives chronic myelomonocytic leukemia through disturbing gene expression/DNA methylation in hematopoietic cells. Proc. Natl. Acad. Sci. USA *111*, 2620–2625.

Yan, X.J., Xu, J., Gu, Z.H., Pan, C.M., Lu, G., Shen, Y., Shi, J.Y., Zhu, Y.M., Tang, L., Zhang, X.W., et al. (2011). Exome sequencing identifies somatic mutations of DNA methyltransferase gene DNMT3A in acute monocytic leukemia. Nat. Genet. *43*, 309–315.

Yang, L., Rau, R., and Goodell, M.A. (2015). DNMT3A in haematological malignancies. Nat. Rev. Cancer *15*, 152–165.

Zhang, J., Wang, J., Liu, Y., Sidik, H., Young, K.H., Lodish, H.F., and Fleming, M.D. (2009). Oncogenic Kras-induced leukemogeneis: hematopoietic stem cells as the initial target and lineage-specific progenitors as the potential targets for final leukemic transformation. Blood *113*, 1304–1314.

Cancer Cell, Volume *30*

Supplemental Information

Epigenetic Perturbations by Arg882-Mutated DNMT3A Potentiate Aberrant Stem Cell Gene-Expression Program and Acute Leukemia Development

Rui Lu, Ping Wang, Trevor Parton, Yang Zhou, Kaliopi Chrysovergis, Shira Rockowitz, Wei-Yi Chen, Omar Abdel-Wahab, Paul A. Wade, Deyou Zheng, and Gang Greg Wang

Supplemental Data

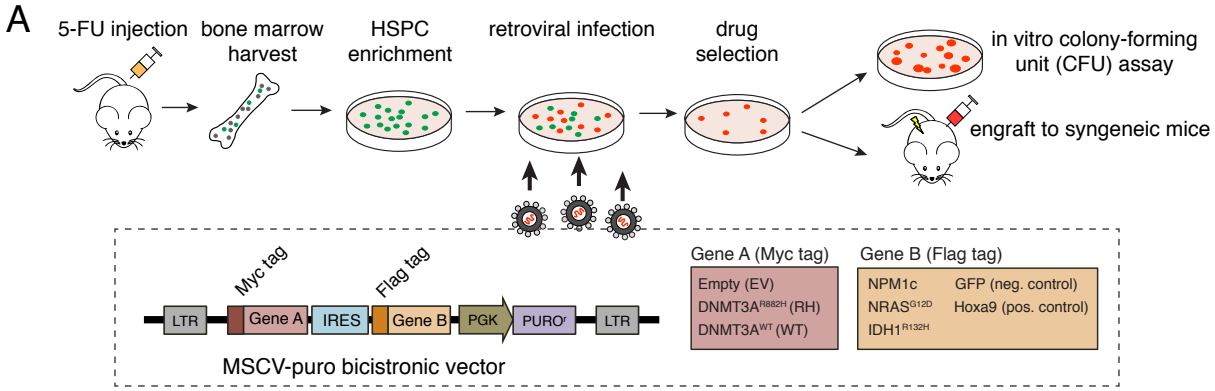

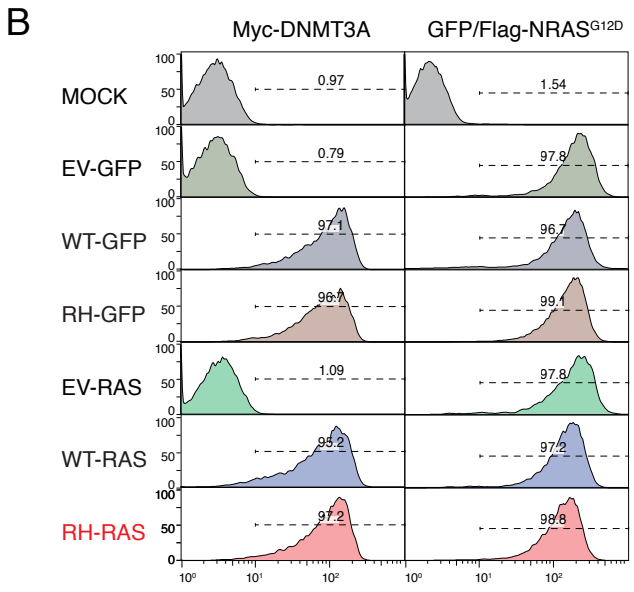

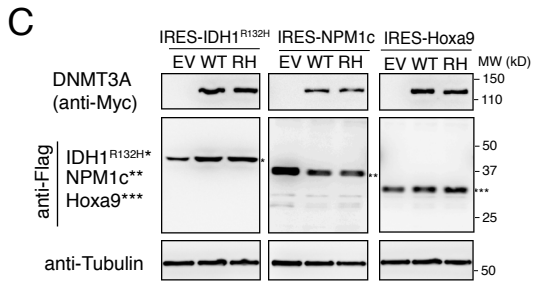

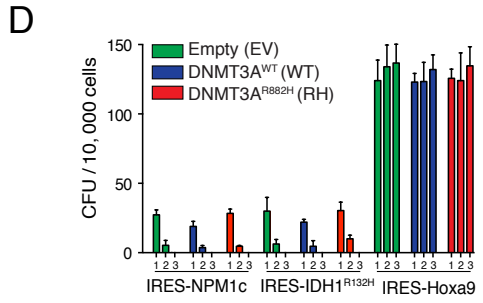

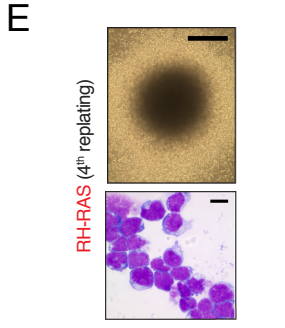

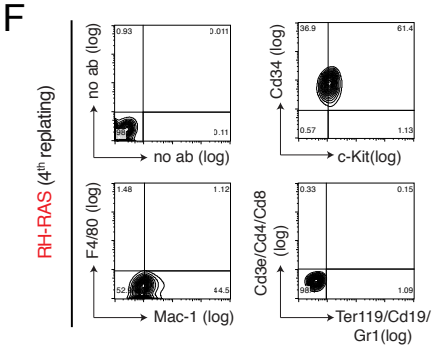

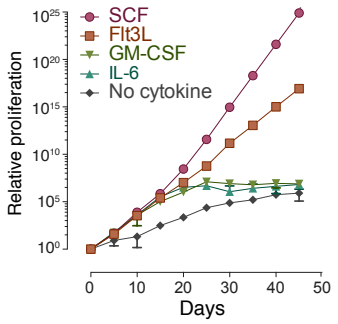

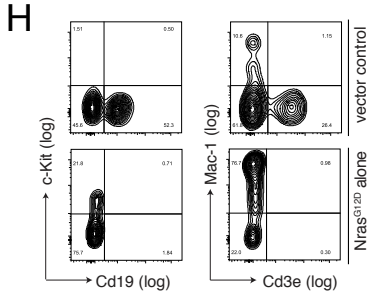

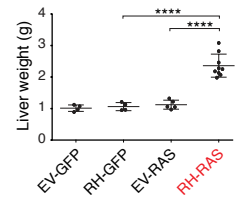

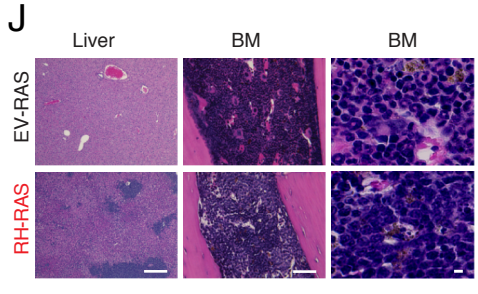

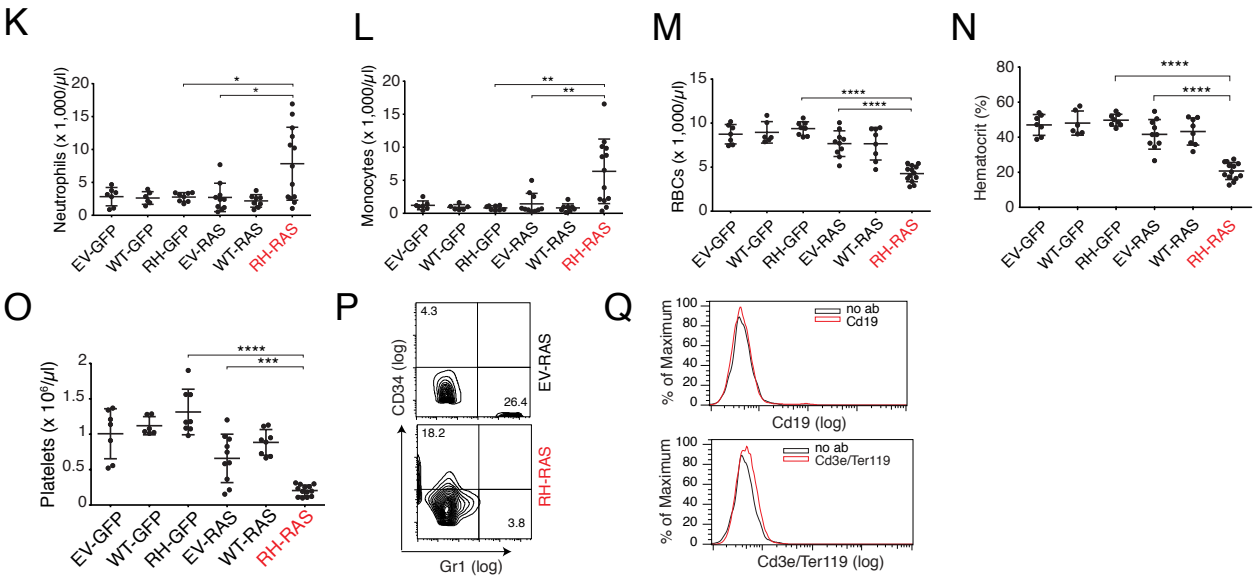

R

Chromosome	Position	Ref	Alt	Gene	Snp_Eff_Effect	Snp_Eff_HGVS	AA_Change	Normal_Alt	Normal_Total	Tumor_Alt	Tumor_Total
Tumor 1											
chr2	180937146	C	T	*Srms*	downstream_gene_variant	c.*1937G>A	No	0	43	19	50
chr3	127023244	G	T	*Ank2*	intron_variant	c.12+18806C>A	No	0	21	8	32
chr7	103517976	G	T	*Odz4*	intron_variant	c.-90+14055G>T	No	0	48	9	40
chr8	121973844	A	G	*Necab2*	intron_variant	c.211-138A>G	No	0	45	9	59
chr8	121973870	G	A	*Necab2*	intron_variant	c.211-112G>A	No	0	32	8	50
chr10	5035165	T	C	*Syne1*	intron_variant	c.6819+312T>C	No	0	31	11	38
chr12	73371371	G	A	*Rtn1*	intron_variant	c.242-46845C>T	No	0	47	20	54
chr14	63495968	T	C	*Wdfy2*	intron_variant	c.138-8679T>C	No	0	35	15	36
chr15	91191312	A	G	*Slc2a13*	intron_variant	c.1002-10751T>C	No	0	74	35	85
chr17	12940301	C	A	*Airn*	intron_variant	n.27+6011C>A	No	0	59	23	59
chr17	25025673	T	G	*Spsb3*	intron_variant	c.55-358T>G	No	0	66	32	73
chr18	12698079	T	C	*Lama3*	intron_variant	c.2458-99T>C	No	0	59	14	53
Tumor 2											
chr3	64503579	T	G	*Vmn2r7*	intron_variant	c.1369-6550A>C	No	0	46	18	48
chr4	18844775	A	G	*Cnbd1*	intron_variant	c.432-10487T>C	No	0	53	12	67
chr5	3344315	A	C	*Cdk6*	5_prime_UTR_variant	c.-52A>C	No	0	27	9	34
chr5	3344338	C	T	*Cdk6*	5_prime_UTR_variant	c.-29C>T	No	0	38	9	39
chr5	31067469	A	C	*Dpysl5*	intron_variant	c.262-12224A>C	No	0	62	46	80
chr5	129513237	C	T	*Stx2*	intron_variant	c.30+1032G>A	No	0	85	43	76
chr6	60083270	G	A	*Gm5570*	intron_variant	n.901-15143G>A	No	0	35	19	40
chr7	8031898	T	G	*AC190408.2*	intron_variant	c.*102-49867A>C	No	0	49	18	42
chr7	13472971	G	T	*Zfp128*	intron_variant	c.290-2374G>T	No	0	183	24	209
chr7	106330699	G	T	*Dgat2*	intron_variant	c.121+203C>A	No	0	33	12	43
chr8	81902933	G	C	*Smad1*	intron_variant	c.-181-6670C>G	No	0	25	8	27
chr8	84127582	C	G	*Inpp4b*	intron_variant	c.-103+130864C>G	No	0	53	25	55
chr8	85517955	G	T	*Rnf150*	intron_variant	c.732+3459G>T	No	0	43	16	68
chr8	122865623	G	A	*Galnt2*	intron_variant	c.21+430784G>A	No	0	57	13	55
chr9	119815293	A	G	*Wdr48*	intron_variant	c.481+678A>G	No	0	25	13	43
chr10	33305020	T	del	*Clvs2*	intron_variant	c.236+10530delA	No	0	24	11	24
chr10	61961300	T	C	*Srgn*	intron_variant	c.74-629A>G	No	0	169	92	185
chr11	67887869	T	C	*Stx8*	intron_variant	c.386-34910T>C	No	0	50	21	50
chr14	43563174	C	A	*Gm3676*	intron_variant	c.491-50G>T	No	0	69	33	59
chr14	52075131	A	G	*Vmn2r89*	intron_variant	c.207-228A>G	No	0	41	27	47
chr15	81208662	T	C	*St13*	intron_variant	c.269-232A>G	No	0	22	10	32
chr15	98639564	G	T	*B130046B21Rik*	intron_variant	n.193+1909G>T	No	0	40	14	45
chr16	20735595	C	G	*Chrd*	intron_variant	c.1092+23C>G	No	0	61	9	46
chr16	37288253	A	del	*Stxbp5l*	intron_variant	c.666+120delT	No	0	28	11	28
chr16	90248725	G	A	*Srsf15*	intron_variant	c.1681+33C>T	No	0	46	26	61
chr17	25385402	C	T	*Baiap3*	intron_variant	c.1155+15G>A	No	0	21	8	30
chr18	63544895	C	T	*Fam38b*	intron_variant	c.-2934+965G>A	No	0	35	13	23
chr19	44155623	C	T	*Chuk*	intron_variant	c.194+813G>A	No	0	72	17	61
chrX	6082010	G	A	*Shroom4*	intron_variant	c.-36-15901G>A	No	0	53	18	63
Tumor 3											
chr1	8679206	A	T	*Sntg1*	intron_variant	c.143-7096T>A	No	0	26	9	36
chr1	74519008	G	A	*Usp37*	intron_variant	c.1026-748C>T	No	0	22	9	15
chr2	76758370	G	T	*Ttn*	intron_variant	c.355+1238C>A	No	0	32	12	26
chr2	77075014	A	del	*Sestd1*	intron_variant	c.215-2218delT	No	0	30	11	38
chr3	5243764	G	C	*Zfhx4*	missense_variant	c.2049G>C,p.Arg683Ser	Yes	0	33	17	36
chr4	115565831	T	G	*6430628N08Rik*	intron_variant	n.296+2265T>G	No	0	21	10	28
chr8	47843058	C	T	*Irf2*	intron_variant	c.-7+17768C>T	No	0	54	25	52
chr8	116993479	G	A	*Wwox*	intron_variant	c.130-19319G>A	No	0	49	8	61
chr9	3020484	C	A	*Gm16869*	intron_variant	n.936-2402G>T	No	0	158	8	161
chr9	3022139	A	T	*Gm16869*	intron_variant	n.936-4057T>A	No	0	102	15	140
chr10	33335118	A	G	*Clvs2*	intron_variant	c.389+7232T>C	No	0	47	25	55
chr11	77295772	G	A	*Ankrd13b*	intron_variant	c.115-4492C>T	No	0	127	61	123
chr14	34170775	C	T	*Arhgap22*	intron_variant	c.122-1529C>T	No	0	77	35	76
chr14	73955585	C	T	*Sucla2*	intron_variant	c.90+2881C>T	No	0	47	15	47

Figure S1, related to Figure 1. DNMT3A^{R882H} acts in concert with mutant RAS to transform murine HSPCs ex vivo and induce AMLs in vivo.

(A) Scheme of in vitro and in vivo leukemic assays (top). Bottom, diagram of a home-made, MSCV retrovirus-based bicistronic co-expression system that carries either empty control (EV), DNMT3A^{WT} (WT) or DNMT3A^{R882H} (RH) upstream of an internal ribosome entry site (IRES) sequence, followed by cDNA of either GFP, NRAS^{G12D}, IDH1^{R132H}, NPM1c, or Hoxa9. Myc and Flag tags were fused in-frame with the first (gene A) and second (gene B) cDNA, respectively.

(B) Flow cytometry analysis of Myc-tagged DNMT3A (left) and Flag-tagged NRAS^{G12D} or GFP (right) expression to assess cell purify and gene transduction rates of murine HSPCs after viral infection and drug selection. HSPCs were infected with retrovirus encoding a bicistronic vector of GFP alone (EV-GFP), GFP with DNMT3A^{WT} (WT-GFP) or DNMT3A^{R882H} (RH-GFP), NRAS^{G12D} alone (EV-RAS), or NRAS^{G12D} with DNMT3A^{WT} (WT-RAS) or DNMT3A^{R882H} (RH-RAS). MOCK, non-infected HSPCs.

(C) Immunoblot of indicated proteins in murine HSPCs post-transduction of retrovirus as shown on top of the blot. EV, empty; WT, DNMT3A^{WT}; RH, DNMT3A^{R882H}. Tubulin was used as a protein loading control.

(D) In vitro serial replating assays that score colony-forming units (CFU) of murine HSPCs post-transduction of retrovirus carrying indicated coexpressed oncogenes.

(E-F) Representative microscopic image (panel E, top), Wright–Giemsa staining (panel E, bottom) and flow cytometry analysis (panel F) of cells prepared from the 4th replating of HSPC colonies transduced with DNMT3A^{R882H}-IRES-NRAS^{G12D} (RH-RAS). Scale bars in panel E represent 1 mm and 10 μm in top and bottom, respectively.

(G) Proliferation of RH-RAS-immortalized progenitors derived from CFU assays in liquid culture medium with indicated cytokines. SCF, stem cell factor; Flt3L, Flt3 ligand; GM-SCF, granulocyte-macrophage colony-stimulating factor; IL-6, interleukin 6.

(H) Flow cytometry analysis of indicated markers using spleen cell populations isolated from recipient mice 3 months post-engraftment of HSPCs transduced with empty vector control (upper; EV-GFP) or NRAS^{G12D} alone (EV-RAS, bottom).

(I) Size of liver in indicated recipient cohorts (n = 4-9) 4 weeks post-engraftment of retrovirally transduced HSPCs (refer to also panel A for the retrovirus-encoded genes).

(J) Hematoxylin and eosin (H&E) staining of liver (left) and bone marrow (middle and right) sections of recipient cohorts 3-4 weeks post-engraftment of HSPCs transduced with EV-RAS (upper) or RH-RAS (bottom). Scale bars in the left, middle and right represent 100, 100 and 10 μm, respectively.

(K-O) Summary of various examined peripheral blood counting parameters among indicated recipient cohorts (n = 6-13) 4 weeks post-engraftment of retrovirally transduced HSPCs (refer to also panel A for identity of the retrovirus-encoded genes).

(P) Flow cytometry analysis of bone marrow cells from mice 4 weeks post-engraftment of HSPCs transduced with RH-RAS, in comparison to those transduced with EV-RAS.

(Q) Flow cytometry analysis of bone marrow cells from murine leukemias induced by RH-RAS. Non-specific IgG (no ab; black) was used as antibody control.

(R) Summary of somatic nucleotide polymorphisms, insertion and deletions (SNP/Indels) from 3 independent RH-RAS-induced murine AMLs as determined by whole exome capture sequencing. Ref, reference nucleotide; Alt, alternate nucleotide; Snp_Eff_Effect, effect of this variant; Snp_Eff_HGVS, HGVS notation of this variant; AA_Change, effect of this variant on amino acid change; Normal_Alt, alternate counts in normal; Normal_Total, total counts in normal; Tumor_Alt, alternate counts in tumor; Tumor_Total, total counts in tumor; del, deletion.

Error bar, +/- SD; *, $p < 0.05$; **, $p < 0.01$; ***, $p < 0.001$; ****, $p < 0.0001$.

Table S1, related to Figure 1. Summary of phenotypic analysis of murine AMLs induced by coexpression of DNMT3A^{R882H} and NRAS^{G12D} (RH-RAS).

Mouse	WBC*	Hematocrit	Spleen	Lymph node	Liver	FACS: bone marrow (positive %)**					FACS: Spleen (positive %)				
ID	(k/μl)	(%)	(mg)	(mg)	(mg)	Mac1$^+$	c-Kit$^+$	Cd19$^+$	Cd3e$^+$	CD34$^+$	Mac1$^+$	c-Kit$^+$	Cd19$^+$	Cd3e$^+$	CD34$^+$
1	35.44	20.2	358	44	1436	58.5	16.1	3.6	0.9	18.4	70.9	10.4	N/D***	N/D	N/D
2	58.8	24.9	521	54	1890	52.1	10.8	4.7	0.9	13.0	58.9	10.9	2.5	1.1	41.5
3	75.82	26	478	75	2250	69.7	20.9	3.4	1.0	18.9	78.7	19.5	2.2	1.2	40.7
4	59.36	23.4	561	97	1567	78.5	21.5	8.0	1.6	20.9	61.7	15.7	2.5	2.5	31.5
5	56.72	16.5	382	77	1546	51.9	19.5	5.0	1.1	19.2	70.9	14.4	4.1	1.8	39.2
6	76.2	23.8	432	47	1742	55.4	12.4	5.4	1.2	16.8	74.6	13.2	3.3	1.6	38.4

*, WBC (1,000/µl), white blood cell count in one microliter of peripheral circulating blood

**, FACS analysis of leukemic mice showing the percentage of cells scored as positive signals using antigen-specific antibodies

***, N/D, not determined

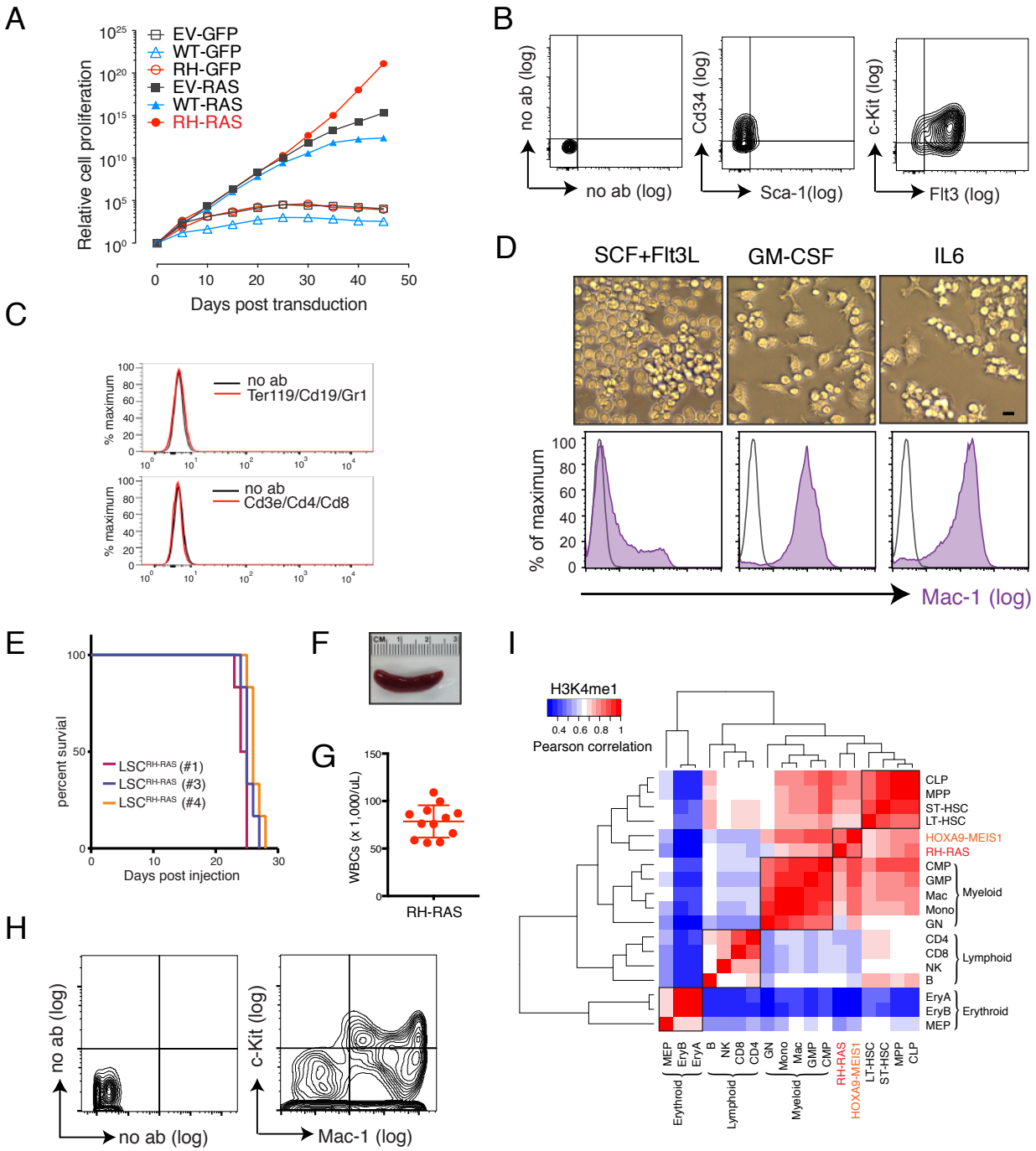
A
Relative cell proliferation
EV-GFP
WT-GFP
RH-GFP
EV-RAS
WT-RAS
RH-RAS
Days post transduction
B
no ab (log)
Cd34 (log)
c-Kit (log)
Sca-1(log)
Flt3 (log)
C
% maximum
no ab
Ter119/Cd19/Gr1
Cd3e/Cd4/Cd8
D
SCF+Flt3L
GM-CSF
IL6
% of maximum
Mac-1 (log)
E
percent survial
LSCRH-RAS (#1)
LSCRH-RAS (#3)
LSCRH-RAS (#4)
Days post injection
F
G
WBCs (x 1,000/uL)
RH-RAS
H
no ab (log)
c-Kit (log)
Mac-1 (log)
I
H3K4me1
Pearson correlation
CLP
MPP
ST-HSC
LT-HSC
HOXA9-MEIS1
RH-RAS
CMP
GMP
Mac
Mono
GN
Myeloid
CD4
CD8
NK
B
Lymphoid
EryA
EryB
MEP
Erythroid
J
Ery
GN
Mono/Mac
B
CD4
CD8
NKT
MEP
CD34-KLS
HSC
MPP1
GMP
CMP
MPP2
CLP
MLL-AF6
RH-RAS
MLL-AF9
NUP98-JARID1A
HOXA9-MEIS1
MLL-ENL
NUP98-NSD1
AML1-ETO

Figure S2, related to Figure 2. R882-mutated DNMT3A establishes leukemia-initiating stem cells (LSCs) ex vivo in the presence of activated RAS.

(A) Proliferation kinetics of murine HSPCs post-transduction of indicated genes.

(B-C) FACS analysis of indicated antigens of RH-RAS immortalized progenitors. Non-specific IgG (no ab) was used as antibody control.

(D) Typical microscopic images (upper) and FACS analysis of Mac-1 (bottom; purple) two weeks post-cultivation of RH-RAS immortalized progenitors in liquid medium with indicated cytokines. Non-specific IgG (open) was used as antibody control in FACS. Scale bar, 10 μm.

(E) Kaplan-Meier survival curve of mice (n = 6 for each progenitor line) engrafted with each of 3 independent RH-RAS immortalized progenitor lines demonstrates a LSC property of these cells.

(F-G) Enlarged spleen (panel F) and increased counts in peripheral white blood cells (WBC, panel G, n = 12; relative to normal WBC counts of ~10,000 per μL) among mice that developed AML post-engraftment of the ex vivo derived $LSC^{RH\text{-}RAS}$ lines.

(H) Flow cytometry analysis of murine AMLs produced by $LSCs^{RH\text{-}RAS}$.

(I) Heatmap showing hierarchical clustering of samples based on their similarities of genome-wide H3K4me1 ChIP-Seq profiles. A non-overlapping 5-kb window was used to count histone ChIP-Seq reads across the mouse genome. The colors represent the scaled Pearson correlation coefficients of the resultant vectors for individual cell lines. The used H3K4me1 ChIP-Seq datasets are those we produced in this current study for $LSCs^{RH\text{-}RAS}$ (RH-RAS; red font) and for a murine AML line established by leukemic TFs HOXA9 plus MEIS1 (HOXA9-MEIS1; orange) (Wang et al., 2005), as well as the publicly available datasets of various normal blood cell types (black) as defined in a previous study (Lara-Astiaso et al., 2014). LT-HSC, long-term HSC; ST-HSC, short-term HSC; MPP, multipotent progenitor; CMP, common myeloid progenitor; CLP, common lymphoid progenitor; GMP, granulocyte-monocyte progenitor; MEP, megakaryocyte-erythroid progenitor; Mac, macrophage; Mono, monocyte; GN, granulocyte; B, $B220^{+}/CD19^{+}$ B-cell; CD4/8, $CD4/8^{+}$ T-cell; NK, natural killer cell; EryA and EryB, $Ter119^{+}/CD71^{+}$ erythroid cell with high and low forward scatter (FSC), respectively.

(J) Hierarchical clustering of samples based on similarity of genome-wide gene expression profiling. The used microarray data are those we generated in this current study for $LSCs^{RH\text{-}RAS}$ and murine leukemogenic (AML) lines carrying MLL-fusion proteins (such as MLL-AF9 or MLL-ENL), as well as publicly available datasets of either normal blood cell types (Bock et al., 2012; Ji et al., 2010; Konuma et al., 2011) or murine leukemogenic (AML) lines established by TF mutations, such as HOXA9 plus MEIS1 (Wang et al., 2005) and AML-ETO (Lo et al., 2012), or by a deregulated chromatin regulator, such as MLL-AF6 (Deshpande et al., 2013), NUP98-JARID1A/KDM5A (Wang et al., 2009) or NUP98-NSD1 (Wang et al., 2007). Besides what is described in panel I, $CD34^{-}KLS$ represents $Cd34^{-}/cKit^{+}/Lineage^{-}/ScaI^{+}$ HSC; MPP1, $Flk2^{-}$ multipotent progenitor; MPP2, $Flk2^{+}$ multipotent progenitor; NKT, natural killer T-cell; Ery, erythroid cell.

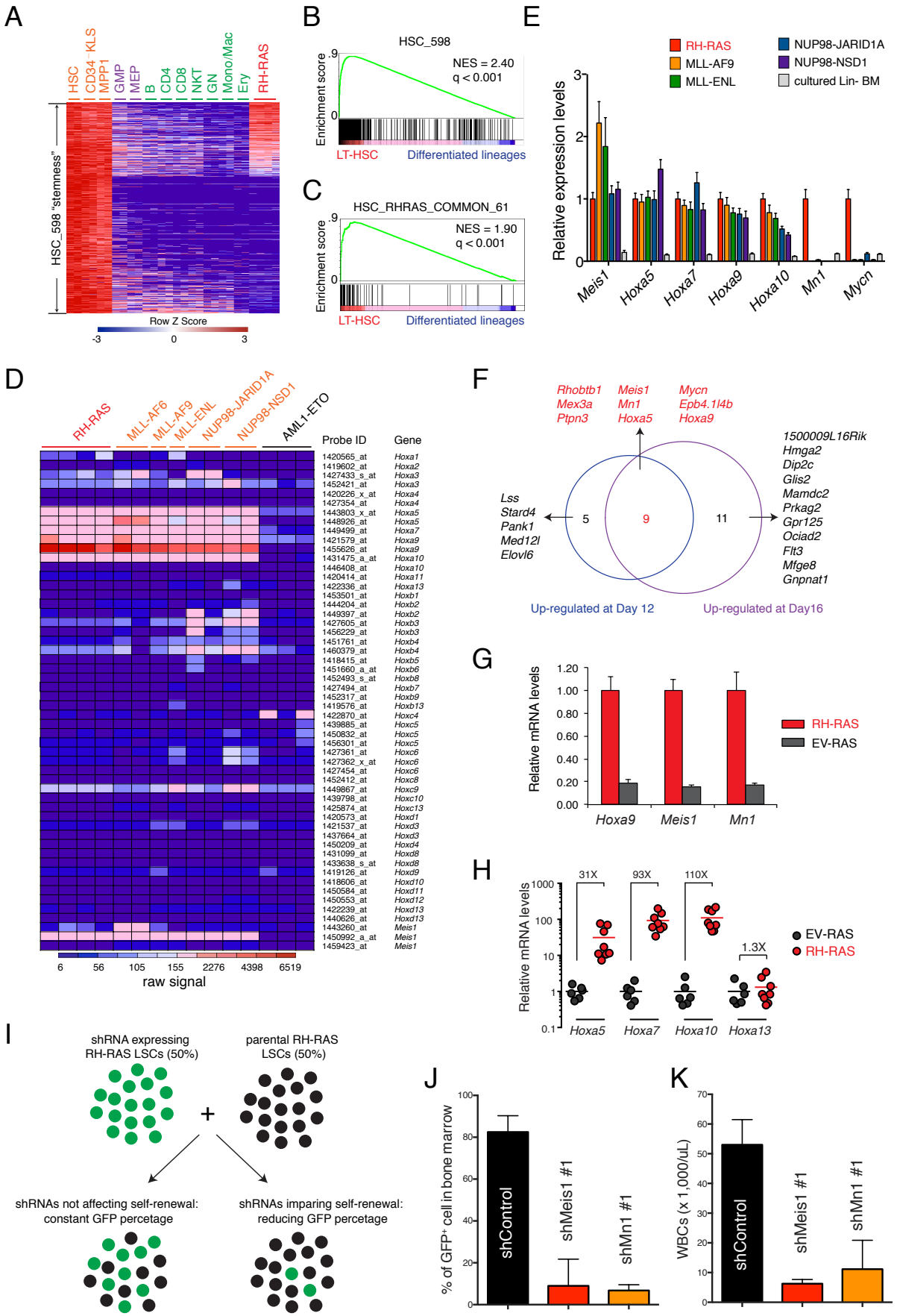
A
HSC
CD34 KLS
MPP1
GMP
MEP
B
CD4
CD8
NKT
GN
Mono/Mac
Ery
RH-RAS
HSC_598 "stemness"
Row Z Score
-3
0
3
B
HSC_598
NES = 2.40
q < 0.001
Enrichment score
LT-HSC
Differentiated lineages
C
HSC_RHRAS_COMMON_61
NES = 1.90
q < 0.001
Enrichment score
LT-HSC
Differentiated lineages
E
RH-RAS
MLL-AF9
MLL-ENL
NUP98-JARID1A
NUP98-NSD1
cultured Lin- BM
Relative expression levels
Meis1
Hoxa5
Hoxa7
Hoxa9
Hoxa10
Mn1
Mycn
D
RH-RAS
MLL-AF6
MLL-AF9
MLL-ENL
NUP98-JARID1A
NUP98-NSD1
AML1-ETO
Probe ID
Gene
raw signal
F
Rhobtb1
Mex3a
Ptpn3
Meis1
Mn1
Hoxa5
Mycn
Epb4.1l4b
Hoxa9
Lss
Stard4
Pank1
Med12l
Elovl6
5
9
11
1500009L16Rik
Hmga2
Dip2c
Glis2
Mamdc2
Prkag2
Gpr125
Ociad2
Flt3
Mfge8
Gnpnat1
Up-regulated at Day 12
Up-regulated at Day16
G
Relative mRNA levels
RH-RAS
EV-RAS
Hoxa9
Meis1
Mn1
H
Relative mRNA levels
31X
93X
110X
1.3X
EV-RAS
RH-RAS
Hoxa5
Hoxa7
Hoxa10
Hoxa13
I
shRNA expressing RH-RAS LSCs (50%)
parental RH-RAS LSCs (50%)
shRNAs not affecting self-renewal: constant GFP percetage
shRNAs imparing self-renewal: reducing GFP percetage
J
% of GFP+ cell in bone marrow
shControl
shMeis1 #1
shMn1 #1
K
WBCs (x 1,000/uL)
shControl
shMeis1 #1
shMn1 #1

Figure S3, related to Figure 3. DNMT3A^{R882H} potentiates activation of 'stemness' genes including a critical *Meis1-Mn1-Hoxa* regulatory node

(A) Heatmap showing relative expression of 598 gene probes (464 genes) uniquely expressed among primitive self-renewing HSPCs (orange font; i.e., HSC, Cd34-/KLS and MPP; also refer to Figures S2I-J for details of cell identity and data source) relative to differentiating (purple) and mature (green) blood cell types (from GMP to Ery), followed by ranking based on higher gene expression in LSCs^{RH-RAS} (red) relative to differentiating and mature blood cell types.

(B-C) GSEA analysis with different datasets from a previous study (Chambers et al., 2007) verifies differential expression of the 598 'stemness' probes identified as specific to primitive self-renewing HSPCs (panel B), as well as the 61 probes identified as unique to both self-renewing HSPC and LSCs^{RH-RAS} (panel C), in LT-HSCs relative to differentiated blood cells.

(D) Heatmap showing expression levels of indicated gene probes using genome-wide gene expression data generated by this current or previously published study for LSCs^{RH-RAS} and various murine leukemogenic (AML) progenitor lines established by MLL-AF6 (Deshpande et al., 2013), MLL-AF9, MLL-ENL, NUP98-JARID1A/KDM5A (Wang et al., 2009), NUP98-NSD1 (Wang et al., 2007), or AML-ETO (Lo et al., 2012). The scale bar shows color-coded values for microarray hybridization signals.

(E) RT-qPCR of *Meis1, Hoxa, Mn1* and *Mycn* in murine leukemogenic progenitor lines transformed by various mutated epigenetic regulators such as RH-RAS, MLL fusion proteins (MLL-AF9 and MLL-ENL), NUP98-JARID1A/KDM5A (Wang et al., 2009) or NUP98-NSD1 (Wang et al., 2007). Y-axis represents mean ± SD of relative gene expression from at least 2-4 independent lines after normalization. In vitro cultured lineage-negative (Lin$^-$; cultured for > 2 weeks) bone marrow (BM) cells serve as control.

(F) Venn diagram shows part of the identified 54 LSC^{RH-RAS} 'stemness' genes consistently upregulated among murine HSPCs at both day 12 and 16 post-transduction of RH-RAS, relative to EV-RAS (also refer to Figure 3B).

(G) RT-qPCR analysis of *Hoxa9*, *Meis1* and *Mn1* expression with samples from the 2nd serial replating of murine HSPCs transduced with EV-RAS or RH-RAS.

(H) RT-qPCR of *Hoxa* expression in murine leukemias induced by RH-RAS (n = 8) or EV-RAS (n = 6).

(I) Scheme of cell competition assays used to assess effects of shRNA-mediated gene knockdown on cell growth. GFP-positive (shRNA-expressing) cells were mixed at a 1:1 ratio with un-transduced (GFP-negative) control cells, followed by in vitro cultivation and measurement of percentage of GFP-positive cells every 2 days.

(J-K) Percentage of GFP-positive cells in bone marrow (panel J) and peripheral WBC counts (panel K) in recipient mice 3 weeks post-transplantation of LSCs^{RH-RAS} carrying the stably expressed vector control or shRNA specific to either *Meis1* or *Mn1*.

Error bar, +/- SD.

Table S2, related to Figure 3 (provided as a separate Excel file). Microarray analysis for genes showing a unique high expression among primitive self-renewing HSPCs in comparison to non-self-renewing differentiating and mature blood cell subtypes, as well as genes showing a unique high expression among both normal self-renewing HSPCs and LSCs^{RH-RAS}.

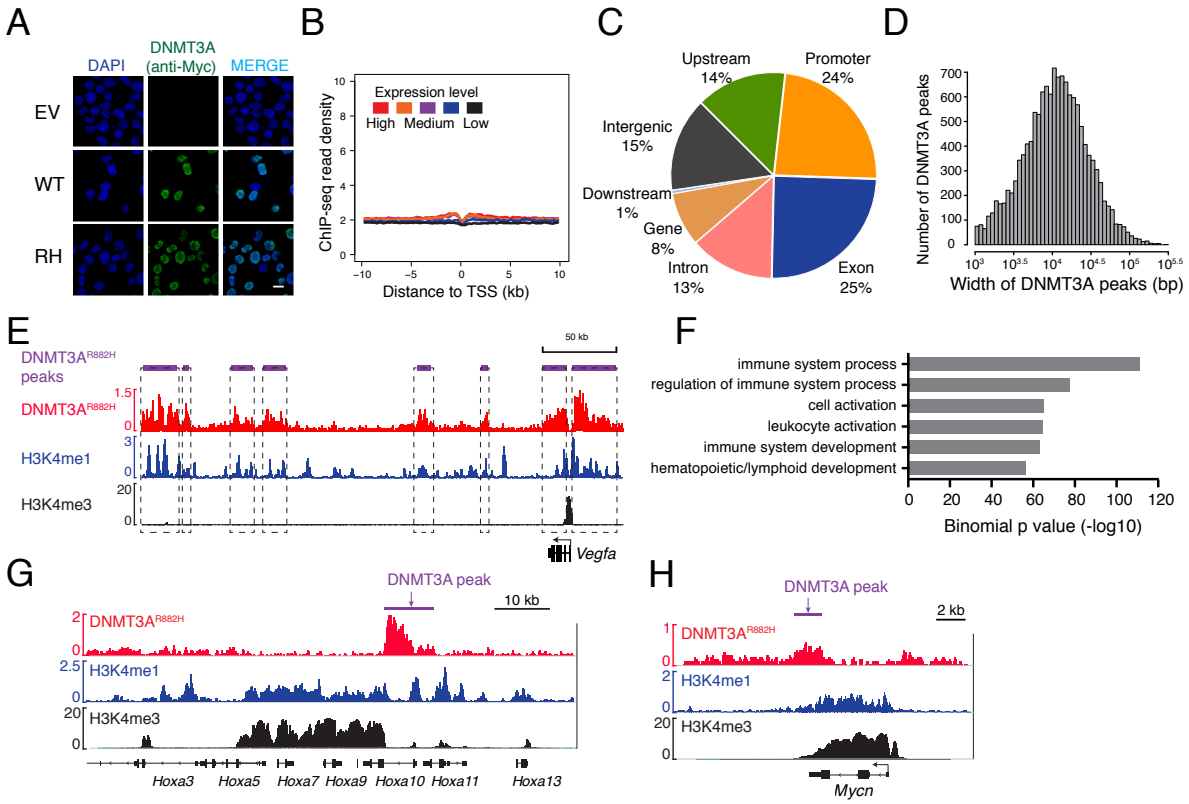

Figure S4, related to Figure 4. ChIP-Seq reveals chromatin context-dependent binding of R882-mutated DNMT3A to genomic regions, including 'stemness' genes such as a *Meis1-Mn1-Hoxa* node.

(A) Anti-Myc immunofluorescence of Myc-tagged DNMT3A^{R882H} and DAPI staining after transduction of either empty control (EV), DNMT3A^{WT} (WT) or DNMT3A^{R882H} (RH). Scale bar, 10 μm.

(B) Average signal densities from anti-Myc ChIP-Seq experiments using EV-RAS-transduced HSPCs, which do not express Myc-DNMT3A^{R882H}, show no enrichment across genes at all expression levels.

(C) Pie-chart showing distribution of the identified 13,705 DNMT3A^{R882H} ChIP-Seq peaks among indicated genomic regions in LSCs$^{RH\text{-}RAS}$.

(D) Distribution plot of DNMT3A^{R882H} ChIP-Seq peaks identified in LSCs$^{RH\text{-}RAS}$ based on the peak width (x-axis, log scale) shows a generally broad binding pattern on chromatin, with a mean size of ~17 kb.

(E) ChIP-Seq peaks of DNMT3A^{R882H} (top), H3K4me1 (middle) and H3K4me3 (bottom) at an intragenic region close to *Vegfa* in LSCs$^{RH\text{-}RAS}$. Boxed areas highlight close proximity and significant overlap of DNMT3A^{R882H} binding and H3K4me1 peaks.

(F) Functional annotation of DNMT3A^{R882H} ChIP-Seq peaks by GREAT tools (with a setting of "single nearest gene, 200.0 kb max extension"). Shown are the top over-represented categories belonging to Gene Ontology (GO) biological processes.

(G-H) ChIP-Seq profiles of DNMT3A^{R882H}, H3K4me1 and H3K4me3 at the LSC$^{RH\text{-}RAS}$ 'stemness' genes *Hoxa* cluster (panel G) and *Mycn* (panel H) in LSCs$^{RH\text{-}RAS}$. Shown in y-axis is ChIP-Seq read coverage normalized to a read depth of 1 million reads. Shown on top (purple) is position of the called DNMT3A^{R882H} ChIP-Seq peaks.

Table S3, related to Figure 4 (provided as a separate Excel file). Summary of DNMT3A^{R882H} ChIP-Seq peaks identified in murine LSCs$^{RH\text{-}RAS}$.

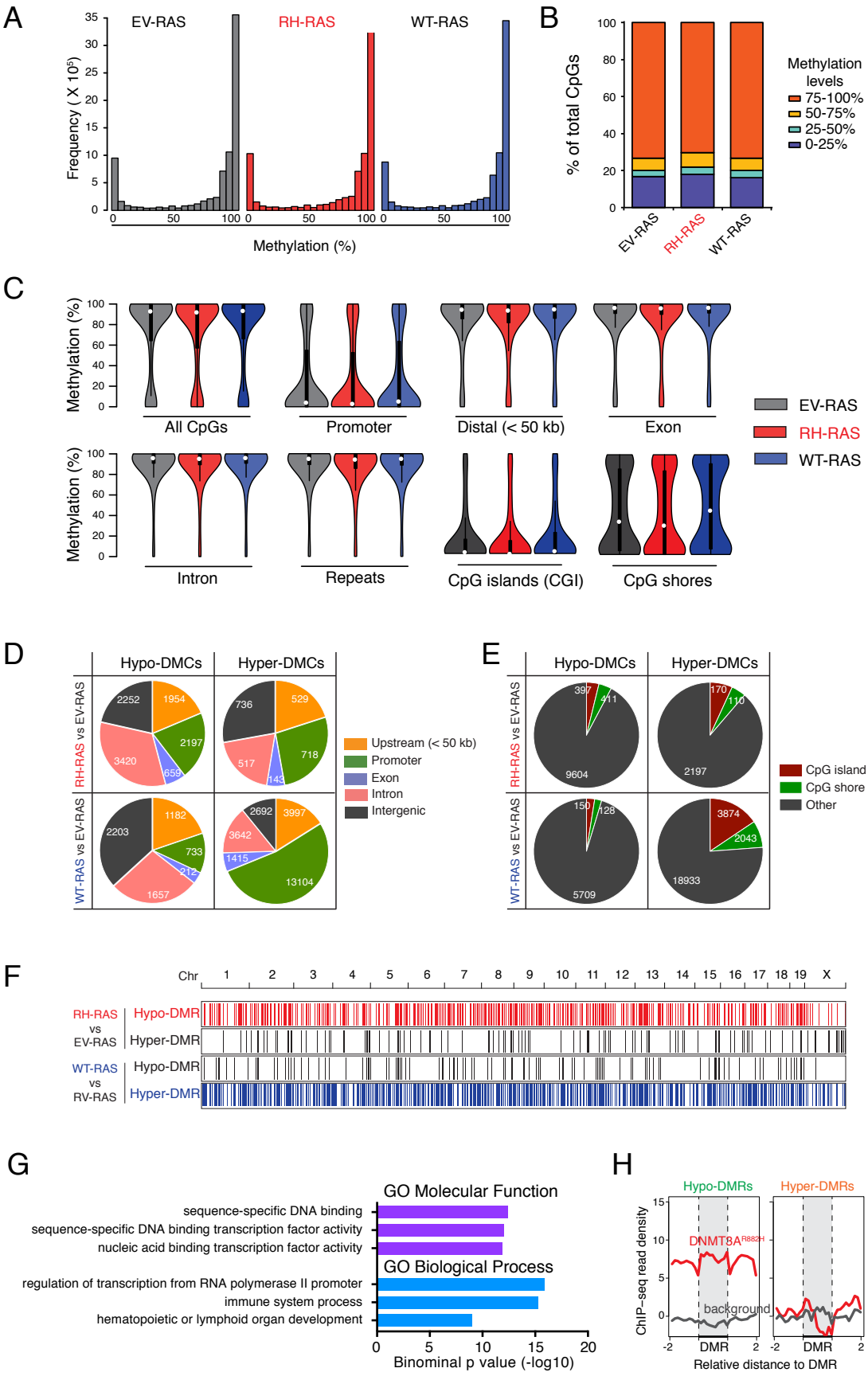
A
EV-RAS
RH-RAS
WT-RAS
Frequency (X 10^5)
Methylation (%)
B
% of total CpGs
Methylation levels
75-100%
50-75%
25-50%
0-25%
EV-RAS
RH-RAS
WT-RAS
C
Methylation (%)
All CpGs
Promoter
Distal (< 50 kb)
Exon
Intron
Repeats
CpG islands (CGI)
CpG shores
EV-RAS
RH-RAS
WT-RAS
D
Hypo-DMCs
Hyper-DMCs
RH-RAS vs EV-RAS
WT-RAS vs EV-RAS
2252
1954
2197
3420
659
736
529
718
517
143
2203
1182
733
212
1657
2692
3997
3642
1415
13104
Upstream (< 50 kb)
Promoter
Exon
Intron
Intergenic
E
Hypo-DMCs
Hyper-DMCs
RH-RAS vs EV-RAS
WT-RAS vs EV-RAS
397
411
9604
170
110
2197
150
128
5709
3874
2043
18933
CpG island
CpG shore
Other
F
Chr
1
2
3
4
5
6
7
8
9
10
11
12
13
14
15
16
17
18
19
X
RH-RAS vs EV-RAS
Hypo-DMR
Hyper-DMR
WT-RAS vs RV-RAS
Hypo-DMR
Hyper-DMR
G
GO Molecular Function
sequence-specific DNA binding
sequence-specific DNA binding transcription factor activity
nucleic acid binding transcription factor activity
GO Biological Process
regulation of transcription from RNA polymerase II promoter
immune system process
hematopoietic or lymphoid organ development
Binominal p value (-log10)
H
Hypo-DMRs
Hyper-DMRs
ChIP−seq read density
DNMT8A^R882H
background
DMR
Relative distance to DMR

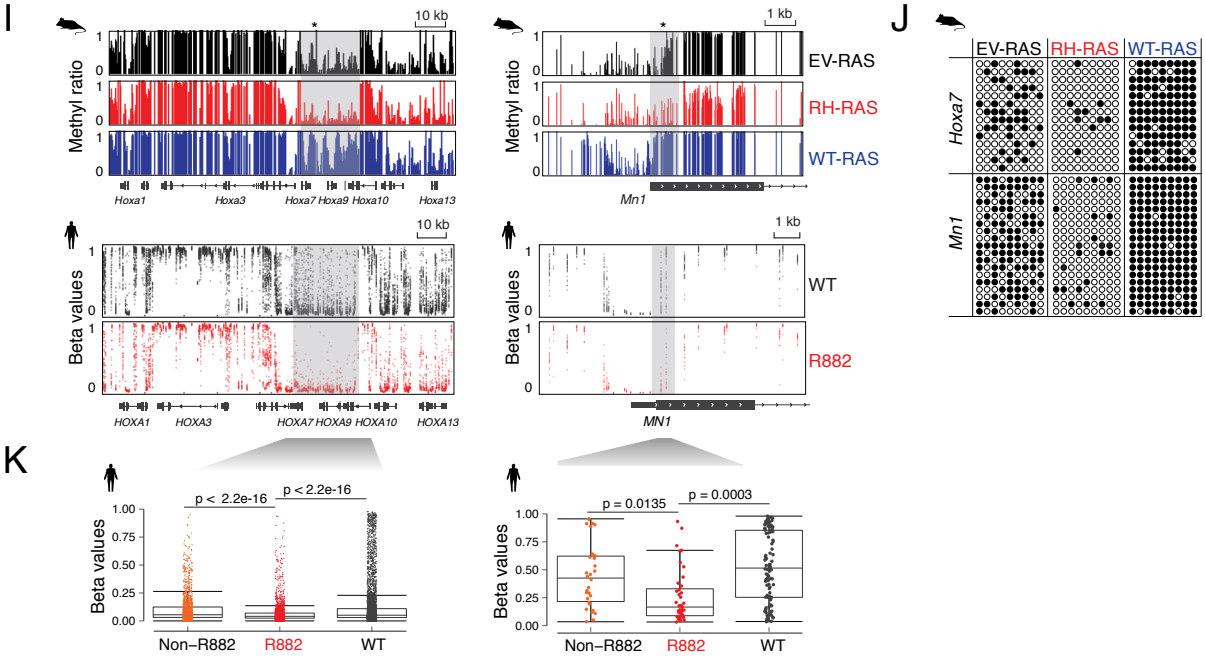

Figure S5, related to Figure 5. DNMT3A^{R882H} induces focal CpG hypomethylations enriched at H3K4me1-demarcated gene-regulatory sites in murine HSPCs.

(A-B) Distribution (panel A) and bar plots (panel B) of absolute methylation levels for a total of ~6.5 million CpG sites detected by eRRBS with >10× coverage among indicated HSPC samples.

(C) Violin plots showing distribution of absolute methylation levels at CpG sites within indicated genomic features among EV-RAS, RH-RAS or WT-RAS HSPCs. White dots are the median and box lines are the first and third quartile of the data. Repeats, repetitive sequence.

(D-E) Pie charts showing distribution of indicated DMCs among various genomic regions.

(F) Distribution of indicated DMRs among chromosomes. Each vertical line represents a DMR.

(G) GREAT annotation of DNMT3A^{R882H}-associated hypo-DMRs. Shown are the top over-represented categories belonging to GO Molecular Function and GO Biological Process.

(H) DNMT3A^{R882H} ChIP-Seq profiles at DNMT3A^{R882H}-associated hypo-DMRs (left), hyper-DMRs (right) and their background controls (grey).

(I) DNA methylation profiles of *Hoxa* (left) and *Mn1* (right) in murine HSPCs (upper panel), as well as those of the human gene homologue (bottom panel) among AML patient samples carrying either WT or R882-mutated *DNMT3A* based on the TCGA dataset (Cancer Genome Atlas Research, 2013; Russler-Germain et al., 2014). Faded points represent individual CpG methylation beta values (WT, n = 50; R882, n = 20). Grey box, DMR detected by both mouse and human studies.

(J) Individual bisulfite sequencing verifies two hypo-DMRs at LSC^{RH-RAS} 'stemness' genes *Hoxa7* and *Mn1* (as indicated with asterisks in panel I) in murine HSPCs after indicated gene transduction.

(K) Box plots of methylation beta values of pooled CpGs from grey marked regions at *HOXA7-HOXA10* and *MN1* in human AMLs carrying WT (n = 50), R882-mutated (n = 20) or non-R882-mutated (n = 15) *DNMT3A* based on the TCGA studies. Horizontal line, median; box, interquartile range; whiskers extend to 1.5× the interquartile range. The p values were calculated by Mann-Whitney U test.

Table S4, related to Figures 5 and 6 (provided as a separate Excel file). Summary of DNMT3A^{R882H}- and DNMT3A^{WT}-associated DMRs identified by eRRBS studies in murine HSPCs.

Table S5, related to Figure 5. List of genes having DNMT3A^{R882H}-associated DMRs identified in murine HSPCs, as well as those associated with hypo-DMRs identified among human normal-karyotype (NK) AML patients carrying R882-mutated DNMT3A in comparison to WT DNMT3A.

ABCC4	*DLG4*	*LHX9*	*RSPO1*
ABLIM1	*EBF1*	*LRRC8D*	*RTKN*
ACOXL	*EDNRB*	*MAN1C1*	*RUSC1*
ADAMTSL5	*EFHD1*	*MARVELD2*	*SBNO2*
ADARB1	*ELK3*	*MBNL1*	*SCARF2*
ADCY4	*F3*	*MEGF11*	*SCRT2*
AHDC1	*FAM171A2*	*MEIS1*	*SCUBE1*
ALDH7A1	*FOXK1*	*MN1*	*SEMA4B*
AMIGO3	*FSCN1*	*MSRB3*	*Sept9*
APC2	*FZD5*	*NAV2*	*SIK3*
APLP1	*GABBR1*	*NCKAP5L*	*SIPA1L3*
ATF6B	*GATA4*	*NCOR2*	*SIX3*
ATP9A	*GBX2*	*NFATC1*	*SLC11A2*
AXL	*GLTP*	*NFIA*	*SLC23A2*
B4GALNT1	*HLCS*	*NGB*	*SLC38A1*
BAHCC1	*HLF*	*NKX2-5*	*SMAD3*
CALCA	*HOXA7*	*NXPH4*	*SYNE2*
CHN2	*HOXB4*	*ONECUT1*	*TBX5*
CIT	*HOXD13*	*PANX2*	*TFAP2A*
CLCF1	*HS3ST2*	*PAX3*	*TIAM1*
CLDN5	*HSF4*	*PBX1*	*TNKS1BP1*
CTBP2	*IRX4*	*PCDHGA11*	*TRAF1*
CXCL12	*ITGB2*	*PCDHGA2*	*TRIM14*
CYP1B1	*ITPK1*	*PMEPA1*	*TRPS1*
CYP26C1	*KCNG3*	*POMC*	*TSPAN4*
DAB2IP	*KCNIP2*	*PRRT1*	*TTC7B*
DHX35	*KDM2B*	*PTPRS*	*USP2*
DLC1	*KIFC2*	*RAI1*	*WWTR1*
DLEU2	*LASP1*	*RILP*	*ZMIZ1*
DLEU7	*LEF1*	*RIN3*	

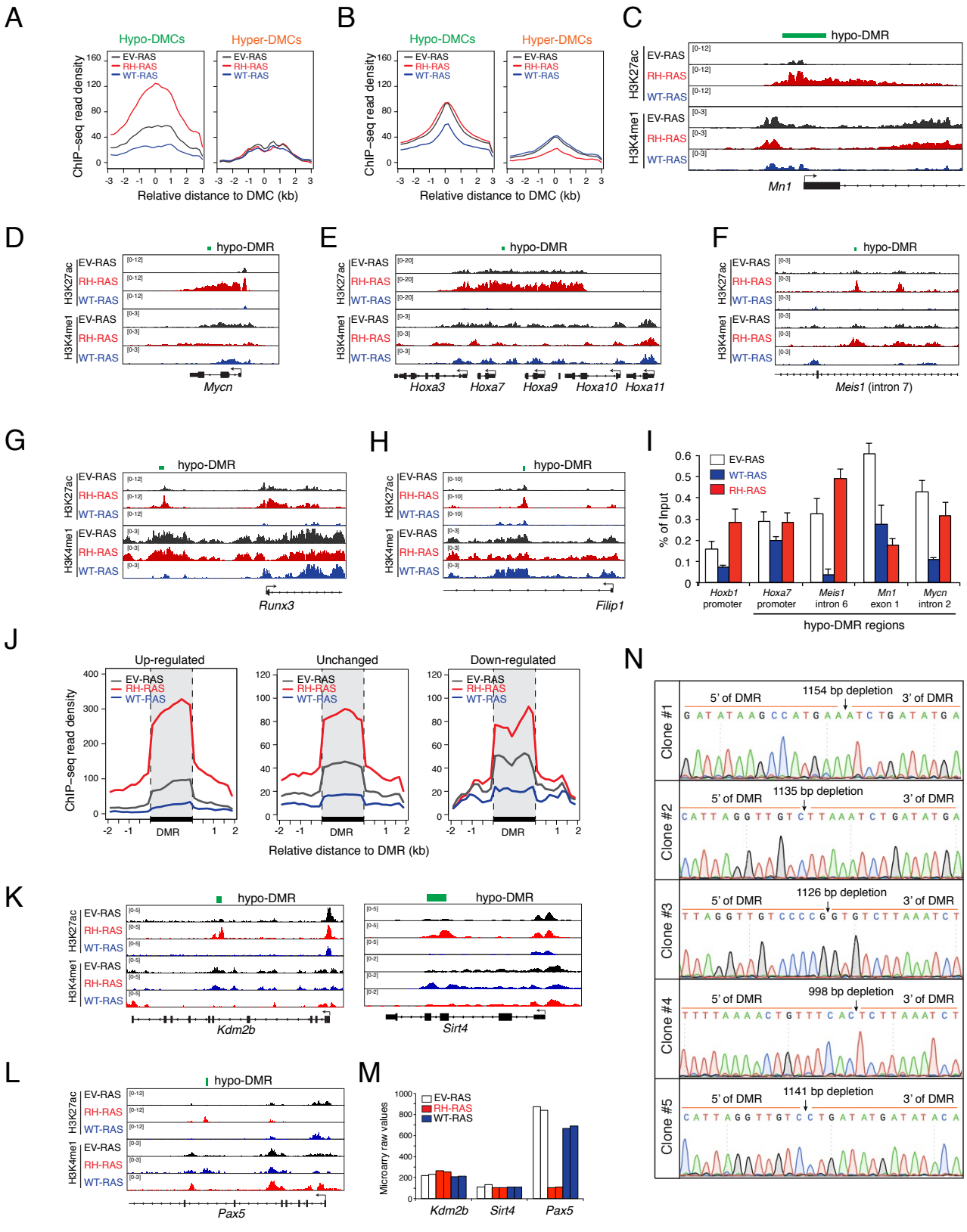
A
Hypo-DMCs
Hyper-DMCs
EV-RAS
RH-RAS
WT-RAS
ChIP−seq read density
Relative distance to DMC (kb)
B
Hypo-DMCs
Hyper-DMCs
ChIP−seq read density
Relative distance to DMC (kb)
C
hypo-DMR
H3K27ac
H3K4me1
Mn1
D
hypo-DMR
Mycn
E
hypo-DMR
Hoxa3
Hoxa7
Hoxa9
Hoxa10
Hoxa11
F
hypo-DMR
Meis1 (intron 7)
G
hypo-DMR
Runx3
H
hypo-DMR
Filip1
I
% of Input
Hoxb1 promoter
Hoxa7 promoter
Meis1 intron 6
Mn1 exon 1
Mycn intron 2
hypo-DMR regions
J
Up-regulated
Unchanged
Down-regulated
ChIP−seq read density
DMR
Relative distance to DMR (kb)
K
hypo-DMR
Kdm2b
Sirt4
L
hypo-DMR
Pax5
M
Microarry raw values
Kdm2b
Sirt4
Pax5
N
Clone #1
5' of DMR
1154 bp depletion
3' of DMR
Clone #2
1135 bp depletion
Clone #3
1126 bp depletion
Clone #4
998 bp depletion
Clone #5
1141 bp depletion

Figure S6, related to Figure 6. DNMT3A^{R882H}-associated hypo-DMRs gain epigenetic alterations associated with gene activation.

(A-B) Enrichment of H3K27ac (panel A) and H3K4me1 (panel B) ChIP-Seq signals at DNMT3A^{R882H}-associated DMCs (with DMCs positioned at the center of x-axis). Plotted were average histone ChIP-Seq read densities at 100-bp bins within +/-3 kb of DMCs in murine HSPCs co-transduced with DNMT3A^{R882H} (RH-RAS, red) in comparison to mock transduction (EV-RAS, grey) or co-transduced with DNMT3A^{WT} (WT-RAS, blue).

(C-H) Histone ChIP-Seq profiles of indicated genes among HSPCs post-transduction of EV-RAS, RH-RAS or WT-RAS. Green bars indicate gained hypo-DMRs upon DNMT3A^{R882H} transduction (RH-RAS) relative to control (EV-RAS) as identified by eRRBS.

(I) ChIP-qPCR of H3K4me1 binding at indicated genomic regions among HSPCs post-transduction of EV-RAS, RH-RAS or WT-RAS.

(J) Enrichment of H3K27ac ChIP-Seq signals at DNMT3A^{R882H}-associated hypo-DMRs (shown in bold on x-axis) associated with three gene subgroups showing either up-regulation (n = 144), down-regulation (n = 89) or no significant changes (n = 821) in their expression levels in murine HSPCs 16 days post-transduction of RH-RAS, relative to EV-RAS (with significant gene expression change defined by fold-of-change > 1.3 and p value < 0.05). Plotted were averaged H3K27ac ChIP-Seq read densities across hypo-DMRs in murine HSPCs post-transduction of EV-RAS, RH-RAS or WT-RAS.

(K-L) H3K4me1 and H3K27ac ChIP-Seq profiles at *Kdm2b* and *Sirt4* (panel K), as well as *Pax5* (panel L) in murine HSPCs post-transduction of EV-RAS, RH-RAS or WT-RAS. Green bars indicate gained hypo-DMRs upon DNMT3A^{R882H} transduction (RH-RAS), relative to control (EV-RAS), as identified by eRRBS.

(M) Microarray analysis shows no expression up-regulation of *Kdm2b, Sirt4* and *Pax5,* the genes with significant gain of H3K27ac at their hypo-DMR as shown in the panels K and L.

(N) Sequencing results verified CRISPR/Cas9-induced genomic deletion of a hypo-DMR found at the *Meis1* intron 6 in LSC^{RH-RAS} lines. The genomic PCR products were generated with the two DMR-flanking primers (i.e. F2 and R2 as shown in Figures 6L-M) followed by direct sequencing.

Error bar, +/- SD.

Table S6, related to Figures 6 and 7. List of DNMT3A^{R882H} signature genes (defined as genes carrying DNMT3A^{R882H}-induced epigenetic changes [CpG hypomethylation and H3K27ac gain] and up-regulated by DNMT3A^{R882H} in HSPCs with RH-RAS, relative to EV-RAS).

2610307P16Rik	*Hoxa7*	*Prrt2*
Alox5ap	*Id2*	*Ptpre*
Anxa2	*Itgae*	*Pxn*
Bace1	*Itpk1*	*Rab27a*
Baiap2	*Itsn1*	*Rab3ip*
Bcl2	*Klhl2*	*Rin3*
Bsn	*Limk1*	*Rora*
Chad	*Lpar2*	*Runx3*
Chst12	*Meis1*	*S1pr3*
Chst14	*Mn1*	*Selplg*
Cpne2	*Mrvi1*	*Sh2d5*
Dnajc6	*Mta3*	*Slc9a9*
Dpp4	*Mycn*	*Snx18*
Emid1	*Nfix*	*Tarm1*
Ephb2	*Nrip1*	*Tifab*
Erap1	*Pan3*	*Trerf1*
Filip1	*Pde4a*	*Tubb6*
Gne	*Plec*	*Uck2*
Golm1	*Plxnc1*	*Zfp217*

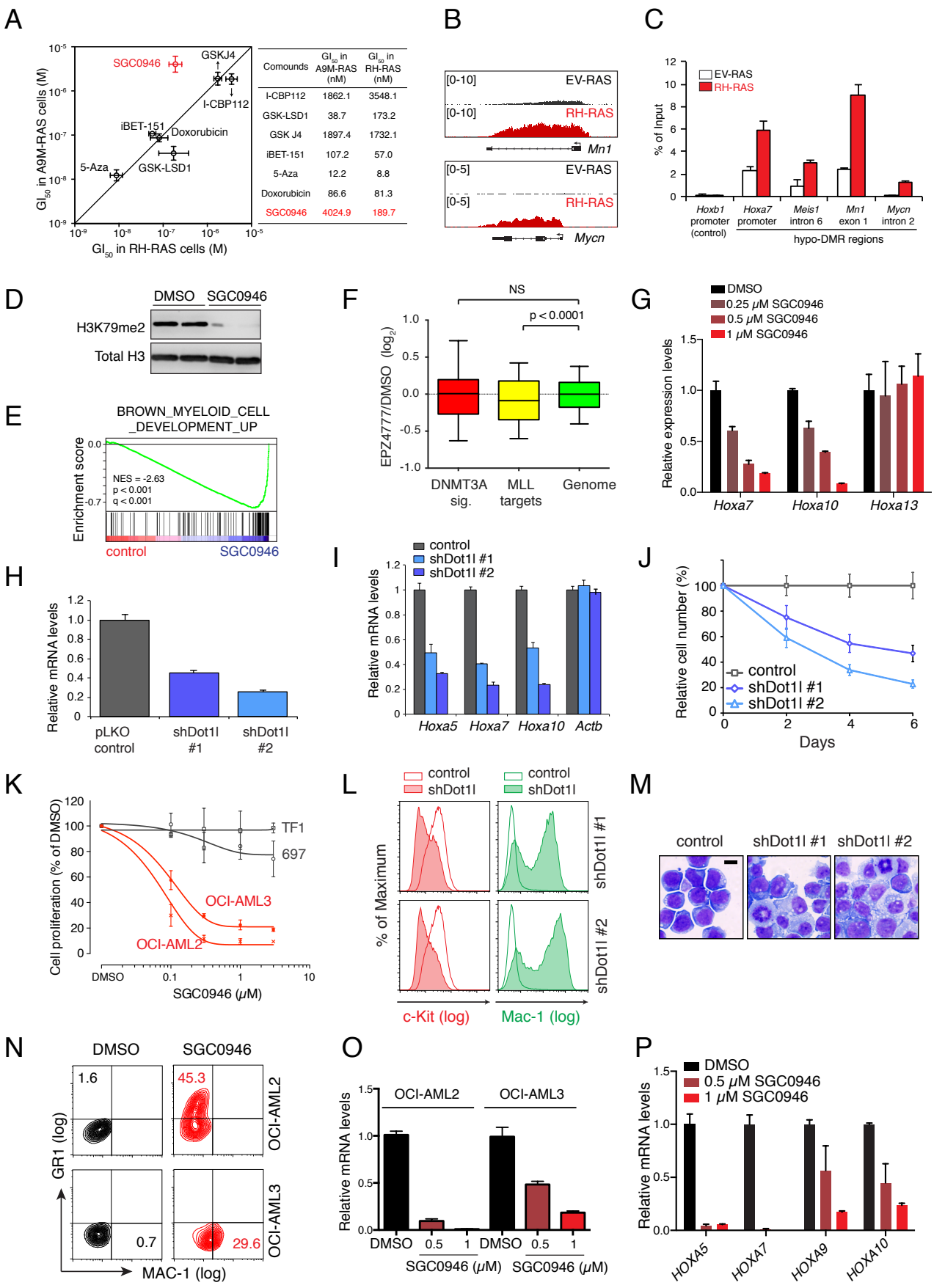
A
SGC0946
GSKJ4
I-CBP112
iBET-151
Doxorubicin
5-Aza
GSK-LSD1
GI50 in A9M-RAS cells (M)
GI50 in RH-RAS cells (M)
Comounds | GI50 in A9M-RAS (nM) | GI50 in RH-RAS (nM)
I-CBP112 | 1862.1 | 3548.1
GSK-LSD1 | 38.7 | 173.2
GSK J4 | 1897.4 | 1732.1
iBET-151 | 107.2 | 57.0
5-Aza | 12.2 | 8.8
Doxorubicin | 86.6 | 81.3
SGC0946 | 4024.9 | 189.7
B
[0-10] EV-RAS
[0-10] RH-RAS
Mn1
[0-5] EV-RAS
[0-5] RH-RAS
Mycn
C
EV-RAS
RH-RAS
% of Input
Hoxb1 promoter (control)
Hoxa7 promoter
Meis1 intron 6
Mn1 exon 1
Mycn intron 2
hypo-DMR regions
D
DMSO SGC0946
H3K79me2
Total H3
E
BROWN_MYELOID_CELL_DEVELOPMENT_UP
Enrichment score
NES = -2.63
p < 0.001
q < 0.001
control
SGC0946
F
NS
p < 0.0001
EPZ4777/DMSO (log2)
DNMT3A sig.
MLL targets
Genome
G
DMSO
0.25 μM SGC0946
0.5 μM SGC0946
1 μM SGC0946
Relative expression levels
Hoxa7
Hoxa10
Hoxa13
H
Relative mRNA levels
pLKO control
shDot1l #1
shDot1l #2
I
control
shDot1l #1
shDot1l #2
Relative mRNA levels
Hoxa5
Hoxa7
Hoxa10
Actb
J
Relative cell number (%)
control
shDot1l #1
shDot1l #2
Days
K
Cell proliferation (% of DMSO)
TF1
697
OCI-AML3
OCI-AML2
DMSO
SGC0946 (μM)
L
control
shDot1l
control
shDot1l
% of Maximum
shDot1l #1
shDot1l #2
c-Kit (log)
Mac-1 (log)
M
control
shDot1l #1
shDot1l #2
N
DMSO
SGC0946
1.6
45.3
0.7
29.6
OCI-AML2
OCI-AML3
GR1 (log)
MAC-1 (log)
O
OCI-AML2
OCI-AML3
Relative mRNA levels
DMSO
0.5
1
SGC0946 (μM)
P
DMSO
0.5 μM SGC0946
1 μM SGC0946
Relative mRNA levels
HOXA5
HOXA7
HOXA9
HOXA10

Figure S7, related to Figure 7. Dot1l inhibition reverses DNMT3A^{R882H}-mediated aberrant trans-activation of stem cell genes, thereby suppressing acute leukemogenicity.

(A) Plots (left) and summary table (right) of the half maximal inhibition of cell proliferation (GI_{50}) of indicated compounds in suppressing in vitro growth of LSCs$^{RH\text{-}RAS}$ and a control line without DNMT3A^{R882H}, i.e., LSCs established by coexpression of NRAS^{G12D} and Hoxa9 plus Meis1. Data were collected 12 days post-treatment. Compounds include bromodomain inhibitor iBET-151, a DNA demethylating agent 5-Aza, topoisomerase inhibitor Doxorubincin, LSD1 inhibitor GSK-LSD1, CBP/p300 inhibitor I-CBP112, Dot1l inhibitor SGC0946, and the jumonji H3K27 demethylase inhibitor GSK-J4.

(B) H3K79me2 ChIP-Seq profiles at indicated LSC$^{RH\text{-}RAS}$ 'stemness' genes in murine HSPCs transduced with EV-RAS or RH-RAS.

(C) ChIP-qPCR of H3K79me2 levels at indicated genomic sites in murine HSPCs post-transduction of EV-RAS or RH-RAS.

(D) Immunoblot of H3K79me2 and total histone H3 in LSCs$^{RH\text{-}RAS}$ 4 days post-treatment with DMSO or 1 μM SGC0946.

(E) GSEA analysis reveals a significant enrichment of myeloid differentiation gene programs in LSCs$^{RH\text{-}RAS}$ 4 days post-treatment with 1 μM SGC0946, relative to DMSO.

(F) Boxplots showing relative expression of DNMT3A^{R882H} signature genes (n = 54), MLL-AF9 target genes (n = 129), and all genes in the genome among MLL-AF9-transformed leukemic lines post-treatment with the Dot1l inhibitor EPZ4777 (3 μM) for 6 days, relative to DMSO. Expression data were obtained from GEO datasets GSE61013 (Chen et al., 2015). Horizontal line, median; box, interquartile range; whiskers, 10 to 90 percentiles. The p values were calculated by Mann-Whitney U test.

(G) RT-qPCR shows a dose-dependent suppression of *Hoxa7* and *Hoxa10,* but not *Hoxa13* (an already repressed *Hoxa* gene), in LSCs$^{RH\text{-}RAS}$ 6 days post-treatment with indicated concentrations of SGC0946, relative to DMSO.

(H-I) RT-qPCR detects relative expression of *Dot1l* (panel H) and *Hoxa* genes (panel I) in LSC$^{RH\text{-}RAS}$ lines stably transduced with either of the two tested *Dot1l*-specific shRNAs, in comparison to pLKO vector control. *Actb* serves as a control for gene expression.

(J) Relative in vitro growth of LSC$^{RH\text{-}RAS}$ lines after stable transduction with either of the two tested *Dot1l*-specific shRNAs in comparison to pLKO vector control.

(K) Relative growth of two *DNMT3A*-mutated human AML cell lines, OCI-AML2 and OCI-AML3*,* and two human leukemia lines with no *DNMT3A* mutation, TF-1 (carrying an activating *NRAS* mutation) and 697 (a pre-B ALL line with translocation of a HOX/MEIS1 cofactor gene, *E2A-PBX1*) 12 days post-treatment with various concentrations of SGC0946 in comparison to DMSO.

(L-M) FACS analysis for c-Kit and Mac-1 (panel L) and Wright–Giemsa staining (panel M; scale bar, 5 μm) of LSC$^{RH\text{-}RAS}$ lines after stable transduction with *Dot1l*-specific shRNAs, relative to pLKO vector control.

(N) FACS analysis for GR1 and MAC-1 expression in the OCI-AML2 and OCI-AML3 human AML cell lines 6 days post-treatment with 1 μM of SGC0946 in comparison to DMSO.

(O) RT-qPCR of *MEIS1* in OCI-AML2 or OCI-AML3 human AML cells 6 days post-treatment with indicated concentrations of SGC0946, relative to DMSO.

(P) RT-qPCR of *HOXA* expression in OCI-AML2 human AML cells 6 days post-treatment with indicated concentrations of SGC0946, relative to DMSO.

Error bar, +/- SD. NS, not significant.

Supplemental Experimental Procedures

Plasmid Construction

MYC-tagged human DNMT3A isoform 1 (also known as DNMT3A1, NCBI accession NP_783328) was generated by PCR-mediated ligation of a MYC tag to N-terminus of DNMT3A1 and then cloned to a MSCV retroviral expression vector (Clontech). For gene co-expression, DNMT3A1 cDNA was inserted to upstream of an internal ribosome entry site (IRES) sequence, followed by either GFP, $NRAS^{G12D}$, $IDH1^{R132H}$ or NPM1c, in a home-made MSCV-based bicistronic system. DNMT3A1, $NRAS^{G12D}$ and NPM1 plasmids were obtained from Addgene and $IDH1^{R132H}$ was kindly provided by Dr. Yue Xiong (UNC at Chapel Hill). Point mutation was generated by site-directed mutagenesis and all used plasmids were confirmed by sequencing. MSCV expression plasmids for Hoxa9 alone or in combination with co-expressed Meis1 were used as previously described (Wang et al., 2005). All plasmids used were confirmed by sequencing.

Cell lines and Tissue Culture

Cell lines of HEK293, NIH3T3, and TF-1 were obtained from ATCC and maintained using recommended culture conditions. Maintenance and cultivation in vitro of murine leukemogenic progenitor lines established by various leukemic factors such as HOXA9 plus MEIS1 (Wang et al., 2006; Wang et al., 2005), MLL-AF9 (Xu et al., 2015), NUP98-NSD1 (Wang et al., 2007) or NUP98-JARID1A/KDM5A (Wang et al., 2009) were described before. A WEHI3B murine AML line that shows high Hoxb8 and Meis2 coexpression (Fujino et al., 2001) and a human pre-B ALL cell line, 697 (Kamps et al., 1991), are obtained from Dr. Mark Kamps (UCSD). Two *DNMT3A*-mutated human AML lines OCI-AML2 and OCI-AML3 (Tiacci et al., 2012) are kind gifts of Dr. Mark Minden (Princess Margaret Hospital).

Retroviral Production

MSCV-based retrovirus was packaged and produced in HEK293 followed by retroviral titration with NIH3T3 cell infection as previously described (Wang et al., 2006).

Purification, Retroviral Transduction, and Cultivation of Primary Murine Hematopoietic Stem/Progenitor Cells (HSPCs)

Bone marrow cells are harvested from femur and tibia of wild-type balb/C mice pre-treated with 5-Fluorouracil (5-FU), followed by a lineage-negative (Lin^-) enrichment protocol to remove cells expressing differentiation antigens as we described before (Wang et al., 2006; Wang et al., 2009). Briefly, 500,000 of Lin^- enriched hematopoietic stem/progenitor cells (HSPCs) were obtained per mouse with ~10% of them c-$Kit^+Lin^-Sca1^+$ (KLS) HSPCs. Before retroviral infection, Lin^--enriched HSPCs were pre-stimulated in the base medium OptiMEM (Invitrogen, 31985), 15% of FBS (Invitrogen, 16000-044), 1% of antibiotics and 50 μM of β-mercaptoethanol) complemented with a cytokine cocktail that contains 10 ng/mL each of SCF (Miltenyi), Flt3 ligand (Flt3L; Sigma), IL3 (Peprotech) and IL6 (Peprotech) for three days as described (Wang et al., 2007; Wang et al., 2006; Wang et al., 2009). Post-infection with the concentrated retrovirus (Retro-X concentrator, Clontech) and drug selection (2 μg/mL puromycin for the first 2-4 days followed by an extended seven-day selection using 1 μg/mL puromycin for the MSCV-puro vector used in the study), rates of purity and exogenous oncogene expression in those retrovirus-transduced, drug-selected murine HSPCs were assessed by flow cytometry of MYC and/or FLAG-tagged proteins, followed by subsequent functional readout assays such as CFU assays in the semi-solid culture system or the growth assay in the liquid

culture medium. For the latter, the above base medium is added with either recombinant murine SCF alone or together with Flt3L; alternatively, we also routinely use home-made cell culture supernatants of mSCF-producer (mSCF-CHO cells, gift of Dr. Mark Kamps, UCSD) and mFlt3-producer (SP2.0-mFlt3L cells, gift of Dr. Robert Rottapel, University of Toronto) cell lines as source of murine SCF and Flt3L, respectively. To test differentiation potency in the presence of myeloid-promoting cytokines such as GM-SCF or IL6 (Peprotech), progenitor cells were rinsed with PBS and seeded in the same base medium that contains 10 ng/mL of each tested cytokine. Cell splitting and replating with fresh medium were carried out every 3-4 days to keep cell number <1.5 million per mL (in a 6- or 12-well plate). In vitro cultured HSPCs were routinely monitored under microscopy and cellular morphology examined by Wright-Giemsa staining and FACS as described (Wang et al., 2006).

In vivo Leukemogenic Assay

To determine potential leukemia-initiating stem cell (LSC) properties possessed by ex vivo immortalized progenitor lines, 0.1 million of these cells were engrafted to syngeneic mice via tail vein injection (The UNC Cancer Center Animal Studies Core). Mice were monitored with complete blood counting (CBC) of the obtained peripheral blood samples and abdomen palpation for early signs of early leukemia such as lethargy, increased white blood cell (WBC) counts and enlarged spleen (Xu et al., 2015). Mice exhibiting full-blown leukemic phenotypes were euthanized followed by pathological and histological analyses as described (Wang et al., 2007; Wang et al., 2006; Wang et al., 2005; Xu et al., 2015). LSCs established ex vivo were used for primary (1^{st}) transplantation assays, and the produced primary leukemias in independent mice were used for secondary (2^{nd}) transplantation.

Flow Cytometry (FACS) Analysis

Cells were blocked with BD FcBlock (2.4G2) and stained on ice with fluro-conjugated antibodies (1:100 dilution of c-$Kit^{FITC/APC}$, Sca-I^{PE-Cy7}, $Cd34^{APC/FITC}$, Mac-1^{APC}, $Gr1^{PE/FITC}$, $Cd19^{PE/FITC}$, $Cd3e^{FITC}$, $Ter119^{FITC}$, $Cd4^{FITC}$, $Cd8^{FITC}$; purchased from BD Biosciences and eBioscience Inc.) and analyzed on the Beckman Coulter CyAn ADP or Becton Dickinson LSR II machine (UNC Flow Cytometry Core Facility) as described before (Wang et al., 2009; Xu et al., 2015). For intracellular staining of FLAG- or MYC-tagged proteins, cells were first prefixed by the fixation/permeability buffer (BD Biosciences) or 100% methanol, respectively, and stained with Fluor-conjugated, DYKDDDDK or c-Myc Alexa antibodies (1:100 dilution, R&D Systems), respectively. Data were analyzed using FlowJo software.

Microarray Analysis

Total RNA was extract using RNeasy Plus Mini Kit (Qiagen) followed by quality check with Bioanalyzer; subsequent sample preparation and hybridization to either Mouse Genome 430 2.0 Arrays (Affymetrix) or Mouse Gene 2.0 ST Arrays (Affymetrix) were carried out according to manufacturer's instruction and by UNC Functional Genomics Core as described before (Wang et al., 2007; Xu et al., 2015). Raw CEL data from Mouse Gene 2.0 ST Arrays were processed with GeneSpring software X12.6 (Agilent Technologies, Inc.) as described before (Xu et al., 2015).

Raw Data of Mouse Genome 430 2.0 Array studies – Gene expression data generated by this current study included those of four independently derived RH-RAS LSC lines (termed as LSC^{RH-RAS} #1, #2, #3 and #4), two RH-RAS LSC lines (LSC^{RH-RAS} #1 and # 3) treated with 1 μM SGC0946 for 4 days and one MLL-AF9-transformed progenitor line. The other datasets in the same Mouse Genome 430 2.0 platform for various normal and leukemogenic hematopoietic cell lines are listed in the following list.

Published Expression Data Used In This Study	GSE datasets	Reference
HSC and MEP	GSE38557	(Bock et al., 2012)
MPP1, MPP2, CLP, CMP and GMP	GSE20244	(Ji et al., 2010)
Cd34$^-$KLS, Ery, GN, Mono/Mac, B, CD4, CD8 and NKT	GSE27787	(Konuma et al., 2011)
LT-HSC and various differentiated lineages	GSE6506	(Chambers et al., 2007)
MLL-AF6 AML	GSE43067	(Deshpande et al., 2013)
AML1-ETO AML	GSE15195	(Lo et al., 2012)
NUP98-JARID1A AML	This study	(Wang et al., 2009)
NUP98-NSD1, HOXA9/MEIS1 and MLL-ENL AML	GSE10071	(Wang et al., 2007)

Data Preprocessing, Hierarchical clustering and Principal component analysis (PCA) – Raw CEL files were subjected to a series of normalization and quality control procedures, similar to a previously described method (Bock et al., 2012). First, CEL files from all experiments were jointly normalized through the Robust Multi-array Average (RMA) method (Irizarry et al., 2003) to remove systematic variations. RMA normalization was performed using the 'affy' package of the Bioconductor suite (http://www.bioconductor.org/). Second, for most cell types, the two replicates with the highest pairwise correlation were selected and used. Third, we performed RMA normalization with these used CEL files to generate final datasets for further analysis. Normalized data were then processed and filtered by floor = 20, ceiling = 20000, min fold change = 3, min delta = 100 for hierarchical clustering and PCA analysis. Hierarchical clustering was performed by average linkage using uncentered Pearson correlation on GenePattern platform (Reich et al., 2006). PCA analysis was performed using the 'prcomp' package in R (www.r-project.org).

Identification of 'stemness gene' signatures – Base on hierarchical clustering and PCA analysis, we used gene expression data of HSC, MPP1 and CD34$^-$KLS from different sources (see the list above; defined as "self-renewing group") to minimize potential unwanted batch effects; gene expression datasets of differentiating or mature blood cell types (i.e., GMP, MEP, B, CD4, CD8, NKT, GN, Mono/Mac, and Ery) represent the "non-self-renewing group". HSC "stemness" genes were defined by two standards: (1) by comparing "self-renewing group" with each category in the "non-self-renewing group", a gene probe should have at least two-fold overexpression and $p < 0.05$ with standard two sample t-test, and (2) by comparing "self-renewing" vs. "non-self-renewing" groups, a gene probe should meet statistical significance $p < 0.001$ with standard two sample t-test. From these, we identified 598 gene probes as HSC "stemness" genes. Next, those 598 HSC "stemness" gene probes that meet the same criteria by comparing RH-RAS LSCs to the "non-self-renewing group" will then be defined as "LSC$^{RH\text{-}RAS}$ 'stemness' genes/programs".

Gene Set Enrichment Analysis (GSEA)

GSEA analysis was performed using GSEA2-2.2.0 software (Subramanian et al., 2005) for testing enrichment of curated gene sets (C2) or customized gene sets as performed before (Xu et al., 2015).

RT-qPCR Analysis

Reverse transcription of RNA was performed using the random hexamer and High Capacity cDNA Reverse Transcription Kits (Applied Biosystems). Usually the PCR amplicon (size ~75-150 bp) is designed to span over large intron regions using NCBI Primer-BLAST. Quantitative PCR was performed in triplicate using SYBR green master mix reagent (Applied Biosystem) on an ABI 7900HT

fast real-time PCR system. The detailed primer sequences for RT-qPCR are provided in the following lists.

Mouse Genes	Forward	Reverse	Reference
Actb	ACCAACTGGGACGACATGGA	GGTCTCAAACATGATCTGGGTCAT	
Hoxa5	GCAAGCTGCACATTAGTCAC	GCATGAGCTATTTCGATCCT	(Wang et al., 2009)
Hoxa7	CGGGCTTATACAATGTCAACAG	AAATGGAATTCCTTCTCCAGTTC	(Wang et al., 2009)
Hoxa9	ACAATGCCGAGAATGAGAGC	CAGCGTCTGGTGTTTTGTGT	
Hoxa10	CTCCAGCCCCTTCAGAAAAC	TGTAAGGGCAGCGTTTCTTC	
Hoxa13	CCAAATGTACTGCCCCAAAG	CCTATAGGAGCTGGCGTCTG	
Meis1	AAGGTGATGGCTTGGACAAC	TGTGCCAACTGCTTTTTCTG	
Mn1	TGATGGCAGAACACAGCACT	CTTGTTGGTGGGGTGGTCAT	
Mycn	CGGAGAGGATACCTTGAGCG	AGTGGTTACCGCCTTGTTGT	
Dot1l	GCGGAACCGTTGGAGGTAAT	TTCACAGTGGCTCCATGTCC	

Human Genes	Forward	Reverse	Reference
GAPDH	AACATCATCCCTGCCTCTACTGG	GTTTTTCTAGACGGCAGGTCAGG	
HOXA5	TCTACCCCTGGATGCGCAAG	AATCCTCCTTCTGCGGGTCA	
HOXA7	TCTGCAGTGACCTCGCCAAA	AGCGTCTGGTAGCGCGTGTA	
HOXA9	AAAAACAACCCAGCGAAGGC	ACCGCTTTTTCCGAGTGGAG	
HOXA10	CCTTCCGAGAGCAGCAAAGC	CAGCGCTTCTTCCGACCACT	
MEIS1	TGACCGTCCATTACGAAACCT	CCAGTCCAACCGAGCAGTAAG	(Abdel-Wahab et al., 2012)

Antibodies and Immunoblotting

Antibodies used for immunoblotting were α-Flag (Sigma; M2), α-MYC (Sigma, 9E10), α-Hoxa9 (Wang et al., 2007; Wang et al., 2005), α-Meis1 (a gift of Dr. Miguel Torres, Centro Nacional de Investigaciones Cardiovasculares, Spain), α-H3K79me2 (Abcam, ab3594) and α-Tubulin (Sigma). Total protein samples were prepared by cell lysis with either SDS-containing Laemmli sample buffer or RIPA lysis buffer as described (Wang et al., 2007; Wang et al., 2005) followed by brief sonication; extracted samples equivalent to 100,000 cells were loaded to SDS-PAGE gels for immunoblotting analysis.

Chromatin immunoprecipitation (ChIP) Followed by Deep Sequencing (ChIP-Seq)

Chromatin samples used for ChIP-Seq were prepared using a previously described protocol (Goldberg et al., 2010; Lee et al., 2006), followed by antibody enrichment, library generation, and parallel sequencing using an Illumina HiSeq-2500 Sequencer (UNC High-throughput Sequencing Facility). Chromatin samples extracted from ~100 million of cells were used for ChIP-Seq of Myc-tagged DNMT3A with the 9E10 anti-Myc antibody (Sigma); other antibodies used for ChIP-Seq were α-H3K4me1 (Abcam, 8895), α-H3K4me3 (Abcam, 8580), α-H3K27me3 (Upstate, 07-449), α-H3K27ac (Abcam, 4729), and α-H3K79me2 (Abcam, 3594). ChIP-Seq data for various normal blood cell subtypes (Lara-Astiaso et al., 2014) were obtained from GEO database (GSE60103).

ChIP-Seq Data Analysis

Briefly, all sequencing reads were mapped to the mouse genome (mm9) using the BWA alignment software (Li and Durbin, 2009), and unique reads mapped to a single best-matching location with no more than two mismatches were kept for data analysis. Duplicated reads, likely generated by PCRs,

were removed using SAMtools (Xu et al., 2015). Bedgraph signal track files for each ChIP-Seq experiment were generated using MACS2 software (Zhang et al., 2008), followed by displaying in the Integrative Genomics Viewer (IGV, Broad Institute) (Robinson et al., 2011). The MACS2 software was also used for peak identification with data from input as controls. DNMT3A^{R882H} ChIP-Seq peaks were called by a window approach as described previously (Goldberg et al., 2010; Xu et al., 2015). In-house scripts were used to assign peaks to annotated genomic features, defined as "promoter proximal" (±2kb of transcription start site, TSS), "promoter distal" or "upstream" (-50kb to -2kb of TSS), introns and exons, using the mouse RefSeq annotation as reference (both coding and non-coding were considered). In the case of broad peaks, we assigned a peak as "gene" if it extends beyond the start and end of an annotated gene. The CpG island annotation from the UCSC browser was used to associate peaks to CpG islands (CGIs), and the 1kb regions flanking CGIs were defined as CpG shores. In all analyses, 1-bp intersection was considered as peak overlapping. In the generation of profiles of ChIP-Seq read densities, a 100-bp window was used to determine ChIP-Seq read counts unless specified otherwise. To account for different peak (or DMR) sizes, peaks (or DMRs) were broken into 10-equal size bins and ChIP-Seq reads in individual bins were summed and normalized to yield reads per 100-bp. All ChIP-Seq profiles were normalized to a read depth of 10 millions for comparison, if necessary. The mapping information of the ChIP-Seq studies is provided in the following list.

Sample / Epitope	Total reads	Uniquely mapped reads
LSC$^{RH\text{-}RAS}$ / Input	18,324,401	15,535,177
LSC$^{RH\text{-}RAS}$ / Myc-DNMT3A^{R882H} (9E10)	29,195,863	21,976,593
LSC$^{RH\text{-}RAS}$ / H3K4me1	32,441,556	29,241,182
LSC$^{RH\text{-}RAS}$ / H3K4me3	37,160,636	24,298,214
HOXA9-MEIS1 / Input	13,813,627	8,567,831
HOXA9-MEIS1 / H3K4me1	26,034,975	24,547,306
EV-RAS / Input	24,486,819	21,306,596
EV-RAS / H3K4me1	12,754,638	11,736,817
EV-RAS / H3K27ac	23,362,273	21,913,284
EV-RAS / H3K79me2	65,883,113	58,669,486
EV-RAS / Input (matched for H3K79me2)	63,142,797	56,204,919
WT-RAS / Input	19,919,007	17,486,043
WT-RAS / H3K4me1	25,580,239	23,773,579
WT-RAS / H3K27ac	12,547,468	11,497,378
RH-RAS / Input	36,252,235	31,338,073
RH-RAS / H3K4me1	67,194,048	59,841,459
RH-RAS / H3K27ac	13,021,014	11,684,066
RH-RAS / H3K79me2	64,436,265	56,961,688
RH-RAS / Input (matched for H3K79me2)	62,786,927	56,304,371

ChIP Followed by qPCR (ChIP-qPCR)

The detailed procedure for ChIP-qPCR was described before (Wang et al., 2007; Wang et al., 2009), and the primer sequences used for ChIP-qPCR are provided in the following list. ChIP signals were produced from 3 independent experiments followed by normalization to input signals and presented as mean ± SD.

Mouse Genes	Primer location	Forward	Reverse	Reference
Hoxa7	upstream/DMR	TGGTGGGCTTCAGCTATTGG	TTCGGGTAGGAATTGGTGGC	
Hoxb1	promoter	GGGACTGCCAAACTCTGGC	CATGTGATCTCTCCCAGGCC	(Bernt et al., 2011)
Meis1	intron 6/DMR	ATCTCTGCTCTCTCCCCGAG	CTTCCCGGGCATATCTGGTC	
Mn1	exon 1/DMR	GAGGGTGACGAACCAAGGAG	GCTGCCCTTCAGAGTCAGAG	
Mycn	intron 2/DMR	ACTGCCAGGCTAGGAGAGAA	CAATTGTTCCGCTTTCCGGT	

Genomic Regions Enrichment of Annotations Tool (GREAT) Analysis

GREAT analysis (McLean et al., 2010) for DNMT3A^{R882H} ChIP-Seq peaks and DNMT3A^{R882H} associated hypo-DMRs was performed at its website (http://great.stanford.edu) using a setting of single nearest gene (200.0 kb max extension) with curated regulatory domains included.

Enhanced Reduced Representation Bisulfite Sequencing (eRRBS)

eRRBS was carried out with a previously described protocol with slight modification (Garrett-Bakelman et al., 2015). Briefly, ~300 ng of genomic DNA were digested with three different enzymes (80 units of MspI, 40 units of BfaI and 40 units of MseI) to enhance genomic fragmentation and coverage. The produced fragments were ligated to pre-annealed adapters containing 5'-methyl-cytosine instead of cytosine, followed by overhang fill-in, 3'-terminal-A extension and purification. Bisulfite treatment of the fragments was done using the EZ DNA Methylation–Lightning kit (Zymo Research). Amplified eRRBS libraries was quality checked with Agilent 2200 TapeStation, followed by deep sequencing on the Illumina HiSeq-2000 genome analyzer with 50 bp SE parameters. Differential methylation of CpGs was determined by the methylKit software (Akalin et al., 2012). A cut-off of $q < 0.05$ was used to define differentially methylation CpGs (DMCs). A slight window approach was used to call differentially methylated regions (DMRs), similar to the previously described method (Russler-Germain et al., 2014). Adjacent Cs within 300 bp apart were merged to form genomic regions and genomic regions < 400 bp were discarded. For the rest, we determined the % of hypo- or hyper-Cs within the regions. If a region contained at least 10 Cs and at least 20% of its Cs exhibited hypo- or hyper-methylation, we performed paired t-test to compute the statistics of methylation difference between samples. At the end, a cutoff of p value < 0.0005 was used to define DMRs. The overlapping of DMRs with genomic features was computed by treating DMRs as ChIP-Seq peaks. The sequencing and mapping information of eRRBS studies is provided in the following list.

eRRBS Sample	Total Read #	Mapped Read #	Unique CpGs
EV-RAS	511,071,807	328,254,404	17,169,526
RH-RAS	493,228,644	324,267,522	16,635,379
WT-RAS	523,165,129	320,339,494	16,190,740

Motif Analysis of DMCs

For enrichment of transcription factor binding motifs, 50-bp sequences centered on individual CpGs were used for predicting transcription factor binding sites presented in the Jaspar database (vertebrate TFs only) (Mathelier et al., 2014) by the software FIMO with default parameter (Grant et al., 2011). The number of Cs matching to a TF in all Cs tested by eRRBS and the corresponding numbers in DMCs were compared by Chi-square test for significant difference.

Analysis of Human Methylome Data and Cross-Comparisons with Mouse eRRBS Data

Human AML patient DNA methylation data are downloaded from The Cancer Genome Atlas (TCGA)

(http://cancergenome.nih.gov/cancersselected/acutemyeloidleukemia). To compare DNA methylation data between human cancer samples and our mouse data, we used the tool liftover from the UCSC genome browser to find the conserved mouse regions of each individual probe (extended to 100 bp) on the Infinium HumanMethylation450 BeadChip platform used in the human/TCGA study. Conserved regions smaller than 150 bp in the mouse genome were kept and the average methylation level of CpGs in the regions were used to compare the human and mouse methylation. In addition, the conserved regions were intersected with mouse DMRs. For a gene having hypo-DMRs identified among murine HSPCs post transduction of RH-RAS relative to EV-RAS and among human normal-karyotype (NK) AML patients carrying R882-mutated *DNMT3A* relative to WT *DNMT3A* ones, we consider the gene with a common DMR in both human and mouse data sets.

Bisulfite Sequencing

Genomic DNA was extracted using DNeasy Blood & Tissue Kit (Qiagen) and bisulfite-conversion carried out using EZ DNA methylation gold kit (Zymo Research) according to manufacturer's instructions. Purified DNA (50 ng) was used as template for PCRs with region-specific primers designed by Methprimer software (Li and Dahiya, 2002). PCR product was gel purified and cloned into pCR4-TOPO vector (Invitrogen), followed by transformation and mini-preps. Plasmids isolated from at least 10 colonies for each sample were sequenced. The detailed primer sequences for bisulfite sequencing are provided in the following list.

Gene	Location	Forward	Reverse
Meis1	intron 6	TTTTGGAGTTTAAATTGTTTAGATT	AAATCCCCTAACCATACCTAATAAC
Hoxa7	promoter	GGGGATTTTGAATTTTTTTAGTTTT	TAACTAAACCAACAACCTCCCTTAC
Mn1	exon 1	GGTTAGGGTTTTGGTTTAGAGGTAGACCCCCACTTTAAAAACAACTTC	

Chromosome Conformation Capture (3C) Followed by qPCR

3C DNA samples were prepared as described previously (Hagege et al., 2007). Briefly, 10 millions cells were cross-linked with 2% formaldehyde for 5 min at room temperature followed by quench in 0.125 M glycine for 5 min. Cells were then washed with ice-cold PBS and lysed in 3C lysis buffer (10 mM Tris-HCl, pH 8.0; 10 mM NaCl; 0.2% NP-40; and 1X Roche Complete Protease Inhibitor Cocktail) for 30 min at 4°C. Nuclei were pelleted by centrifugation at 1000 × g and digested with 600U of high concentration BglII (New England Biolabs) in 1× NEB buffer 3 plus 0.3% SDS and 1.8% Triton-X at 37°C for overnight. After enzyme inactivation with 1.6% SDS at 65°C, samples were brought up to a final volume of 7 ml in 1× NEB T4 ligase buffer plus 1% Triton-X, and added with 6000U of T4 DNA ligase (New England Biolabs). Samples were incubated at 16°C for 4 hr followed by 30-min incubation at room temperature. After ligation, samples were treated with RNase A and proteinase K, extracted with a phenol-chloroform protocol, and precipitated by ethanol. About 100 ng of 3C DNA sample was used as template with a primer pair (one test primer and the constant primer) for qPCR analysis. For testing *Meis1* enhancer-promoter 'looping' in the RH-RAS LSC cells, we employed a negative control cell line, *HOXA9/MEIS1*-coexpressing AML lines (Wang et al., 2005) that are known to have a repressed endogenous *Meis1* gene locus (Wang et al., 2007; Wang et al., 2009). The qPCR signal was first normalized with that of *Gapdh* for input normalization, followed by a second normalization to that of negative cell control (i.e., cells with a silenced endogenous *Meis1)* for calculating relative crosslinking frequency to demonstrate 'looping' specificity. The detailed primer sequences for 3C-qPCR at *Meis1* locus are provided in the following list.

Primer	Location	Sequence (5' to 3')
P0 (constant)	chr11:18,925,586-18,925,605	CCTTGGTGCAAGGACTCTTC
P1 (test)	chr11:18,900,080-18,900,101	TGTTGTCTCCAAGAATTTCCAA
P2 (test)	chr11:18,900,816-18,900,835	GGCAGAGGAACTTGGAAAAA
P3 (test)	chr11:18,904,495-18,904,514	TGGCTATCCTGGCACTTTCT
P4 (test)	chr11:18,907,527-18,907,545	AAAGTTCCCAGGCCCATTT
P5 (test)	chr11:18,909,825-18,909,844	GACTCTCCCGCTGACACTTC

Whole Exome Sequencing and Data Analysis

Genomic DNA was extracted from bone marrow of murine leukemic and normal mice. Whole-exome captures and 50× sequencing experiments were carried out by Otogenetics (Norcross, GA). The sequencing reads were aligned to mm10 reference genome by using BWA (Li and Durbin, 2009), PCR-produced tag duplicates removed by Picard Tools, and base quality score recalibration and Indel (insert/deletion) realignment using the Genome Analysis Toolkit GATK (McKenna et al., 2010). SNP and Indel discovery and genotyping were performed on all samples simultaneously with GATK Lite 2.3.9 using mm10 reference genome as reference. The called SNP/Indels were further filtered for high-quality variants (total counts ≥ 20, alternate counts ≥ 8). Known SNPs from dbSNP137 and variants present in the normal control samples were removed for identifying tumor-specific variants. Lastly, identified variants matching sequences of transduced human *DNMT3A* or *NRAS* cDNA were discarded. The SNP/Indels were annotated with snpEff v3.6 (Cingolani et al., 2012).

Luciferase Reporter Analysis

pCpGL-CMV/EF1a, a CpG-free, luciferase-containing reporter vector designed for assessing regulatory effects of CpG methylations on the introduced cis-element, was kindly provided by Dr. Rehli (University Hospital Regensburg University Hospital Regensburg, Regensburg, Germany). To specifically assess their putative enhancer activity, the hypo-DMR genomic regions were obtained by genomic PCR followed by cloning into the PstI and SpeI sites of pCpGL-CMV/EF1a vector to replace the CMV enhancer with the hypo-DMR sequences. These generated reporter plasmids were either mock-treated or methylated in vitro with recombinant CpG methyltransferase M.SssI (New England Biolabs) for 4 h at 37°C, followed by plasmid purification with QIAquick PCR Purification Kit (Qiagen). 3 X 10^5 Hela cells were transfected with 1.0 μg of each reporter plasmid and 0.2 μg of pRL-TK Renilla luciferase control reporter using the standard Lipofectamine 2000 transfection protocol (Invitrogen). Triplicate transfections were harvested 36 hr post-transfection. Cell lysates were assayed for firefly and Renilla luciferase activities using the Dual-Luciferase Reporter Assay System (Promega). The firefly luciferase activity for each transfection was normalized to that of Renilla luciferase. Relative luciferase units are generated by normalization to those of Renilla and then to empty vector controls. The detailed primer sequences for cloning of each tested DMR are provided in the following list.

Gene	DMR location	Forward Primer (with PstI site)	Reverse Primer (with SpeI site)
Hoxa7	Upstream	ATCGctgcagGCTCAGAGGCCTGGTGAAAT	ATCGactagtCCAACGCTGTCCCAGAACTA
Meis1	Intron 7	ATCGctgcagTCTATGGCTGGGTTGTGCTG	ATCGactagtTGAAGAAAACGCCTCCTGCT
Meis1	Intron 6	ATCGctgcagTCCTAGGGGTTCACGGTCTT	ATCGactagtCATTAGGTTGTCCCCGCCTT
Runx3	Upstream	ATCGctgcagAGGAGAGCCAGGTGTAGAGG	ATCGactagtGGTTAGACCACAGGCTGGAC
Mycn	Intron 2	ATCGctgcagTGTCTGTGCCTTGACAGCTT	ATCGactagtCCAGTCTGCCCCATGGATTT
Filip1	Intron 1	ATCGctgcagTACACTTGGTCCAGCAAGGC	ATCGactagtGAGGCAAGAGCTGATGCAGA

CRISPR/Cas9-mediated genomic editing of putative enhancers

LentiCas9-Venus and LentiGuide-Crimson plasmids were kindly provided by Drs. Daniel Bauer (Harvard Medical School) and Feng Zhang (MIT and Broad Institute). CRISPR/Cas9-mediated deletion of a specific genomic region was performed as previously described (Canver et al., 2015). Briefly, two sgRNA sequences that specifically target the boundary sequences of a putative *Meis1* enhancer located in intron 6 were designed using an online CRISPR design tool (crispr.mit.edu). Top ranked sgRNAs (with minimal predicted off-targets) at either side of target region (sgRNA-5' or sgRNA-3'; see also a list below) were selected and cloned into a BsmBI site of LentiGuide-Crimson vector. To generate a single vector with tandem sgRNA expression cassette (i.e., sgRNA-5' plus sgRNA-3'), LentiGuide-Crimson carrying sgRNA-5' was first digested with PspXI and XmaI, and then inserted with PspXI/XmaI-digested PCR products (which contain sgRNA-3') amplified by using LentiGuide-Crimson with sgRNA-3' as the template and specific primers (5'-GGCCGGCC-gctcgaggGAGGGCCTATTTCC-3' and 5'-CCGGCCGGcccgggTTGTGGATGAATACTGCCATTT-3'). The detailed sgRNA sequences are provided below.

sgRNA	Position	Target sequence
sgRNA-5'	5' of Meis1 DMR at intron 6	TTAGGTTGTCCCCGCCTTAC
sgRNA-3'	3' of Meis1 DMR at intron 6	AATAGGATTACAGCTTCTAC

Stable LentiCas9-Venus expressing cell lines were produced by infection with LentiCas9-Venus lentivirus, followed by Venus sorting on FACSAria II (BD Biosciences). Lentivirus carrying either the LentiGuide-Crimson empty vector or that with a tandem sgRNA expression cassette was prepared and used for infecting cell lines with stable LentiCas9-Venus expression, followed by sorting of cells expressing both Venus and E2-Crimson 48 hr post-infection. The sorted single cells (200-300 in total) were plated into 96-well plates. After growth for 1-2 weeks, single-cell colonies carrying the desired CRISPR/cas9-induced genomic targeting/deletion were first screened out by PCR using primer pairs either flanking or located within target genomic region (which serves positive or negative selection primers), and further confirmed by direct sequencing of genomic PCR products flanking target genomic region. The detailed genotyping PCR primer sequences are provided below.

Primer Location	Forward Primer	Reverse Primer	Product Size
Within DMR	GTTCCCAGGCCCATTTGAGA	CACTACCGGATGTCGCCTTT	579 bp
Outside of DMR	ACCCACTGCTGGTTGTATCC	AAGACACCGAGGTTGCCATT	~ 382 bp

Compound Treatment

SGC0946 and other used compounds in the study was kindly provided by Drs. Matthieu Schapira and Cheryl Arrowsmith at Structural Genomics Consortium (SGC) in Toronto and used as described before (Yu et al., 2012).

shRNA Knockdown

The pLKO.1 lentiviral shRNA plasmids for *Dot1l* knockdown were obtained from Sigma. Lentivirus production and infection was performed using provider's protocols. An $LSC^{RH\text{-}RAS}$ cell line (#1) generated using a puromycin-free MSCV vector similar to the one shown in Figure S1A was used for *Dot1l* knockdown. Stable shRNA-expressing cell lines were established by puromycin (1-2 μg/mL) selection. The detailed target sequences for *Dot1l*-specific shRNAs are provided below.

shRNA	Clone ID	Target sequence	Vector
shDot1l #1	TRCN0000125102	CGGCAGAATCGTATCCTCAAA	pLKO.1
shDot1l #2	TRCN0000125100	GCTGACCTACAATGACCTGAT	pLKO.1

The lentivirus-based shRNA plasmids for knocking down *Meis1* or *Mn1* were generated by cloning a 19-mer shRNA sequence into HpaI and XhoI sites in LentiLox 5.0 vector (kind gift from Dr. James Bear, UNC at Chapel Hill). Stable shRNA-expressing cell lines were obtained by GFP sorting on FACSAria II (BD Biosciences). The detailed target sequences for *Meis1* or *Mn1*-specific shRNAs are provided below.

shRNA	Target sequence	Vector	Reference
shMeis1 #1	GGATAACAGCAGTGAGCAA	LentiLox 5.0	(Kumar et al., 2009)
shMeis1 #2	GCGTGGCATCTTTCCCAAA	LentiLox 5.0	
shMn1 #1	GGTACATGCCACCTGACAA	LentiLox 5.0	
shMn1 #2	GCTTGAACATGGAGCCCTA	LentiLox 5.0	

Supplemental References

Abdel-Wahab, O., Adli, M., LaFave, L. M., Gao, J., Hricik, T., Shih, A. H., Pandey, S., Patel, J. P., Chung, Y. R., Koche, R.*,* et al*.* (2012). ASXL1 mutations promote myeloid transformation through loss of PRC2-mediated gene repression. Cancer cell *22*, 180-193.

Akalin, A., Kormaksson, M., Li, S., Garrett-Bakelman, F. E., Figueroa, M. E., Melnick, A., and Mason, C. E. (2012). methylKit: a comprehensive R package for the analysis of genome-wide DNA methylation profiles. Genome Biol *13*, R87.

Bock, C., Beerman, I., Lien, W. H., Smith, Z. D., Gu, H., Boyle, P., Gnirke, A., Fuchs, E., Rossi, D. J., and Meissner, A. (2012). DNA methylation dynamics during in vivo differentiation of blood and skin stem cells. Molecular cell *47*, 633-647.

Canver, M. C., Smith, E. C., Sher, F., Pinello, L., Sanjana, N. E., Shalem, O., Chen, D. D., Schupp, P. G., Vinjamur, D. S., Garcia, S. P.*,* et al*.* (2015). BCL11A enhancer dissection by Cas9-mediated in situ saturating mutagenesis. Nature *527*, 192-197.

Chambers, S. M., Boles, N. C., Lin, K. Y., Tierney, M. P., Bowman, T. V., Bradfute, S. B., Chen, A. J., Merchant, A. A., Sirin, O., Weksberg, D. C.*,.* (2007). Hematopoietic fingerprints: an expression database of stem cells and their progeny. Cell stem cell *1*, 578-591.

Cingolani, P., Platts, A., Wang le, L., Coon, M., Nguyen, T., Wang, L., Land, S. J., Lu, X., and Ruden, D. M. (2012). A program for annotating and predicting the effects of single nucleotide polymorphisms, SnpEff: SNPs in the genome of Drosophila melanogaster strain w1118; iso-2; iso-3. Fly *6*, 80-92.

Deshpande, A. J., Chen, L., Fazio, M., Sinha, A. U., Bernt, K. M., Banka, D., Dias, S., Chang, J., Olhava, E. J., Daigle, S. R.*,* et al*.* (2013). Leukemic transformation by the MLL-AF6 fusion oncogene requires the H3K79 methyltransferase Dot1l. Blood *121*, 2533-2541.

Fujino, T., Yamazaki, Y., Largaespada, D. A., Jenkins, N. A., Copeland, N. G., Hirokawa, K., and Nakamura, T. (2001). Inhibition of myeloid differentiation by Hoxa9, Hoxb8, and Meis homeobox genes. Exp Hematol *29*, 856-863.

Garrett-Bakelman, F. E., Sheridan, C. K., Kacmarczyk, T. J., Ishii, J., Betel, D., Alonso, A., Mason, C. E., Figueroa, M. E., and Melnick, A. M. (2015). Enhanced reduced representation bisulfite sequencing for assessment of DNA methylation at base pair resolution. J Vis Exp, e52246.

Goldberg, A. D., Banaszynski, L. A., Noh, K. M., Lewis, P. W., Elsaesser, S. J., Stadler, S., Dewell, S., Law, M., Guo, X., Li, X.*,* et al*.* (2010). Distinct factors control histone variant H3.3 localization at specific genomic regions. Cell *140*, 678-691.

Grant, C. E., Bailey, T. L., and Noble, W. S. (2011). FIMO: scanning for occurrences of a given motif. Bioinformatics *27*, 1017-1018.

Hagege, H., Klous, P., Braem, C., Splinter, E., Dekker, J., Cathala, G., de Laat, W., and Forne, T. (2007). Quantitative analysis of chromosome conformation capture assays (3C-qPCR). Nature protocols *2*, 1722-1733.

Irizarry, R. A., Hobbs, B., Collin, F., Beazer-Barclay, Y. D., Antonellis, K. J., Scherf, U., and Speed, T. P. (2003). Exploration, normalization, and summaries of high density oligonucleotide array probe level data. Biostatistics *4*, 249-264.

Ji, H., Ehrlich, L. I., Seita, J., Murakami, P., Doi, A., Lindau, P., Lee, H., Aryee, M. J., Irizarry, R. A., Kim, K., et al. (2010). Comprehensive methylome map of lineage commitment from haematopoietic progenitors. Nature *467*, 338-342.

Kamps, M. P., Look, A. T., and Baltimore, D. (1991). The human t(1;19) translocation in pre-B ALL produces multiple nuclear E2A-Pbx1 fusion proteins with differing transforming potentials. Genes & development *5*, 358-368.

Konuma, T., Nakamura, S., Miyagi, S., Negishi, M., Chiba, T., Oguro, H., Yuan, J., Mochizuki-Kashio, M., Ichikawa, H., Miyoshi, H., et al. (2011). Forced expression of the histone demethylase Fbxl10 maintains self-renewing hematopoietic stem cells. Exp Hematol *39*, 697-709 e695.

Kumar, A. R., Li, Q., Hudson, W. A., Chen, W., Sam, T., Yao, Q., Lund, E. A., Wu, B., Kowal, B. J., and Kersey, J. H. (2009). A role for MEIS1 in MLL-fusion gene leukemia. Blood *113*, 1756-1758.

Lee, T. I., Johnstone, S. E., and Young, R. A. (2006). Chromatin immunoprecipitation and microarray-based analysis of protein location. Nature protocols *1*, 729-748.

Li, H., and Durbin, R. (2009). Fast and accurate short read alignment with Burrows-Wheeler transform. Bioinformatics *25*, 1754-1760.

Li, L. C., and Dahiya, R. (2002). MethPrimer: designing primers for methylation PCRs. Bioinformatics *18*, 1427-1431.

Lo, M. C., Peterson, L. F., Yan, M., Cong, X., Jin, F., Shia, W. J., Matsuura, S., Ahn, E. Y., Komeno, Y., Ly, M., et al. (2012). Combined gene expression and DNA occupancy profiling identifies potential therapeutic targets of t(8;21) AML. Blood *120*, 1473-1484.

Mathelier, A., Zhao, X., Zhang, A. W., Parcy, F., Worsley-Hunt, R., Arenillas, D. J., Buchman, S., Chen, C. Y., Chou, A., Ienasescu, H., et al. (2014). JASPAR 2014: an extensively expanded and updated open-access database of transcription factor binding profiles. Nucleic acids research *42*, D142-147.

McKenna, A., Hanna, M., Banks, E., Sivachenko, A., Cibulskis, K., Kernytsky, A., Garimella, K., Altshuler, D., Gabriel, S., Daly, M., and DePristo, M. A. (2010). The Genome Analysis Toolkit: a MapReduce framework for analyzing next-generation DNA sequencing data. Genome research *20*, 1297-1303.

McLean, C. Y., Bristor, D., Hiller, M., Clarke, S. L., Schaar, B. T., Lowe, C. B., Wenger, A. M., and Bejerano, G. (2010). GREAT improves functional interpretation of cis-regulatory regions. Nature biotechnology *28*, 495-501.

Reich, M., Liefeld, T., Gould, J., Lerner, J., Tamayo, P., and Mesirov, J. P. (2006). GenePattern 2.0. Nature genetics *38*, 500-501.

Subramanian, A., Tamayo, P., Mootha, V. K., Mukherjee, S., Ebert, B. L., Gillette, M. A., Paulovich, A., Pomeroy, S. L., Golub, T. R., Lander, E. S., and Mesirov, J. P. (2005). Gene set enrichment analysis: a knowledge-based approach for interpreting genome-wide expression profiles. Proceedings of the National Academy of Sciences of the United States of America *102*, 15545-15550.

Tiacci, E., Spanhol-Rosseto, A., Martelli, M. P., Pasqualucci, L., Quentmeier, H., Grossmann, V., Drexler, H. G., and Falini, B. (2012). The NPM1 wild-type OCI-AML2 and the NPM1-mutated OCI-AML3 cell lines carry DNMT3A mutations. Leukemia *26*, 554-557.

Wang, G. G., Calvo, K. R., Pasillas, M. P., Sykes, D. B., Hacker, H., and Kamps, M. P. (2006). Quantitative production of macrophages or neutrophils ex vivo using conditional Hoxb8. Nature methods *3*, 287-293.

Wang, J., Liu, Y., Li, Z., Wang, Z., Tan, L. X., Ryu, M. J., Meline, B., Du, J., Young, K. H., Ranheim, E.*,* et al*.* (2011). Endogenous oncogenic Nras mutation initiates hematopoietic malignancies in a dose- and cell type-dependent manner. Blood *118*, 368-379.

Xu, B., On, D. M., Ma, A., Parton, T., Konze, K. D., Pattenden, S. G., Allison, D. F., Cai, L., Rockowitz, S., Liu, S.*,* et al*.* (2015). Selective inhibition of EZH2 and EZH1 enzymatic activity by a small molecule suppresses MLL-rearranged leukemia. Blood *125*, 346-357.

Yu, W., Chory, E. J., Wernimont, A. K., Tempel, W., Scopton, A., Federation, A., Marineau, J. J., Qi, J., Barsyte-Lovejoy, D., Yi, J.*,* et al*.* (2012). Catalytic site remodelling of the DOT1L methyltransferase by selective inhibitors. Nat Commun *3*, 1288.

Zhang, Y., Liu, T., Meyer, C. A., Eeckhoute, J., Johnson, D. S., Bernstein, B. E., Nusbaum, C., Myers, R. M., Brown, M., Li, W., and Liu, X. S. (2008). Model-based analysis of ChIP-Seq (MACS). Genome Biol *9*, R137.

Regular Article

MYELOID NEOPLASIA

Selective inhibition of EZH2 and EZH1 enzymatic activity by a small molecule suppresses *MLL*-rearranged leukemia

Bowen Xu,[1,2] Doan M. On,[1,2] Anqi Ma,[3] Trevor Parton,[2] Kyle D. Konze,[3] Samantha G. Pattenden,[4] David F. Allison,[1,2] Ling Cai,[1,2] Shira Rockowitz,[5,6] Shichong Liu,[7] Ying Liu,[8] Fengling Li,[9] Masoud Vedadi,[9] Stephen V. Frye,[2,4] Benjamin A. Garcia,[7] Deyou Zheng,[5,6] Jian Jin,[3] and Gang Greg Wang[1,2]

[1]Department of Biochemistry and Biophysics, and [2]Lineberger Comprehensive Cancer Center, University of North Carolina at Chapel Hill, Chapel Hill, NC; [3]Department of Structural and Chemical Biology, Icahn School of Medicine at Mount Sinai, New York, NY; [4]Center for Integrative Chemical Biology and Drug Discovery, University of North Carolina at Chapel Hill, Chapel Hill, NC; [5]Department of Genetics, and [6]Departments of Neurology and Neuroscience, Albert Einstein College of Medicine, Bronx, NY; [7]Epigenetics Program, Department of Biochemistry and Biophysics, Perelman School of Medicine, University of Pennsylvania, Philadelphia, PA; [8]Ansary Stem Cell Institute and Department of Genetic Medicine, Weill Cornell Medical College, New York, NY; and [9]Structural Genomics Consortium, University of Toronto, Toronto, ON, Canada

Key Points

- We characterize active vs inactive analog compounds suitable for inhibition of both PRC2-EZH2 and PRC2-EZH1 ex vivo and in vivo.
- This study is the first to show oral delivery of an EZH2 and EZH1 dual inhibitor as promising therapeutics for *MLL*-rearranged leukemia.

Enhancer of zeste homolog 2 (EZH2) and related EZH1 control gene expression and promote tumorigenesis via methylating histone H3 at lysine 27 (H3K27). These methyltransferases are ideal therapeutic targets due to their frequent hyperactive mutations and overexpression found in cancer, including hematopoietic malignancies. Here, we characterized a set of small molecules that allow pharmacologic manipulation of EZH2 and EZH1, which include UNC1999, a selective inhibitor of both enzymes, and UNC2400, an inactive analog compound useful for assessment of off-target effect. UNC1999 suppresses global H3K27 trimethylation/dimethylation (H3K27me3/2) and inhibits growth of mixed lineage leukemia (*MLL*)–rearranged leukemia cells. UNC1999-induced transcriptome alterations overlap those following knockdown of embryonic ectoderm development, a common cofactor of EZH2 and EZH1, demonstrating UNC1999's on-target inhibition. Mechanistically, UNC1999 preferentially affects distal regulatory elements such as enhancers, leading to derepression of polycomb targets including *Cdkn2a*. Gene derepression correlates with a decrease in H3K27me3 and concurrent gain in H3K27 acetylation. UNC2400 does not induce such effects. Oral administration of UNC1999 prolongs survival of a well-defined murine leukemia model bearing *MLL-AF9*. Collectively, our study provides the detailed profiling for a set of chemicals to manipulate EZH2 and EZH1 and establishes specific enzymatic inhibition of polycomb repressive complex 2 (PRC2)–EZH2 and PRC2-EZH1 by small-molecule compounds as a novel therapeutics for *MLL*-rearranged leukemia. (*Blood*. 2015;125(2):346-357)

Introduction

Covalent histone modification provides a fundamental means to control gene expression and define cellular identities.[1-3] Dysregulation of histone modification represents a central oncogenic pathway in human cancers.[1,3,4] As the regulatory factors involved in the installation, removal, or recognition of histone modification (often termed as epigenetic "writers," "erasers," and "readers"[1]) are increasingly considered to be "druggable,"[5-7] development of epigenetic modulators holds promise for novel therapeutic interventions.[7,8]

Polycomb repressive complex 2 (PRC2), the sole enzymatic machinery that uses either enhancer of zeste homolog 2 (EZH2) or related EZH1 as a catalytic subunit to induce trimethylation of histone H3 at lysine 27 (H3K27me3), has been shown to play critical roles in gene silencing[9] and in hematopoietic lineage specification at various developmental stages.[10-13] Extensive evidence has linked PRC2 deregulation to malignant hematopoiesis. Recurrent *EZH2* gain-of-function mutations were found in germinal center B-cell lymphoma patients,[14,15] and constitutive expression of wild-type or lymphoma-associated mutant *EZH2* in hematopoietic lineages induced myeloproliferative diseases[16] and lymphomagenesis,[13,17] respectively, in murine models. Furthermore, EZH1 compensates the function of EZH2[9,18] and emerges as regulator of myeloid neoplasms.[19,20] Inhibitors selective to EZH2 have recently been developed and shown to be effective in killing lymphoma cells with *EZH2* mutation,[21-23] however, these inhibitors demonstrated minimal effects on proliferation or gene transcription among lymphomas carrying the wild-type EZH2[21,22,24] and are expected to be ineffective for tumors that rely on both wild-type EZH2 and EZH1.

Submitted June 9, 2014; accepted November 3, 2014. Prepublished online as *Blood* First Edition paper, November 13, 2014; DOI 10.1182/blood-2014-06-581082.

B.X., D.M.O., and A.M. contributed equally to this study.

The ChIP-seq data reported in this article have been deposited in the Gene Expression Omnibus database (accession number GSE62437). The microarray data reported in this article have been deposited in the Gene Expression Omnibus database (accession number GSE62198).

The online version of this article contains a data supplement.

The publication costs of this article were defrayed in part by page charge payment. Therefore, and solely to indicate this fact, this article is hereby marked "advertisement" in accordance with 18 USC section 1734.

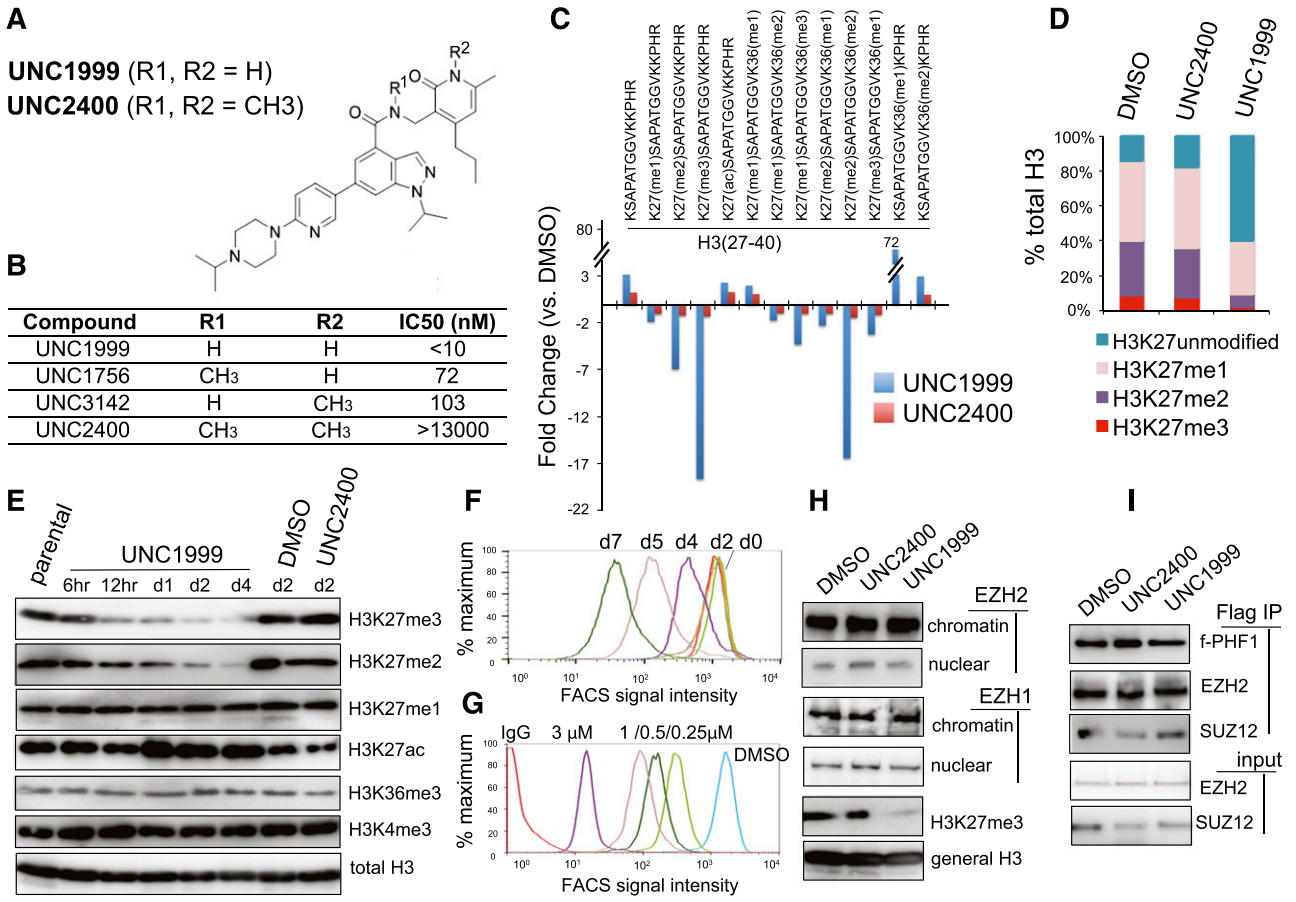

Compound	R1	R2	IC50 (nM)
UNC1999	H	H	<10
UNC1756	CH_3	H	72
UNC3142	H	CH_3	103
UNC2400	CH_3	CH_3	>13000

Figure 1. A small-molecule UNC1999, and not its inactive analog UNC2400, selectively and potently suppresses H3K27 methylation. (A) Chemical structure of UNC1999 and UNC2400, with the positions R1 and R2 modified with 2 N-methyl groups (CH_3) in UNC2400. (B) Summary of modification at R1 and R2 in UNC1999 and derivatives, and their IC_{50} measured by in vitro methyltransferase assay. (C) Quantitative mass spectrometry analysis detects the change in relative abundance of various peptide species covering histone H3 amino acids 27-40 after treatment with 3 μM UNC1999 (blue) or UNC2400 (red) for 4 days. Y-axis represents fold-change in relative abundances normalized to DMSO-treated samples; the sequence and modification of H3 peptide are shown on top. (D) Overall percentages of histone H3 with the lysine 27 either unmodified, monomethylated, dimethylated, or trimethylated (H3K27me1/2/3) following compound treatments. (E) Immunoblot of the indicated histone modifications in *MLL-AF9*–transformed leukemia progenitor cells after treatment with DMSO, or 3 μM UNC1999 or UNC2400. (F-G) Flow cytometry with H3K27me3-specific antibodies revealing time-dependent (F, 2 μM UNC1999) and dose-dependent suppression of H3K27me3 by UNC1999 (G, 7-day treatment) in *MLL-AF9*–transformed murine leukemia cells and *EOL-1* human leukemia cells, respectively. DMSO and nonspecific IgG are used as control. (H) Immunoblots detecting the chromatin-bound and nucleoplasmic fraction of EZH2 or EZH1 after treatment with 2 μM of the indicated compounds for 5 days. (I) Co-IP of PRC2 complex components following Flag IP with extracts of a Flag-PHF1 stable expression cell line[34] in the presence of 2 μM of the indicated compounds. ac, acetylation; Co-IP, coimmunoprecipitation; FACS, fluorescence-activated cell sorter; Ig, immunoglobulin; IP, immunoprecipitation; me1/2/3, mono/di/trimethylation.

Recently, we have discovered a series of small-molecule compounds for specific targeting of both EZH2 and EZH1, including UNC1999, an EZH2 and EZH1 dual inhibitor, and UNC2400, an inactive analog compound useful for assessment of off-target effect.[25] Here, we characterized molecular and cellular effects by these translational tools and aim to establish novel therapeutics for cancer types that rely on PRC2-EZH2 and PRC2-EZH1 both. We choose to focus on leukemia bearing chromosomal rearrangement of mixed lineage leukemia (*MLL*), a gene encoding histone H3 lysine 4 (H3K4)–specific methyltransferase.[1,26] *MLL* rearrangements are responsible for ~70% of infant acute myeloid or lymphoid leukemia and ~7% to 10% of adult cases,[26] and leukemia with *MLL* rearrangement displays poor prognosis with low survival rates, highlighting a special need for new interventions.[27,28] Oncoproteins produced by *MLL* rearrangements inappropriately recruit epigenetic factors and/or transcriptional elongation machineries to enforce abnormal gene expression.[1,26-28] Recent studies show that PRC2 acts in parallel with *MLL* rearrangements by controlling a distinctive gene program to sustain leukemogenicity.[19,20,29] Specifically, EZH2 and EZH1 compensate one another to promote acute leukemogenesis, and genetic disruption of both enzymes was required to inhibit growth of leukemia carrying *MLL-AF9*, a common form of *MLL* rearrangements.[19,20] Therefore, chemical agents that can target both PRC2-EZH2 and PRC2-EZH1 shall represent a new way for treating *MLL*-rearranged leukemia.

In this study, we use a series of proteomics, genomics, and tumorigenic assays to profile the effects of our unique EZH2 and EZH1 dual inhibitor, UNC1999, and its inactive analog, UNC2400, among *MLL*-rearranged leukemia. UNC1999, and not UNC2400, specifically suppressed H3K27me3/2 and induced a range of anti-leukemia effects including anti-proliferation, differentiation, and apoptosis. The UNC1999-responsive gene signatures include *Cdkn2a* and developmental genes, and significantly overlapped those induced by knockdown of EED, an essential subunit of PRC2-EZH2 and PRC2-EZH1. Mechanistically, we unveiled preferential "erasure" of H3K27me3 associated with distal regulatory elements such as enhancers following UNC1999 treatment, whereas H3K27me3 peaks at proximal promoters are largely retained,

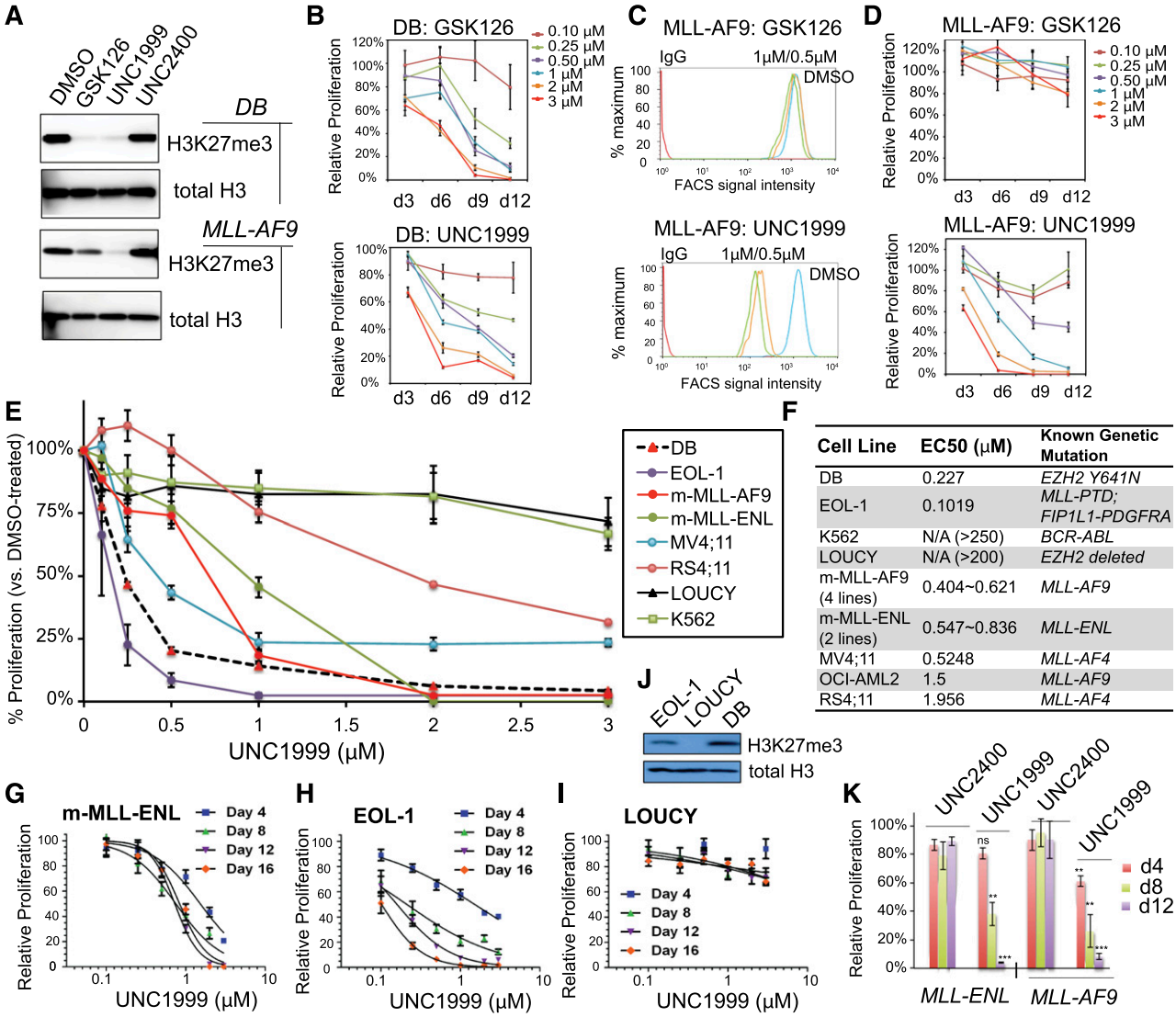

Cell Line	EC50 (μM)	Known Genetic Mutation
DB	0.227	*EZH2 Y641N*
EOL-1	0.1019	*MLL-PTD; FIP1L1-PDGFRA*
K562	N/A (>250)	*BCR-ABL*
LOUCY	N/A (>200)	*EZH2 deleted*
m-MLL-AF9 (4 lines)	0.404~0.621	*MLL-AF9*
m-MLL-ENL (2 lines)	0.547~0.836	*MLL-ENL*
MV4;11	0.5248	*MLL-AF4*
OCI-AML2	1.5	*MLL-AF9*
RS4;11	1.956	*MLL-AF4*

Figure 2. UNC1999, but not GSK126, efficiently suppresses H3K27me3 in *MLL*-rearranged leukemia cells and inhibits their growth. (A) Immunoblots of the global H3K27me3 level after treatment of *DB* lymphoma cells (top) or *MLL-AF9*–transformed murine leukemia progenitors (bottom) with 2 μM of the indicated compounds for 5 days. General H3 serves as control. (B) Relative proliferation of *DB* cells treated with a range of concentrations of GSK126 (top) or UNC1999 (bottom) for the indicated duration. Y-axis represents the relative percentage of accumulative cell numbers normalized to DMSO treatment, and is presented as the mean of triplicates ± SD. (C) Flow cytometry analysis of H3K27me3 in *MLL-AF9*–transformed murine leukemia progenitors following treatment with various concentrations of GSK126 (top) or UNC1999 (bottom) for 4 days. DMSO serves as control. (D) Relative proliferation of *MLL-AF9*–transformed leukemia progenitors treated with a range of concentrations of GSK126 (top) or UNC1999 (bottom) for the indicated duration. Y-axis represents the relative percentage of cell numbers after normalization to DMSO treatment, and is presented as the mean of triplicates ± SD. (E) Relative proliferation of a panel of leukemia or lymphoma cell lines treated with various concentrations of UNC1999 for 16 days. Y-axis, presented as the mean of triplicates ± SD, represents the relative percentage of accumulative cell numbers after normalization to DMSO treatment. Shown as a dashed line is *DB*, an *EZH2*-mutated (Y641N) lymphoma line known to be sensitive to EZH2 inhibition.[22] (F) Summary of EC_{50} of a panel of cell lines in response to UNC1999. m-MLL-AF9 and m-MLL-ENL represent murine leukemia lines established by *MLL-AF9* and *MLL-ENL*, respectively. (G-I) Relative proliferation of murine *MLL-ENL*–bearing leukemia cells (G) and *EOL-1* (H) and *LOUCY* (I) human leukemia cells treated with a range of UNC1999 concentrations for the indicated duration. Y-axis represents relative percentage of accumulative cell numbers after normalization to DMSO treatment, and is presented as the mean of triplicates ± SD. (J) Immunoblot of H3K27me3 and general H3 in *EOL-1*, *LOUCY*, and *DB* cells. (K) Relative proliferation of murine leukemia cells bearing *MLL-AF9* or *MLL-ENL* after treatment with UNC1999 or UNC2400 and normalization to DMSO treatment. **P* < .05; ***P* < .01; ****P* < .001; ns, not significant.

despite a shrinking in their average peak size. Gene derepression correlates with decrease in H3K27me3 and concurrent gain in H3K27 acetylation (H3K27ac). None of these effects were seen following UNC2400 treatment, further verifying on-target effect by UNC1999. *Cdkn2a* is a crucial mediator for UNC1999-induced growth inhibition. Importantly, oral dosing of UNC1999 prolongs survival of *MLL-AF9*–induced murine leukemia models. Thus, our study provides a detailed characterization of a pair of small-molecule compounds available to the community for studying EZH2 and EZH1 in health and disease. This study also represents the first one to establish chemical inhibition of both EZH2 and EZH1 as a promising therapeutics for *MLL*-rearranged leukemia.

Methods

Compound synthesis and usage

UNC1999 and UNC2400 were synthesized as previously described.[25] Synthesis of UNC1756 and UNC3142 is described in supplemental Materials

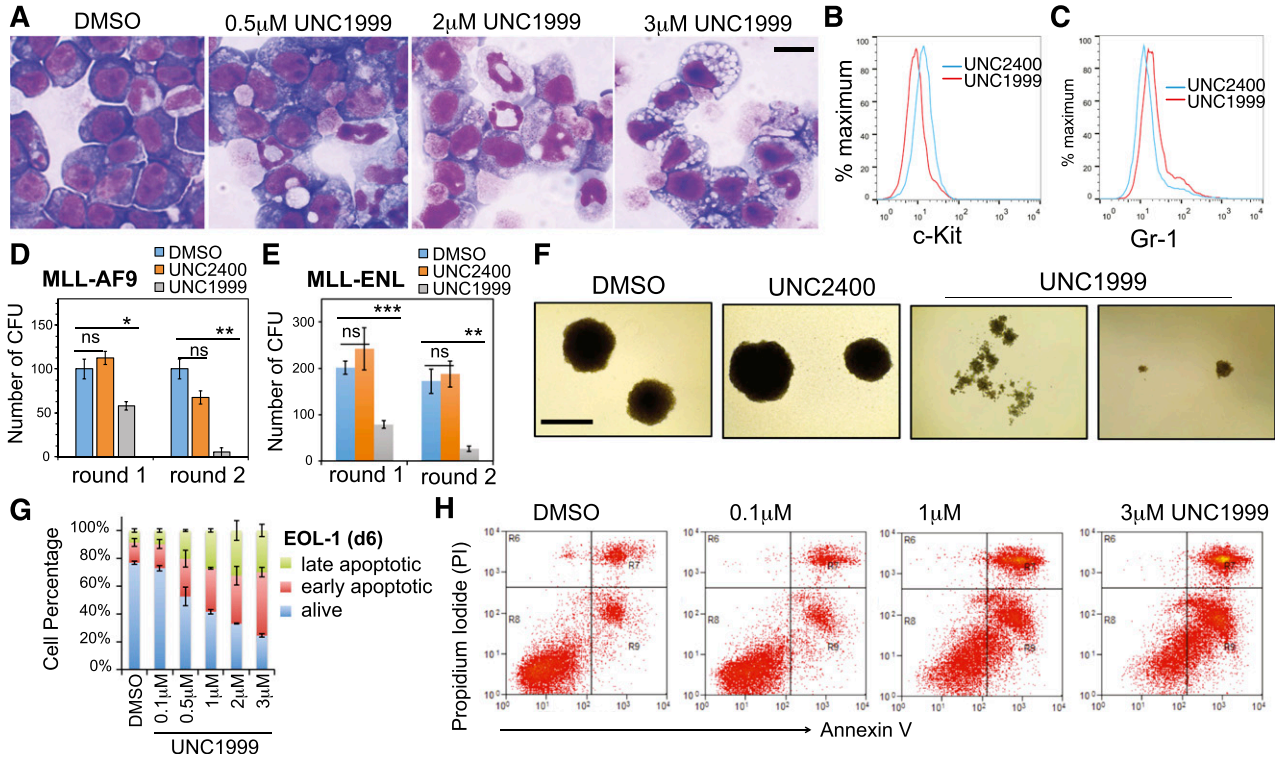

Figure 3. UNC1999, and not UNC2400, promotes differentiation, suppresses colony formation, and induces apoptosis of *MLL*-rearranged leukemia cells. (A) Representative light micrographs show Wright-Giemsa staining of *MLL-AF9*–transformed leukemic progenitors after treatment with the indicated concentration of UNC1999 for 8 days. Black bar, 10 μm. (B-C) Flow cytometry analysis of c-Kit and Gr-1 after treatment with 3 μM of the indicated compounds for 8 days. (D-E) Quantification of colony-forming units from *MLL-AF9*– (D) or *MLL-ENL*–transformed leukemia progenitors (E) after serial replating into the cytokine-rich, methylcellulose medium containing DMSO or 3 μM UNC2400 or UNC1999. Data are shown as the mean ± SD of experiments in duplicate. *$P < .05$; **$P < .01$; ***$P < .001$. (F) Light micrographs show typical morphology of the single-cell colonies derived from *MLL-AF9*–transformed leukemia progenitors following serial replating in the presence of DMSO or 3 μM UNC2400 or UNC1999. Black bar, 1 mm. (G) Percentage of live and apoptotic subpopulations of *EOL-1* leukemia cells after the indicated compound treatments for 6 days. (H) Typical profiles of staining with PI and annexin V after treatment of *EOL-1* cells with DMSO or the indicated concentration of UNC1999 for 6 days. PI, propidium iodide.

(available on the *Blood* Web site). UNC1999 and derivatives were dissolved in dimethylsulfoxide (DMSO) as 5 mM stocks before use.

Mass spectrometry–based quantification

Total histones were prepared and subject to mass spectrometry analysis as previously described.[30]

Purification, culture, and leukemia transformation of primary hematopoietic stem and progenitor cells

Wild-type Balb/C mice and *p16Ink4a*$^{-/-}$;*p19Arf*$^{-/-}$ knockout mice (strain number 01XB2) were purchased from the NCI at Frederick Mouse Repository. Bone marrow isolated from femur and tibia of mice was subject to lineage-negative enrichment, followed by cytokine stimulation and retroviral transduction of oncogenes (*MLL-AF9*) as described.[31,32] Freshly immortalized leukemia progenitor cell lines were generated, characterized, and maintained with the previously described procedures.[31-33] The detailed procedures for flow cytometry, antibody and immunoblot, and various assays of cell proliferation, Wright-Giemsa staining, colony-forming units by serial replating, cell-cycle profiling, and apoptosis are described in supplemental Materials.

Microarray analysis

Total RNA was isolated followed by quantification of the transcript expression levels with Affymetrix GeneChip MOGene_2.1_ST. After RNA hybridization, scanning, and signal quantification (UNC Genomics Core), hybridization signals were retrieved, followed by normalization, differential expression analysis, gene ontology (GO) analysis, gene set enrichment analysis (GSEA), and statistical analysis using GeneSpring Analysis Platform GX12.6 (Agilent Technologies) as described.[34] GSEA was also carried out with the downloaded GSEA software (www.broadinstitute.org/gsea) by exploring the Molecular Signatures Database (www.broadinstitute.org/gsea/msigdb/annotate.jsp).

ChIP followed by deep sequencing

Chromatin samples used for chromatin immunoprecipitation (ChIP) followed by deep sequencing (ChIP-Seq) were prepared using a previously described protocol,[35] followed by antibody enrichment, library generation, and parallel sequencing using an Illumina HiSeq-2000 Sequencer (UNC High-throughput Sequencing Facility) as described before.[36] The detailed procedures of ChIP-Seq data alignment, filtration, peak calling and assignment, and cross-sample comparison and analysis are described in supplemental Materials.

Real-time PCR

The quantitative polymerase chain reaction (qPCR) following reverse transcription (RT-qPCR) or ChIP (ChIP-qPCR) was carried out as previously described.[34] Information on primers used is described in supplemental Table 6.

In vivo leukemogenic assay and compound treatment

MLL-AF9–induced murine leukemia was generated as previously described,[31,32] followed by compound treatment. The powder of UNC1999 (verified by high-performance liquid chromatography and mass spectrometry) was slowly dissolved and incorporated in vehicle (0.5% of sodium carboxymethylcellulose and 0.1% of Tween 80 in sterile water) with continuous trituration by a pestle in a mortar. UNC1999 or vehicle was administered by oral gavage twice daily at a dose of 50 mg/kg. The detailed descriptions of murine leukemia generation, compound usage and delivery, animal care and dissection, and pathological analysis are described in supplemental Materials.

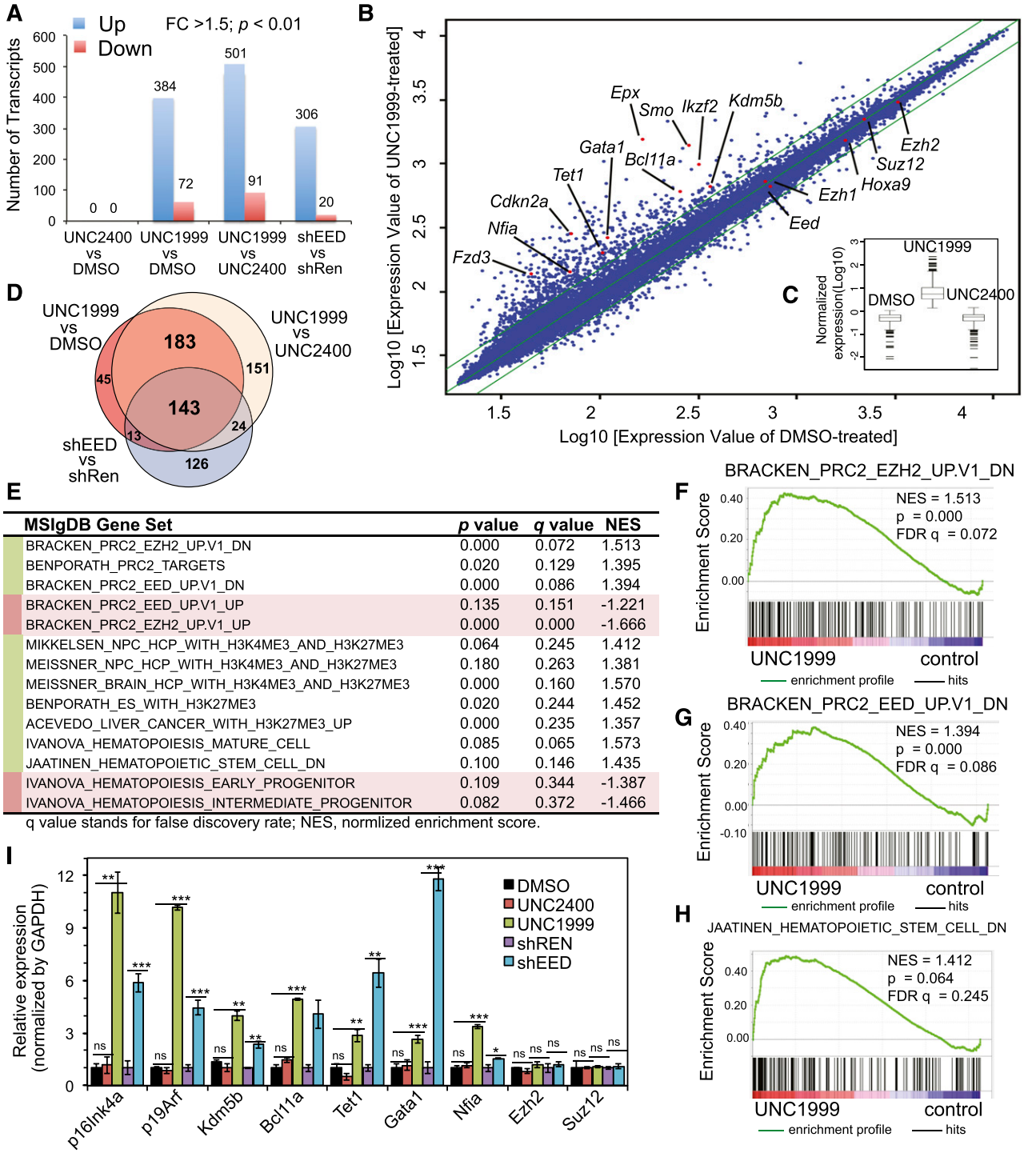

MSIgDB Gene Set	*p* value	*q* value	NES
BRACKEN_PRC2_EZH2_UP.V1_DN	0.000	0.072	1.513
BENPORATH_PRC2_TARGETS	0.020	0.129	1.395
BRACKEN_PRC2_EED_UP.V1_DN	0.000	0.086	1.394
BRACKEN_PRC2_EED_UP.V1_UP	0.135	0.151	-1.221
BRACKEN_PRC2_EZH2_UP.V1_UP	0.000	0.000	-1.666
MIKKELSEN_NPC_HCP_WITH_H3K4ME3_AND_H3K27ME3	0.064	0.245	1.412
MEISSNER_NPC_HCP_WITH_H3K4ME3_AND_H3K27ME3	0.180	0.263	1.381
MEISSNER_BRAIN_HCP_WITH_H3K4ME3_AND_H3K27ME3	0.000	0.160	1.570
BENPORATH_ES_WITH_H3K27ME3	0.020	0.244	1.452
ACEVEDO_LIVER_CANCER_WITH_H3K27ME3_UP	0.000	0.235	1.357
IVANOVA_HEMATOPOIESIS_MATURE_CELL	0.085	0.065	1.573
JAATINEN_HEMATOPOIETIC_STEM_CELL_DN	0.100	0.146	1.435
IVANOVA_HEMATOPOIESIS_EARLY_PROGENITOR	0.109	0.344	-1.387
IVANOVA_HEMATOPOIESIS_INTERMEDIATE_PROGENITOR	0.082	0.372	-1.466

q value stands for false discovery rate; NES, normlized enrichment score.

Figure 4. UNC1999, and not UNC2400, derepresses the PRC2 gene targets. (A) Summary of the upregulated (blue) and downregulated (red) transcripts in 2 independent *MLL-AF9*–transformed leukemia lines after a 5-day treatment with 3 μM of compounds or after knockdown of *EED* vs *Renilla*, as identified by microarray analysis with a cutoff of FC of >1.5 and a *P* value of <.01. (B) Scatter plot to compare the global gene expression pattern in *MLL-AF9*–transformed leukemia cells following DMSO (x-axis) vs UNC1999 treatment (y-axis). Plotted are Log10 values of the signal intensities of all transcripts on gene microarrays after normalization. The flanking lines in green indicate 1.5-fold change in gene expression. (C) Boxplots showing the expression levels of upregulated transcripts in the compound- vs DMSO-treated samples. Y-axis represents the Log10 value of signal intensities detected by microarray. (D) Venn diagram of the upregulated transcripts shown in panel A. (E) Summary of GSEA using the MSIgDB. Green and red indicate the positive and negative correlation to UNC1999-treated cells, respectively. (F-H) GSEA revealing significant enrichment of the EZH2-repressed (F) or EED-repressed gene signatures (G) and those negatively associated with hematopoietic stem cells (H) in the UNC1999- vs DMSO-treated cells. (I) RT-qPCR detects relative expression levels of the indicated genes in *MLL-AF9*–transformed leukemia cells following treatment with 3 μM of compounds or *EED* knockdown (shEED) for 5 days. Y-axis represents fold-change after normalization to *GAPDH* and to control (DMSO treatment or *Renilla* knockdown [shRen]), and error bars represent SD of triplicates. **P* < .05; ***P* < .01; ****P* < .001. FC, fold-change; FDR, false discovery rate; GAPDH, glyceraldehyde-3-phosphate dehydrogenase; MSIgDB, Molecular Signatures Database; NES, normalized enrichment score; Ren, *Renilla*; shEED, shRNA against EED; shREN, shRNA against Renilla.

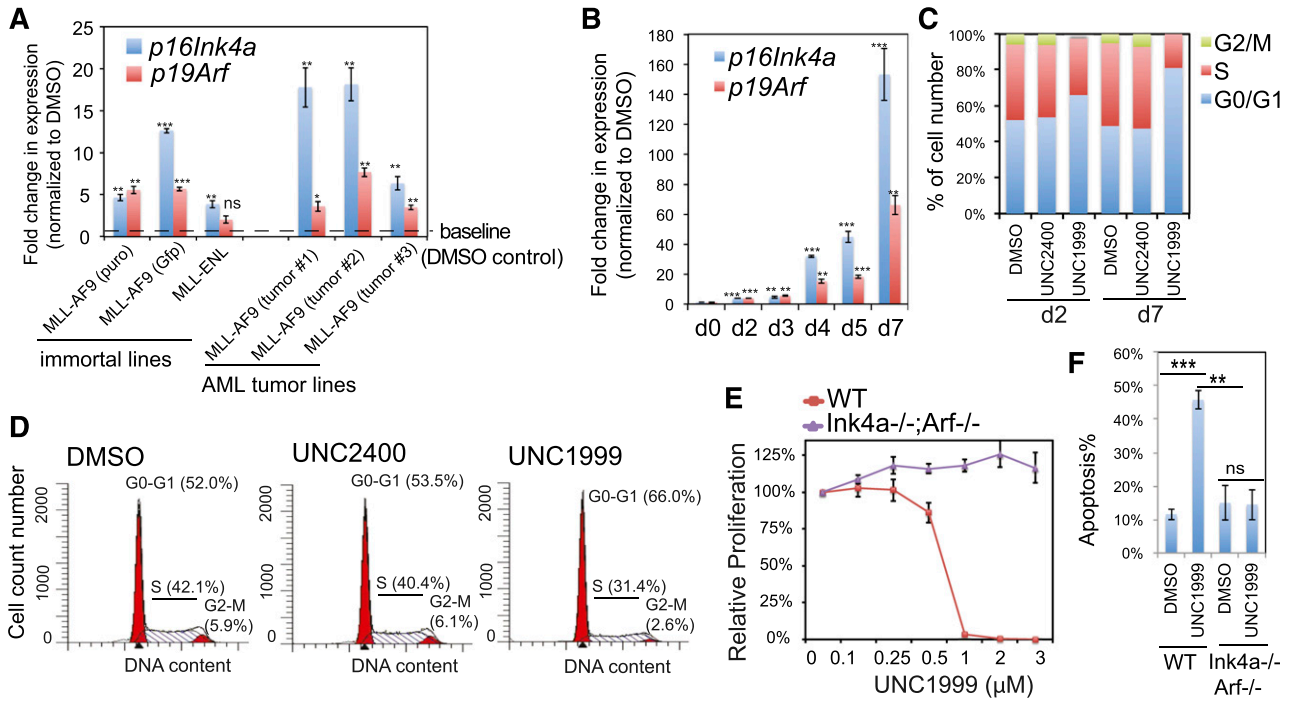

Figure 5. *Cdkn2a* reactivation plays a critical role in UNC1999-mediated growth inhibition. (A) Change in *p16Ink4a* and *p19Arf* gene expression following a 3-day treatment with 3 μM UNC1999 among 6 independent murine leukemia lines, either freshly immortalized by *MLL-AF9* or *MLL-ENL* (left) or derived from *MLL-AF9*–induced primary murine leukemia (right). Y-axis represents fold-change in gene expression after normalization to *GAPDH* and DMSO treatment, and error bars represent SD of triplicates. $^{*}P < .05$; $^{**}P < .01$; $^{***}P < .001$. (B) RT-qPCR shows time-dependent derepression of *p16Ink4a* and *p19Arf* by UNC1999 in a leukemia line derived from *MLL-AF9*–induced primary tumors. $^{*}P < .05$; $^{**}P < .01$; $^{***}P < .001$. (C) Summary of cell-cycle status of *MLL-AF9*–transformed murine leukemia progenitors following 2-day or 7-day treatment with DMSO, or 3 μM UNC2400 or UNC1999. (D) Representative histograms showing DNA contents measured by PI staining of *MLL-AF9*–transformed leukemia cells after treatment with 3 μM of compounds for 2 days. (E) Relative proliferation of *MLL-AF9*–transformed murine leukemia cells, either wild-type (red) or *p16Ink4a*$^{-/-}$/*p19Arf*$^{-/-}$ (purple), after treatment with various concentrations of UNC1999 for 12 days. Y-axis, presented as the mean of triplicates ± SD, represents the relative percentage of cell numbers after normalization to DMSO treatment. (F) Summary of apoptotic induction in *MLL-AF9*–transformed murine leukemia progenitors, either wild-type (WT) or *p16Ink4a/p19Arf*-deficient, following a 6-day treatment with 3 μM of compounds as assayed by PI staining. $^{**}P < .01$; $^{***}P < .005$. WT, wild type.

Statistical analysis

Data are presented as the mean ± standard deviation (SD) for 3 independent experiments unless otherwise noted. Statistical analysis was performed with the Student *t* test, except for nonparametric analysis that used the log-rank (Mantel-Cox) test.

Results

A small-molecule UNC1999, and not its inactive analog UNC2400, selectively and potently suppresses H3K27me3/2

Previously, using an in vitro methyltransferase assay, we have shown that UNC1999 (Figure 1A) exhibits highly selective and potent inhibition of EZH2 and EZH1 over other unrelated methyltransferases with half-maximal inhibitory concentration (IC_{50}) for EZH2 and EZH1 measured at <10 nM (Figure 1B) and 45 nM, respectively.[25] UNC2400, an inactive analog compound (with IC_{50} of >13 000 nM), was generated by modifying UNC1999 with 2 N-methyl groups (Figure 1A-B). Via docking studies with the recently solved apo structure of the EZH2 SET domain,[37,38] we found that the 2 N-methyl modifications presumably disrupt the critical hydrogen bonds formed by UNC1999 with the side-chain carbonyl of *Asn*688 and the N-terminal nitrogen of *His*689 of EZH2 (supplemental Figure 1A). Modifying UNC1999 with both N-methyl groups is required to abrogate its potency because UNC3142 and UNC1756 (supplemental Figure 1B), 2 compounds with a single N-methyl modification at either position, merely modestly interfered with EZH2-mediated methylation (Figure 1B).

To assess the effect of our active vs inactive compounds on the landscape of histone modifications, we used mass spectrometry proteomic techniques[30] to quantify histone modification levels following compound treatment of a murine leukemia line established by *MLL-ENL*,[32] a common form of *MLL* rearrangements.[26,27] Of 55 detected histone peptides carrying the single or combinatorial modification, only peptides covering the H3 residues 27-40 were found altered in relative abundance with fold-change of >2 following UNC1999 vs DMSO treatment (Figure 1C, blue; supplemental Table 1). Peptides with a single H3K27me3 or H3K27me2 modification showed the greatest decreases. H3(27-40) peptide can also be modified by H3K36 methylation and, indeed, following UNC1999 treatment, several peptides with dual methylations of H3K27 and H3K36 were either undetectable (H3K27me3-K36me2) or found decreased (H3K27me3-K36me1 and H3K27me2-K36me2/1) (Figure 1C, blue; supplemental Table 1). Due to H3K27 "demethylation" by UNC1999 on these dually methylated peptides, the relative abundance of certain peptide species bearing H3K36me1/2 (supplemental Figure 1C-D, see increases in blue in bar graph, UNC1999 vs mock) was found increased accordingly (Figure 1C; supplemental Table 1), a phenomenon also seen in cells deficient in *Suz12*, an essential subunit of PRC2 (supplemental Figure 1E, blue in bar graph).[39] Overall, global H3K36me1/2 does not show significant change as examined by mass spectrometry (supplemental Figure 1F) and immunoblot (supplemental Figure 1G); indeed, at the concentrations applied to cells (<3 μM), UNC1999 had no effect on all 4 known H3K36-specific methyltransferases (supplemental Figure 1H-K). These findings collectively demonstrated specific targeting of PRC2 by UNC1999. As a result, the overall percentage of H3K27me3 and

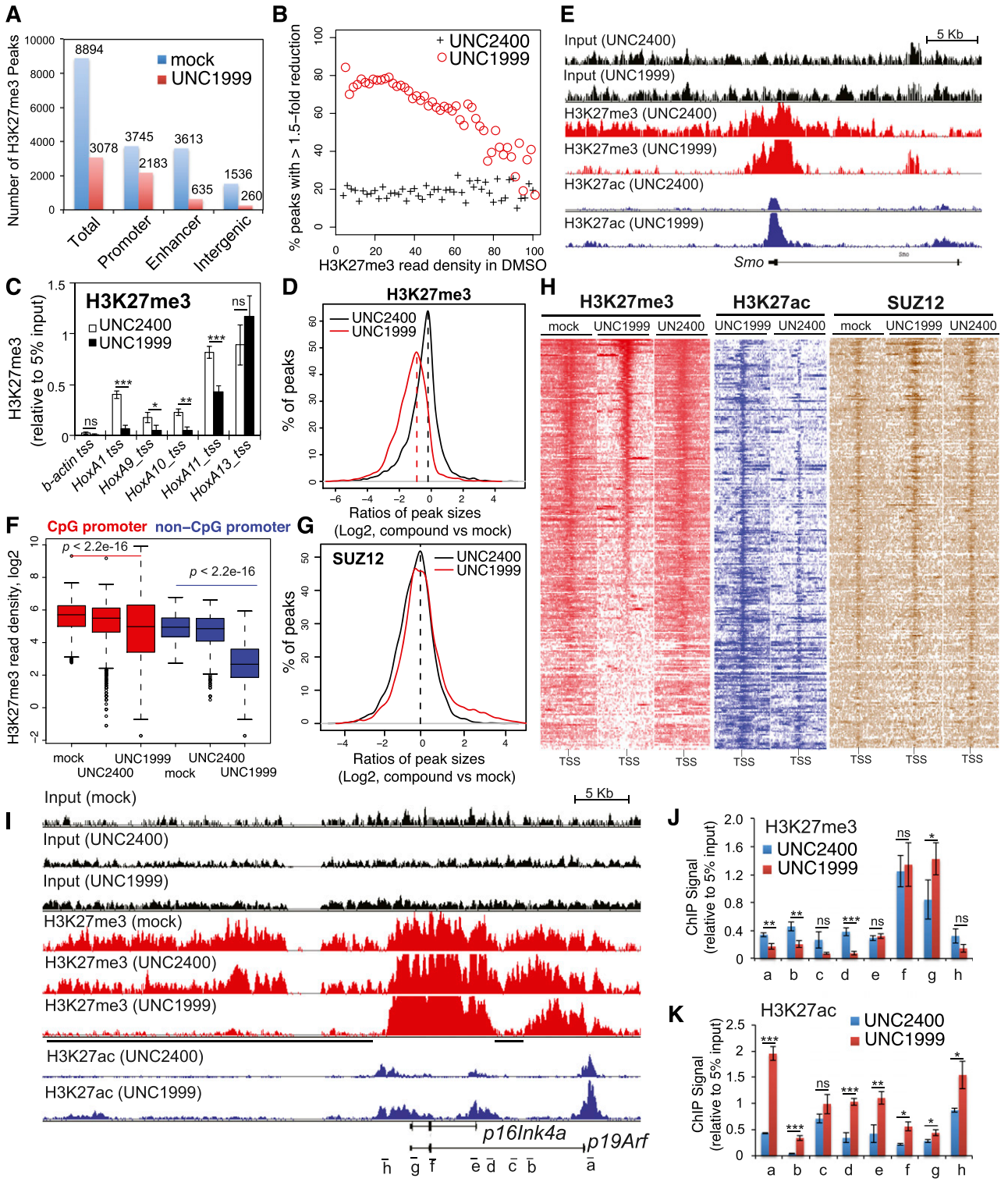

Figure 6. ChIP-Seq reveals UNC1999-induced loss of H3K27me3 and concurrent gain of H3K27ac in *MLL-AF9*–transformed leukemia progenitors. (A) Summary of H3K27me3 peaks showing loss in the UNC1999- (red) vs mock-treated (blue) samples. X-axis indicates all H3K27me3 peaks (left) or those associated with promoters, enhancers, or intergenic regions. (B) The fractions of H3K27me3 peaks showing reduction in ChIP-Seq signals by 1.5-fold or more in UNC1999-treated (red circle) or UNC2400-treated (cross) samples in comparison with mock treatment. The H3K27me3 peaks and their densities shown on x-axis were first defined and then grouped by the number of ChIP-Seq reads identified in the mock-treated sample; y-axis represents the fraction in each group of H3K27me3 peaks that show reduction by >1.5-fold in the compound- vs mock-treated samples, after normalization of ChIP-Seq reads to the sequencing depths and peak sizes. (C) ChIP-qPCR detects H3K27me3 at the TSS of several *Hox-A* genes in *MLL-AF9*–transformed leukemia progenitors after treatment with 3 μM UNC2400 or UNC1999 for 4 days. ChIP signals (y-axis) were normalized to 5% of input and presented as mean ± SD. TSS of *β-actin* was used as negative control. *$P < .05$; **$P < .01$; ***$P < .001$. (D) Plot showing a global reduction in the H3K27me3 peak sizes following UNC1999 treatment (red). X-axis shows the ratios (in their Log2 values) of peak sizes following UNC1999 (red) or UNC2400 (black) treatment in comparison with mock; y-axis shows the relative fraction of peaks at each individual ratio. The dashed vertical lines mark the mean value of peak size ratios. (E) IGB view showing the distribution of input (black), H3K27me3 (red) and H3K27ac (blue) ChIP-Seq read densities (normalized by the ChIP-seq read depths) at the Smoothened (*Smo*) gene in *MLL-AF9* leukemia progenitors after treatment with 3 μM UNC2400 or UNC1999 for 4 days. (F) Boxplots showing a significantly greater reduction of ChIP-Seq enrichment at the non-CpG- than the CpG-contained promoter associated H3K27me3 peaks after UNC1999 treatment in comparison with mock treatment. (G) Plot showing

H3K27me2 was reduced from 8.5% and 30.9% of total H3 in mock-treated cells, respectively, to 1.3% and 7.1% in UNC1999-treated cells, H3K27me1 slightly altered from 45.6% to 30.7%, whereas the nonmethylated H3K27 increased accordingly from 14.8% to 60.4% (Figure 1D). Consistent with antagonism between PRC2 and H3K27 acetylation (H3K27ac),[40] we detected significantly increased H3K27ac after UNC1999 treatment (Figure 1C; supplemental Table 1).

None of these alterations were seen following UNC2400 treatment (Figure 1C, red; supplemental Table 1). By immunoblot (Figure 1E) and flow cytometry (Figure 1F-G; supplemental Figure 1L-N), we verified "erasure" of H3K27me3/2 and concurrent elevation of H3K27ac by UNC1999, its negligible effects on other histone methylations, and undetectable effects by UNC2400. UNC1999-mediated suppression of H3K27me3 was time- and concentration-dependent (Figure 1F-G; supplemental Figure 1L-N). UNC1999 did not alter total levels of PRC2 (supplemental Figure 1O-P) or chromatin-bound EZH2 and EZH1 (Figure 1H), and did not affect the stability or assembly of PRC2 (Figure 1I), indicating that UNC1999 acts primarily via enzymatic inhibition of EZH2 and EZH1 on chromatin.

Taken together, UNC1999 induces potent and selective suppression of H3K27me3/2, whereas UNC2400 does not, highlighting them as a pair of compounds useful to manipulate both PRC2-EZH2 and PRC2-EZH1.

An EZH2 and EZH1 dual inhibitor UNC1999, but not an EZH2-selective inhibitor GSK126, effectively inhibits growth of *MLL*-rearranged leukemia

Recent studies have shown that genetic disruption of both EZH2 and EZH1 is required to inhibit growth of *MLL*-rearranged leukemia,[19,20] which prompted us to ask whether UNC1999 provides a unique way for treating *MLL*-rearranged leukemia. First, we compared the effect of UNC1999 to GSK126, a recently disclosed EZH2-selective inhibitor (with ~150-fold selectivity of EZH2 over EZH1).[22] As expected, both GSK126 and UNC1999 efficiently inhibited the global H3K27me3 in *DB* cells, a lymphoma line bearing the $EZH2^{Y641N}$ mutation,[22,25] as measured by both immunoblot (Figure 2A, top) and quantitative flow cytometry (supplemental Figure 2A), and efficiently suppressed *DB* cell proliferation (Figure 2B). However, using 3 independent *MLL-AF9*–transformed murine leukemia lines, we found that only UNC1999, and not GSK126, efficiently inhibited their H3K27me3 (Figure 2A, bottom and 2C) and suppressed cell proliferation (Figure 2D; supplemental Figure 2B-E). *MLL-AF9*–transformed murine leukemia cells coexpress *EZH2* and *EZH1* (supplemental Figure 2F). These data indicate uniqueness of UNC1999 in treating cancers that rely on PRC2-EZH2 and PRC2-EZH1 both.

Next, we applied UNC1999 to a larger panel of leukemia cell lines. All of the 10 lines bearing *MLL* rearrangements including *MLL-AF9*, *MLL-ENL, MLL-PTD*, or *MLL-AF4* showed sensitivity to UNC1999 (Figure 2E-H; supplemental Figure 2G-I) with half-maximal effective concentration (EC_{50}) ranging from 102 nM to 1.96 μM (Figure 2F). Notably, multiple *MLL*-rearranged lines demonstrated a comparable UNC1999 sensitivity to *DB* (Figure 2E-F). UNC1999 did not induce nonspecific toxicity, for it did not affect proliferation of *LOUCY* (Figure 2I), a T-cell acute lymphoblastic leukemia line without detectable H3K27me3 due to *EZH2* genomic deletion[41] (Figure 2J). Moreover, *K562*, a *BCR-ABL*–bearing myeloid leukemia line, also did not respond to UNC1999 (Figure 2E-F). UNC1999-mediated growth suppression was time-dependent and dose-dependent (Figure 2D-H). UNC2400 had no detectable effect on cell growth (Figure 2K).

Collectively, UNC1999, an EZH2 and EZH1 dual inhibitor, efficiently suppresses proliferation of *MLL*-rearranged leukemia cells that coexpress *EZH2* and *EZH1*.

UNC1999, and not UNC2400, suppresses colony-forming abilities of *MLL*-rearranged leukemia cells and promotes their differentiation and apoptosis

Wright-Giemsa staining revealed dose-dependent alterations by UNC1999 in cell morphology from leukemic myeloblasts to differentiated cells (Figure 3A; supplemental Figure 3A), which was concurrent with the increased differentiation markers and decreased c-Kit, a hematopoietic stem/progenitor marker (Figure 3B-C; supplemental Figure 3B). We used serial replating assays to assess the repopulating ability of clonogenic cells, an ex vivo indicator of leukemia stem cells.[42] Following treatment with UNC1999, and not DMSO or UNC2400, *MLL-AF9*– or *MLL-ENL*–transformed leukemia cells exhibited a dramatic reduction in the number of outgrowing colonies (Figure 3D-E) and morphologic alterations from the primarily large and compact colonies to the small and diffuse ones characteristic of differentiated cell clusters (Figure 3F). We also examined cell viability and found time- and concentration-dependent induction of apoptosis in several tested lines after treatment with UNC1999, and not UNC2400 (Figure 3G-H; supplemental Figure 3C). Taken together, UNC1999, but not UNC2400, suppresses growth of *MLL*-rearranged leukemia by inhibiting repopulating ability and promoting cell differentiation and apoptosis.

Identification of UNC1999-responsive gene signatures in *MLL*-rearranged leukemia

To dissect the underlying mechanisms for the UNC1999-induced anti-leukemia effect, we performed microarray analysis with 2 independent *MLL-AF9*–transformed murine leukemia lines following compound treatments. UNC1999 altered the expression of a few hundred transcripts (Figure 4A-B; supplemental Figure 4A, supplemental Table 2), and consistent with the silencing role of PRC2,[43] significantly more genes showed upregulation than downregulation after UNC1999 treatment (Figure 4A-B; supplemental Figure 4A). In contrast, UNC2400 induced little changes (Figure 4A,C;

Figure 6 (continued) the relative size of SUZ12 peaks after compound treatments. X-axis shows the ratios (in their Log2 values) of peak sizes following UNC1999 (red) or UNC2400 (black) treatment in comparison with mock; y-axis shows the relative fraction of peaks at each individual ratio. The dashed vertical lines mark the mean value of peak size ratios. (H) Heatmap showing the ChIP-Seq read densities of H3K27me3 (red), H3K27ac (blue), and SUZ12 (brown) across the TSS (±20 kb) of upregulated genes following UNC1999 vs mock treatment (Figure 4A). Color represents the degree of ChIP-Seq signal enrichment, with the lowest set to white. The data indicate that a large majority (top of the heatmaps) of the UNC1999-derepressed genes contains H3K27me3 across TSS prior to compound treatment, and following UNC1999 treatment, H3K27me3 peaks become narrower and sharper. (I) IGB profiles showing the distribution of ChIP-Seq read densities (normalized by the ChIP-seq read depths) for input (black), H3K27me3 (red), and H3K27ac (blue) at *p16Ink4a* and *p19Arf*. Black bars under the track of H3K27me3 (UNC1999) mark the regulatory regions showing loss or reduction of H3K27me3 after UNC1999 treatment in comparison with mock or UNC2400. (J-K) ChIP-qPCR of H3K27me3 (J) and H3K27ac (K) across the *Cdkn2a* locus in *MLL-AF9*–transformed leukemia progenitors after treatment with 3 μM UNC2400 (blue) or UNC1999 (red) for 4 days. The genomic organization of *p16Ink4a* and *p19Arf* and positions of each ChIP PCR amplicon (labeled alphabetically, not drawn to scale) are depicted at the bottom of panel I. ChIP signals (y-axis) from independent experiments were normalized to input and presented as mean ± SD. $^{*}P < .05$; $^{**}P < .01$; $^{***}P < .001$. IGB, Integrated Genome Browser.

supplemental Table 2), demonstrating its overall inactivity in transcriptional modulation. Importantly, the transcripts upregulated by UNC1999 largely overlapped those after knockdown of *EED*, a common cofactor of EZH2 and EZH1, demonstrating on-target effects of UNC1999 (Figure 4D; supplemental Figure 4A-C, supplemental Table 2-3). GSEA revealed significant enrichment of PRC2-repressed genes (Figure 4E-G) and those associated with H3K27me3 (supplemental Figure 4D-E) or myeloid differentiation (Figure 4E,H) in UNC1999- vs DMSO-treated cells. GO analysis showed UNC1999-derepressed genes enriched with pathways related to development, myeloid differentiation, and proliferation (supplemental Figure 4F), which are the hallmark of polycomb targets.[43] For example, similar to *EED* knockdown (supplemental Table 3), UNC1999 treatment derepressed the differentiation-associated (*Epx*), proliferation-associated (*Cdkn2a*), and development-associated genes (*Bcl11a*, *Ikzf2*, *Gata1*, *Tet1*, *Kdm5b*, *Smo*, *Fzd3*), whereas expression of all PRC2-encoding genes were unaltered (Figure 4B). By RT-qPCR, we verified the gene expression changes following UNC1999 vs UNC2400 treatments or after *EED* knockdown (Figure 4I).

Taken together, treatment of *MLL*-rearranged leukemias with UNC1999, an EZH2 and EZH1 dual inhibitor, derepresses their PRC2 gene targets.

Cdkn2a reactivation is crucial for UNC1999-induced growth suppression

We performed similar gene array analysis either with milder compound treatment or with *MLL-ENL*–transformed leukemia cells and identified a common UNC1999-responsive signature, which included *Cdkn2a* (supplemental Table 4). We closely examined *Cdkn2a* because this polycomb target encodes 2 crucial cell-cycle regulators, *p16Ink4a* and *p19Arf*. UNC1999 consistently induced reactivation of *p16Ink4a* and *p19Arf* in multiple lines bearing *MLL-AF9* or *MLL-ENL,* and such derepression was concentration- and time-dependent (Figure 5A-B; supplemental Figure 5A). *Cdkn2a* reactivation was modest after 2-day treatment and dramatic 7 days posttreatment, with >150-fold and >60-fold upregulation of *p16Ink4a* and *p19Arf* observed in sensitive lines, respectively (Figure 5A-B). UNC1999 induced cell-cycle arrest at the G1-to-S transition (Figure 5C-D; supplemental Figure 5B). In contrast, UNC2400 did not alter the expression of *Cdkn2a* (Figure 4C,I) or cell-cycle progression (Figure 5C-D; supplemental Figure 5B). To examine whether UNC1999-induced phenotypes depend on *Cdkn2a*, we derived several *MLL-AF9*–transformed leukemia lines with bone marrow from mice deficient in *p16Ink4a* and *p19Arf* (supplemental Figure 5C). Compared with their wild-type counterparts, these $p16Ink4a^{-/-}/p19Arf^{-/-}$ leukemia cells no longer responded to UNC1999 with no detectable change in their proliferation (Figure 5E) or apoptosis (Figure 5F) following treatment. Collectively, *Cdkn2a* is a critical downstream mediator of UNC1999-induced growth inhibition.

ChIP-Seq reveals UNC1999-induced local suppression of H3K27me3 and concurrent gain of H3K27ac in *MLL*-rearranged leukemia

To further dissect how UNC1999 alters the chromatin landscape of *MLL-AF9*–transformed leukemia progenitors, we used ChIP-Seq to profile distribution of H3K27me3 and its antagonizing H3K27ac. We found a global reduction of H3K27me3 following UNC1999 treatment: ~66% of a total of 8894 H3K27me3 peaks showed complete loss (Figure 6A) whereas 8% showed increases (>1.5-fold, data not shown). ChIP-Seq also unveiled preferential removal of H3K27me3 by UNC1999 at loci containing a relatively lower level of H3K27me3 whereas those harboring the highest H3K27me3 remained generally intact (Figure 6B). For example, UNC1999 completely "erased" a domain with lower H3K27me3 upstream of *HoxA1* whereas a domain with higher H3K27me3 covering *HoxA11-A13* was unaltered (supplemental Figure 6A red); using ChIP followed by qPCR, we verified such site-specific "demethylation" by UNC1999 at *Hox-A* genes (Figure 6C). Furthermore, H3K27me3 peaks associated with distal nonpromoter regulatory elements, including enhancers and intergenic regions, often demonstrate complete loss, whereas H3K27me3 peaks associated with proximal promoters are largely retained (Figure 6A; supplemental Figure 6D), despite a shrinking in their average peak size (Figure 6D) or signal reduction at peak shoulders, as exemplified by developmental genes *Smo* (Figure 6E, red), *Evx1*, *Bcl11a*, and *Fzd3* (supplemental Figure 6A-C, red). In addition, we found UNC1999 preferentially affected non-CpG promoters compared with CpG promoters (Figure 6F). We also performed ChIP-Seq of SUZ12, an essential cofactor of EZH2 and EZH1, and did not observe significant decreases in SUZ12 binding following compound treatments (Figure 6G; supplemental Figure 6E), which is consistent with our finding that UNC1999 does not affect PRC2 complex stability (Figure 1I). To correlate the transcriptome alteration with ChIP-Seq, we examined UNC1999-derepressed genes. Indeed, following UNC1999 vs mock or UNC2400 treatment, these genes displayed either loss or shrinking of H3K27me3 centered on transcriptional start sites (TSSs) (Figure 6H, red) and concurrent gain in H3K27ac (Figure 6H, blue), whereas the associated SUZ12 was not decreased (Figure 6H, brown). We then closely examined *Cdkn2a*, a crucial UNC1999-responsive gene. Again, ChIP-Seq revealed preferential "erasure" of H3K27me3 by UNC1999 at multiple regulatory elements (Figure 6I, black lines under the track of "H3K27me3-UNC1999") of *p16Ink4a* or *p19Arf* without altering *Cdkn2a*-associated SUZ12 (supplemental Figure 6F); TSS-associated H3K27ac was significantly increased (Figure 6I, blue). By ChIP-qPCR, we verified site-specific decreases in H3K27me3 (Figure 6J) and increases in H3K27ac (Figure 6K) across *Cdkn2a* after UNC1999 vs UNC2400 treatment.

Collectively, UNC1999, but not UNC2400, preferentially "erases" H3K27me3 associated with distal regulatory regions such as enhancers and reshapes the landscape of H3K27me3 vs H3K27ac at proximal promoters in *MLL-AF9*–transformed leukemia cells, leading to gene derepression.

UNC1999 prolongs survival of an *MLL-AF9*–induced murine leukemia model in vivo

We generated murine leukemia with *MLL-AF9* followed by bone marrow transplantation of primary tumors to syngeneic recipients, which developed aggressive leukemia with a consistent latency of 20 to 35 days (Figure 7A, blue). To examine the effect of UNC1999 on in vivo leukemogenesis, we administered either vehicle or 50 mg/kg UNC1999 by oral gavage to mice twice per day and starting from 7 days posttransplantation when the white blood cell (WBC) counts in peripheral blood started to accumulate when compared with nonengrafted controls. We then monitored leukemia progression by periodic assessment of peripheral blood samples and found that, despite steady accumulation of WBCs in both vehicle- and UNC1999-treated cohorts, UNC1999-treated animals displayed significant reduction in WBC counts (Figure 7B-D), indicating a delayed leukemic progression. Indeed, UNC1999-treated leukemic mice exhibited a significantly prolonged survival, with a latency of 36.6 ± 11.7 days in contrast to 24 ± 6.7 days for vehicle-treated

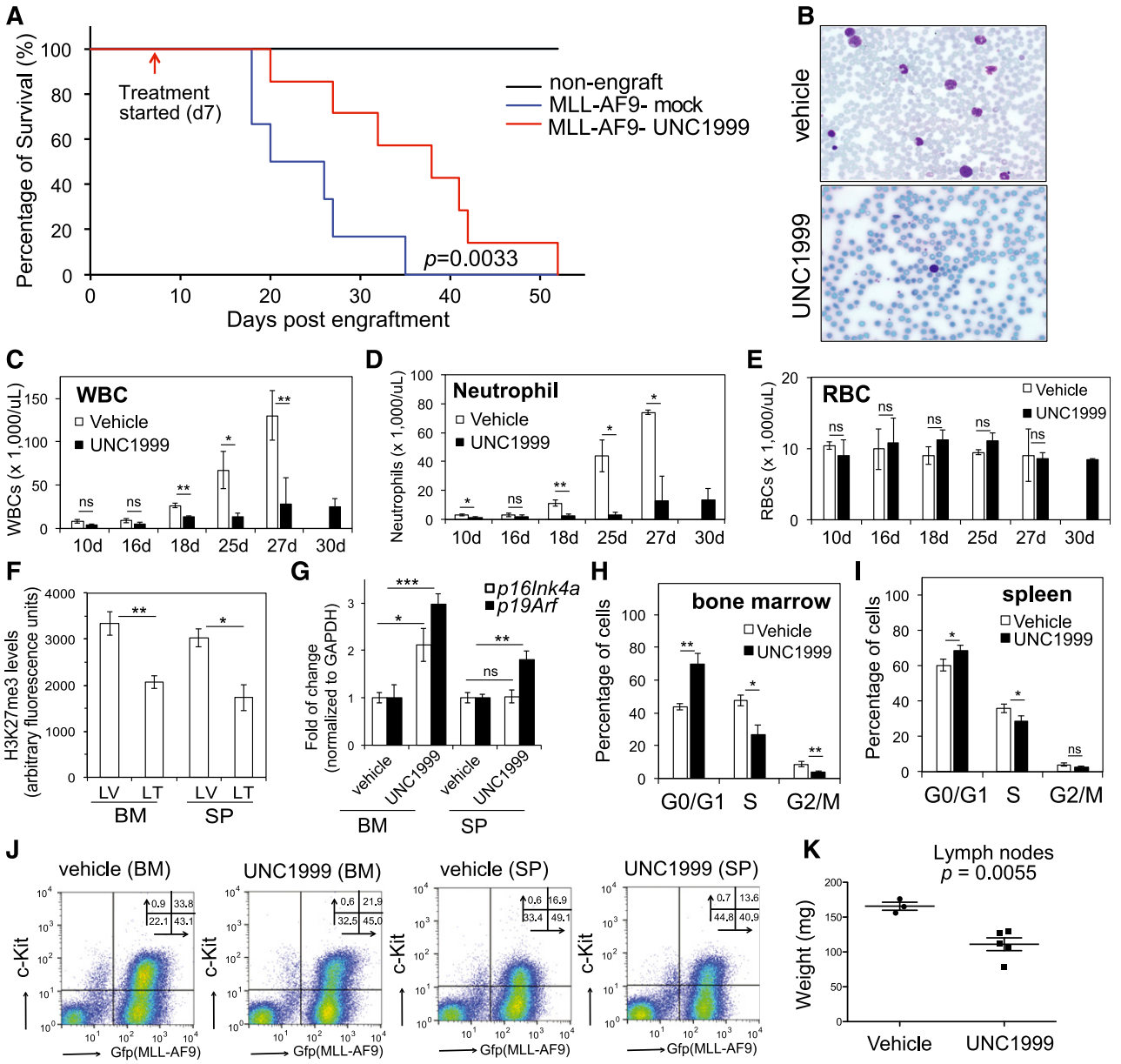

Figure 7. UNC1999 prolongs survival of *MLL-AF9*–induced murine leukemia models in vivo. (A) Kaplan-Meier curve showing leukemia kinetics after transplantation of *MLL-AF9*–induced primary murine leukemia into syngeneic mice. Starting from day 7 posttransplantation, mice received oral administration of either vehicle (blue) or 50 mg/kg UNC1999 (red) twice per day. Black lines (top) represent nontransplanted normal mice treated with vehicle or UNC1999. Cohort size, 6 to 7 mice. (B) Typical Wright-Giemsa staining images of the peripheral blood smears prepared from the vehicle- (top) and UNC1999-treated (bottom) leukemia mice 25 days posttransplantation. (C-E) Summary of counts of the WBCs (C), neutrophils (D), and RBCs (E) in the peripheral blood of vehicle- (white) or UNC1999-treated (black) leukemia mice at the indicated date posttransplantation. $*P < .05$; $**P < .01$; $***P < .001$. (F) Summary of H3K27me3 levels in cells isolated from bone marrow or spleen of vehicle- (LV) and UNC1999-treated (LT) leukemia mice as quantified by flow cytometry. $*P < .05$; $**P < .01$. (G) Fold-change in *p16Ink4a* and *p19Arf* gene expression in cells isolated from bone marrow or spleen of the UNC1999-treated (black) leukemia mice in comparison with vehicle-treated (white). $*P < .05$; $**P < .01$. (H-I) Summary of cell-cycle status of cells isolated from bone marrow (H) or spleen (I) of vehicle- (white) and UNC1999-treated (black) leukemia mice 25 days posttransplantation. $*P < .05$; $**P < .01$. (J) Flow cytometry (performed 25 days posttransplantation) detects leukemia cells (labeled by bicistronic *GFP* expression in x-axis) and their *c-Kit* expression (y-axis) in the bone marrow or spleen after treating mice with either vehicle or 50 mg/kg UNC1999. (K) Comparison of sizes of lymph nodes isolated from the *MLL-AF9*–induced leukemia mice after treatment with either vehicle or 50 mg/kg UNC1999. BM, bone marrow; GFP, green fluorescent protein; LT, UNC1999-treated leukemia mice; LV, vehicle-treated leukemia mice; RBC, red blood cell; SP, spleen.

mice (Figure 7A, $P = .0033$). UNC1999 treatment did not affect the counts of red blood cells (Figure 7E) or platelets (supplemental Figure 7A). We closely examined leukemia cells collected from moribund mice. Compared with vehicle, UNC1999 treatment significantly decreased H3K27me3 in cells isolated from bone marrow and spleen (Figure 7F), significantly elevated their *p16Ink4a* or *p19Arf* expression (Figure 7G), and caused the G1-to-S cell-cycle arrest (Figure 7H-I; supplemental Figure 7B). UNC1999 treatment also significantly reduced the total number of leukemia cells (labeled by bicistronic *GFP* expression) or c-Kit–positive leukemia progenitors (c-Kit$^+$/GFP$^+$) in bone marrow and spleen (Figure 7J; supplemental Figure 7C-D). Furthermore, the size of lymph nodes was significantly smaller in UNC1999- vs vehicle-treated mice (Figure 7K); both cohorts showed similar severity of splenomegaly.

Collectively, oral administration of UNC1999 delays *MLL-AF9*–induced leukemogenicity in vivo and our EZH2 and EZH1 dual inhibitor provides a new therapeutics for *MLL*-rearranged leukemia.

Discussion

Our study represents the first to show specific enzymatic inhibition of EZH2 and EZH1 by oral delivery of a small-molecule compound as a promising therapeutic intervention for *MLL*-rearranged leukemia, a genetically defined malignancy with poor prognosis. Previously, several methods were reported to disrupt PRC2 function in cancer. 3-Deazaneplanocin A (DZNep), an inhibitor of S-adenosylhomocysteine hydrolase that depletes PRC2 via an unclear mechanism,[44] demonstrated a tumor-suppressive effect in cancers including *MLL*-rearranged leukemia[45]; however, increasing evidence has indicated that DZNep lacks specificity.[46,47] Inhibitors highly selective to EZH2[21-23] or to EZH2 and EZH1[25,48] have been discovered, some of which demonstrated early success in treating *EZH2*-mutated lymphoma[22] and *SNF5*-inactivated malignant rhabdoid tumors.[49] Furthermore, a hydrocarbon-stapled peptide (SAH-EZH2) has recently been developed to disrupt interaction of EED with EZH2 and EZH1, leading to degradation of PRC2.[50] Prior to our study, an orally bioavailable inhibitor of PRC2 remains to be established in both in vitro and in vivo settings to treat cancer that relies on PRC2-EZH2 and PRC2-EZH1 both. Here, we used a series of proteomics, genomics, and leukemogenic approaches to show that UNC1999, an EZH2 and EZH1 dual inhibitor, suppresses growth of *MLL*-rearranged leukemia ex vivo and in vivo, whereas an EZH2-selective inhibitor GSK126 failed to efficiently inhibit H3K27me3 or proliferation of *MLL*-rearranged leukemia cells. Our translational tool may represent novel therapeutics for cancer types that coexpress *EZH2* and *EZH1*.

UNC1999-responsive genes largely overlapped the defined PRC2 targets. Derepression of PRC2 target genes associates with suppression of H3K27me3 and concurrent gain in H3K27ac. Unlike DZNep[44] or SAH-EZH2,[50] UNC1999 does not degrade PRC2 and, thus, the UNC1999-derepressed genes are likely to be silenced by PRC2 via its methyltransferase activity per se, and not via silencing factors recruited by PRC2. This difference may partly explain why a subset of genes were upregulated by *EED* knockdown and not by UNC1999 (Figure 4D). We also show that deletion of *Cdkn2a* largely reversed the UNC1999-induced antiproliferation effect in vitro, suggesting that the status of *CDKN2A* might be a useful predictor for drug resistance vs efficacy of PRC2 inhibitors. It would be also interesting to investigate into the status of *CDKN2A* among certain non-*MLL*-rearranged myeloid malignancies and T-cell acute lymphoblastic leukemia where PRC2 inactivation occurs due to the damaging mutation of *EZH2*, *EED*, or *SUZ12*.[51,52] Furthermore, we demonstrated overall inactivity of an analog compound UNC2400 in modulation of H3K27me3 or gene expression, making it an ideal chemical control for UNC1999. Thus, this study provides the first detailed molecular characterization of a pair of active vs inactive small-molecule compounds suitable for studying EZH2 and EZH1 in the in vitro and in vivo settings.

Mechanistically, UNC1999 preferentially "erases" H3K27me3 peaks associated with distal regulatory elements such as enhancers and remodels the landscape of H3K27me3 vs H3K27ac at proximal promoters and TSSs. We speculate that the local concentration and/or composition of PRC2 and associated factors may influence the efficacy of UNC1999, as we observed a higher level of SUZ12 at TSS where H3K27me3 tends to be retained following UNC1999 treatment (Figure 6H). However, the causal relationship remains to be defined. Furthermore, we noticed that UNC1999 had a weaker effect in vivo and only modestly delayed *MLL-AF9*–induced leukemogenesis. Partial in vivo efficacy has previously been seen for specific inhibitors of BRD4[53,54] and DOT1L.[55] Further optimization of potency, selectivity, and drug metabolism and pharmacokinetics are needed to enhance their in vivo antitumor effect. With accumulating evidence demonstrating a general "druggability" of many cancer-associated epigenetic "writers," "erasers," and "readers,"[1] development of epigenetic modulators shall provide novel therapeutic interventions in the near future.

Acknowledgments

The authors thank Drs Chris Vakoc, Robert Slany, and Vittorio Sartorelli for providing plasmids used in this study. The authors thank Mike Vernon and the University of North Carolina at Chapel Hill (UNC) Genomics Core for microarray analysis, Charlene Satos and the UNC Animal Studies Core for in vivo studies, and Piotr Mieczkowski and the UNC High-Throughput Sequencing Facility (HTSF) Core for deep-sequencing studies.

This work was supported by the National Institutes of Health (NIH), National Cancer Institute K99/R00 "Pathway to Independence" Award CA151683 (G.G.W.), an NIH Institute of General Medical Sciences grant R01GM103893 (J.J.), a US Department of Defense Congressionally Directed Medical Research Programs grant CA130247 (G.G.W.), and the University Cancer Research Fund of North Carolina State. The Structural Genomics Consortium is a registered charity (no. 1097737) that receives funds from the Canada Foundation for Innovation, Eli Lilly Canada, GlaxoSmithKline, the Ontario Ministry of Economic Development and Innovation, the Novartis Research Foundation, Pfizer, AbbVie, Takeda, Janssen, Boehringer Ingelheim, and the Wellcome Trust. G.G.W. is an American Society of Hematology Scholar in Basic Science, a Kimmel Scholar of the Sidney Kimmel Foundation for Cancer Research, and is also supported by grants from the Gabrielle's Angel Foundation and the Concern Foundation of Cancer Research. D.F.A. and L.C. are supported by postdoctoral fellowships from the American Association for Cancer Research–Debbie's Dream Foundation and Department of Defense, respectively, and K.D.K. is supported by a predoctoral fellowship from the American Chemical Society Medicinal Chemistry Division.

Authorship

Contribution: G.G.W. and J.J. designed the research; B.X., D.M.O., A.M., T.P., K.D.K., S.G.P., D.F.A., L.C., S.L., D.F.A., F.L., S.V.F., M.V., B.A.G., J.J., and G.G.W. performed the research; S.R., Y.L., G.G.W., and D.Z. analyzed ChIP-Seq data; B.X., D.M.O., and G.G.W. performed overall analysis and data interpretation; G.G.W. wrote the paper; and all authors checked the final version of the manuscript.

Conflict-of-interest disclosure: The authors declare no competing financial interests.

Correspondence: Greg G. Wang, Department of Biochemistry and Biophysics, UNC Lineberger Comprehensive Cancer Center, University of North Carolina at Chapel Hill, 450 West Dr, CB 7295, Chapel Hill, NC 27599; e-mail: greg_wang@med.unc.edu.

References

1. Chi P, Allis CD, Wang GG. Covalent histone modifications—miswritten, misinterpreted and mis-erased in human cancers. *Nat Rev Cancer.* 2010;10(7):457-469.
2. Strahl BD, Allis CD. The language of covalent histone modifications. *Nature.* 2000;403(6765):41-45.
3. Greer EL, Shi Y. Histone methylation: a dynamic mark in health, disease and inheritance. *Nat Rev Genet.* 2012;13(5):343-357.
4. Esteller M. Cancer epigenomics: DNA methylomes and histone-modification maps. *Nat Rev Genet.* 2007;8(4):286-298.
5. Karberg S. Switching on epigenetic therapy. *Cell.* 2009;139(6):1029-1031.
6. Dawson MA, Kouzarides T. Cancer epigenetics: from mechanism to therapy. *Cell.* 2012;150(1):12-27.
7. Arrowsmith CH, Bountra C, Fish PV, Lee K, Schapira M. Epigenetic protein families: a new frontier for drug discovery. *Nat Rev Drug Discov.* 2012;11(5):384-400.
8. Helin K, Dhanak D. Chromatin proteins and modifications as drug targets. *Nature.* 2013; 502(7472):480-488.
9. Margueron R, Li G, Sarma K, et al. Ezh1 and Ezh2 maintain repressive chromatin through different mechanisms. *Mol Cell.* 2008;32(4): 503-518.
10. Mochizuki-Kashio M, Mishima Y, Miyagi S, et al. Dependency on the polycomb gene Ezh2 distinguishes fetal from adult hematopoietic stem cells. *Blood.* 2011;118(25):6553-6561.
11. Hidalgo I, Herrera-Merchan A, Ligos JM, et al. Ezh1 is required for hematopoietic stem cell maintenance and prevents senescence-like cell cycle arrest. *Cell Stem Cell.* 2012;11(5):649-662.
12. Caganova M, Carrisi C, Varano G, et al. Germinal center dysregulation by histone methyltransferase EZH2 promotes lymphomagenesis. *J Clin Invest.* 2013;123(12):5009-5022.
13. Béguelin W, Popovic R, Teater M, et al. EZH2 is required for germinal center formation and somatic EZH2 mutations promote lymphoid transformation. *Cancer Cell.* 2013;23(5):677-692.
14. Morin RD, Johnson NA, Severson TM, et al. Somatic mutations altering EZH2 (Tyr641) in follicular and diffuse large B-cell lymphomas of germinal-center origin. *Nat Genet.* 2010;42(2): 181-185.
15. Sneeringer CJ, Scott MP, Kuntz KW, et al. Coordinated activities of wild-type plus mutant EZH2 drive tumor-associated hypertrimethylation of lysine 27 on histone H3 (H3K27) in human B-cell lymphomas. *Proc Natl Acad Sci USA.* 2010; 107(49):20980-20985.
16. Herrera-Merchan A, Arranz L, Ligos JM, de Molina A, Dominguez O, Gonzalez S. Ectopic expression of the histone methyltransferase Ezh2 in haematopoietic stem cells causes myeloproliferative disease. *Nat Commun.* 2012;3:623.
17. Berg T, Thoene S, Yap D, et al. A transgenic mouse model demonstrating the oncogenic role of mutations in the polycomb-group gene EZH2 in lymphomagenesis. *Blood.* 2014;123(25): 3914-3924.
18. Shen X, Liu Y, Hsu Y-J, et al. EZH1 mediates methylation on histone H3 lysine 27 and complements EZH2 in maintaining stem cell identity and executing pluripotency. *Mol Cell.* 2008;32(4):491-502.
19. Neff T, Sinha AU, Kluk MJ, et al. Polycomb repressive complex 2 is required for MLL-AF9 leukemia. *Proc Natl Acad Sci USA.* 2012;109(13): 5028-5033.
20. Shi J, Wang E, Zuber J, et al. The Polycomb complex PRC2 supports aberrant self-renewal in a mouse model of MLL-AF9;Nras(G12D) acute myeloid leukemia. *Oncogene.* 2013;32(7): 930-938.
21. Knutson SK, Wigle TJ, Warholic NM, et al. A selective inhibitor of EZH2 blocks H3K27 methylation and kills mutant lymphoma cells. *Nat Chem Biol.* 2012;8(11):890-896.
22. McCabe MT, Ott HM, Ganji G, et al. EZH2 inhibition as a therapeutic strategy for lymphoma with EZH2-activating mutations. *Nature.* 2012; 492(7427):108-112.
23. Qi W, Chan H, Teng L, et al. Selective inhibition of Ezh2 by a small molecule inhibitor blocks tumor cells proliferation. *Proc Natl Acad Sci USA.* 2012; 109(52):21360-21365.
24. Knutson SK, Kawano S, Minoshima Y, et al. Selective inhibition of EZH2 by EPZ-6438 leads to potent antitumor activity in EZH2-mutant non-Hodgkin lymphoma. *Mol Cancer Ther.* 2014; 13(4):842-854.
25. Konze KD, Ma A, Li F, et al. An orally bioavailable chemical probe of the lysine methyltransferases EZH2 and EZH1. *ACS Chem Biol.* 2013;8(6): 1324-1334.
26. Dou Y, Hess JL. Mechanisms of transcriptional regulation by MLL and its disruption in acute leukemia. *Int J Hematol.* 2008;87(1):10-18.
27. Krivtsov AV, Armstrong SA. MLL translocations, histone modifications and leukaemia stem-cell development. *Nat Rev Cancer.* 2007;7(11): 823-833.
28. Slany RK. The molecular biology of mixed lineage leukemia. *Haematologica.* 2009;94(7):984-993.
29. Tanaka S, Miyagi S, Sashida G, et al. Ezh2 augments leukemogenicity by reinforcing differentiation blockage in acute myeloid leukemia. *Blood.* 2012;120(5):1107-1117.
30. Lin S, Garcia BA. Examining histone posttranslational modification patterns by high-resolution mass spectrometry. *Methods Enzymol.* 2012;512:3-28.
31. Wang GG, Song J, Wang Z, et al. Haematopoietic malignancies caused by dysregulation of a chromatin-binding PHD finger. *Nature.* 2009; 459(7248):847-851.
32. Wang GG, Cai L, Pasillas MP, Kamps MP. NUP98-NSD1 links H3K36 methylation to Hox-A gene activation and leukaemogenesis. *Nat Cell Biol.* 2007;9(7):804-812.
33. Wang GG, Calvo KR, Pasillas MP, Sykes DB, Häcker H, Kamps MP. Quantitative production of macrophages or neutrophils ex vivo using conditional Hoxb8. *Nat Methods.* 2006;3(4):287-293.
34. Cai L, Rothbart SB, Lu R, et al. An H3K36 methylation-engaging Tudor motif of polycomb-like proteins mediates PRC2 complex targeting. *Mol Cell.* 2013;49(3):571-582.
35. Lee TI, Johnstone SE, Young RA. Chromatin immunoprecipitation and microarray-based analysis of protein location. *Nat Protoc.* 2006;1(2):729-748.
36. Goldberg AD, Banaszynski LA, Noh KM, et al. Distinct factors control histone variant H3.3 localization at specific genomic regions. *Cell.* 2010;140(5):678-691.
37. Antonysamy S, Condon B, Druzina Z, et al. Structural context of disease-associated mutations and putative mechanism of autoinhibition revealed by x-ray crystallographic analysis of the EZH2-SET domain. *PLoS ONE.* 2013;8(12):e84147.
38. Wu H, Zeng H, Dong A, et al. Structure of the catalytic domain of EZH2 reveals conformational plasticity in cofactor and substrate binding sites and explains oncogenic mutations. *PLoS ONE.* 2013;8(12):e83737.
39. Jung HR, Pasini D, Helin K, Jensen ON. Quantitative mass spectrometry of histones H3.2 and H3.3 in Suz12-deficient mouse embryonic stem cells reveals distinct, dynamic post-translational modifications at Lys-27 and Lys-36. *Mol Cell Proteomics.* 2010;9(5):838-850.
40. Pasini D, Malatesta M, Jung HR, et al. Characterization of an antagonistic switch between histone H3 lysine 27 methylation and acetylation in the transcriptional regulation of Polycomb group target genes. *Nucleic Acids Res.* 2010;38(15):4958-4969.
41. Nagel S, Venturini L, Marquez VE, et al. Polycomb repressor complex 2 regulates HOXA9 and HOXA10, activating ID2 in NK/T-cell lines. *Mol Cancer.* 2010;9:151.
42. Somervaille TC, Cleary ML. Identification and characterization of leukemia stem cells in murine MLL-AF9 acute myeloid leukemia. *Cancer Cell.* 2006;10(4):257-268.
43. Margueron R, Reinberg D. The Polycomb complex PRC2 and its mark in life. *Nature.* 2011; 469(7330):343-349.
44. Tan J, Yang X, Zhuang L, et al. Pharmacologic disruption of Polycomb-repressive complex 2-mediated gene repression selectively induces apoptosis in cancer cells. *Genes Dev.* 2007;21(9): 1050-1063.
45. Ueda K, Yoshimi A, Kagoya Y, et al. Inhibition of histone methyltransferase EZH2 depletes leukemia stem cell of mixed lineage leukemia fusion leukemia through upregulation of p16. *Cancer Sci.* 2014;105(5):512-519.
46. Miranda TB, Cortez CC, Yoo CB, et al. DZNep is a global histone methylation inhibitor that reactivates developmental genes not silenced by DNA methylation. *Mol Cancer Ther.* 2009;8(6): 1579-1588.
47. Lee JK, Kim KC. DZNep, inhibitor of S-adenosylhomocysteine hydrolase, down-regulates expression of SETDB1 H3K9me3 HMTase in human lung cancer cells. *Biochem Biophys Res Commun.* 2013;438(4):647-652.
48. Garapaty-Rao S, Nasveschuk C, Gagnon A, et al. Identification of EZH2 and EZH1 small molecule inhibitors with selective impact on diffuse large B cell lymphoma cell growth. *Chem Biol.* 2013; 20(11):1329-1339.
49. Knutson SK, Warholic NM, Wigle TJ, et al. Durable tumor regression in genetically altered malignant rhabdoid tumors by inhibition of methyltransferase EZH2. *Proc Natl Acad Sci USA.* 2013;110(19):7922-7927.
50. Kim W, Bird GH, Neff T, et al. Targeted disruption of the EZH2-EED complex inhibits EZH2-dependent cancer. *Nat Chem Biol.* 2013;9(10): 643-650.
51. Simon C, Chagraoui J, Krosl J, et al. A key role for EZH2 and associated genes in mouse and human adult T-cell acute leukemia. *Genes Dev.* 2012; 26(7):651-656.
52. Shih AH, Abdel-Wahab O, Patel JP, Levine RL. The role of mutations in epigenetic regulators in myeloid malignancies. *Nat Rev Cancer.* 2012; 12(9):599-612.
53. Zuber J, Shi J, Wang E, et al. RNAi screen identifies Brd4 as a therapeutic target in acute myeloid leukaemia. *Nature.* 2011;478(7370): 524-528.
54. Filippakopoulos P, Qi J, Picaud S, et al. Selective inhibition of BET bromodomains. *Nature.* 2010; 468(7327):1067-1073.
55. Daigle SR, Olhava EJ, Therkelsen CA, et al. Selective killing of mixed lineage leukemia cells by a potent small-molecule DOT1L inhibitor. *Cancer Cell.* 2011;20(1):53-65.

2015 125: 346-357
doi:10.1182/blood-2014-06-581082 originally published online November 13, 2014

Selective inhibition of EZH2 and EZH1 enzymatic activity by a small molecule suppresses *MLL*-rearranged leukemia

Bowen Xu, Doan M. On, Anqi Ma, Trevor Parton, Kyle D. Konze, Samantha G. Pattenden, David F. Allison, Ling Cai, Shira Rockowitz, Shichong Liu, Ying Liu, Fengling Li, Masoud Vedadi, Stephen V. Frye, Benjamin A. Garcia, Deyou Zheng, Jian Jin and Gang Greg Wang

Blood (print ISSN 0006-4971, online ISSN 1528-0020), is published weekly by the American Society of Hematology, 2021 L St, NW, Suite 900, Washington DC 20036.

ELSEVIER

Experimental Hematology

Experimental Hematology 2015;■:■–■

Targeting EZH2 and PRC2 dependence as novel anticancer therapy

Bowen Xu[a], Kyle D. Konze[b], Jian Jin[b], and Gang Greg Wang[a]

[a]*Department of Biochemistry and Biophysics, The Lineberger Comprehensive Cancer Center, University of North Carolina at Chapel Hill, Chapel Hill, North Carolina, USA;* [b]*Department of Structural and Chemical Biology, Icahn School of Medicine at Mount Sinai, New York, New York, USA*

(Received 5 April 2015; revised 1 May 2015; accepted 5 May 2015)

Distinctive patterns of chromatin modification control gene expression and define cellular identity during development and cell differentiation. Polycomb repressive complex 2 (PRC2), the sole mammalian enzymatic complex capable of establishing gene-repressive high-degree methylation of histone H3 at lysine 27 (H3K27), plays crucial roles in regulation of normal and malignant hematopoiesis. Recently, increasing evidence has indicated that recurrent gain-of-function mutation and overexpression of EZH2, the catalytic subunit of PRC2, drive and promote malignant transformation such as B-cell lymphomagenesis, providing a rationale for PRC2 inhibition as a novel anticancer strategy. Here, we summarize the recently developed strategies for inhibition of PRC2, which include a series of highly specific, highly potent, small-molecule inhibitors of EZH2 and EZH1, an EZH2-related methyltransferase. PRC2 establishes functional crosstalk with numerous epigenetic machineries during dynamic regulation of gene transcription. Perturbation of such functional crosstalk caused by genetic events observed in various hematologic cancers, such as inactivation of *SNF5* and somatic mutation of *UTX*, confers PRC2 dependence, thus rendering an increased sensitivity to PRC2 inhibition. We discuss our current understanding of EZH2 somatic mutations frequently found in B-cell lymphomas and recurrent mutations in various other epigenetic regulators as novel molecular predictors and determinants of PRC2 sensitivity. As recent advances have indicated a critical developmental or tumor-suppressive role for PRC2 and EZH2 in various tissue types, we discuss concerns over potentially toxic or even adverse effects associated with EZH2/1 inhibition in certain biological contexts or on cancer genetic background. Collectively, inhibition of PRC2 catalytic activity has emerged as a promising therapeutic intervention for the precise treatment of a range of genetically defined hematologic malignancies and can be potentially applied to a broader spectrum of human cancers that bear similar genetic and epigenetic characteristics.

Chromatin modification provides a fundamental means for regulating DNA accessibility in a wide range of DNA-templated processes such as gene transcription and DNA damage repair [1]. At the very least, the regulatory mechanisms for defining distinctive chromatin states include DNA methylation [2], posttranslational modification of histones [3], ATP-dependent chromatin remodeling [4], and utility of histone variants [5]. Deregulation of these chromatin regulatory mechanisms is directly involved in oncogenesis, including hematopoietic malignancies [3,4,6–9].

Polycomb repressive complex 2 (PRC2) probably represents the only enzymatic machinery capable of catalyzing the high-level methylation of histone H3 at lysine 27 (H3K27me3/2) in mammalian cells [10,11]. H3K27 trimethylation (H3K27me3) strongly associates with transcriptional repression [10,11]. Extensive studies have indicated that PRC2 and, by extension, H3K27me3 play critical roles in cell fate determination during development including hematopoietic lineage specification [12–15]. Biochemically, PRC2 uses either enhancer of zeste homologue 2 (EZH2) or a related homolog (EZH1) as the catalytic subunit, and other core components such as EED and SUZ12 are requisite for forming a stable and enzymatically active methyltransferase complex [10,11]. The DNA- and histone-binding properties harbored by PRC2 core components [10,11] and several PRC2-associated proteins [16–20]

BX and KDK contributed equally to this article.

Offprint requests to: Greg Wang, Department of Biochemistry and Biophysics, The Lineberger Comprehensive Cancer Center, University of North Carolina at Chapel Hill, Chapel Hill, NC 27599, USA; E-mail: greg_wang@med.unc.edu

0301-472X/
http://dx.doi.org/10.1016/j.exphem.2015.05.001

or noncoding RNAs [21] have been found to regulate PRC2's target specificity and mediate its chromatin association and/or spreading on chromatin. Hyperactivation of PRC2 caused by mutation or overexpression of EZH2 has been identified as a frequent genetic event among B-cell lymphomas [22–24]. In the next sections, we focus on our current understanding of the lymphoma-associated EZH2 mutations and recent exciting advances in developing EZH2/1-specific inhibitors as a novel molecularly targeted therapy. Because of the high degree of crosstalk between PRC2 and other chromatin regulatory machineries, we also cover recent findings of novel molecular determinants yielding sensitivity to PRC2 inhibition and discuss the potential applications for small-molecule PRC2 inhibitors as therapies in several genetically defined hematologic cancers.

Lymphoma-associated gain-of-function mutation of *EZH2*

During germinal-center (GC) B-cell development, EZH2 exhibits a dynamic expression pattern: it is massively upregulated when B cells undergo rapid proliferation and immunoglobulin affinity maturation on immune activation, and decreased after completion of these processes [14,25], suggesting a key role for EZH2 in GC development. EZH2 is expressed in a wide range of B-cell neoplasms including Burkitt's lymphoma, mantle cell lymphomas (MCLs), follicular lymphoma (FL), and diffuse large B-cell lymphomas (DLBCLs) [26,27]. It is upregulated in MCLs as compared with the normal tissue counterparts from which the lymphoma derived [28]. EZH2 deregulation indeed associates with B-cell lymphomagenesis [26], with its expression levels positively correlated with aggressiveness and unfavorable prognosis [29,30]. The importance of PRC2 in lymphomagenesis is further strengthened by the recent identification of recurrent, heterozygous missense mutations of *EZH2* in B-cell lymphomas of GC origin such as DLBCLs and FLs. These mutations specifically target the catalytic SET domain of EZH2. The most prevalent is a point mutation of the Tyr641 residue found mutated to either Asn, Phe, Cys, Ser, or His (Fig. 1A, the numeration of EZH2 amino acids based on a short isoform [NCBI Accession No. Q15910.2]) in ~10%–20% of DLBCLs and FLs [22,31,32]; two other rare EZH2 mutations, A677G and A687V (Fig. 1A), were reported in about ~1%–3% of B-cell lymphoma cases [23,31–33].

Biochemically, lymphoma-associated *EZH2* mutations alter substrate specificity of the PRC2 complex [31,34,35]. EZH2 can induce mono-, di-, and trimethylation of H3K27 (i.e., H3K27me1/2/3), with H3K27me3/2 most strongly associated with gene silencing. Kinetic studies in vitro indicate that PRC2 complexes assembled by the wild-type EZH2 (i.e., PRC2-EZH2^{WT}) have the greatest

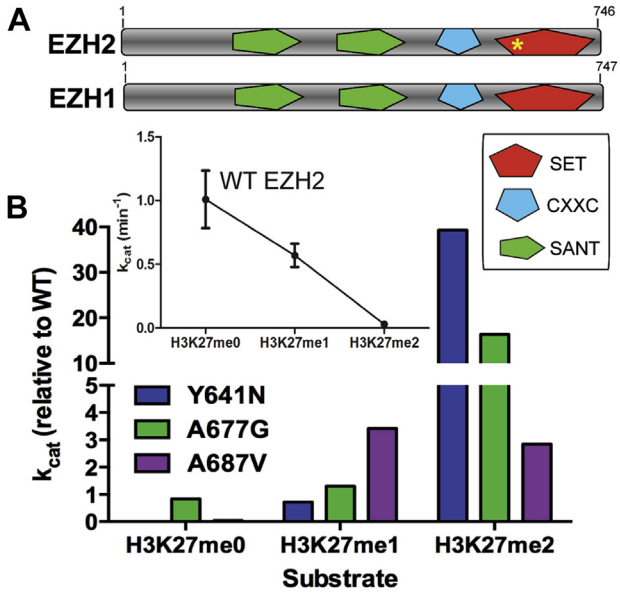

Figure 1. Gain-of-function EZH2 mutations affect substrate specificity of the PRC2 complex. (**A**) Depiction of EZH2 and EZH1 domain structure with the site of gain-of-function mutations (either the hotspot Y641 mutation, A667G, or A687V) in the catalytic SET domain of EZH2 highlighted with a *yellow asterisk*. (**B**) Wild-type EZH2 is more efficient at catalyzing the turnover of H3K27me0 and H3K27me1 than H3K27me2 (shown in inset, *black line*). Y641N (*blue bars*) and A677G (*green bars*) exhibit the opposite trend. A687V (*purple bars*) is equipotent at catalyzing the turnover of H3K27me1 and H3K27me2, relative to WT EZH2. *WT* = wild-type.

catalytic efficiency for converting nonmethylated H3K27 (H3K27me0) to monomethylated H3K27 (H3K27me1) and exhibit diminished efficiency for subsequent (H3K27me1 to H3K27me2 and H3K27me2 to H3K27me3) reactions [31,34,35] (Fig. 1B, inset). In contrast, PRC2 complexes bearing a lymphoma-associated EZH2 Tyr641 hotspot mutation such as Y641N (i.e., PRC2-EZH2^{Y641N}) display very limited ability to methylate nonmethylated H3K27, but once H3K27 is monomethylated, they can catalyze the turnover of H3K27me1 to H3K27me2 and, then, much more rapidly catalyze the H3K27me2-to-H3K27me3 reaction [31,34,35] (Fig. 1B, *blue bars*). The enzymatic differences between PRC2-EZH2^{WT} and PRC2-EZH2^{Y641N} require cooperation to produce the abnormally high level of H3K27me3 seen in the lymphoma cells [31,34,35]; a similar phenomenon was observed for other Tyr641 mutations such as Y641F [31,34,35]. Two other rare EZH2 SET domain mutations, A677G and A687V (Fig. 1A), also affect the substrate specificity of PRC2; however, they have kinetic properties that differ from those of the Y641 mutants [31,32,36,37]. For example, the A677G mutation leads to a form of EZH2 that is capable of efficiently methylating all the H3K27 substrates (Fig. 1B, *green bars*). Contrarily, the A687V mutation yields a PRC2 complex that is equipotent at methylating H3K27me1 and H3K27me2, but like

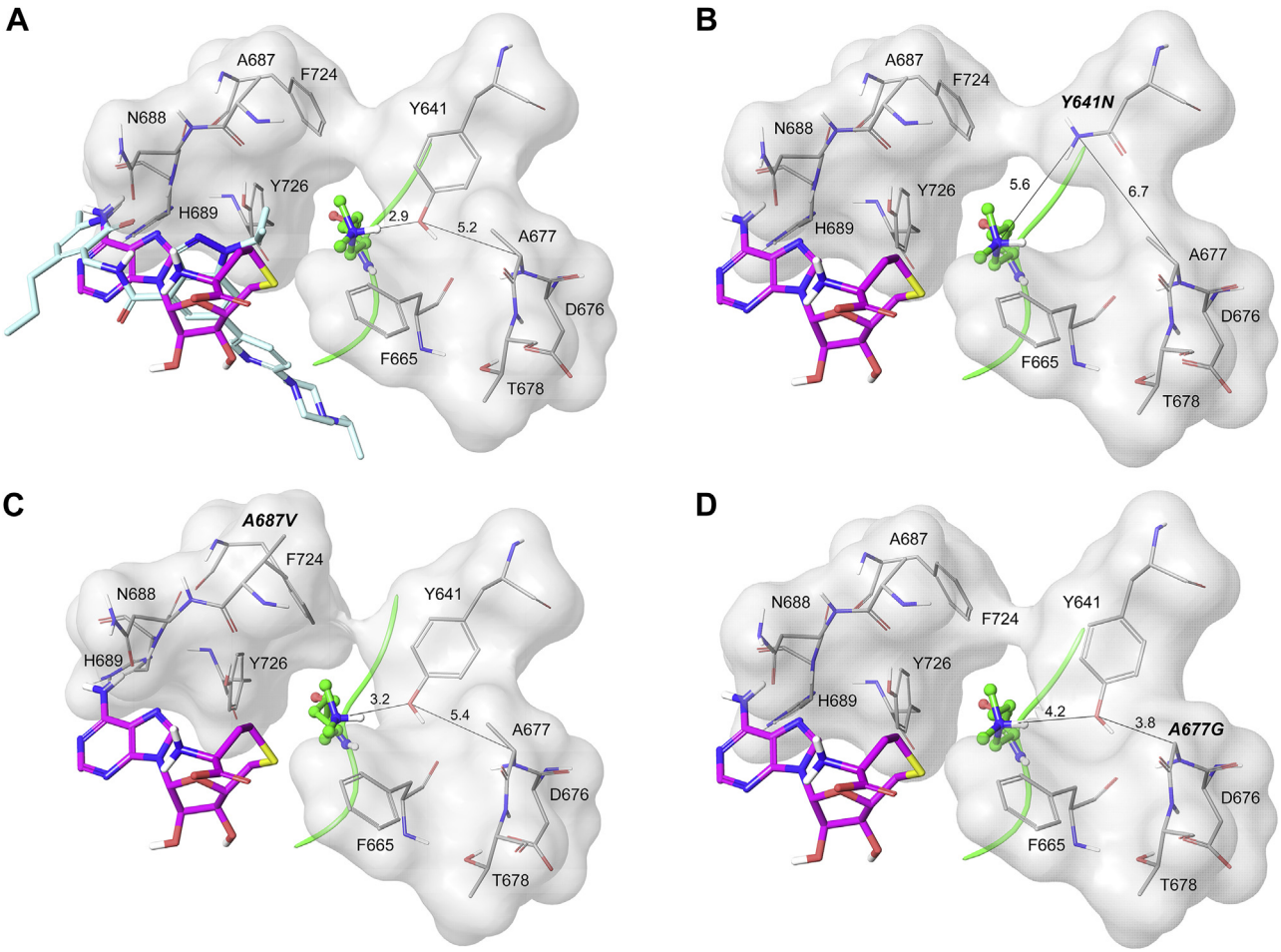

Figure 2. Mechanistic insights into substrate selectivity of EZH2 mutants. (**A**) Wild-type EZH2 uses Y641 to control the methylation state of H3K27 by maintaining a hydrogen bond (*dotted line*, 2.9 Å) with the dimethylated substrate (*green*). SAH (*purple*), the methylation product of cofactor SAM, and the SAM-competitive EZH2 inhibitor UNC1999 (*light blue*) are also included in the model to illustrate their overlapped binding sites. (**B**) Mutation to Y641N enlarges the pocket and reduces the propensity for a hydrogen bond between the asparagine and H3K27me2 (*dotted line*, 5.6 Å), promoting trimethylation of H3K27. (**C**) Mutation of A677 to the smaller glycine residue (A677G) leads to a slight conformational change, enlarging the pocket and weakening the hydrogen bond between Y641 and H3K27me2 (*dotted line*, 4.2 Å), which enhances the ability of $EZH2^{A677G}$ to trimethylate H3K27. (**D**) Mutation of A687 to valine (A687V) leads to a similar conformational change, which leads to a slightly larger pocket, and reduces the strength of the hydrogen bond between Y641 and H3K27me2 (*dotted line*, 3.2 Å). *SAM* = *S*-adenosylmethionine.

$PRC2\text{-}EZH2^{Y641N}$, is incapable of methylating H3K27me0 [31,32,36,37] (Fig. 1B, *purple bars*). Collectively, lymphoma-associated mutations of *EZH2* are gain-of-function mutations and induce PRC2 hyperactivity through distinct molecular mechanisms, leading to a globally elevated H3K27me3 phenotype seen in patient-derived lymphoma cells [26]. The reduced ability to methylate H3K27me0 by EZH2 bearing the hotspot mutation provides an explanation for the exclusively heterozygous mutation pattern observed in lymphoma patients [22,31,32]. A potentially additional aspect of this "cooperative" model is existence of EZH1 in vivo, to which we believe the model can be extended. In the future, generation of a murine *EZH2* Y641-mutated knockin model that faithfully recapitulates the human disease would be very useful for proving the "cooperative" model genetically.

Homology modeling [31,34] and the recently solved apo structure of the EZH2 SET domain [38,39] have provided mechanistic insights into the aforementioned trends in substrate specificity that was seen with the EZH2 gain-of-function mutants. Y641 is believed to be important for both recognizing and limiting the H3K27 methylation states. Specifically, the ε-amino lysine nitrogen of the H3K27 substrate is within proximity of the phenolic oxygen of Y641 to create a hydrogen bond (Fig. 2A, *dashed line*, 2.9 Å) [31,34]. This hydrogen bond is maintained through successive steps of mono- and dimethylation and is believed to be part of the reason $EZH2^{WT}$ prefers to stop methylation with an H3K27me2 product [31]. The functional relevance of this hydrogen bond is manifold [31]: first, it is important for engaging H3K27me0 as substrate, because all Y641 mutants possess little catalytic

activity with unmethylated substrates (Fig. 1B, H3K27me0); second, Y641 helps create a constrained "pocket" that reduces the ability of H3K27me2 to rotate and accept a third methyl group from the methyl donor (Fig. 2A). A mutation that results in a smaller amino acid at the Y641 position, such as $EZH2^{Y641N}$ (Fig. 2B), changes both the hydrogen bonding ability and local geometry of the substrate-binding pocket. $EZH2^{Y641N}$ is not as proficient at hydrogen bonding with H3K27, because the mutated N641 form is no longer within the acceptable range to form a hydrogen bond [31] (Fig. 2B, *dashed line*, 5.6 Å). Furthermore, as the pocket dimensions change, the dimethylated lysine of the H3K27me2 substrate is able to rotate more freely, which accelerates the transfer of an additional methyl group. Similar effects were observed for other EZH2 Y641 mutations (Y641 to F, C, S, or H), but the most drastic effects were seen with $EZH2^{Y641N}$ [31].

Structural modeling also provided an explanation for the altered substrate preference associated with the EZH2 A677G and A687V mutations. A677 and A687 are two residues that surround the substrate recognition groove and appear to play no direct role in substrate recognition (Fig. 2C, D); however, their mutation leads to a change in geometry of the substrate binding groove, which alters the kinetics of the corresponding PRC2 complex. This change in geometry has two effects on substrate recognition [31,37]: first, both mutations result in a slightly larger pocket, which allows for more rotation of the lysine residue; second, the phenolic oxygen of Y641 is shifted further away from H3K27, resulting in a less stable hydrogen bond, which reduces the ability of EZH2 to recognize the methylation state (Fig. 2C and D, 3.2 Å and 4.2 Å). Because of the smaller effect on pocket dimensions seen in the A677G and A687V mutants, they are less effective in generating H3K27me3 than Y641N mutants (Fig. 1B, H3K27me2 bars) [31], but $EZH2^{A677G}$ is as effective as $EZH2^{WT}$ at methylating H3K27me0 (Fig. 1B, *green bars*). A recent electron microscopy analysis of PRC2 complexes has indicated that the EZH2 SET domain can form intracomplex interactions with other PRC2 components [40]. Therefore, further investigations aimed at solving the structural details of PRC2 complexes will allow a better understanding of PRC2/EZH2 enzymology and its lymphoma-associated mutations.

Development of PRC2 inhibitors

As EZH2 overexpression is frequently found in various human cancers [3], EZH2 and PRC2 are proposed as attractive drug targets for cancer therapy, which has inspired several pharmaceutical companies to endeavor on high-throughput screening campaigns for inhibitors of EZH2. Independent efforts by Epizyme, GlaxoSmithKline (GSK), and Novartis have revealed a structurally similar, cofactor-competitive, small molecule, which potently suppresses EZH2-catalyzed H3K27me3 [41–47] (Table 1). These independent hits were then optimized via traditional medicinal chemistry to enhance the drug-likeness of these compounds.

The first two published EZH2 inhibitors are EPZ005687 [42] and GSK126 [41] (Table 1), which potently inhibit wild-type and lymphoma-associated mutants of EZH2 and are highly selective for EZH2 over a range of unrelated methyltransferases. Although EPZ005687 from Epizyme was not suitable for *in vivo* studies, it was an essential tool compound for target validation and overall study of EZH2 biology. GSK126 from GSK exhibited *in vivo* potency via intraperitoneal administration [41]. These compounds share very similar pharmacophoric features and are fairly selective for EZH2 versus EZH1, the only EZH2-related enzyme (50- to 150-fold selectivity [Table 1]), indicating the high specificity of these compounds. Soon after the disclosure of GSK126, GSK343 was published with similar potency against EZH2, and differs from GSK126 in that it contains an indazole core and several different substitutions such as the piperazine-substituted pyridine (Table 1). El1 (Table 1) is a compound that was optimized from a hit of a high-throughput screening campaign at Novartis [43] and has structural features and selectivity similar to those of EPZ005687 and GSK126, but did not have any *in vivo* activity. UNC1999 (Table 1) represents the first orally bioavailable inhibitor of EZH2 and is the most panactive EZH2/1 inhibitor to date [44]. UNC1999 is similar in structure to GSK343, differing only in the substitution of the pyridine and the capping group of the piperazine. However, this small modification has a large effect on the pharmacokinetic properties of the compound and EZH2/1 selectivity. EZH1 compensates the function of EZH2 [48,49] and emerges as a regulator of hematopoietic neoplasms [50,51]. This EZH2/1 panactivity poses a potential advantage for UNC1999 in cancer cells that rely on both EZH enzymes such as *MLL*-rearranged acute leukemia. Epizyme also released an orally bioavailable derivative of EPZ005687—EPZ-6438 [45] (Table 1). Unlike previously published compounds that contain a bicyclic core, EPZ-6438 has a phenyl core. The only non–pyridone-containing inhibitor of EZH2 is Constellation Pharmaceuticals compound 3 (Table 1) [46]. This compound is not suitable for *in vivo* studies and has about tenfold selectivity for EZH2 versus EZH1. All of these inhibitors exhibit high potency and high selectivity toward wild-type EZH2 and its lymphoma-associated mutant forms [41–47] (Table 1). In addition, enzymology assays revealed that all of the EZH2/1 inhibitors block EZH2 enzymatic activity through a cofactor *S*-adenosylmethionine (SAM)-competitive mechanism (Fig. 2A; inhibitor in *purple* overlapped with SAM shown in *cyan*), rather than disruption of PRC2 complex formation or alteration of PRC2 protein stability.

Table 1. Structures of the disclosed small-molecule inhibitors of EZH2, as well as their activity against EZH2, either wild-type (WT) or mutant, and EZH1[a]

Compound	Structure	*In vitro* activity, IC_{50} (nmol/L)[b]					*In vivo* activity?	Orally bioavailable?	Fold selectivity for EZH2
		WT	Y641N	A677G	A687V	EZH1			
EPZ005687	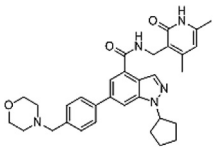	54	41	10	ND	2713	No	No	50
GSK126	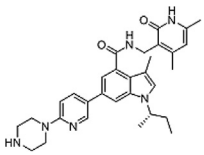	10	29	24	441	680	Yes	No	150
GSK343	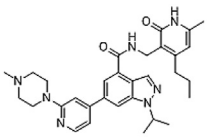	4	ND	ND	ND	240	No	No	60
El1	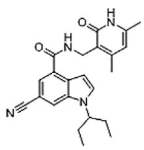	9	ND	ND	ND	1340	No	No	140
UNC1999	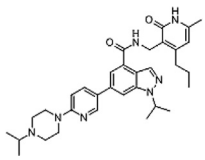	10	46	ND	ND	45	Yes	Yes	5
EPZ6438	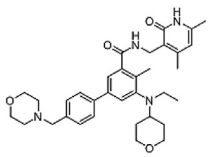	11	38	2	2	392	Yes	Yes	35
Constellation Compound 3	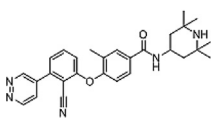	21	197	ND	ND	213	No	No	10

ND = not determined.

[a]Compounds appear in the order they were disclosed in the literature. All compounds except Constellation compound 3 bear a dimethylpyridone motif that is requisite for activity. Additionally, all compounds remain active against EZH2 gain-of-function mutants tested and are fairly selective for EZH2 over EZH1, with UNC1999 displaying the most EZH1 inhibition. GSK126 exhibited the first activity *in vivo*, and UNC1999 was the first EZH2/1 inhibitor to exhibit oral bioavailability.

[b]IC_{50} values were calculated on the basis of the Cheng–Prusoff equation for competitive inhibitors.

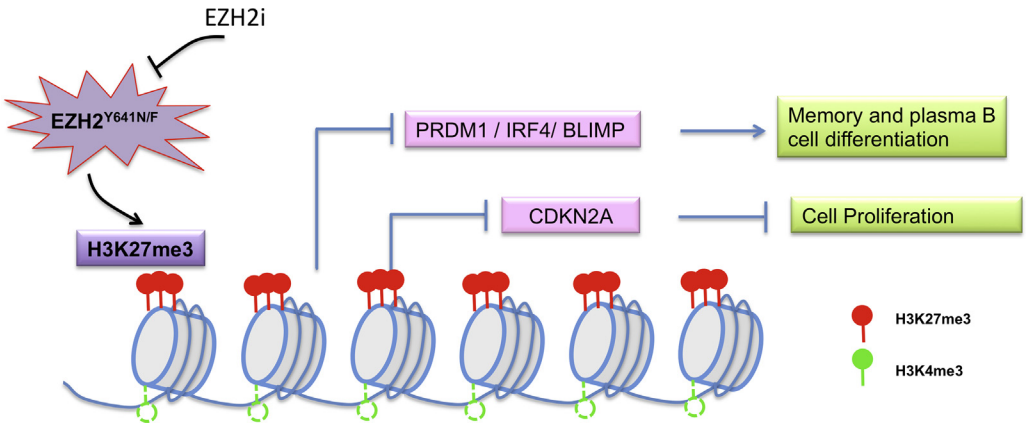

Figure 3. EZH2 gain-of-function mutations in driving B-cell lymphomagenesis. H3K27me3 and H3K4me3 often coexist at multiple genomic loci in germinal-center B cells, rendering these genes in a repressive but poised status. EZH2 gain-of-function mutants reinforce H3K27me3 occupancy and repression of the "bivalent genes" that are crucial for antiproliferation (such as *CDKN2A*) or terminal differentiation (such as PRDM1, IRF4, and BLIMP), promoting hyperplasia or cancerous transformation of germinal-center B cells.

Targeting EZH2 hyperactivity for B-cell lymphoma therapy

Recent studies have indicated that acquisition of EZH2 gain-of-function mutations indeed perturbs normal B-cell development and promotes lymphomagenesis in animal models [14,15,53,54]. Mechanistically, EZH2 gain-of-function mutations cause increased H3K27me3 occupancy and transcriptional repression of critical genes associated with B-cell differentiation, such as *BLIMP1*, *IRF4*, and *PRDM1*, as well as the cell cycle regulator genes *CDKN2A* and *CDKN1A/1B* [14,15,53,54] (Fig. 3). Thus, lymphoma-associated EZH2 mutations are supposed to reinforce B cells at an immature and proliferative state and represent ideal molecular targets. Indeed, early success has been achieved using highly selective EZH2 inhibitors for treatment of GC-cell lymphomas bearing EZH2 gain-of-function mutations [15,41–47]. Studies with GSK126 [41], EPZ005687, and EPZ-6438 [42,55] indicate their preferential effectiveness in suppressing growth of *EZH2*-mutated lymphomas in comparison to those with wild-type EZH2. However, B-cell studies performed in DLBCLs [15], MCLs, and Burkitt's lymphoma [47,56] indicate that overexpression of *EZH2* may confer a similar PRC2 addiction, arguing a general sensitivity to EZH2 inhibitors regardless of EZH2 mutations. Besides cell-based studies, early success with EZH2-selective inhibitors *in vivo* was also achieved in treatment of xenografted DLBCL models in which GSK126 was well tolerated [41]. It remains to be evaluated by several ongoing clinical studies whether the selective PRC2 inhibitors can provide clinical benefits to lymphoma patients. It is, however, noteworthy that the first two patients reported as responders in a recent Epizyme clinical trial are actually EZH2 wild type, with a mediastinal B-cell lymphoma patient reportedly bearing no germinal center features [57]. These unexpected findings raise questions regarding what genetic markers in these responder cases render sensitivity to EZH2 inhibitors clinically or which of the molecular response predictors identified in preclinical mouse and cell line studies will actually translate to the clinic.

Collectively, PRC2 inhibition represents a promising way to treat B-cell lymphomas, especially those DLBCLs, FLs, and MCLs that exhibit PRC2 dependency because of *EZH2* somatic mutation or overexpression.

Crosstalk between PRC2 and other chromatin regulatory pathways

Evidence from different cellular and organismal systems has revealed complex crosstalk between PRC2 and other chromatin machineries. PRC2 activity is influenced by a myriad of cooperative and antagonistic interactions, allowing dynamic regulation of PRC2 target genes and the landscape of H3K27me3. It can be anticipated that certain genetic events during cancer development may affect these crosstalk and genetic interactions, thus conferring a "synthetic" or collateral sensitivity to PRC2 or EZH2 blockade.

Several mechanisms were found to reverse or interfere with PRC2 enzymatic activity (Fig. 4). While PRC2 establishes or "writes" H3K27me3 on chromatin, the KDM6 family of H3K27 demethylases such as UTX removes or "erases" the mark by converting H3K27me3 to the low- or unmethylated H3K27 [58]. Furthermore, catalysis of H3K27me3 is influenced by the surrounding chromatin environment, such as the existence of other histone modifications [59,60] and nucleosomal density [61]. Methylation of histone H3 Lys 4 (H3K4me) and methylation of histone H3 Lys 36 (H3K36me) are two prominent histone marks that demarcate the promoter and gene body regions, respectively, of actively transcribed genes [3,62]. Pre-existence of H3K4me3 or H3K36me2/3 on nucleosomes directly inhibits enzymatic activities of PRC2 [59,60]. In addition,

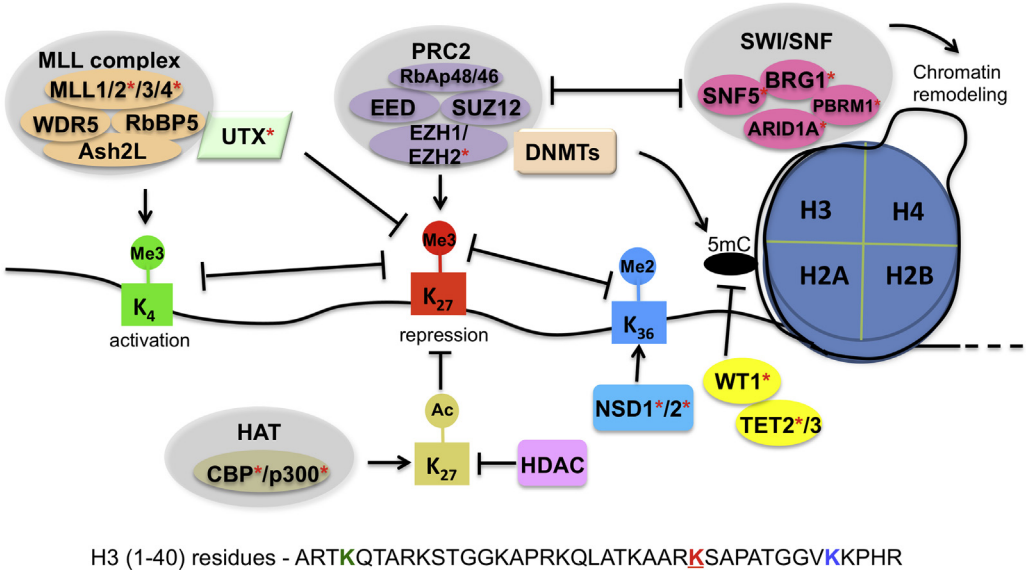

Figure 4. Crosstalk between PRC2 and other epigenetic factors. PRC2 is the sole methyltransferase complex capable of catalyzing H3K27me3 to induce and enforce gene repression. Various epigenetic machineries have crosstalk with PRC2 complex, either cooperatively or antagonistically. The KDM6 family of lysine demethylases such as UTX removes H3K27me3. Methylations of H3K4 and H3K36, as well as acetylation of H3K27, are prominent histone marks associated with transcriptional activation, which are established by the MLL complexes, the NSD family proteins, and the CBP/p300 acetyltransferases, respectively; preinstallation of H3K4me3, H3K36me2/3, and/or H3K27ac inhibits the activity of PRC2 and interferes with H3K27me3 installation. UTX physically interacts with the MLL complex linking H3K4 methylation with H3K27 demethylation. SWI/SNF is an ATP-dependent chromatin remodeling complex that can also antagonize PRC2. PRC2 was found to interact with other epigenetic factors such as histone deacetylases (HDACs) and DNA methyltransferases (DNMTs) to further reinforce a repressive state of polycomb target genes. WT1, however, serves as a platform for recruiting DNA demethylases TET2 and TET3, thus facilitating conversion of 5-methylcytosine (5 mC) to 5-hydroxymethylcytosine (5hmC) and attenuating the DNA methylation-mediated repression. Genetic alterations that affect such a myriad of epigenetic factors (*red stars*) are identified as the recurrent event in various hematopoietic malignancies, causing global or focal perturbation of PRC2 activity and H3K27me3 and thereby rendering cancer cells sensitive to PRC2 inhibition.

because a single lysine cannot be simultaneously modified by methylation and acetylation at the ε-amino group, acetylation of H3K27 (H3K27ac) by histone acetyltransferases such as p300 and CBP also strongly suppresses addition of H3K27me3 by PRC2 [63,64]. Thus, the existence of active histone marks (H3K4me3, H3K36me3/2, H3K27ac) and associated enzymatic machineries directly inhibits PRC2-mediated H3K27me3 establishment (Fig. 4).

Furthermore, genetic studies in *Drosophila* have revealed that the SWI/SNF family of chromatin remodeling complexes antagonizes PRC2 (Fig. 4): mutation of *SWI/SNF* suppressed developmental defects caused by mutation of PRC2 homologues in flies [65]. Although the exact underlying mechanism remains unclear, SWI/SNF remodeling complexes modify DNA accessibility and nucleosomal density [66], a factor known to influence PRC2 enzymatic activity [61]. It has been hypothesized that interplay between SWI/SNF and PRC2 complexes defines a dynamic balance of the chromatin state [67].

Factors also exist that cooperate with PRC2 and promote its function (Fig. 4). For instance, PRC2 physically interacts with the histone deacetylases HDAC1-3 [68], which remove the acetyl group from H3K27ac and thus make the lysine available for methylation by PRC2. PRC2 also associates with *de novo* DNA methyltransferases [69], and it was reported that H3K27me3 and PRC2 targets are positively correlated to DNA methylation [11,69–71].

Taken together, mounting data have indicated that PRC2 activity and functional outcomes are regulated by additional chromatin contexts. Epigenetic factors that influence PRC2 activity or catalytic outcomes such as UTX [72,73] and MMSET/NSD2 [74,75] were recurrently found mutated in a range of hematopoietic malignancies. We therefore anticipate that these genetic lesions may potentially affect PRC2 and confer tumor cell sensitivity to PRC2 inhibition. In the next sections, we summarize recent studies that have indicated PRC2 inhibition as a promising therapeutic option in several genetically defined hematologic malignancies. These studies have expanded the potential applications of PRC2 inhibitors and will improve the personalized medicine and treatment of hematologic cancers in future.

Genetic lesions that confer PRC2 dependence and sensitivity to PRC2 inhibition

UTX mutation

UTX (also known as KDM6A) is a ubiquitously expressed H3K27 demethylase that antagonizes PRC2 in gene regulation and development [76–78]. Localized on the X

chromosome, *UTX* is one of a limited number of genes known to escape X inactivation in females [79]. Somatic mutations of *UTX* were frequently identified in a range of tumors including hematologic cancers such as multiple myeloma (MM), acute lymphoblastic leukemia (ALL), and myeloid leukemia [72,73,80–83] (Fig. 5A). These *UTX* mutations are often loss-of-function gene deletions, truncations and frameshifts, or missense mutations found centered in a hotspot region within the demethylase enzymatic domain [72,80,81]. *UTX* mutations coexist with the hyperactivation mutation of *NOTCH1*, one of the most common lesions associated with T-cell ALLs (T-ALLs) [80]. Deletion of *UTX* significantly accelerated tumor progression in a *NOTCH1* mutation-induced T-ALL model [80], whereas restoration of *UTX* expression in *UTX*-mutated T-ALL cell lines induced apoptosis and suppressed tumor growth [81]. These observations support a *bona fide* tumor-suppressive role for UTX. Although *UTX* deficiency did not change the global levels of H3K27me3 or H3K4me3, it caused a genomewide redistribution of H3K27me3 [72,80,81]. In the *NOTCH1* mutation-induced T-ALL model, loss of *Utx* aberrantly repressed several putative tumor suppressors such as *Pcgf2* and *Lzts2*, which is concurrent with gain in H3K27me3 at their promoters [80] (Fig. 5A). Conversely, gene derepression after *UTX* restoration in *UTX*-null tumor lines was associated with a decrease in H3K27me3 occupancy at target genes [72,80], demonstrating direct involvement of UTX-mediated demethylation in dynamic control of critical gene expression and malignant transformation. Considering the aberrant H3K27me3 accumulation and accompanying gene repression at critical location upon *UTX* mutation, it is reasonable to postulate that *UTX*-mutated leukemia and lymphoma would be more sensitive to PRC2 inhibition. Indeed, van der Meulen et al. have recently reported that *UTX*-mutated T-ALL lines are more sensitive to DZNep, a nonspecific methyltransferase inhibitor that causes EZH2 degradation, than *UTX* wild-type T-ALL lines, despite the similar reduction in H3K27me3 seen in tested lines after compound treatment [80]. Similarly, Ezponda et al. recently reported

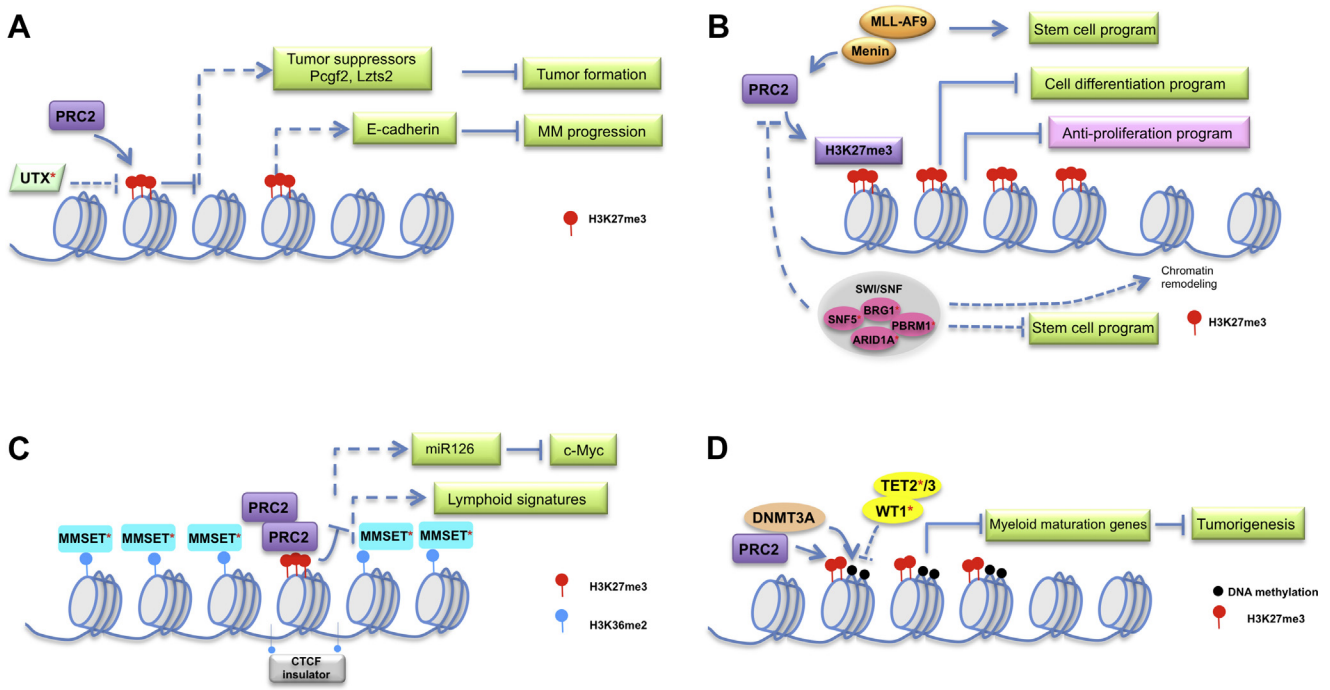

Figure 5. Genetic mutations found in hematopoietic malignancies confer on cancer cells sensitivity to PRC2 or EZH2 inhibition. (**A**) Although they do not affect the global H3K27me3 level, *UTX* inactivating mutations cause focal H3K27me3 enrichment in genes involved in antiproliferation and cell adhesion to promote cancerous transformation. *denotes mutation of the labeled gene found in hematological cancers. (**B**) Biallelic inactivation of a core component of the SWI/SNF chromatin remodeling complex, *SNF5* (also known as *SMARCB1*), enhances PRC2-mediated suppression of antiproliferation and lineage differentiation signature genes; other subunits of the SWI/SNF complex also function as tumor suppressors and their mutations in malignancies may confer a similar PRC2 dependence. Similarly, PRC2 is also required for acute leukemia caused by *MLL* rearrangements such as MLL-AF9. In addition to leukemia stem cell programs, MLL-AF9 oncoproteins directly promote expression of *EZH2*. PRC2 complexes assembled by both EZH2 and EZH1 repress myeloid differentiation and antiproliferation programs to promote acute leukemogenicity. (**C**) Because of the abnormal chromosomal translocation or gain-of-function somatic mutation (E1099K) found in multiple myeloma patients, hyperactivation of MMSET/NSD2 causes a global increase in H3K36me2 and decrease in H3K27me3. However, H3K27me3 is maintained and even enriched at certain critical regions protected by CTCF, an insulator factor. Focal enrichment of EZH2 leads to an enhanced suppression of lymphoid signatures and miR126, a negative regulator of c-*MYC*, thus enhancing tumorigenesis. (**D**) Loss-of-function mutation of *WT1* induces a DNA hypermethylation phenotype in patients with acute myeloid leukemia (AML). Methylated genes found specific to *WT1*-mutated AMLs largely overlap with PRC2 gene targets such as myeloid maturation signatures, indicating cooperation between DNMTs and PRC2. *WT1*-mutated AMLs exhibit sensitivity to PRC2 inhibition.

that GSK343 (Table 1) is more effective in treating *UTX*-mutant MM lines in comparison to the *UTX*–wild-type lines [84]. These findings provide rationale for treating *UTX*-mutated hematopoietic tumors with the more specific PRC2 inhibitors.

Loss-of-function mutation of the SWI/SNF *complex*

The mammalian SWI/SNF complex is an ATP-dependent chromatin remodeling complex that is critical for regulating cell differentiation and proliferation [85]. Loss-of-function mutations that "hit" various components of the SWI/SNF complex have been reported in nearly 20% of human cancers, including hematologic cancers, indicating its tumor suppressive role [86,87] (Figs. 4 [*stars*] and 5B). SNF5 is the first subunit of SWI/SNF functionally linked to PRC2 deregulation during tumorigenesis [88]. Biallelic inactivation of *SNF5* exists in a majority of human malignant rhabdoid tumors (MRTs) [89,90] and sporadic cases of T-cell malignancies [91]. Conditional inactivation of *Snf5* in mouse peripheral T cells causes completely penetrant CD8+ T-cell lymphomas [88]. It has been found that *Snf5* mutation drives tumor progression by disrupting several key pathways related to tumor suppression, differentiation, and cell cycle progression [66]. The mechanisms that underlie functional antagonisms between SNF5 and PRC2 are manifold: first, SNF5 directly downregulates *EZH2* gene expression in tumor cells [88]; in addition, the SWI/SNF complex restricts the recruitment and/or spreading of PRC2 at its critical target genes such as the tumor-suppressive locus $p16^{INK4a}$ and numerous lineage differentiation genes [67,88]. PRC2-mediated repression of $p16^{INK4a}$ is counteracted by SNF5, and occupancy of H3K27me3 was elevated at $p16^{INK4a}$ in *SNF5*-deficient lymphomas [67,88]; restoration of SNF5 in MRT cells caused eviction of polycomb proteins and loss of H3K27me3 at the $p16^{INK4a}$ gene, as well as concomitant increased occupancy of transactivators, leading to its elevated transcription [67] (Fig. 5B). A similar phenomenon was seen at differentiation genes in these *SNF5*-deficient lymphomas [88]. Therefore, in tumors carrying *SNF5* deficiency such as T-cell lymphomas, PRC2 complexes abnormally enforce repression of genes critical for tumor suppression and cell differentiation, keeping cancer cells in a proliferative, undifferentiated state. Indeed, knockdown or deletion of *EZH2* in the *SNF5*-deficient cells reversed $p16^{INK4a}$ repression [88]. These findings indicate PRC2 dependence in *SNF5*-deficient cancers. A recent study found that blockade of PRC2 activity by an EZH2 inhibitor specifically suppressed growth of *SNF5*-deleted and not wild-type MRTs, by inducing apoptosis and cell differentiation in the mutant MRTs [45]. As mutations of other SWI/SNF complex components such as BRG1, ARID1A, and PBRM1 (Figs. 4 and 5B, *stars*) were found in various cancers and are generally less well understood, it would be intriguing to examine if these mutations also confer SWI/SNF loss-of-function and, thus, PRC2/EZH2 dependence. Indeed, two recent studies have reported that *BRG1*-mutated non–small-cell lung cancer (NSCLC) cells [92] and *ARID1A*-mutated ovarian cancer cells [93] exhibit sensitivity to GSK126 (Table 1), an EZH2-selective inhibitor, in comparison to cancer cells without such a lesion. Hematopoietic cancers bearing the similar mutations might be equally sensitive to PRC2 inhibition.

MLL gene rearrangement

The mammalian *mixed lineage leukemia* (*MLL*) gene encodes an H3K4-specific methyltransferase [3,94]. Rearrangement of *MLL* is responsible for ~70% of infant acute myeloid, lymphoid, or mixed-lineage leukemias and ~7%–10% of adult cases [94]. Acute leukemia with *MLL* rearrangement has a poor prognosis with low survival rates, highlighting the need for novel molecularly targeted interventions [95,96]. It has been found that MLL fusion oncoproteins produced by *MLL* gene rearrangements recruit epigenetic factors and/or transcriptional elongation-promoting complexes such as DOT1L and bromodomain proteins (BRD4) to enforce abnormal activation of oncogenes such as *HOX*, *MEIS1*, and *c-MYC* [3,94–96]. In addition, studies have also found that MLL fusion oncoproteins are recruited to the promoter of *EZH2* and promote its transcription [97] (Fig. 5B), indicating a role for PRC2 in *MLL*-rearranged leukemia. Indeed, several works have found that PRC2 acts in parallel with *MLL* rearrangements by controlling a distinctive program to sustain leukemogenicity [50,51,98]. In detail, PRC2 directly represses genes that are critical for myeloid differentiation such as *EGR1*, as well as genes that limit proliferation and self-renewal of hematopoietic cells such as *CDKN2A* [50,51,98]. In addition, EZH2 was also found to physically interact with C/EBPα, a differentiation-promoting transcription factor, and repressed the C/EBPα-mediated prodifferentiation program [97]. In the *MLL*-rearranged acute leukemia, both *EZH2* and *EZH1* are expressed and compensate one another to promote acute leukemogenesis [50,51]. Disruption of both enzymes is required to inhibit growth of leukemia carrying *MLL-AF9*, a common form of *MLL* rearrangements [50,51]. UNC1999, the most panactive inhibitor of both EZH1 and EZH2 to date (Table 1), indeed demonstrated a unique growth-suppressing effect on a panel of *MLL*-rearranged leukemia cells *in vitro* by inhibiting their repopulating ability and promoting cell differentiation and apoptosis, whereas GSK126, the EZH2-selective inhibitor with much less activity against EZH1 (Table 1), failed to efficiently inhibit H3K27me3 or suppress proliferation of *MLL*-rearranged leukemia cells [52]. Genomic profiling by ChIP-seq revealed the molecular events following PRC2 enzymatic inhibition: UNC1999 preferentially "erases" H3K27me3 associated with distal regulatory

elements such as enhancers and remodels the landscape of H3K27me3 versus H3K27ac at proximal promoters, leading to derepression of numerous PRC2 target genes that include *CDKN2A* and development/differentiation-related genes [52]. Oral administration of UNC1999 prolonged survival of a well-defined murine leukemia model bearing *MLL-AF9*, a common form of *MLL* rearrangement [52]. Therefore, the targeting of both PRC2-EZH2 and PRC2-EZH1 with small-molecule compounds such as UNC1999 represents a new way of treating *MLL*-rearranged leukemia; a similar tumor-suppressing phenomenon was also observed in *MLL*-rearranged leukemia using a hydrocarbon-stapled peptide recently developed to disrupt physical interactions of EZH2 and EZH1 with its cofactor EED, which leads to the proteasome-mediated degradation of PRC2 complexes [99].

Translocation and activating mutation of MMSET/NSD2

MMSET (also known as NSD2 or WHSC1) is a histone methyltransferase that catalyzes dimethylation of histone H3 at lysine 36 (H3K36me2), a histone modification associated with transcriptional initiation and/or elongation [100]. Reciprocal t(4;14) translocation, which results in *MMSET* fusion to the immunoglobulin heavy chain locus and, hence, overexpression of *MMSET*, was reported in 15%–20% of multiple myeloma patients [101]. This genetic event is believed to drive tumorigenesis of myeloma and is associated with lower survival rates of myeloma patients [102–105]. Consistently, a recurrent gain-of-function mutation of *MMSET* (E1099 K) was also identified in a subset of ALL patients [74,75] and specifically targets the catalytic SET domain of MMSET. In both cases, the activated MMSET reprograms the landscape of histone modifications, inducing a global increase in H3K36me2 and concurrent decrease in H3K27me3, caused by the antagonistic effect of H3K36me2 on PRC2 and, thus, H3K27 methylation (Figs. 4 and 5C) [74,106,107]. However, despite a genomewide net loss of H3K27me3, this silencing mark is maintained and even enriched further at certain specific loci [106]. Motif analysis suggested that CTCF, a known genome organizer and insulator, is likely to be responsible for preventing these PRC2/H3K27me3 domains from the intrusion of MMSET [106]. This study indicates that although the hyperactivated MMSET restricts the binding and activity of PRC2 at H3K36me2-demarcated loci, it also induces a collateral effect at putative "CTCF-protected" loci because the free pool of PRC2 has nowhere else to bind [106]. As a result, the latter loci end up with enhanced PRC2 binding and a concomitant elevated level of H3K27me3, leading to abnormal repression of the embedded genes [106] (Fig. 5C). Further genomic profiling revealed that genes embedded within the retained PRC2 domains include the GC B cell-associated gene signatures, as well as critical microRNAs such as miR-126, a negative regulator of *c-MYC* [106] (Fig. 5C), suggesting a critical role for certain newly acquired PRC2-binding sites in promotion of growth and aggressiveness of myeloma cells with MMSET hyperactivation. Indeed, myeloma cells carrying t(4;14) *MMSET* translocations exhibit more sensitivity to GSK343 (Table 1) than t(4;14)-negative myeloma cells [106]. GSK343 treatment also led to elevated miR-126 levels and concomitant decreased MYC levels. Therefore, although additional studies need to be carried out, PRC2 inhibitors represent a promising therapeutic agent for treatment of myeloma patients with MMSET hyperactivity.

Inactivating mutations of WT1

The *Wilms' tumor 1* (*WT1*) gene encodes a sequence-specific zinc finger transcription factor that was originally identified as a tumor suppressor in Wilms' tumor, a rare kidney cancer [108]. WT1 has been linked to regulation of critical differentiation genes in various biological processes, particularly nephrogenesis and hematopoiesis [109]. Heterozygous somatic mutations of *WT1* were identified in approximately 10% of cases of acute myeloid leukemia (AML), with the hotspot mutations centered within the DNA-binding zinc finger domains [110,111]. These loss-of-function mutations of *WT1* correlate with poor prognosis and chemotherapy resistance in AML patients, but the role of WT1 and oncogenic mechanisms that underlie *WT1*-mutated AMLs is unclear [111]. Recent studies have linked *WT1* mutations to regulation of DNA methylation [112–114] (Figs. 4 and 5D). WT1 physically interacts with the methylcytosine dioxygenases TET2 and TET3, and serves as one of the mechanisms responsible for recruitment of TET2/3 to target loci (Fig. 4), where TET proteins mediate DNA demethylation via conversion of 5-methylcytosine (5 mC) to 5-hydroxymethylcytosine (5hmC) and subsequent oxidative derivatives [112,113]. Inactivated mutants of WT1 in AMLs lack the critical DNA binding domains, leading to a DNA hypermethylation phenotype in the affected AMLs [112–114]. Indeed, introduction of mutant *WT1* into *WT1*–wild-type AML cells is sufficient in inducing DNA hypermethylation, indicating a causal role for *WT1* mutation in regulating DNA methylation [114]. Intriguingly, the DNA hypermethlylated loci were found enriched with signature of known PRC2 targets such as differentiation genes [114], indicating cooperation between DNA hypermethylation and PRC2 (Fig. 5D). Consistently, the mutant and not wild-type WT1 blocked myeloid differentiation of hematopoietic stem cells [114]. Moreover, EZH2 is significantly overexpressed in *WT1*-mutated AMLs compared with *WT1*–wild-type cases [114] (Fig. 5D). EZH2 knockdown or its blockade with the inhibitor GSK126 promoted myeloid differentiation in AML cells carrying *WT1* mutations [114]. These studies have provided rationale for using EZH2 inhibitors in the treatment of *WT1*-mutated AMLs.

Potential adverse, side, and toxic effects of PRC2 or EZH2 inhibition

Despite enthusiasm shared by the community for EZH2/1 inhibitors as a future cancer therapy, recent studies have raised concerns over the potentially side, toxic, or even adverse effects caused by PRC2/EZH2 blockade.

First, in contrast to the oncogenic function of PRC2 and EZH2 described above, inactivating mutation of EZH2 and other PRC2 components has emerged as a recurrent theme in a range of human cancers, which demonstrates a dichotomous role for PRC2 in different biological contexts and raises concerns over PRC2 and EZH2 inhibition in clinical treatment. Specifically, various damaging mutations, such as biallelic deletion and missense, frameshifting, or truncation mutations, that "hit" either the PRC2 core component (EZH2, EED, and SUZ12) [115–117] or cofactor genes (JARID2 [118] and ASXL1 [119]) are recurrent in a range of myeloid neoplasms such as myelodysplastic syndromes (MDSs), primary myelofibrosis (PMF), myeloproliferative neoplasms (MPNs), and chronic myelomonocytic leukemia (CMML); similar PRC2-inactivating somatic mutations also occur frequently among human T-ALL [120–122] and solid tumors such as malignant peripheral nerve sheath tumors (MPNSTs) [123–126]. These PRC2-inactivating mutations are associated with adverse prognostic outcomes of MDS and PMF patients [127]. The tumor-suppressive role of PRC2 has been verified with several murine cancer models: deletion of *Ezh2* alone in hematopoietic systems is sufficient to cause spontaneous T-ALL with an average latency of 150 days in mice [122]; *Ezh2* loss also led to development of an MDS/MPN-like phenotype following serial bone marrow transplantation [128]; loss of PRC2 caused aberrant gene transcription programs and significantly enhanced *in vivo* tumorigenesis driven by mutant RAS signaling [123–126]. These recent findings have collectively indicated that EZH2 and PRC2 act as *bona fide* tumor suppressors in certain cell lineages or biological contexts.

In addition, EZH2/1 or PRC2 was also reported to be important in normal development. In particular, *EZH1* is documented as a crucial factor in maintaining the self-renewal capacity of adult HSCs by protecting them from senescence [13]; similar developmental roles for EZH2 or EZH1 were reported as well in other tissue-specific stem and progenitor cells [129,130]. A dual EZH2 and EZH1 inhibitor may therefore cause greater toxicity by impairing normal functions of the PRC2 assembled by both enzymes.

Collectively, these recent advances have urged the field to re-evaluate the clinical application of PRC2 and EZH2 inhibitors with more caution. A safe therapeutic window needs to be determined to eradicate cancer cells over generation of the unwanted toxic or even adverse effect during treatment. Furthermore, efforts are required to explore the cancer genetic backgrounds that define either beneficial or adverse effects of PRC2/EZH2 inhibition. Indeed, a recent study of NSCLCs indicated that usage of EZH2 inhibitors can cause differential or even opposite effects among NSCLC patients carrying different genetic backgrounds: although EZH2 inhibition sensitizes the *BRG1*-mutated NSCLCs to etoposide, a topoisomerase II inhibitor, and improves cancer treatment, the same EZH2 inhibitor causes an opposite effect by conferring *BRG1* wild-type NSCLC resistance on topoisomerase II inhibitors [92].

Combination therapy and drug resistance

PRC2 inhibitors can be potentially used with other Food and Drug Administration-approved agents, either sequentially or in a combinational therapeutic strategy, to further enhance their therapeutic value. Indeed, pretreatment with EZH2 inhibitor sensitized *BRG1*-mutated NSCLCs to the topoisomerase II inhibitors, and dual treatment with EZH2 and topoisomerase II inhibitors provided synergy in reversing oncogenicity [92]. A similar and dramatic synergistic antitumor effect was observed when combining EZH2 inhibitors with Food and Drug Administration-approved glucocorticoid receptor agonists such as prednisolone and dexamethasone in the treatment of lymphomas, regardless of *EZH2* mutation status [131]. However, the molecular basis for these described synergistic effects remains unclear. Use of a PRC2 inhibitor in combination therapy with other developed agents, for example, inhibitor of histone deacetylase, will also be explored (Fig. 4), because PRC2 and histone deacetylase are known to interact physically in their coordinated action in mediating gene silencing [26].

In addition, it is probably not of a total surprise that tumor cells may develop strategies such as the acquired additional mutations that confer resistance to EZH2/1 inhibitors, because clinically relevant and inhibitor-resistant mutations were found during treatment with inhibitors of oncogenic kinase such as BCR-ABL [132] and B-RAF [133]. Indeed, a very recent cell line–based study identified the two missense mutations of *EZH2* that affect compound binding and therefore confer resistance to several tested EZH2 inhibitors [134]. One of such acquired mutations, *Y661D*, occurs *cis* in the *EZH2 Y641*-mutated allele and is in the vicinity of the SAM pocket where these inhibitors are believed to bind (Fig. 2A); however, the other mutation, *Y111L*, is found in the wild-type *EZH2* allele, thus providing additional support for the model of cooperativity between wild-type and mutant EZH2 enzymes. The fact that Y111L is far from the SAM-binding pocket (located between the EED-binding domain and the SANT domain) suggests a long-range interaction potentially via formation of a high-order PRC2 complex for mediating regulation or formation of an active methyltransferase domain of EZH2. Research is required to learn the structural details of EZH2/1 inhibitors bound to EZH2 or the PRC2 complex, which will enable the rational design of new strategies for inhibiting the inhibitor-resistant mutations that tumors can acquire during treatment.

Conclusions

Therapeutic targeting of PRC2 initially emerged from studies reporting that overexpression or hyperactive mutation of *EZH2* can initiate, promote, or maintain oncogenesis. The already developed small-molecule inhibitors of PRC2 or EZH2/1 have achieved early success in the laboratory and are currently under clinical evaluation for the treatment of germinal-center B-cell lymphomas bearing *EZH2* mutations, which account for about 15%–20% of all cases. Studies have revealed the genetic interaction and functional crosstalk (either cooperative or antagonistic) of PRC2 with a variety of other chromatin modifiers and epigenetic regulators such as SWI/SNF, UTX, and MMSET. Somatic mutations that affect these epigenetic factors have been identified as a recurrent genetic event in a range of hematopoietic malignancies, which cause a collateral dependence of PRC2 and an increased sensitivity to pharmacologic inhibition of PRC2 or EZH2. In addition, increasing evidence has started to reveal the PRC2-independent roles of EZH2/1 in various cancer and biological contexts [135–137], and further investigations shall be extended to studies of their nonhistone substrates [138] and/or noncanonical gene-activation roles [139,140]. Thus, we expect to see an increasing list of such PRC2 or EZH2 dependencies in the future. For example, the trithorax group proteins, such as the MLL family of H3K4-specific methyltransferases and histone acetyltransferases CBP/p300, are known to antagonize PRC2 (Fig. 4) [3], and inactivating somatic mutations of *MLL2*, *MLL4*, *CBP*, and *p300* are frequent in lymphomas [23,24,141]. In addition to EZH2 gain-of-function mutations, identification of collateral PRC2 or EZH2 dependency in various hematopoietic malignancies has expanded the potential application of the already developed PRC2 inhibitors and will promote the precision medicine and personalized therapy. However, considering the fact that PRC2 or EZH2 has a tumor-suppressive role with loss-of-function mutations recurrently identified in various human cancers, we need to avoid treating cancer patients with certain genetic lesions and backgrounds with EZH2 or PRC2 inhibitors because such blockade could accelerate cancer progression, as reported in recent studies [92,123–126]. Although ongoing efforts continue to optimize the pharmacokinetic and pharmacodynamic properties of the currently existing PRC2 and EZH2/1 inhibitors, as well as development of second-generation inhibitors to target additional mutations of *EZH2* that tumors acquire to produce inhibitor resistance, we remain optimistic and excited about their future clinical applications in hematologic cancer, as well as a broader spectrum of human cancers being unraveled to show PRC2 dependency and, thus, PRC2 inhibitor sensitivity.

Acknowledgments

KDK is supported by an American Chemical Society Medicinal Chemistry Predoctoral Fellowship. JJ is supported by National Institutes of Health Institute of General Medical Sciences Grant R01GM103893. GGW is supported by a National Cancer Institute "Pathway to Independence" Award in Cancer Research (CA151683), a Department of Defense Career Development award (CA130247), and grants from Gabrielle's Angel Foundation and Concern Foundation. GGW is also a Kimmel Scholar of Sidney Kimmel Foundation for Cancer Research and an American Society of Hematology (ASH) Scholar in Basic Science.

Conflict of interest disclosure

The authors have no conflicting financial interests to disclose.

References

1. Strahl BD, Allis CD. The language of covalent histone modifications. Nature. 2000;403:41–45.
2. Schubeler D. Function and information content of DNA methylation. Nature. 2015;517:321–326.
3. Chi P, Allis CD, Wang GG. Covalent histone modifications—Miswritten, misinterpreted and mis-erased in human cancers. Nat Rev Cancer. 2010;10:457–469.
4. Wang GG, Allis CD. ChiChromatin remodeling and cancer: Part II. ATP-dependent chromatin remodeling. Trends Mol Med. 2007;13:373–380.
5. Weber CM, Henikoff S. Histone variants: Dynamic punctuation in transcription. Genes Dev. 2014;28:672–682.
6. Shih AH, Abdel-Wahab O, Patel JP, Levine RL. The role of mutations in epigenetic regulators in myeloid malignancies. Nat Rev Cancer. 2012;12:599–612.
7. Dawson MA, Kouzarides T. Cancer epigenetics: From mechanism to therapy. Cell. 2012;150:12–27.
8. Rodriguez-Paredes M, Esteller M. Cancer epigenetics reaches mainstream oncology. Nat Med. 2011;17:330–339.
9. Arrowsmith CH, Bountra C, Fish PV, Lee K, Schapira M. Epigenetic protein families: A new frontier for drug discovery. Nat Rev Drug Discov. 2012;11:384–400.
10. Margueron R, Reinberg D. The polycomb complex PRC2 and its mark in life. Nature. 2011;469:343–349.
11. Di Croce L, Helin K. Transcriptional regulation by polycomb group proteins. Nat Struct Mol Biol. 2013;20:1147–1155.
12. Mochizuki-Kashio M, Mishima Y, Miyagi S, et al. Dependency on the polycomb gene Ezh2 distinguishes fetal from adult hematopoietic stem cells. Blood. 2011;118:6553–6561.
13. Hidalgo I, Herrera-Merchan A, Ligos JM, et al. Ezh1 is required for hematopoietic stem cell maintenance and prevents senescence-like cell cycle arrest. Cell Stem Cell. 2012;11:649–662.
14. Caganova M, Carrisi C, Varano G, et al. Germinal center dysregulation by histone methyltransferase EZH2 promotes lymphomagenesis. J Clin Invest. 2013;123:5009–5022.
15. Beguelin W, Popovic R, Teater M, et al. EZH2 is required for germinal center formation and somatic EZH2 mutations promote lymphoid transformation. Cancer Cell. 2013;23:677–692.
16. Musselman CA, Gibson MD, Hartwick EW, et al. Binding of PHF1 Tudor to H3K36me3 enhances nucleosome accessibility. Nat Commun. 2013;4:2969.
17. Cai L, Rothbart SB, Lu R, et al. An H3K36 methylation-engaging Tudor motif of polycomb-like proteins mediates PRC2 complex targeting. Mol Cell. 2013;49:571–582.
18. Ballare C, Lange M, Lapinaite A, et al. Phf19 links methylated Lys36 of histone H3 to regulation of polycomb activity. Nat Struct Mol Biol. 2012;19:1257–1265.

19. Pasini D, Cloos PA, Walfridsson J, et al. JARID2 regulates binding of the polycomb repressive complex 2 to target genes in ES cells. Nature. 2010;464:306–310.
20. Li G, Margueron R, Ku M, Chambon P, Bernstein BE, Reinberg D. Jarid2 and PRC2, partners in regulating gene expression. Genes Dev. 2010;24:368–380.
21. Brockdorff N. Noncoding RNA and polycomb recruitment. RNA. 2013;19:429–442.
22. Morin RD, Johnson NA, Severson TM, et al. Somatic mutations altering EZH2 (Tyr641) in follicular and diffuse large B-cell lymphomas of germinal-center origin. Nat Genet. 2010;42:181–185.
23. Morin RD, Mendez-Lago M, Mungall AJ, et al. Frequent mutation of histone-modifying genes in non-Hodgkin lymphoma. Nature. 2011; 476:298–303.
24. Okosun J, Bodör C, Wang J, et al. Integrated genomic analysis identifies recurrent mutations and evolution patterns driving the initiation and progression of follicular lymphoma. Nat Genet. 2014;46: 176–181.
25. Van Galen JC, Dukers DF, Giroth C, et al. Distinct expression patterns of polycomb oncoproteins and their binding partners during the germinal center reaction. Eur J Immunol. 2004;34:1870–1881.
26. Wang GG, Konze KD, Tao J. Polycomb genes, miRNA, and their deregulation in B-cell malignancies. Blood. 2015;125:1217–1225.
27. Van Kemenade FJ, Raaphorst FM, Blokzijl T, et al. Coexpression of BMI-1 and EZH2 polycomb-group proteins is associated with cycling cells and degree of malignancy in B-cell non-Hodgkin lymphoma. Blood. 2001;97:3896–3901.
28. Visser HP, Gunster MJ, Kluin-Nelemans HC, et al. The polycomb group protein EZH2 is upregulated in proliferating, cultured human mantle cell lymphoma. Br J Haematol. 2001;112:950–958.
29. Abd Al Kader L, Oka T, Takata K, et al. In aggressive variants of non-Hodgkin lymphomas, Ezh2 is strongly expressed and polycomb repressive complex PRC1.4 dominates over PRC1.2. Virchows Arch. 2013;463:697–711.
30. Van Galen JC, Muris JJF, Oudejans JJ, et al. Expression of the polycomb-group gene BMI1 is related to an unfavourable prognosis in primary nodal DLBCL. J Clin Pathol. 2007;60:167–172.
31. McCabe MT, Graves AP, Ganji G, et al. Mutation of A677 in histone methyltransferase EZH2 in human B-cell lymphoma promotes hypertrimethylation of histone H3 on lysine 27 (H3K27). Proc Natl Acad Sci U S A. 2012;109:2989–2994.
32. Majer CR, Lei J, Scott MP, et al. A687V EZH2 is a gain-of-function mutation found in lymphoma patients. FEBS Lett. 2012;586:3448–3451.
33. Bodör C, Grossmann V, Popov N, et al. EZH2 mutations are frequent and represent an early event in follicular lymphoma. Blood. 2013; 122:3165–3168.
34. Yap DB, Chu J, Berg T, et al. Somatic mutations at EZH2 Y641 act dominantly through a mechanism of selectively altered PRC2 catalytic activity, to increase H3K27 trimethylation. Blood. 2011;117: 2451–2459.
35. Sneeringer CJ, Scott MP, Kuntz KW, et al. Coordinated activities of wild-type plus mutant EZH2 drive tumor-associated hypertrimethylation of lysine 27 on histone H3 (H3K27) in human B-cell lymphomas. Proc Natl Acad Sci U S A. 2010;107:20980–20985.
36. Swalm BM, Knutson SK, Warholic NM, et al. Reaction coupling between wild-type and disease-associated mutant EZH2. ACS Chem Biol. 2014;9:2459–2464.
37. Ott HM, Graves AP, Pappalardi MB, et al. A687V EZH2 is a driver of histone H3 lysine 27 (H3K27) hypertrimethylation. Mol Cancer Ther. 2014;13:3062.
38. Antonysamy S, Condon B, Druzina Z, et al. Structural context of disease-associated mutations and putative mechanism of autoinhibition revealed by X-ray crystallographic analysis of the EZH2-SET domain. PLoS One. 2013;8:e84147.
39. Wu H, Zeng H, Dong A, et al. Structure of the catalytic domain of EZH2 reveals conformational plasticity in cofactor and substrate binding sites and explains oncogenic mutations. PLoS One. 2013;8: e83737.
40. Ciferri C, Lander GC, Maiolica A, Herzog F, Aebersold R, Nogales E. Molecular architecture of human polycomb repressive complex 2. ELife. 2012;1:e00005.
41. McCabe MT, Ott HM, Ganil G, et al. EZH2 inhibition as a therapeutic strategy for lymphoma with EZH2-activating mutations. Nature. 2012;492:108–112.
42. Knutson SK, Wigle TJ, Warholic NM, et al. A selective inhibitor of EZH2 blocks H3K27 methylation and kills mutant lymphoma cells. Nat Chem Biol. 2012;8:890–896.
43. Qi W, Chan HM, Teng L, et al. Selective inhibition of Ezh2 by a small molecule inhibitor blocks tumor cells proliferation. Proc Natl Acad Sci U S A. 2012;109:21360–21365.
44. Konze KD, Ma A, Li FL, et al. An orally bioavailable chemical probe of the lysine methyltransferases EZH2 and EZH1. ACS Chem Biol. 2013;8:1324–1334.
45. Knutson SK, Warholic NM, Wigle TJ, et al. Durable tumor regression in genetically altered malignant rhabdoid tumors by inhibition of methyltransferase EZH2. Proc Natl Acad Sci U S A. 2013;110: 7922–7927.
46. Garapaty-Rao S, Nasveschuk C, Gagnon A, et al. Identification of EZH2 and EZH1 small molecule inhibitors with selective impact on diffuse large B cell lymphoma cell growth. Chem Biol. 2013; 20:1329–1339.
47. Bradley WD, Arora S, Busby J, et al. EZH2 Inhibitor efficacy in non-Hodgkin's lymphoma does not require suppression of H3K27 monomethylation. Chem Biol. 2014;21:1463–1475.
48. Shen X, Liu YC, Hsu YJ, et al. EZH1 mediates methylation on histone H3 lysine 27 and complements EZH2 in maintaining stem cell identity and executing pluripotency. Mol Cell. 2008;32:491–502.
49. Margueron R, Li G, Sarma K, et al. Ezh1 and Ezh2 maintain repressive chromatin through different mechanisms. Mol Cell. 2008;32: 503–518.
50. Neff T, Sinha AU, Kluk MJ, et al. Polycomb repressive complex 2 is required for MLL-AF9 leukemia. Proc Natl Acad Sci U S A. 2012; 109:5028–5033.
51. Shi J, Wang E, Zuber J, et al. The polycomb complex PRC2 supports aberrant self-renewal in a mouse model of MLL-AF9;Nras(G12D) acute myeloid leukemia. Oncogene. 2013;32:930–938.
52. Xu B, On DM, Ma A, et al. Selective inhibition of EZH2 and EZH1 enzymatic activity by a small molecule suppresses MLL-rearranged leukemia. Blood. 2015;125:346–357.
53. Velichutina I, Shaknovich R, Geng H, et al. EZH2-mediated epigenetic silencing in germinal center B cells contributes to proliferation and lymphomagenesis. Blood. 2010;116:5247–5255.
54. Berg T, Thoene S, Yap D, et al. A transgenic mouse model demonstrating the oncogenic role of mutations in the polycomb-group gene EZH2 in lymphomagenesis. Blood. 2014;123:3914–3924.
55. Knutson SK, Kawano S, Minoshima Y, et al. Selective inhibition of EZH2 by EPZ-6438 leads to potent antitumor activity in EZH2 mutant non-Hodgkin lymphoma. Mol Cancer Ther. 2014;13:842–854.
56. Zhang X, Zhao X, Fiskus W, et al. Coordinated silencing of MYC-mediated miR-29 by HDAC3 and EZH2 as a therapeutic target of histone modification in aggressive B-cell lymphomas. Cancer Cell. 2012;22:506–523.
57. Copeland RA, Keilhack H, Italiano A, et al. EZH2 inhibitor EPZ-6438 (E7438) in non-hodgkin lymphoma: Pre-clinical models and early clinical observations. Presented at the annual American Society of Hematology (ASH) meeting, 12 August 2014.
58. Mosammaparast N, Shi Y. Reversal of histone methylation: Biochemical and molecular mechanisms of histone demethylases. Annu Rev Biochem. 2010;79:155–179.

59. Schmitges FW, Prusty AB, Faty M, et al. Histone methylation by PRC2 is inhibited by active chromatin marks. Mol Cell. 2011;42:330–341.
60. Yuan W, Xu M, Huang C, Liu N, Chen S, Zhu B. H3K36 methylation antagonizes PRC2-mediated H3K27 methylation. J Biol Chem. 2011;286:7983–7989.
61. Yuan W, Wu T, Fu H, et al. Dense chromatin activates polycomb repressive complex 2 to regulate H3 lysine 27 methylation. Science. 2012;337:971–975.
62. Barski A, Cuddapah S, Cui K, et al. High-resolution profiling of histone methylations in the human genome. Cell. 2007;129:823–837.
63. Pasini D, Malatesta M, Jung HR, et al. Characterization of an antagonistic switch between histone H3 lysine 27 methylation and acetylation in the transcriptional regulation of polycomb group target genes. Nucleic Acids Res. 2010;38:4958–4969.
64. Tie F, Banerjee R, Stratton CA, et al. CBP-mediated acetylation of histone H3 lysine 27 antagonizes Drosophila polycomb silencing. Development. 2009;136:3131–3141.
65. Kennison JA, Tamkun JW. Dosage-dependent modifiers of polycomb and antennapedia mutations in Drosophila. Proc Natl Acad Sci U S A. 1988;85:8136–8140.
66. Wilson BG, Roberts CW. SWI/SNF nucleosome remodellers and cancer. Nat Rev Cancer. 2011;11:481–492.
67. Kia SK, Gorski MM, Giannakopoulos S, Verrijzer CP. SWI/SNF mediates polycomb eviction and epigenetic reprogramming of the INK4b-ARF-INK4a locus. Mol Cell Biol. 2008;28:3457–3464.
68. Van der Vlag J, Otte AP. Transcriptional repression mediated by the human polycomb-group protein EED involves histone deacetylation. Nat Genet. 1999;23:474–478.
69. Vire E, Brenner C, Deplus R, et al. The polycomb group protein EZH2 directly controls DNA methylation. Nature. 2006;439:871–874.
70. Ohm JE, McGarvey KM, Yu X, et al. A stem cell-like chromatin pattern may predispose tumor suppressor genes to DNA hypermethylation and heritable silencing. Nat Genet. 2007;39:237–242.
71. Schlesinger Y, Straussman R, Keshet I, et al. Polycomb-mediated methylation on Lys27 of histone H3 pre-marks genes for de novo methylation in cancer. Nat Genet. 2007;39:232–236.
72. Van Haaften G, Dalgliesh GL, Davies H, et al. Somatic mutations of the histone H3K27 demethylase gene UTX in human cancer. Nat Genet. 2009;41:521–523.
73. Mar BG, Bullinger L, Basu E, et al. Sequencing histone-modifying enzymes identifies UTX mutations in acute lymphoblastic leukemia. Leukemia. 2012;26:1881–1883.
74. Oyer JA, Huang X, Zheng Y, et al. Point mutation E1099K in MMSET/NSD2 enhances its methyltranferase activity and leads to altered global chromatin methylation in lymphoid malignancies. Leukemia. 2014;28:198–201.
75. Jaffe JD, Wang Y, Chan HM, et al. Global chromatin profiling reveals NSD2 mutations in pediatric acute lymphoblastic leukemia. Nat Genet. 2013;45:1386–1391.
76. Agger K, Cloos PA, Christensen J, et al. UTX and JMJD3 are histone H3K27 demethylases involved in HOX gene regulation and development. Nature. 2007;449:731–734.
77. Lan F, Bayliss PE, Rinn JL, et al. A histone H3 lysine 27 demethylase regulates animal posterior development. Nature. 2007;449:689–694.
78. Lee MG, Villa R, Trojer P, et al. Demethylation of H3K27 regulates polycomb recruitment and H2A ubiquitination. Science. 2007;318:447–450.
79. Greenfield A, Carrel L, Pennisi D, et al. The UTX gene escapes X inactivation in mice and humans. Hum Mol Genet. 1998;7:737–742.
80. Van der Meulen J, Sanghvi V, Mavrakis K, et al. The H3K27me3 demethylase UTX is a gender-specific tumor suppressor in T-cell acute lymphoblastic leukemia. Blood. 2015;125:13–21.
81. Ntziachristos P, Tsirigos A, Welstead GG, et al. Contrasting roles of histone 3 lysine 27 demethylases in acute lymphoblastic leukaemia. Nature. 2014;514:513–517.
82. Jankowska AM, Makishima H, Tiu RV, et al. Mutational spectrum analysis of chronic myelomonocytic leukemia includes genes associated with epigenetic regulation: UTX, EZH2, and DNMT3A. Blood. 2011;118:3932–3941.
83. Kar SA, Jankowska A, Makishima H, et al. Spliceosomal gene mutations are frequent events in the diverse mutational spectrum of chronic myelomonocytic leukemia but largely absent in juvenile myelomonocytic leukemia. Haematologica. 2013;98:107–113.
84. Ezponda T, Popovic R, Zheng Y. Loss of the histone demethylase UTX contributes to multiple myeloma and sensitizes cells to EZH2 inhibitors. Blood. 2014;124(21):611. Available at. http://www.bloodjournal.org/content/124/21/611.abstract. [Accessed December 6, 2014].
85. De la Serna IL, Ohkawa Y, Imbalzano AN. Chromatin remodelling in mammalian differentiation: Lessons from ATP-dependent remodellers. Nat Rev Genet. 2006;7:461–473.
86. Kadoch C, Hargreaves DC, Hodges C, et al. Proteomic and bioinformatic analysis of mammalian SWI/SNF complexes identifies extensive roles in human malignancy. Nat Genet. 2013;45:592–601.
87. Shain AH, Pollack JR. The spectrum of SWI/SNF mutations, ubiquitous in human cancers. PLoS One. 2013;8:e55119.
88. Wilson BG, Wang X, Shen X, et al. Epigenetic antagonism between polycomb and SWI/SNF complexes during oncogenic transformation. Cancer Cell. 2010;18:316–328.
89. Versteege I, Sévenet N, Lange J, et al. Truncating mutations of hSNF5/INI1 in aggressive paediatric cancer. Nature. 1998;394:203–206.
90. Biegel JA, Zhou JY, Rorke LB, Stenstrom C, Wainwright LM, Fogelgren B. Germ-line and acquired mutations of INI1 in atypical teratoid and rhabdoid tumors. Cancer Res. 1999;59:74–79.
91. Yuge M, Nagai H, Uchida T, et al. HSNF5/INI1 gene mutations in lymphoid malignancy. Cancer Genet Cytogenet. 2000;122:37–42.
92. Fillmore CM, Xu C, Desai PT, et al. EZH2 inhibition sensitizes BRG1 and EGFR mutant lung tumours to TopoII inhibitors. Nature. 2015;520:239–242.
93. Bitler BG, Aird KM, Garipov A, et al. Synthetic lethality by targeting EZH2 methyltransferase activity in ARID1A-mutated cancers. Nat Med. 2015;21:231–238.
94. Dou Y, Hess JL. Mechanisms of transcriptional regulation by MLL and its disruption in acute leukemia. Int J Hematol. 2008;87:10–18.
95. Krivtsov AV, Armstrong SA. MLL translocations, histone modifications and leukaemia stem-cell development. Nat Rev Cancer. 2007;7:823–833.
96. Slany RK. The molecular biology of mixed lineage leukemia. Haematologica. 2009;94:984–993.
97. Thiel AT, Feng Z, Pant DK, et al. The trithorax protein partner menin acts in tandem with EZH2 to suppress C/EBPalpha and differentiation in MLL-AF9 leukemia. Haematologica. 2013;98:918–927.
98. Tanaka S, Miyagi S, Sashida G, et al. Ezh2 augments leukemogenicity by reinforcing differentiation blockage in acute myeloid leukemia. Blood. 2012;120:1107–1117.
99. Kim W, Bird GH, Neff T, et al. Targeted disruption of the EZH2–EED complex inhibits EZH2-dependent cancer. Nat Chem Biol. 2013;9:643–650.
100. Wagner EJ, Carpenter PB. Understanding the language of Lys36 methylation at histone H3. Nat Rev Mol Cell Biol. 2012;13:115–126.
101. Keats JJ, Reiman T, Belch AR, Pilarski LM. Ten years and counting: so what do we know about t(4;14)(p16;q32) multiple myeloma. Leuk Lymphoma. 2006;47:2289–2300.
102. Keats JJ, Reiman T, Maxwell CA, et al. In multiple myeloma, t(4;14)(p16;q32) is an adverse prognostic factor irrespective of FGFR3 expression. Blood. 2003;101:1520–1529.

103. Santra M, Zhan F, Tian E, Barlogie B, Shaughnessy J Jr. A subset of multiple myeloma harboring the t(4;14)(p16;q32) translocation lacks FGFR3 expression but maintains an IGH/MMSET fusion transcript. Blood. 2003;101:2374–2376.
104. Avet-Loiseau H, Facon T, Grosbois B, et al. Oncogenesis of multiple myeloma: 14q32 and 13q chromosomal abnormalities are not randomly distributed, but correlate with natural history, immunological features, and clinical presentation. Blood. 2002;99:2185–2191.
105. Fonseca R, Blood E, Rue M, et al. Clinical and biologic implications of recurrent genomic aberrations in myeloma. Blood. 2003;101:4569–4575.
106. Popovic R, Martinez-Garcia E, Giannopoulou EG, Zhang QW, Zhang QY, Exponda T. Histone methyltransferase MMSET/NSD2 alters EZH2 binding and reprograms the myeloma epigenome through global and focal changes in H3K36 and H3K27 methylation. PLoS Genet. 2014;10:e1004566.
107. Zheng Y, Sweet SM, Popovic R, et al. Total kinetic analysis reveals how combinatorial methylation patterns are established on lysines 27 and 36 of histone H3. Proc Natl Acad Sci U S A. 2012;109:13549–13554.
108. Haber DA, Buckler AJ, Glaser T, et al. An internal deletion within an 11p13 zinc finger gene contributes to the development of Wilms' tumor. Cell. 1990;61:1257–1269.
109. Huff V. Wilms' tumours: About tumour suppressor genes, an oncogene and a chameleon gene. Nat Rev Cancer. 2011;11:111–121.
110. King-Underwood L, Pritchard-Jones K. Wilms' tumor (WT1) gene mutations occur mainly in acute myeloid leukemia and may confer drug resistance. Blood. 1998;91:2961–2968.
111. Virappane P, Gale R, Hills R, et al. Mutation of the Wilms' tumor 1 gene is a poor prognostic factor associated with chemotherapy resistance in normal karyotype acute myeloid leukemia: The United Kingdom Medical Research Council Adult Leukaemia Working Party. J Clin Oncol. 2008;26:5429–5435.
112. Wang Y, Xiao M, Chen X, et al. WT1 recruits TET2 to regulate Its target gene expression and suppress leukemia cell proliferation. Mol Cell. 2015;57:662–673.
113. Rampal R, Alkalin A, Madzo J, et al. DNA hydroxymethylation profiling reveals that WT1 mutations result in loss of TET2 function in acute myeloid leukemia. Cell Rep. 2014;9:1841–1855.
114. Sinha S, Thomas D, Yu L, et al. Mutant WT1 is associated with DNA hypermethylation of PRC2 targets in AML and responds to EZH2 inhibition. Blood. 2015;125:316–326.
115. Ernst T, Chase AJ, Score J, et al. Inactivating mutations of the histone methyltransferase gene EZH2 in myeloid disorders. Nat Genet. 2010;42:722–726.
116. Nikoloski G, Langemeijer SMC, Kuiper RP, et al. Somatic mutations of the histone methyltransferase gene EZH2 in myelodysplastic syndromes. Nat Genet. 2010;42:665–667.
117. Score J, Hidalgo-Curtis C, Jones AV, et al. Inactivation of polycomb repressive complex 2 components in myeloproliferative and myelodysplastic/myeloproliferative neoplasms. Blood. 2012;119:1208–1213.
118. Puda A, Milosevic JD, Berg T, et al. Frequent deletions of JARID2 in leukemic transformation of chronic myeloid malignancies. Am J Hematol. 2012;87:245–250.
119. Abdel-Wahab O, Adli M, LaFave LM, et al. ASXL1 mutations promote myeloid transformation through loss of PRC2-mediated gene repression. Cancer Cell. 2012;22:180–193.
120. Zhang J, Ding L, Holmfeldt L, et al. The genetic basis of early T-cell precursor acute lymphoblastic leukaemia. Nature. 2012;481:157–163.
121. Ntziachristos P, Tsirigos A, van Vlierberghe P, et al. Genetic inactivation of the polycomb repressive complex 2 in T cell acute lymphoblastic leukemia. Nat Med. 2012;18:298–301.
122. Simon C, Chagraoui J, Krost J, et al. A key role for EZH2 and associated genes in mouse and human adult T-cell acute leukemia. Genes Dev. 2012;26:651–656.
123. Baude A, Lindroth AM, Plass C. PRC2 loss amplifies Ras signaling in cancer. Nat Genet. 2014;46:1154–1155.
124. Lee W, Teckie S, Wiesner T, et al. PRC2 is recurrently inactivated through EED or SUZ12 loss in malignant peripheral nerve sheath tumors. Nat Genet. 2014;46:1227–1232.
125. Zhang M, Wang Y, Jones S, et al. Somatic mutations of SUZ12 in malignant peripheral nerve sheath tumors. Nat Genet. 2014;46:1170–1172.
126. De Raedt T, Beert E, Pasmant E, et al. PRC2 loss amplifies Ras-driven transcription and confers sensitivity to BRD4-based therapies. Nature. 2014;514:247–251.
127. Woods BA, Levine RL. The role of mutations in epigenetic regulators in myeloid malignancies. Immunol Rev. 2015;263:22–35.
128. Muto T, Santida G, Oshima M, et al. Concurrent loss of Ezh2 and Tet2 cooperates in the pathogenesis of myelodysplastic disorders. J Exp Med. 2013;210:2627–2639.
129. Bardot ES, Valdes VJ, Zhang J, et al. Polycomb subunits Ezh1 and Ezh2 regulate the Merkel cell differentiation program in skin stem cells. EMBO J. 2013;32:1990–2000.
130. Pal B, Boouras T, Shi W, et al. Global changes in the mammary epigenome are induced by hormonal cues and coordinated by Ezh2. Cell Rep. 2013;3:411–426.
131. Knutson SK, Warholic NM, Johnston LD, et al. Synergistic antitumor activity of EZH2 inhibitors and glucocorticoid receptor agonists in models of germinal center non-Hodgkin lymphomas. PLoS One. 2014;9:e111840.
132. Weisberg E, Manley PW, Coean-Jacob SW, Hochhaus A, Griffin JD. Second generation inhibitors of BCR-ABL for the treatment of imatinib-resistant chronic myeloid leukaemia. Nat Rev Cancer. 2007;7:345–356.
133. Lito P, Rosen N, Solit DB. Tumor adaptation and resistance to RAF inhibitors. Nat Med. 2013;19:1401–1409.
134. Gibaja V, Shen F, Haran J, et al. Development of secondary mutations in wild-type and mutant EZH2 alleles cooperates to confer resistance to EZH2 inhibitors. Oncogene. 2015; Article in press.
135. Lee ST, Li Z, Wu Z, et al. Context-specific regulation of NF-kappaB target gene expression by EZH2 in breast cancers. Mol Cell. 2011;43:798–810.
136. Jung HY, Jun S, Lee M, et al. PAF and EZH2 induce Wnt/beta-catenin signaling hyperactivation. Mol Cell. 2013;52:193–205.
137. Xu K, Wu ZJ, Groner AC, et al. EZH2 oncogenic activity in castration-resistant prostate cancer cells is polycomb-independent. Science. 2012;338:1465–1469.
138. He A, Shen X, Ma Q, et al. PRC2 directly methylates GATA4 and represses its transcriptional activity. Genes Dev. 2012;26:37–42.
139. Xu J, Shao Z, Li D, et al. Developmental control of polycomb subunit composition by GATA factors mediates a switch to non-canonical functions. Mol Cell. 2015;57:304–316.
140. Konski A, Weiss C, Rosier R, et al. The use of postoperative irradiation for the prevention of heterotopic bone after total hip replacement with biologic fixation (porous coated) prosthesis: An animal model. Int J Radiat Oncol Biol Phys. 1990;18:861–865.
141. Pasqualucci L, Dominguez-Sola D, Chiarenza A, et al. Inactivating mutations of acetyltransferase genes in B-cell lymphoma. Nature. 2011;471:189–195.

frontiers in Oncology

MINI REVIEW
published: 12 October 2017
doi: 10.3389/fonc.2017.00241

Pharmacologic Targeting of Chromatin Modulators As Therapeutics of Acute Myeloid Leukemia

Rui Lu[1,2] *and Gang Greg Wang*[1,2]*

[1] Lineberger Comprehensive Cancer Center, University of North Carolina at Chapel Hill School of Medicine, Chapel Hill, NC, United States, [2] Department of Biochemistry and Biophysics, University of North Carolina at Chapel Hill, Chapel Hill, NC, United States

Acute myeloid leukemia (AML), a common hematological cancer of myeloid lineage cells, generally exhibits poor prognosis in the clinic and demands new treatment options. Recently, direct sequencing of samples from human AMLs and pre-leukemic diseases has unveiled their mutational landscapes and significantly advanced the molecular understanding of AML pathogenesis. The newly identified recurrent mutations frequently "hit" genes encoding epigenetic modulators, a wide range of chromatin-modifying enzymes and regulatory factors involved in gene expression regulation, supporting aberration of chromatin structure and epigenetic modification as a main oncogenic mechanism and cancer-initiating event. Increasing body of evidence demonstrates that chromatin modification aberrations underlying the formation of blood cancer can be reversed by pharmacological targeting of the responsible epigenetic modulators, thus providing new mechanism-based treatment strategies. Here, we summarize recent advances in development of small-molecule inhibitors specific to chromatin factors and their potential applications in the treatment of genetically defined AMLs. These compounds selectively inhibit various subclasses of "epigenetic writers" (such as histone methyltransferases MLL/KMT2A, G9A/KMT1C, EZH2/KMT6A, DOT1L/KMT4, and PRMT1), "epigenetic readers" (such as BRD4 and plant homeodomain finger proteins), and "epigenetic erasers" (such as histone demethylases LSD1/KDM1A and JMJD2C/KDM4C). We also discuss about the molecular mechanisms underpinning therapeutic effect of these epigenetic compounds in AML and favor their potential usage for combinational therapy and treatment of pre-leukemia diseases.

Keywords: epigenetic modulator, small-molecule inhibitors, acute myeloid leukemia, bromodomain, MLL, EZH2, DNMT3A, DOT1L

OPEN ACCESS

Edited by:
Keisuke Ito, Albert Einstein College of Medicine, United States

Reviewed by:
Kathrin Maria Bernt, Children's Hospital of Philadelphia, United States
Rachel Rau, Baylor College of Medicine, United States

***Correspondence:**
Gang Greg Wang
greg_wang@med.unc.edu

Specialty section:
This article was submitted to Molecular and Cellular Oncology, a section of the journal Frontiers in Oncology

Received: *29 July 2017*
Accepted: *21 September 2017*
Published: *12 October 2017*

Citation:
Lu R and Wang GG (2017) Pharmacologic Targeting of Chromatin Modulators As Therapeutics of Acute Myeloid Leukemia. Front. Oncol. 7:241. doi: 10.3389/fonc.2017.00241

INTRODUCTION

Epigenetic modifications, including DNA methylation and a myriad of post-translational modifications of the DNA-packaging histone proteins, represent a fundamental means for regulating gene expression and other DNA-templated processes (1–4). These modifications of DNA or histones are increasingly appreciated to be dynamically regulated by epigenetic modulators, a broad class of proteins that consist of "epigenetic writer" enzymes catalyzing chromatin modification, "epigenetic eraser" enzymes removing the modification, "epigenetic readers" or "effectors" recognizing the

modification to elicit biological consequences, and various other cellular regulators that indirectly influence the level or readout of epigenetic modification (2, 5). While the dynamic regulation of epigenetic modification enables cells to adapt and function differently in response to developmental and environmental cues, their mis-regulation often perturbs gene expression and cellular function leading to pathogenesis of human disease such as cancer. Indeed, recent deep sequencing of human cancer patient samples has identified novel recurrent mutations in genes encoding a wide range of epigenetic modulators and even histones themselves (6–9).

Acute myeloid leukemia (AML), a common malignancy of myeloid-lineage precursor cells in the blood, is characterized by two hallmarks, uncontrolled cell proliferation and impaired differentiation. Previously, progression and characteristics of AML were linked to several key pathways (10, 11), including inactivation of tumor suppressors [such as TP53 and *Wilm's Tumor-1* (WT1)], gain-of-function mutation of oncogenic kinases (such as FLT3, NRAS, and KRAS), and stem cell transcription factors (TFs) [such as rearrangement and/or overexpression of HOX cluster genes and their cofactors such as MEIS1 (12–14)], as well as inactivating mutation of differentiation-promoting TFs (such as PU.1 and CEBP/α). Recently, deep sequencing of samples from human patients with AML and pre-leukemia diseases such as myelodysplastic syndrome (MDS) and clonal hematopoiesis of indeterminate potential (CHIP) additionally revealed frequent somatic mutations of genes involved in epigenetic modulation or RNA splicing (11, 15–26). Among the various affected epigenetic pathway genes include the *DNA (cytosine-5)-methyltransferase 3 A* (DNMT3A, a DNA methylation "writer"), *Tet Methylcytosine dioxygenase 2* (TET2, a DNA methylation "eraser" or demethylase), *Enhancer of zeste homolog 2* [EZH2/KMT6A, a "writer" mediating methylation of histone H3, Lys27 (H3K27)], *Additional Sex Combs Like 1 and 2* (ASXL1 and ASXL2, an EZH2-associated cofactor family), the Cohesin complex (SMC3-SMC1-RAD21-STAG) genes, and *Isocitrate Dehydrogenase 1* and *2* (IDH1 and IDH2). These newly identified somatic mutations of DNA/chromatin modifiers and structural organizers are in agreement with previous karyotyping/FISH-based analyses of AML patients, which already identified recurrent chromosomal translocation or abnormality of genes encoding various members of epigenetic "writers" (MLL/KMT2A, NSD1/KMT3B, NSD3/WHSC1L1/KMT3F) (27–31), "erasers" (JARID1A/KDM5A) (32, 33), and "readers" (PHF23) (32, 34). Importantly, mutations of *DNMT3A*, *TET2*, *IDH1/2*, or *ASXL1* were frequently detected among apparently healthy individuals with clonal hematopoiesis or CHIP (22, 24, 35, 36) and in AML patients who received complete disease remission after chemotherapy (26, 35, 37–39), supporting the pivotal roles of epigenetic deregulation in initiation, clonal evolution and relapse of AMLs.

In contrast to significant advances in molecular appreciation of human AML's mutational landscape and putative "driving" pathways, chemotherapy remains as the frontline treatment for most AML patients, with an exception of all-trans retinoic acid (ATRA) used as targeted therapy of the acute promyelocytic leukemia (APL) subtype. AML patients still suffer from low overall survival and a high rate of recurrence, demanding new treatments to be developed. Recent studies of AML and other tumors have increasingly shown that genetic lesion of epigenetic modulator often induces a subsequent chain reaction leading to aberrations in chromatin modification/remodeling, gene-expression program, and cellular states during tumorigenesis (2, 5, 29, 40–43). Thus, pharmacologic targeting of epigenetic players responsible for the above chromatin/gene mis-regulation shall represent new mechanism-based strategies for therapeutic intervention. This review aims to summarize recent advances in specific inhibition of histone-modifying enzymes and regulatory proteins as potential AML therapeutics, with the already discovered inhibitors sub-grouped into the categories targeting either the "writing," "reading," or "erasing" function of epigenetic modulators (**Table 1**).

TARGETING CHROMATIN "WRITERS"

MLL Inhibitors (MLLi)

The *Mixed-Lineage Leukemia* gene (*MLL/MLL1/KMT2A*) encodes one of the KMT2 family of methyltransferase enzymes that contain multiple structural domains, including a C-terminal SET domain catalyzing methylation of histone H3, Lys4 (H3K4) (44–46). *MLL* rearrangement and translocation, which typically affect one allele, are responsible for about 70% of infant leukemias and 5–10% of childhood and adult AML cases (28, 29). Often, the leukemia-associated *MLL* gene rearrangement produces the MLL fusion oncoprotein that loses MLL's C-terminal SET domain and gains a partial sequence from its fusion partner such as AF4, AF9, AF10, or ENL, which recruits the DOT1L-associated transcription elongation complexes. MLL fusion oncoproteins still retain MLL's N-terminal domains, which mediate chromatin association and interaction with functional cofactors such as Menin. Previously, the remaining wild-type *MLL* allele in cancer cells was shown to be critical for leukemogenesis induced by MLL fusion (47); however, a recent study reported that MLL2/KMT2B, another trithorax family methyltransferase that is most closely related to MLL/KMT2A (48), sustains growth of *MLL*-rearranged leukemia and represents a more relevant drug target (49). While the transcription elongation activity acquired by MLL fusion remains as an attractive targeting strategy (see the section of DOT1Li), these studies have justified development of MLL1/2 inhibitors (MLLi) for the treatment of *MLL*-rearranged leukemias.

Using the structure-guided design, Cao et al. developed an MLLi termed MM-401 (**Figure 1A**, left and **Table 1**) to disrupt direct interaction of MLL1 with WDR5, a cofactor associated with the SET domain of MLL/KMT2 enzymes, and thus inhibit MLL1's methylase or "writer" function (50). *In vitro* biochemical assays showed that MM-401 specifically targets WDR5 interaction to MLL1, and not other MLL/KMT2 family enzymes. Treatment with MM-401 blocked proliferation and induced myeloid differentiation of *MLL*-rearranged leukemia cells while not significantly affecting normal blood stem/progenitor cells (50). A recent study reported that MLL2 represents a more relevant therapeutic target in a range of *MLL*-rearranged leukemia

TABLE 1 | Epigenetic therapies in acute myeloid leukemia (AML): targets, compounds, and clinical development.

Targets	Role in epigenetic regulation	Representative compounds	Indications	Clinical development
Writers				
MLL protein complex	H3K4 methyltransferase	MM-401 MIV-6R[a] MI-503[a]	MLL-rearranged AML	Preclinical
G9A	H3K9 methyltransferase	UNC0648	HOXA9-overexpressed AML	Preclinical
EZH2	H3K27 methyltransferase	GSK126 UNC1999 EPZ005687 Tazemetostat	MLL-rearranged AML	Preclinical
DOT1L	H3K79 methyltransferase	SGC0946 EPZ-5676	MLL-rearranged AML, and others	Phase I
PRMT1	H4R3 methyltransferase	AMI-408	MLL-EEN/GAS7, MOZ-TIF2 and AML1-ETO AML	Preclinical
Readers				
Bromodomain proteins	Histone acetylation readers	JQ1 I-BET151 I-BED762 CPI-0610 OTX015 TEN-01 FT-1101 GSK525762	MLL-rearranged AML, and others	Phase I and Phase II
NUP98-PHF23 or NUP98-JARID1A	H3K4me3 readers	Disulfiram	AMLs with NUP98-PHF23 or NUP98-JARID1A	Preclinical
Erasers				
Histone deacetylases	Histone deacetylases	Vorinostat Romidepsin Panobinostat Givinostat Mocetinostat Ricolinostat AR-42 CUDC-907	AML	Phase I and Phase II for AML; FDA approved for T cell lymphoma and multiple myeloma
LSD1	H3K4 demethylase	GSK2879552 ORY-1001	MLL-rearranged AML, and others	Phase I
KDM4C	H3K9 demethylase	SD70	MLL-EEN/GAS7 and MOZ-TIF2 AML	Preclinical

[a]*MLL/Menin inhibitor is likely to act through inhibiting MLL fusion and not wild-type MLL proteins and probably should not be listed among the "writer" inhibitor category.*

models and that MLL2 and MLL1 collaborate to maintain oncogenesis *via* regulating distinctive gene-expression pathways (49). Therefore, dual inhibitors of MLL2 and MLL1 or a specific one against MLL2 need to be developed and may provide a more effective treatment strategy.

Menin, a cofactor associated with the N-terminal region of both MLL fusion and wild-type MLL1/2 proteins, is required for MLL- and MLL fusion-mediated target gene activation and for leukemic transformation caused by *MLL* rearrangement (51–55). Menin is required for association and/or recruitment of MLL and MLL fusion proteins to their gene targets and represents a validated drug target of *MLL*-rearranged leukemia. Recently, through high-throughput screening and structure-based development, a series of MLLi, including MIV-6R (56), MI-463, and MI-503 (57), were discovered and optimized to disrupt MLL–Menin interaction, with some achieving *in vitro* inhibition in the nanomole range (**Figure 1A**, right; **Table 1**). These MLL–Menin inhibitors efficiently suppressed growth of *MLL*-rearranged leukemia cells *in vitro*/vivo and did not affect that of non-*MLL*-rearranged leukemias. Treatment with these MLLi led to down-regulation of gene-expression programs enforced by MLL fusion, such as *HOXA9* and *MEIS1*, in the leukemia cells. The effect of MLL–Menin inhibitors on steady-state normal hematopoiesis appears to be small (57), suggesting that their anti-leukemia effect is mainly through inhibiting Menin interaction to MLL fusion and not wild-type MLL1 proteins. For this reason, MLL–Menin inhibitors should not be categorized as the "writer" inhibitor. However, it is worthy noting that, besides MLL1/KMT2A, Menin also interacts with MLL2/KMT2B through conserved interfaces (46, 51, 53). It remains to be determined whether the above MLLi also targets MLL2, a recently validated oncoprotein that sustains *MLL*-rearranged leukemias (49). For convenience, we decide to list the MLL–Menin inhibitors as MLLi and "writer" inhibitors (**Table 1**).

G9A Inhibitors (G9Ai)

Euchromatic histone lysine methyltransferase 2 (*EHMT2*, also known as *G9A/KMT1C*) encodes a methyltransferase that catalyzes mono/di-methylation of histone H3, Lys9 (H3K9me1/2), a histone modification correlated with gene silencing. Knockout

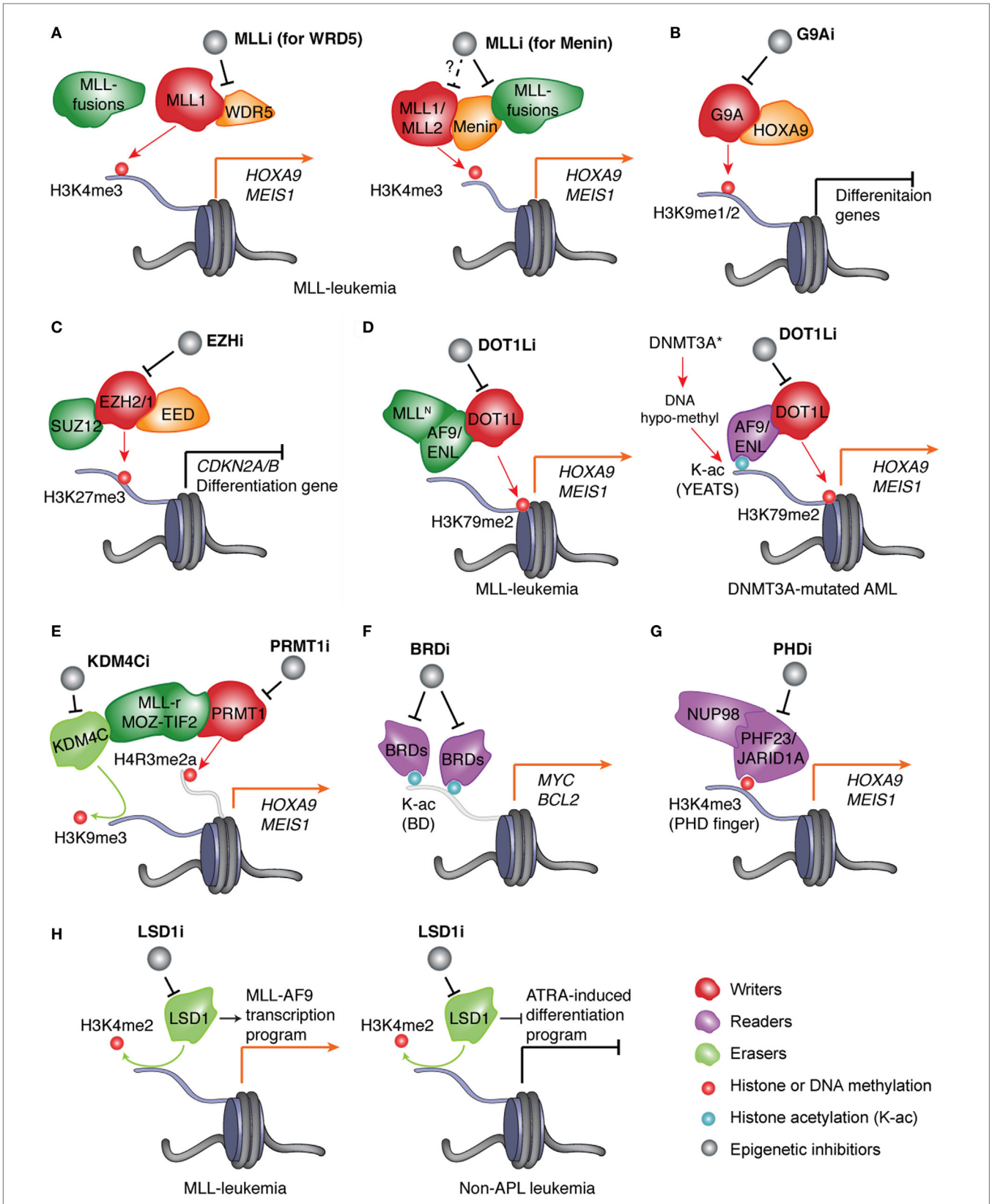

FIGURE 1 | Continued

FIGURE 1 | Continued
Pharmacological inhibition of the epigenetic "writers," "readers," or "erasers" responsible for deregulation of chromatin modification and gene expression in AMLs. **(A)** In leukemias with *MLL* rearrangement (MLL-r), protein complexes assembled by the wild-type MLL and aberrant MLL fusion proteins induce H3K4me3 and H3K79me2, respectively, to cooperatively mediate activation of MLL targets such as "stemness" genes *HOXA9* and *MEIS1*. Inhibitor of MLL (MLLi) disrupts physical association of MLL (MLL1 or MLL2) and MLL-fusion to its interacting partner, either WDR5 (left) or Menin (right), thereby preventing target gene activation and AML development. **(B)** HOXA9, a transcription factor (TF) found overexpressed in ~50–70% of AML patients, promotes leukemogenesis partly through recruiting G9A, an H3K9me1/2-specific "writer" enzyme, to suppress gene-expression programs crucial for myeloid differentiation. Inhibitor of G9A (G9Ai) targets this differentiation-arrest mechanism in AMLs with HOXA9 overexpression. **(C)** In AMLs, treatment with inhibitor of EZH2 and/or EZH1 (EZHi) results in suppression of H3K27me3 and de-repression of polycomb repressive complex 2 (PRC2) target genes, which include tumor suppressor genes (such as CDKN2A/B) and myeloid differentiation-associated genes. **(D)** Left panel: in *MLL*-rearranged leukemias, MLL fusion partners such as AF9 and ENL recruit DOT1L, an H3K79me2-specific "writer" enzyme, to maintain high expression of target genes such as *MEIS1* and *HOXA9*. Right panel: in normal-karyotype AMLs with *DNMT3A* mutation, focal decrease of DNA methylation (i.e., hypo-methylation) results in increase of histone acetylation (K-ac) and binding of the YEAST domain-containing K-ac "reader" proteins AF9 and ENL, which subsequently recruit DOT1L to promote H3K79me2 and transcriptional activation/elongation of "stemness" genes. In both genetically defined AML subtypes, inhibitor of DOT1L (DOT1Li) blocks the above oncogenic program and leukemia progression. **(E)** In leukemias with aberrant fusion of MLL or MOZ-TIF2, PRMT1, an H4R3-specific methyltransferase/"writer," and KDM4C, an H3K9-specific demethylase/"eraser," are recruited by leukemic fusion oncoproteins to modulate histone methylation and promote target gene activation. Blockage of PRMT1 or KDM4C provides a new treatment strategy. **(F)** In AMLs, inhibitor of bromodomain (BRD)-containing K-ac "readers" (BRDi) selectively blocks interaction of bromodomain proteins (BRD4 and related BRD2/3) with K-ac and represses expression of vital oncogenes such as *MYC* and *BCL2*, thus suppressing leukemic growth. **(G)** In AML patients, aberrant rearrangement of the gene encoding the H3K4me3-"reading" proteins JARID1A/KDM5A and PHF23 produces the leukemogenic fusion protein NUP98-JARID1A and NUP98-PHF23, respectively, which rely on their H3K4me3-"reading" plant homeodomain (PHD) finger domains to maintain high expression of AML-associated genes. Inhibitor of PHD fingers (PHDi) shall provide an attractive therapeutic method for these AML patients. **(H)** Left: in MLL-rearranged leukemia, inhibitor of LSD1 (LSD1i) downregulates MLL target genes and inhibits leukemia development. Right: in non-acute promyelocytic leukemia (APL) leukemia, LSD1i promotes all-trans retinoic acid (ATRA)-induced cell differentiation thereby suppressing leukemogenesis.

of *G9A* in hematopoietic systems led to decreased proliferation of myeloid progenitors without affecting the function of long-term repopulating hematopoietic stem cells (58). In mouse AMLs induced by *HOXA9*, a homeodomain TF gene found over-expressed in about 50–70% of human AMLs, loss of *G9A* suppressed leukemogenesis. Mechanistically, G9A physically interacts with HOXA9. Inhibition of G9A led to de-repression of HOXA9 target genes (58). UNC0638 (59), a recently developed G9Ai, demonstrated similar AML therapeutic effect (**Figure 1B**; **Table 1**). While no method is currently available for directly targeting HOXA9 oncoprotein, the above studies provide an alternative strategy.

EZH Inhibitors (EZHi)

EZH2/KMT6A serves as the catalytic subunit of the polycomb repressive complex 2 (PRC2) mediating transcriptional repression through tri-methylation of H3K27 (H3K27me3) (60). EZH1, an EZH2-related methylase, can partially compensate EZH2's functions on a subset of gene targets when assembled in a separate complex with the same set of PRC2 components such as SUZ12 and EED (60, 61). Genomic deletion and loss-of-function mutations of *EZH2/KMT6A* were frequently found in MDS and other myeloid malignancies (62), whereas its gain-of-function mutations occur in 10–20% of B-cell lymphoma patients (63–65). Such *EZH2/KMT6A* somatic mutation is rare among AMLs (66). Recent investigation of animal blood cancer models, however, has shown that complete loss of *EZH2* promotes MDS development but prevents AML transformation (67). MDS induced by *EZH2* loss requires EZH1 for disease progression (68), indicating a context-dependent role of these PRC2 enzymatic complexes in development of MDS and blood malignancy. Furthermore, several studies demonstrated that the *MLL*-rearranged leukemias require functionality of EZH2 and/or EZH1 to maintain leukemogenecity (69–74). Mechanistically, these PRC2 enzymes suppress genes related to tumor suppression (such as *Cdkn2a/b*) and cell differentiation (such as *Egr1*) through inducing gene-repressive H3K27me3/2 (**Figure 1C**). Additionally, PRC2 was found to promote expression of MYC-associated gene signatures probably *via* an indirect mechanism. Furthermore, about 5–10% of AML patients carry the inactivating mutation of the *WT1* gene, which was shown to induce a DNA hyper-methylation phenotype through interfering with WT1-mediated recruitment of TET DNA demethylases (75, 76). The induced DNA hyper-methylation sites were found enriched in myeloid differentiation genes and PRC2 targets, and *EZH2* is highly expressed in *WT1*-mutated AMLs to maintain repression of genes with DNA hyper-methylation, leading to cell differentiation block (77). Importantly, in cellular and murine models of *MLL*-rearranged (69, 70, 72) or *WT1*-mutated AMLs (77), knockdown or knockout of PRC2 inhibited cell proliferation and restored gene-expression programs involved in myeloid differentiation. These studies unveiled the oncogenic function of PRC2 and EZH2 in these genetically defined AMLs, supporting PRC2 as a drug target of AML.

Due to frequent overexpression and gain-of-function mutation of *EZH2* in solid cancer and lymphoma, several pharmaceutical companies have embarked on high-throughput screening campaigns leading to discovery of a series of small-molecule compounds (**Table 1**) that compete binding of S-adenosyl-methionine (SAM), the methyl donor of PRC2, thereby suppressing PRC2's methyltransferase activity (78–82). These EZHi compounds demonstrate high selectivity and high potency toward EZH2 and/or EZH1. In *MLL*-rearranged AML models, dual inhibition of EZH2 and EZH1 by an EZHi, UNC1999, derepressed PRC2 target genes and significantly suppressed AML malignant growth *in vitro* and *in vivo* (74) (**Figure 1C**). Treatment of *WT1*-mutated AML cells with GSK126 (79), an EZH2-selective inhibitor, had similar anti-cancer effect (77). Currently, several EZHis show

drug-like properties and are used in clinical trials of lymphoma treatment. Their potential therapeutic effect in AMLs remains to be determined in clinical settings.

DOT1L Inhibitors (DOT1Li)

Disruptor of telomeric silencing 1-like (DOT1L/KMT4) is a histone H3 Lys79 (H3K79)-specific methyltransferase that regulates gene transcriptional elongation, telomeric silencing, and DNA damage response (83). Biochemical interaction studies found that DOT1L interacts with transcriptional elongation factors including AF4, AF9, AF10, and ENL, which are also common fusion partners of *MLL*-rearrangement in AMLs (29, 84–86). DOT1L loss-of-function studies in *MLL*-rearranged leukemias support its crucial role in leukemogeneicity, possibly through maintaining expression of target transcripts of MLL-fusion such as *HOX* cluster genes and *MEIS1* (84, 87–91).

Structure-based design has led to development of several DOT1Li (**Table 1**) that specifically targets the SAM-binding pocket of DOT1L enzymes (92, 93). Consistent with DOT1L loss-of-function studies, these DOT1Li also selectively inhibited expression of MLL-fusion target genes such as *HOXA9* and *MEIS1* and selectively killed *MLL*-rearranged leukemia cells and xenografted tumors (90–92, 94). Furthermore, recent investigation supports that DOT1L can potentially serve as a therapeutic target of other genetically defined AMLs, which include the subtype with translocation of *NUP98-NSD1* (95), somatic mutation of *DNMT3A* (96, 97), *NPM1* (98) or *IDH1/2* (99), or overexpression of *MN1* (100). While *NUP98-NSD1* induced leukemic transformation through direct targeting and epigenetic modulation of AML-promoting "stemness" genes (*HOX* gene clusters and *MEIS1*) (30), a *DNMT3A* hotspot mutation ($DNMT3A^{R882H}$) was recently found to focally suppress DNA methylation at cis-regulatory elements of these genes thereby promoting their transcription activation (96). In addition, aberrant over-expression of *HOX* cluster genes is a hallmark of AMLs that harbor *NPM1* mutation (98), and overexpression of *MN1* was found to induce an aggressive myeloid leukemia that strictly relies on the same "stemness" genes-expression program in the leukemia-initiating cells (100). Leukemia cells from the above AML subtypes were found generally sensitive to DOT1Li, and DOT1Li treatments repressed "stemness" gene-expression programs, supporting a broader role of DOT1L and "stemness" TF nodes in AML biology (**Figure 1D**). EPZ-5676 (94) represents the first DOT1Li used for clinical trials for *MLL*-rearranged leukemia; however, drug-like properties of the disclosed DOT1Li such as half-life *in vivo* are generally poor and need to be improved.

PRMT1 Inhibitors (PRMT1i)

Protein arginine methyltransferase 1 (*PRMT1*) encodes a methyltransferase for histone H4 arginine-3 (H4R3) and associates with gene activation. PRMT1 was shown to interact with AML1-ETO, a gene fusion product defining AML with t(8;21) translocation, activate the downstream target genes of AML1-ETO, and promote progression of AML1-ETO-asssociated leukemia (101). Recent studies have additionally demonstrated specific requirement of PRMT1 in leukemogenesis induced by *MLL*-rearrangement (such as *MLL-GAS7*) or the *MOZ-TIF2* translocation (102, 103). Similar to what was found in t(8;21) AMLs, PRMT1 physically associates with these leukemic fusion oncoproteins and is required for high expression of their target genes such as *HOX* and *MEIS1*, supporting targeting PRMT1 as new AML therapeutics. Indeed, in various leukemia cell lines and animal models with *MLL* fusion or *MOZ-TIF2*, AMI-408 (104), a PRMT1i, suppressed AML growth (103) (**Figure 1E**; **Table 1**). These works have established a foundation for further validation of PRMT1i's therapeutic effect in clinical settings.

TARGETING CHROMATIN "READERS"

Epigenetic or chromatin "readers" are a subclass of factors that specifically recognize DNA or histone modification to induce subsequent events and elicit functional readout of the modification (1, 2, 105–107). Compared to a generally high druggability of chromatin-modifying "writer" or "eraser" enzymes, that of various epigenetic "reader" families varies (108). Despite challenges, targeting chromatin "reader" function is increasingly considered as promising partly due to recent success in discovery of bromodomain (BRD) protein inhibitors.

BRD Inhibitors (BRDi)

BRD-containing proteins BRD4 and related BRD2/3 recognize histone lysine acetylations subsequently recruiting pTEFb, a CDK9/Cyclin-T kinase complex, to activate RNA polymerase II and target gene expression (109). Originally, these BRD genes were found aberrantly rearranged in malignant NUT midline carcinomas. A pioneering functional genomics screening of chromatin regulators in *MLL*-rearranged leukemia unveiled a role for BRD4 in maintenance of *C-MYC* expression and leukemia oncogenicity (110). Since advent of JQ1, the first highly selective and highly potent BRDi (showing a nano-molar range inhibition of BRDs) that competes BRD4 off acetylated histone ligands (111), multiple BRDis have been developed and their therapeutic effect seen in a wide range of human diseases including AML and other cancers (109). Mechanistically, BRDi such as JQ1 and I-BET151 repressed expression of a number of key oncogenic nodes including *C-MYC* and *BCL2* in mouse and human leukemia models carrying *MLL*-rearrangement (110, 112) (**Figure 1F**). BRDi was also found effective in treating non-*MLL*-rearranged AMLs such as those with *NPM1* mutation (113) or deletion of chromosome 7 and 7q [−7/del(7q)] (114), supporting their broader application in AML therapeutics. Even more potent BRDi, including a degrader derivative that can both inhibit BRD's "reading" function and induce its proteasome-mediated degradation (115), have been developed, with several currently under clinical evaluation for the treatment of refractory AMLs (109). Following these encouraging advances, inhibitors of other RNA Pol-II activators such as the CDK7 and CDK9 kinases are on the horizon becoming a strategy to target transcriptional addiction to vital oncogenes seen in cancer (116, 117).

Plant Homeodomain (PHD) Finger Inhibitors (PHDi)

The PHD finger-containing proteins comprise a large class of chromatin-associated proteins, some of which harbor the "reading" specificity toward H3K4 methylation (2, 106). In human AMLs, genes encoding the PHD finger-containing protein JARID1A (also known as KDM5A, a PHD finger-containing histone demethylase) and PHF23 were altered due to chromosomal abnormalities, resulting in in-frame fusion of their C-terminal H3K4me3-"reading" PHD finger to NUP98, a promiscuous gene translocation partner in human AMLs (32, 106). Despite generally low frequency of these genetic abnormalities in AMLs, the *NUP98-JARID1A/KDM5A* translocation was reported to be recurrent and detected in ~10% of the pediatric acute megakaryoblastic leukemia subtype (33). The produced NUP98-JARID1A or NUP98-PHF23 oncoproteins were highly potent in inducing AML transformation *in vitro*/vivo and rely on their H3K4me3-"reading" PHD finger domain to maintain high expression of "stemness" nodes, notably *HOX* and *MEIS1* (32, 118). Disulfiram, a previously FDA-approved drug, was found to carry the ability to inhibit binding of these PHD fingers to H3K4me3 possibly through structural alteration (119) and to selectively kill the leukemic cells transformed by *NUP98-PHF23* or *NUP98-JARID1A/KDM5A* (118) (**Figure 1G**). However, the potency and selectivity of disulfiram appear poor and the ligand-competitive inhibitors still remain to be developed for these PHD fusion oncoproteins.

TARGETING CHROMATIN "ERASERS"

HDAC Inhibitors (HDACi)

Histone deacetylases (HDACs) remove acetylation off histones to influent gene expression. HDACi (**Table 1**) including Vorinostat (also known as SAHA) and Panobinostat are the earliest inhibitors of epigenetic "erasers" approved by FDA for treatment of cutaneous T cell lymphoma and, recently, multiple myeloma. Currently, HDACi is under phase I/II trials of relapsed AML patients. As HDACs also deacetylate numerous non-histone substrates, effect of HDACi remains controversial as of the detailed mechanisms, especially through targeting histone versus non-histone proteins.

LSD1 Inhibitors (LSD1i)

Lysine-specific demethylase 1 (LSD1/KDM1A) is the first identified histone demethylase with specificity toward H3K4 mono/di-methylation (H3K4me1/2) (120). Several LSD1i have been developed. In the *MLL*-rearranged leukemias, terminal differentiation arrest was partially enforced by LSD1, and LSD1i treatment induced myeloid differentiation and suppressed leukemogenesis *in vivo* (**Figure 1H**) (121). Mechanistically, LSD1i may perturb the H3K4me3/H3K4me2 ratio at MLL target genes thus reducing their transcription (121). Also, therapeutic effect of LSD1i was reported in AMLs without *PML-RARA* (i.e., non-APL AML), where LSD1i sensitized the pro-differentiation effect of ATRA, an agent only for *PML-RARA*-positive APLs (**Figure 1H**) (122). Here, combinational treatment of non-APL human AMLs with ATRA and LSD1i showed a potent anti-leukemic effect, with increased H3K4me2 and expression found at the myeloid differentiation genes (122). Several LSD1i are now in clinical trials in refractory AMLs.

KDM4C Inhibitors

KDM4C (also known as *JMJD2C/GASC1*) encodes an "eraser" carrying the H3K9-demethylating and gene-activating activities. Like PRMT1, KDM4C was also found to interact with various AML oncoproteins including MLL-GAS7 and MOZ-TIF2 (103). Knockdown of *KDM4C* partially reversed target gene activation mediated by these AML fusion proteins. Moreover, pharmacological inhibition of KDM4C can be achieved by an inhibitor SD70 and proposed to be a potentially new AML treatment strategy (103) (**Figure 1E**).

PERSPECTIVES

In short, epigenetic modulators emerge rapidly as potential drug targets for the treatment of currently incurable AMLs. With many showing high selectivity, high potency and/or promising drug-like properties, the already developed epigenetic inhibitors shall provide potential alternatives or adjuvants to current therapeutic arsenal that frequently relies on non-specific cytotoxic agents. While the area is in its infancy, we wish to pinpoint several directions that may broaden application of epigenetic inhibitors.

Newly Validated Epigenetic Factors and Cancer Cell Dependency Pathways Remain to Be Targeted

An existing advance in understanding the biology of gene activation is recent identification of a YEATS family of protein domains as a new "reader" class of histone acylation such as acetylation and crotonylation (123, 124). In the *MLL*-rearranged AML cells, a YEATS domain harbored in ENL was recently shown to be crucial for tethering/stabilizing the MLL fusion proteins at sites with histone acetylation to induce downstream gene activation (125, 126). Similar mechanisms might be also functional among *DNMT3A*-mutated leukemias (**Figure 1D**, right) where *DNMT3A* mutations perturb efficient CpG methylation at cis-regulatory sites leading to elevated histone acetylation and increased binding of DOT1L-associated complexes that harbor YEATS-containing AF9 and ENL (96). Furthermore, LEDGF (lens epithelium-derived growth factor), a protein that mediates chromatin association of the MLL complex, was previously found to be essential for *MLL*-rearrangement-induced leukemic transformation (55). A recent work reports that the PWWP domain of LEDGF recognizes and "reads" H3K36 methylation added by the ASH1L methyltransferase at proximal promoter chromatin, and this event was found critical for recruiting/stabilizing MLL fusions onto target sites to activate gene expression in leukemia cells (127). Additionally, NSD1 and NSD3, two related H3K36 methyltransferases, were previously found to be aberrantly rearranged in ~15% of pediatric AMLs (31) and their "writing" SET domains represent the validated site that remains to be

pharmacologically targeted (30). Thus, these discovered circuits should offer additional therapeutic opportunities, both in the "reading" domains (YEATS of AF9 or ENL; PWWP of LEDGF) and the catalytic "writing" domains (SET of ASH1L and NSD1/3), for AML treatment.

Identification of BRD4 as a novel AML dependency was achieved through shRNA-based functional screening of epigenetic factors (110). Small-guide RNA-based CRISPR/Cas9 technology has provided an alternative system to perform screening in human AML cell lines, which recently led to identification of the histone acetyltransferase KAT2A/GCN5 as an AML dependency gene (128). In future, functional genomics studies using a range of AML cell lines that represent various genetically defined AML subtypes, as well as validation with primary human AML samples, are likely to produce useful information for subtype-specific dependencies on epigenetic modulators, which would guide drug discovery efforts aiming to developing the personalized AML treatment.

Implication in the Treatment of Pre-leukemic Disease

Somatic mutations of several epigenetic modulators (DNMT3A, TET2, IDH1/2) occur frequently among patients with pre-leukemia diseases such as MDS and apparently healthy individuals with clonal hematopoiesis or CHIP, an aging-related phenotype associated with increased risk of AML (21, 22, 25, 26). These mutations and resultant epigenetic deregulations are likely to be the "founder" lesion initiating pre-malignant disease and shaping subsequent malignant formation. Identification of the epigenetic vulnerabilities associated with these gene mutations in the context of AML shall provide useful information on how to treat premalignant diseases. For example, using a murine AML model harboring the coexisting kinase and *DNMT3A* mutations, a recent study demonstrated that *DNMT3A* mutation induced epigenetic dysregulation to promote "stemness" gene-expression programs, a process that can be reversed by DOT1L inhibitors (**Figure 1D**, right) (96). We speculate that the same mechanism/pathways act among premalignant diseases, and if so, the similar epigenetic inhibitors could reverse the premalignant alternations thus preventing malignant development in individuals with MDS or CHIP. In support, the epigenetic inhibitors and hypomethyating agents such as 5-Aza delay malignant transformation of MDS and are FDA-approved drugs for its treatment. However, as a life-threatening disease with a risk of conversion into AML, MDS has additional immediate needs to treat other complications such as anemia and transfusion associated iron overload, bleeding and infectious risk associated with the cytopenias. Currently, the definitive cure of MDS-associated leukemia risk is still allogeneic HSC transplantation. As for CHIP, there is consensus in the field that the relatively low risk of transformation of CHIP does not warrant the targeted therapies. Potential application of targeted epigenetic inhibitors in the treatment of pre-AML diseases such as MDS and myeloproliferative neoplasms warrants further investigation.

Potential Drug Resistance and Combinational Therapy

Resistance to drug remains a challenge in achieving durable remissions in cancer and epigenetically targeted drugs are no exception. The molecular understanding of resistance in epigenetic therapy is just at its beginning. For example, *MLL*-rearranged leukemias with PRC2 loss, either pre-existing or acquired, are resistant to BRDi presumably due to enhanced transcription of oncogenes such as *MYC* (129); furthermore, recent reports documented acquisition of somatic mutation by blood cancer cells during resistance to BRDi or EZHi (129, 130). Conceptually, combinational treatment using two or more drugs that target multiple cancer cell dependencies should help overcome treatment resistance. Furthermore, regardless of drug resistance, combinational therapy should improve treatment when their potential toxic effect can be mitigated. As mentioned above, a good example is that LSD1i sensitizes non-APL AML cells to ATRA treatment (122). In addition, DOT1Li and BRDi are shown to be synergistic in treating *MLL*-rearranged leukemia, possibly due to functional collaboration between DOT1L and BRD4 at the highly transcribed super-enhancer genes (131). Future studies of drug resistance, toxicity, and combinational treatment strategies would be necessary to further develop and optimize the existing leads into those useful compounds for clinical trials.

AUTHOR CONTRIBUTIONS

RL and GW wrote the manuscript and generated the figures/tables.

FUNDING

GW is supported by a Kimmel Scholar award and the NCI grants R01CA211336 and R01CA215284.

REFERENCES

1. Strahl BD, Allis CD. The language of covalent histone modifications. *Nature* (2000) 403(6765):41–5. doi:10.1038/47412
2. Chi P, Allis CD, Wang GG. Covalent histone modifications – miswritten, misinterpreted and mis-erased in human cancers. *Nat Rev Cancer* (2010) 10(7):457–69. doi:10.1038/nrc2876
3. Meissner A. Epigenetic modifications in pluripotent and differentiated cells. *Nat Biotechnol* (2010) 28(10):1079–88. doi:10.1038/nbt.1684
4. Portela A, Esteller M. Epigenetic modifications and human disease. *Nat Biotechnol* (2010) 28(10):1057–68. doi:10.1038/nbt.1685
5. Dawson MA, Kouzarides T. Cancer epigenetics: from mechanism to therapy. *Cell* (2012) 150(1):12–27. doi:10.1016/j.cell.2012.06.013
6. Baylin SB, Jones PA. A decade of exploring the cancer epigenome – biological and translational implications. *Nat Rev Cancer* (2011) 11(10):726–34. doi:10.1038/nrc3130
7. Schwartzentruber J, Korshunov A, Liu XY, Jones DT, Pfaff E, Jacob K, et al. Driver mutations in histone H3.3 and chromatin remodelling genes in paediatric glioblastoma. *Nature* (2012) 482(7384):226–31. doi:10.1038/nature10833
8. Abdel-Wahab O, Levine RL. Mutations in epigenetic modifiers in the pathogenesis and therapy of acute myeloid leukemia. *Blood* (2013) 121(18):3563–72. doi:10.1182/blood-2013-01-451781

9. Garraway LA, Lander ES. Lessons from the cancer genome. *Cell* (2013) 153(1):17–37. doi:10.1016/j.cell.2013.03.002
10. Estey E, Dohner H. Acute myeloid leukaemia. *Lancet* (2006) 368(9550): 1894–907. doi:10.1016/S0140-6736(06)69780-8
11. Khwaja A, Bjorkholm M, Gale RE, Levine RL, Jordan CT, Ehninger G, et al. Acute myeloid leukaemia. *Nat Rev Dis Primers* (2016) 2:16010. doi:10.1038/nrdp.2016.10
12. Kroon E, Thorsteinsdottir U, Mayotte N, Nakamura T, Sauvageau G. NUP98-HOXA9 expression in hemopoietic stem cells induces chronic and acute myeloid leukemias in mice. *EMBO J* (2001) 20(3):350–61. doi:10.1093/emboj/20.3.350
13. Wang GG, Pasillas MP, Kamps MP. Meis1 programs transcription of FLT3 and cancer stem cell character, using a mechanism that requires interaction with Pbx and a novel function of the Meis1 C-terminus. *Blood* (2005) 106(1):254–64. doi:10.1182/blood-2004-12-4664
14. Alharbi RA, Pettengell R, Pandha HS, Morgan R. The role of HOX genes in normal hematopoiesis and acute leukemia. *Leukemia* (2013) 27(5):1000–8. doi:10.1038/leu.2012.356
15. Ley TJ, Ding L, Walter MJ, McLellan MD, Lamprecht T, Larson DE, et al. DNMT3A mutations in acute myeloid leukemia. *N Engl J Med* (2010) 363(25):2424–33. doi:10.1056/NEJMoa1005143
16. Dolnik A, Engelmann JC, Scharfenberger-Schmeer M, Mauch J, Kelkenberg-Schade S, Haldemann B, et al. Commonly altered genomic regions in acute myeloid leukemia are enriched for somatic mutations involved in chromatin remodeling and splicing. *Blood* (2012) 120(18):e83–92. doi:10.1182/blood-2011-12-401471
17. Patel JP, Gonen M, Figueroa ME, Fernandez H, Sun Z, Racevskis J, et al. Prognostic relevance of integrated genetic profiling in acute myeloid leukemia. *N Engl J Med* (2012) 366(12):1079–89. doi:10.1056/NEJMoa1112304
18. Shih AH, Abdel-Wahab O, Patel JP, Levine RL. The role of mutations in epigenetic regulators in myeloid malignancies. *Nat Rev Cancer* (2012) 12(9):599–612. doi:10.1038/nrc3343
19. Cancer Genome Atlas Research Network. Genomic and epigenomic landscapes of adult de novo acute myeloid leukemia. *N Engl J Med* (2013) 368(22):2059–74. doi:10.1056/NEJMoa1301689
20. Kon A, Shih LY, Minamino M, Sanada M, Shiraishi Y, Nagata Y, et al. Recurrent mutations in multiple components of the cohesin complex in myeloid neoplasms. *Nat Genet* (2013) 45(10):1232–7. doi:10.1038/ng.2731
21. Genovese G, Kahler AK, Handsaker RE, Lindberg J, Rose SA, Bakhoum SF, et al. Clonal hematopoiesis and blood-cancer risk inferred from blood DNA sequence. *N Engl J Med* (2014) 371(26):2477–87. doi:10.1056/NEJMoa1409405
22. Jaiswal S, Fontanillas P, Flannick J, Manning A, Grauman PV, Mar BG, et al. Age-related clonal hematopoiesis associated with adverse outcomes. *N Engl J Med* (2014) 371(26):2488–98. doi:10.1056/NEJMoa1408617
23. Genovese G, Jaiswal S, Ebert BL, McCarroll SA. Clonal hematopoiesis and blood-cancer risk. *N Engl J Med* (2015) 372(11):1071–2. doi:10.1056/NEJMc1500684
24. Steensma DP, Bejar R, Jaiswal S, Lindsley RC, Sekeres MA, Hasserjian RP, et al. Clonal hematopoiesis of indeterminate potential and its distinction from myelodysplastic syndromes. *Blood* (2015) 126(1):9–16. doi:10.1182/blood-2015-03-631747
25. Ganguly BB, Kadam NN. Mutations of myelodysplastic syndromes (MDS): an update. *Mutat Res Rev Mutat Res* (2016) 769:47–62. doi:10.1016/j.mrrev.2016.04.009
26. Koeffler HP, Leong G. Preleukemia: one name, many meanings. *Leukemia* (2017) 31(3):534–42. doi:10.1038/leu.2016.364
27. Rosati R, La Starza R, Veronese A, Aventin A, Schwienbacher C, Vallespi T, et al. NUP98 is fused to the NSD3 gene in acute myeloid leukemia associated with t(8;11)(p11.2;p15). *Blood* (2002) 99(10):3857–60. doi:10.1182/blood.V99.10.3857
28. Hess JL. MLL: a histone methyltransferase disrupted in leukemia. *Trends Mol Med* (2004) 10(10):500–7. doi:10.1016/j.molmed.2004.08.005
29. Krivtsov AV, Armstrong SA. MLL translocations, histone modifications and leukaemia stem-cell development. *Nat Rev Cancer* (2007) 7(11):823–33. doi:10.1038/nrc2253
30. Wang GG, Cai L, Pasillas MP, Kamps MP. NUP98-NSD1 links H3K36 methylation to Hox-A gene activation and leukaemogenesis. *Nat Cell Biol* (2007) 9(7):804–12. doi:10.1038/ncb1608
31. Hollink IH, van den Heuvel-Eibrink MM, Arentsen-Peters ST, Pratcorona M, Abbas S, Kuipers JE, et al. NUP98/NSD1 characterizes a novel poor prognostic group in acute myeloid leukemia with a distinct HOX gene expression pattern. *Blood* (2011) 118(13):3645–56. doi:10.1182/blood-2011-04-346643
32. Wang GG, Song J, Wang Z, Dormann HL, Casadio F, Li H, et al. Haematopoietic malignancies caused by dysregulation of a chromatin-binding PHD finger. *Nature* (2009) 459(7248):847–51. doi:10.1038/nature08036
33. de Rooij JD, Hollink IH, Arentsen-Peters ST, van Galen JF, Berna Beverloo H, Baruchel A, et al. NUP98/JARID1A is a novel recurrent abnormality in pediatric acute megakaryoblastic leukemia with a distinct HOX gene expression pattern. *Leukemia* (2013) 27(12):2280–8. doi:10.1038/leu.2013.87
34. Reader JC, Meekins JS, Gojo I, Ning Y. A novel NUP98-PHF23 fusion resulting from a cryptic translocation t(11;17)(p15;p13) in acute myeloid leukemia. *Leukemia* (2007) 21(4):842–4.
35. Shlush LI, Zandi S, Mitchell A, Chen WC, Brandwein JM, Gupta V, et al. Identification of pre-leukaemic haematopoietic stem cells in acute leukaemia. *Nature* (2014) 506(7488):328–33. doi:10.1038/nature13038
36. Xie M, Lu C, Wang J, McLellan MD, Johnson KJ, Wendl MC, et al. Age-related mutations associated with clonal hematopoietic expansion and malignancies. *Nat Med* (2014) 20(12):1472–8. doi:10.1038/nm.3733
37. Wakita S, Yamaguchi H, Omori I, Terada K, Ueda T, Manabe E, et al. Mutations of the epigenetics-modifying gene (DNMT3a, TET2, IDH1/2) at diagnosis may induce FLT3-ITD at relapse in de novo acute myeloid leukemia. *Leukemia* (2013) 27(5):1044–52. doi:10.1038/leu.2012.317
38. Corces-Zimmerman MR, Hong WJ, Weissman IL, Medeiros BC, Majeti R. Preleukemic mutations in human acute myeloid leukemia affect epigenetic regulators and persist in remission. *Proc Natl Acad Sci U S A* (2014) 111(7):2548–53. doi:10.1073/pnas.1324297111
39. Ploen GG, Nederby L, Guldberg P, Hansen M, Ebbesen LH, Jensen UB, et al. Persistence of DNMT3A mutations at long-term remission in adult patients with AML. *Br J Haematol* (2014) 167(4):478–86. doi:10.1111/bjh.13062
40. Wang GG, Allis CD, Chi P. Chromatin remodeling and cancer, part II: ATP-dependent chromatin remodeling. *Trends Mol Med* (2007) 13(9): 373–80. doi:10.1016/j.molmed.2007.07.004
41. Lu C, Ward PS, Kapoor GS, Rohle D, Turcan S, Abdel-Wahab O, et al. IDH mutation impairs histone demethylation and results in a block to cell differentiation. *Nature* (2012) 483(7390):474–8. doi:10.1038/nature10860
42. Coombs CC, Tallman MS, Levine RL. Molecular therapy for acute myeloid leukaemia. *Nat Rev Clin Oncol* (2016) 13(5):305–18. doi:10.1038/nrclinonc.2015.210
43. Wainwright EN, Scaffidi P. Epigenetics and cancer stem cells: unleashing, hijacking, and restricting cellular plasticity. *Trends Cancer* (2017) 3(5): 372–86. doi:10.1016/j.trecan.2017.04.004
44. Milne TA, Briggs SD, Brock HW, Martin ME, Gibbs D, Allis CD, et al. MLL targets SET domain methyltransferase activity to Hox gene promoters. *Mol Cell* (2002) 10(5):1107–17. doi:10.1016/S1097-2765(02)00741-4
45. Dou Y, Milne TA, Ruthenburg AJ, Lee S, Lee JW, Verdine GL, et al. Regulation of MLL1 H3K4 methyltransferase activity by its core components. *Nat Struct Mol Biol* (2006) 13(8):713–9. doi:10.1038/nsmb1128
46. Shilatifard A. The COMPASS family of histone H3K4 methylases: mechanisms of regulation in development and disease pathogenesis. *Annu Rev Biochem* (2012) 81:65–95. doi:10.1146/annurev-biochem-051710-134100
47. Thiel AT, Blessington P, Zou T, Feather D, Wu X, Yan J, et al. MLL-AF9-induced leukemogenesis requires coexpression of the wild-type Mll allele. *Cancer Cell* (2010) 17(2):148–59. doi:10.1016/j.ccr.2009.12.034
48. Froimchuk E, Jang Y, Ge K. Histone H3 lysine 4 methyltransferase KMT2D. *Gene* (2017) 627:337–42. doi:10.1016/j.gene.2017.06.056
49. Chen Y, Anastassiadis K, Kranz A, Stewart AF, Arndt K, Waskow C, et al. MLL2, not MLL1, plays a major role in sustaining MLL-rearranged acute myeloid leukemia. *Cancer Cell* (2017) 31(6):755–770e756. doi:10.1016/j.ccell.2017.05.002
50. Cao F, Townsend EC, Karatas H, Xu J, Li L, Lee S, et al. Targeting MLL1 H3K4 methyltransferase activity in mixed-lineage leukemia. *Mol Cell* (2014) 53(2):247–61. doi:10.1016/j.molcel.2013.12.001
51. Hughes CM, Rozenblatt-Rosen O, Milne TA, Copeland TD, Levine SS, Lee JC, et al. Menin associates with a trithorax family histone methyltransferase

complex and with the hoxc8 locus. *Mol Cell* (2004) 13(4):587–97. doi:10.1016/S1097-2765(04)00081-4
52. Yokoyama A, Wang Z, Wysocka J, Sanyal M, Aufiero DJ, Kitabayashi I, et al. Leukemia proto-oncoprotein MLL forms a SET1-like histone methyltransferase complex with menin to regulate Hox gene expression. *Mol Cell Biol* (2004) 24(13):5639–49. doi:10.1128/MCB.24.13.5639-5649.2004
53. Yokoyama A, Somervaille TC, Smith KS, Rozenblatt-Rosen O, Meyerson M, Cleary ML. The menin tumor suppressor protein is an essential oncogenic cofactor for MLL-associated leukemogenesis. *Cell* (2005) 123(2):207–18. doi:10.1016/j.cell.2005.09.025
54. Caslini C, Yang Z, El-Osta M, Milne TA, Slany RK, Hess JL. Interaction of MLL amino terminal sequences with menin is required for transformation. *Cancer Res* (2007) 67(15):7275–83. doi:10.1158/0008-5472.CAN-06-2369
55. Yokoyama A, Cleary ML. Menin critically links MLL proteins with LEDGF on cancer-associated target genes. *Cancer Cell* (2008) 14(1):36–46. doi:10.1016/j.ccr.2008.05.003
56. He S, Senter TJ, Pollock J, Han C, Upadhyay SK, Purohit T, et al. High-affinity small-molecule inhibitors of the menin-mixed lineage leukemia (MLL) interaction closely mimic a natural protein-protein interaction. *J Med Chem* (2014) 57(4):1543–56. doi:10.1021/jm401868d
57. Borkin D, He S, Miao H, Kempinska K, Pollock J, Chase J, et al. Pharmacologic inhibition of the Menin-MLL interaction blocks progression of MLL leukemia in vivo. *Cancer Cell* (2015) 27(4):589–602. doi:10.1016/j.ccell.2015.02.016
58. Lehnertz B, Pabst C, Su L, Miller M, Liu F, Yi L, et al. The methyltransferase G9a regulates HoxA9-dependent transcription in AML. *Genes Dev* (2014) 28(4):317–27. doi:10.1101/gad.236794.113
59. Vedadi M, Barsyte-Lovejoy D, Liu F, Rival-Gervier S, Allali-Hassani A, Labrie V, et al. A chemical probe selectively inhibits G9a and GLP methyltransferase activity in cells. *Nat Chem Biol* (2011) 7(8):566–74. doi:10.1038/nchembio.599
60. Margueron R, Reinberg D. The polycomb complex PRC2 and its mark in life. *Nature* (2011) 469(7330):343–9. doi:10.1038/nature09784
61. Shen X, Liu Y, Hsu YJ, Fujiwara Y, Kim J, Mao X, et al. EZH1 mediates methylation on histone H3 lysine 27 and complements EZH2 in maintaining stem cell identity and executing pluripotency. *Mol Cell* (2008) 32(4):491–502. doi:10.1016/j.molcel.2008.10.016
62. Ernst T, Chase AJ, Score J, Hidalgo-Curtis CE, Bryant C, Jones AV, et al. Inactivating mutations of the histone methyltransferase gene EZH2 in myeloid disorders. *Nat Genet* (2010) 42(8):722–U109. doi:10.1038/ng.621
63. Morin RD, Johnson NA, Severson TM, Mungall AJ, An J, Goya R, et al. Somatic mutations altering EZH2 (Tyr641) in follicular and diffuse large B-cell lymphomas of germinal-center origin. *Nat Genet* (2010) 42(2):181–5. doi:10.1038/ng.518
64. Sneeringer CJ, Scott MP, Kuntz KW, Knutson SK, Pollock RM, Richon VM, et al. Coordinated activities of wild-type plus mutant EZH2 drive tumor-associated hypertrimethylation of lysine 27 on histone H3 (H3K27) in human B-cell lymphomas. *Proc Natl Acad Sci U S A* (2010) 107(49):20980–5. doi:10.1073/pnas.1012525107
65. Wang GG, Konze KD, Tao J. Polycomb genes, miRNA, and their deregulation in B-cell malignancies. *Blood* (2015) 125(8):1217–25. doi:10.1182/blood-2014-10-606822
66. Ley TJ, Miller C, Ding L, Raphael BJ, Mungall AJ, Robertson AG, et al. Genomic and epigenomic landscapes of adult de novo acute myeloid leukemia. *N Engl J Med* (2013) 368(22):2059–74. doi:10.1056/NEJMoa1301689
67. Sashida G, Harada H, Matsui H, Oshima M, Yui M, Harada Y, et al. Ezh2 loss promotes development of myelodysplastic syndrome but attenuates its predisposition to leukaemic transformation. *Nat Commun* (2014) 5:4177. doi:10.1038/ncomms5177
68. Mochizuki-Kashio M, Aoyama K, Sashida G, Oshima M, Tomioka T, Muto T, et al. Ezh2 loss in hematopoietic stem cells predisposes mice to develop heterogeneous malignancies in an Ezh1-dependent manner. *Blood* (2015) 126(10):1172–83. doi:10.1182/blood-2015-03-634428
69. Neff T, Sinha AU, Kluk MJ, Zhu N, Khattab MH, Stein L, et al. Polycomb repressive complex 2 is required for MLL-AF9 leukemia. *Proc Natl Acad Sci U S A* (2012) 109(13):5028–33. doi:10.1073/pnas.1202258109
70. Tanaka S, Miyagi S, Sashida G, Chiba T, Yuan J, Mochizuki-Kashio M, et al. Ezh2 augments leukemogenicity by reinforcing differentiation blockage in acute myeloid leukemia. *Blood* (2012) 120(5):1107–17. doi:10.1182/blood-2011-11-394932
71. Kim W, Bird GH, Neff T, Guo G, Kerenyi MA, Walensky LD, et al. Targeted disruption of the EZH2-EED complex inhibits EZH2-dependent cancer. *Nat Chem Biol* (2013) 9(10):643–50. doi:10.1038/nchembio.1331
72. Shi J, Wang E, Zuber J, Rappaport A, Taylor M, Johns C, et al. The polycomb complex PRC2 supports aberrant self-renewal in a mouse model of MLL-AF9;Nras(G12D) acute myeloid leukemia. *Oncogene* (2013) 32(7):930–8. doi:10.1038/onc.2012.110
73. Danis E, Yamauchi T, Echanique K, Haladyna J, Kalkur R, Riedel S, et al. Inactivation of Eed impedes MLL-AF9-mediated leukemogenesis through Cdkn2a-dependent and Cdkn2a-independent mechanisms in a murine model. *Exp Hematol* (2015) 43(11):930–935e936. doi:10.1016/j.exphem.2015.06.005
74. Xu B, On DM, Ma A, Parton T, Konze KD, Pattenden SG, et al. Selective inhibition of EZH2 and EZH1 enzymatic activity by a small molecule suppresses MLL-rearranged leukemia. *Blood* (2015) 125(2):346–57. doi:10.1182/blood-2014-06-581082
75. Rampal R, Alkalin A, Madzo J, Vasanthakumar A, Pronier E, Patel J, et al. DNA hydroxymethylation profiling reveals that WT1 mutations result in loss of TET2 function in acute myeloid leukemia. *Cell Rep* (2014) 9(5):1841–55. doi:10.1016/j.celrep.2014.11.004
76. Wang Y, Xiao M, Chen X, Chen L, Xu Y, Lv L, et al. WT1 recruits TET2 to regulate its target gene expression and suppress leukemia cell proliferation. *Mol Cell* (2015) 57(4):662–73. doi:10.1016/j.molcel.2014.12.023
77. Sinha S, Thomas D, Yu L, Gentles AJ, Jung N, Corces-Zimmerman MR, et al. Mutant WT1 is associated with DNA hypermethylation of PRC2 targets in AML and responds to EZH2 inhibition. *Blood* (2015) 125(2):316–26. doi:10.1182/blood-2014-03-566018
78. Knutson SK, Wigle TJ, Warholic NM, Sneeringer CJ, Allain CJ, Klaus CR, et al. A selective inhibitor of EZH2 blocks H3K27 methylation and kills mutant lymphoma cells. *Nat Chem Biol* (2012) 8(11):890–6. doi:10.1038/nchembio.1084
79. McCabe MT, Ott HM, Ganji G, Korenchuk S, Thompson C, Van Aller GS, et al. EZH2 inhibition as a therapeutic strategy for lymphoma with EZH2-activating mutations. *Nature* (2012) 492(7427):108–12. doi:10.1038/nature11606
80. Qi W, Chan H, Teng L, Li L, Chuai S, Zhang R, et al. Selective inhibition of Ezh2 by a small molecule inhibitor blocks tumor cells proliferation. *Proc Natl Acad Sci U S A* (2012) 109(52):21360–5. doi:10.1073/pnas.1210371110
81. Garapaty-Rao S, Nasveschuk C, Gagnon A, Chan EY, Sandy P, Busby J, et al. Identification of EZH2 and EZH1 small molecule inhibitors with selective impact on diffuse large B cell lymphoma cell growth. *Chem Biol* (2013) 20(11):1329–39. doi:10.1016/j.chembiol.2013.09.013
82. Konze KD, Ma A, Li F, Barsyte-Lovejoy D, Parton T, Macnevin CJ, et al. An orally bioavailable chemical probe of the lysine methyltransferases EZH2 and EZH1. *ACS Chem Biol* (2013) 8(6):1324–34. doi:10.1021/cb400133j
83. Nguyen AT, Zhang Y. The diverse functions of Dot1 and H3K79 methylation. *Genes Dev* (2011) 25(13):1345–58. doi:10.1101/gad.2057811
84. Okada Y, Feng Q, Lin YH, Jiang Q, Li YQ, Coffield VM, et al. hDOT1L links histone methylation to leukemogenesis. *Cell* (2005) 121(2):167–78. doi:10.1016/j.cell.2005.02.020
85. Mohan M, Herz HM, Takahashi YH, Lin C, Lai KC, Zhang Y, et al. Linking H3K79 trimethylation to Wnt signaling through a novel Dot1-containing complex (DotCom). *Genes Dev* (2010) 24(6):574–89. doi:10.1101/gad.1898410
86. He N, Chan CK, Sobhian B, Chou S, Xue Y, Liu M, et al. Human polymerase-associated factor complex (PAFc) connects the super elongation complex (SEC) to RNA polymerase II on chromatin. *Proc Natl Acad Sci U S A* (2011) 108(36):E636–45. doi:10.1073/pnas.1107107108
87. Chang M-J, Wu H, Achille NJ, Reisenauer MR, Chou C-W, Zeleznik-Le NJ, et al. Histone H3 lysine 79 methyltransferase dot1 is required for immortalization by MLL oncogenes. *Cancer Res* (2010) 70(24):10234–42. doi:10.1158/0008-5472.can-10-3294
88. Anh Tram N, Taranova O, He J, Zhang Y. DOT1L, the H3K79 methyltransferase, is required for MLL-AF9-mediated leukemogenesis. *Blood* (2011) 117(25):6912–22. doi:10.1182/blood-2011-02-334359

89. Bernt KM, Zhu N, Sinha AU, Vempati S, Faber J, Krivtsov AV, et al. MLL-rearranged leukemia is dependent on aberrant H3K79 methylation by DOT1L. *Cancer Cell* (2011) 20(1):66–78. doi:10.1016/j.ccr.2011.06.010
90. Chen L, Deshpande AJ, Banka D, Bernt KM, Dias S, Buske C, et al. Abrogation of MLL-AF10 and CALM-AF10-mediated transformation through genetic inactivation or pharmacological inhibition of the H3K79 methyltransferase Dot1l. *Leukemia* (2013) 27(4):813–22. doi:10.1038/leu.2012.327
91. Deshpande AJ, Chen L, Fazio M, Sinha AU, Bernt KM, Banka D, et al. Leukemic transformation by the MLL-AF6 fusion oncogene requires the H3K79 methyltransferase Dot1l. *Blood* (2013) 121(13):2533–41. doi:10.1182/blood-2012-11-465120
92. Daigle SR, Olhava EJ, Therkelsen CA, Majer CR, Sneeringer CJ, Song J, et al. Selective killing of mixed lineage leukemia cells by a potent small-molecule DOT1L inhibitor. *Cancer Cell* (2011) 20(1):53–65. doi:10.1016/j.ccr.2011.06.009
93. Yu W, Chory EJ, Wernimont AK, Tempel W, Scopton A, Federation A, et al. Catalytic site remodelling of the DOT1L methyltransferase by selective inhibitors. *Nat Commun* (2012) 3:1288. doi:10.1038/ncomms2304
94. Daigle SR, Olhava EJ, Therkelsen CA, Basavapathruni A, Jin L, Boriack-Sjodin PA, et al. Potent inhibition of DOT1L as treatment of MLL-fusion leukemia. *Blood* (2013) 122(6):1017–25. doi:10.1182/blood-2013-04-497644
95. Deshpande AJ, Deshpande A, Sinha AU, Chen L, Chang J, Cihan A, et al. AF10 regulates progressive H3K79 methylation and HOX gene expression in diverse AML subtypes. *Cancer Cell* (2014) 26(6):896–908. doi:10.1016/j.ccell.2014.10.009
96. Lu R, Wang P, Parton T, Zhou Y, Chrysovergis K, Rockowitz S, et al. Epigenetic perturbations by Arg882-mutated DNMT3A potentiate aberrant stem cell gene-expression program and acute leukemia development. *Cancer Cell* (2016) 30(1):92–107. doi:10.1016/j.ccell.2016.05.008
97. Rau RE, Rodriguez BA, Luo M, Jeong M, Rosen A, Rogers JH, et al. DOT1L as a therapeutic target for the treatment of DNMT3A-mutant acute myeloid leukemia. *Blood* (2016) 128(7):971–81. doi:10.1182/blood-2015-11-684225
98. Kuhn MW, Song E, Feng Z, Sinha A, Chen CW, Deshpande AJ, et al. Targeting chromatin regulators inhibits leukemogenic gene expression in NPM1 mutant leukemia. *Cancer Discov* (2016) 6(10):1166–81. doi:10.1158/2159-8290.CD-16-0237
99. Sarkaria SM, Christopher MJ, Klco JM, Ley TJ. Primary acute myeloid leukemia cells with IDH1 or IDH2 mutations respond to a DOT1L inhibitor in vitro. *Leukemia* (2014) 28(12):2403–6. doi:10.1038/leu.2014.235
100. Riedel SS, Haladyna JN, Bezzant M, Stevens B, Pollyea DA, Sinha AU, et al. MLL1 and DOT1L cooperate with meningioma-1 to induce acute myeloid leukemia. *J Clin Invest* (2016) 126(4):1438–50. doi:10.1172/JCI80825
101. Shia W-J, Okumura AJ, Yan M, Sarkeshik A, Lo M-C, Matsuura S, et al. PRMT1 interacts with AML1-ETO to promote its transcriptional activation and progenitor cell proliferative potential. *Blood* (2012) 119(21):4953–62. doi:10.1182/blood-2011-04-347476
102. Cheung N, Chan LC, Thompson A, Cleary ML, So CWE. Protein arginine-methyltransferase-dependent oncogenesis. *Nat Cell Biol* (2007) 9(10):1208–15. doi:10.1038/ncb1642
103. Cheung N, Fung TK, Zeisig BB, Holmes K, Rane JK, Mowen KA, et al. Targeting aberrant epigenetic networks mediated by PRMT1 and KDM4C in acute myeloid leukemia. *Cancer Cell* (2016) 29(1):32–48. doi:10.1016/j.ccell.2015.12.007
104. Dillon MB, Bachovchin DA, Brown SJ, Finn MG, Rosen H, Cravatt BF, et al. Novel inhibitors for PRMT1 discovered by high-throughput screening using activity-based fluorescence polarization. *ACS Chem Biol* (2012) 7(7):1198–204. doi:10.1021/cb300024c
105. Ruthenburg AJ, Allis CD, Wysocka J. Methylation of lysine 4 on histone H3: intricacy of writing and reading a single epigenetic mark. *Mol Cell* (2007) 25(1):15–30. doi:10.1016/j.molcel.2006.12.014
106. Baker LA, Allis CD, Wang GG. PHD fingers in human diseases: disorders arising from misinterpreting epigenetic marks. *Mutat Res* (2008) 647(1–2):3–12. doi:10.1016/j.mrfmmm.2008.07.004
107. Musselman CA, Lalonde ME, Cote J, Kutateladze TG. Perceiving the epigenetic landscape through histone readers. *Nat Struct Mol Biol* (2012) 19(12):1218–27. doi:10.1038/nsmb.2436
108. Arrowsmith CH, Bountra C, Fish PV, Lee K, Schapira M. Epigenetic protein families: a new frontier for drug discovery. *Nat Rev Drug Discov* (2012) 11(5):384–400. doi:10.1038/nrd3674
109. French CA. Small-molecule targeting of BET proteins in cancer. *Adv Cancer Res* (2016) 131:21–58. doi:10.1016/bs.acr.2016.04.001
110. Zuber J, Shi J, Wang E, Rappaport AR, Herrmann H, Sison EA, et al. RNAi screen identifies Brd4 as a therapeutic target in acute myeloid leukaemia. *Nature* (2011) 478(7370):524–U124. doi:10.1038/nature10334
111. Filippakopoulos P, Qi J, Picaud S, Shen Y, Smith WB, Fedorov O, et al. Selective inhibition of BET bromodomains. *Nature* (2010) 468(7327):1067–73. doi:10.1038/nature09504
112. Dawson MA, Prinjha RK, Dittmann A, Giotopoulos G, Bantscheff M, Chan W-I, et al. Inhibition of BET recruitment to chromatin as an effective treatment for MLL-fusion leukaemia. *Nature* (2011) 478(7370):529–33. doi:10.1038/nature10509
113. Dawson MA, Gudgin EJ, Horton SJ, Giotopoulos G, Meduri E, Robson S, et al. Recurrent mutations, including NPM1c, activate a BRD4-dependent core transcriptional program in acute myeloid leukemia. *Leukemia* (2014) 28(2):311–20. doi:10.1038/leu.2013.338
114. Chen C, Liu Y, Rappaport AR, Kitzing T, Schultz N, Zhao Z, et al. MLL3 is a haploinsufficient 7q tumor suppressor in acute myeloid leukemia. *Cancer Cell* (2014) 25(5):652–65. doi:10.1016/j.ccr.2014.03.016
115. Winter GE, Buckley DL, Paulk J, Roberts JM, Souza A, Dhe-Paganon S, et al. Drug development. Phthalimide conjugation as a strategy for in vivo target protein degradation. *Science* (2015) 348(6241):1376–81. doi:10.1126/science.aab1433
116. Chipumuro E, Marco E, Christensen CL, Kwiatkowski N, Zhang T, Hatheway CM, et al. CDK7 inhibition suppresses super-enhancer-linked oncogenic transcription in MYCN-driven cancer. *Cell* (2014) 159(5):1126–39. doi:10.1016/j.cell.2014.10.024
117. Kwiatkowski N, Zhang T, Rahl PB, Abraham BJ, Reddy J, Ficarro SB, et al. Targeting transcription regulation in cancer with a covalent CDK7 inhibitor. *Nature* (2014) 511(7511):616–20. doi:10.1038/nature13393
118. Gough SM, Lee F, Yang F, Walker RL, Zhu YJ, Pineda M, et al. NUP98-PHF23 is a chromatin-modifying oncoprotein that causes a wide array of leukemias sensitive to inhibition of PHD histone reader function. *Cancer Discov* (2014) 4(5):564–77. doi:10.1158/2159-8290.CD-13-0419
119. Wagner EK, Nath N, Flemming R, Feltenberger JB, Denu JM. Identification and characterization of small molecule inhibitors of a plant homeodomain finger. *Biochemistry* (2012) 51(41):8293–306. doi:10.1021/bi3009278
120. Shi YJ, Lan F, Matson C, Mulligan P, Whetstine JR, Cole PA, et al. Histone demethylation mediated by the nuclear amine oxidase homolog LSD1. *Cell* (2004) 119(7):941–53. doi:10.1016/j.cell.2004.12.012
121. Harris WJ, Huang X, Lynch JT, Spencer GJ, Hitchin JR, Li Y, et al. The histone demethylase KDM1A sustains the oncogenic potential of MLL-AF9 leukemia stem cells. *Cancer Cell* (2012) 21(4):473–87. doi:10.1016/j.ccr.2012.03.014
122. Schenk T, Chen WC, Goellner S, Howell L, Jin L, Hebestreit K, et al. Inhibition of the LSD1 (KDM1A) demethylase reactivates the all-trans-retinoic acid differentiation pathway in acute myeloid leukemia. *Nat Med* (2012) 18(4):605–11. doi:10.1038/nm.2661
123. Li Y, Wen H, Xi Y, Tanaka K, Wang H, Peng D, et al. AF9 YEATS domain links histone acetylation to DOT1L-mediated H3K79 methylation. *Cell* (2014) 159(3):558–71. doi:10.1016/j.cell.2014.09.049
124. Zhao D, Li Y, Xiong X, Chen Z, Li H. YEATS domain-a histone acylation reader in health and disease. *J Mol Biol* (2017) 429(13):1994–2002. doi:10.1016/j.jmb.2017.03.010
125. Erb MA, Scott TG, Li BE, Xie H, Paulk J, Seo HS, et al. Transcription control by the ENL YEATS domain in acute leukaemia. *Nature* (2017) 543(7644):270–4. doi:10.1038/nature21688
126. Wan L, Wen H, Li Y, Lyu J, Xi Y, Hoshii T, et al. ENL links histone acetylation to oncogenic gene expression in acute myeloid leukaemia. *Nature* (2017) 543(7644):265–9. doi:10.1038/nature21687
127. Zhu L, Li Q, Wong SH, Huang M, Klein BJ, Shen J, et al. ASH1L links histone H3 lysine 36 dimethylation to MLL leukemia. *Cancer Discov* (2016) 6(7):770–83. doi:10.1158/2159-8290.CD-16-0058
128. Tzelepis K, Koike-Yusa H, De Braekeleer E, Li Y, Metzakopian E, Dovey OM, et al. A CRISPR dropout screen identifies genetic vulnerabilities

and therapeutic targets in acute myeloid leukemia. *Cell Rep* (2016) 17(4): 1193–205. doi:10.1016/j.celrep.2016.09.079

129. Rathert P, Roth M, Neumann T, Muerdter F, Roe J-S, Muhar M, et al. Transcriptional plasticity promotes primary and acquired resistance to BET inhibition. *Nature* (2015) 525(7570):543–7. doi:10.1038/nature14898
130. Xu B, Konze KD, Jin J, Wang GG. Targeting EZH2 and PRC2 dependence as novel anticancer therapy. *Exp Hematol* (2015) 43(8):698–712. doi:10.1016/j.exphem.2015.05.001
131. Gilan O, Lam EY, Becher I, Lugo D, Cannizzaro E, Joberty G, et al. Functional interdependence of BRD4 and DOT1L in MLL leukemia. *Nat Struct Mol Biol* (2016) 23(7):673–81. doi:10.1038/nsmb.3249

Conflict of Interest Statement: The authors declare that the research was conducted in the absence of any commercial or financial relationships that could be construed as a potential conflict of interest.

Polycomb genes, miRNA, and their deregulation in B-cell malignancies

Gang Greg Wang,[1] Kyle D. Konze,[2] and Jianguo Tao[3]

[1]Department of Biochemistry and Biophysics, Lineberger Comprehensive Cancer Center, and [2]Center for Integrative Chemical Biology and Drug Discovery, University of North Carolina at Chapel Hill, Chapel Hill, NC; and [3]Departments of Hematopathology and Laboratory Medicine, H. Lee Moffitt Cancer Center and Research Institute, Tampa, FL

Posttranslational modifications of histone proteins represent a fundamental means to define distinctive epigenetic states and regulate gene expression during development and differentiation. Aberrations in various chromatin-modulation pathways are commonly used by tumors to initiate and maintain oncogenesis, including lymphomagenesis. Recently, increasing evidence has demonstrated that polycomb group (PcG) proteins, a subset of histone-modifying enzymes known to be crucial for B-cell maturation and differentiation, play a central role in malignant transformation of B cells. PcG hyperactivity in B-cell lymphomas is caused by overexpression or recurrent mutations of PcG genes and deregulation of microRNAs (miRNAs) or transcription factors such as c-MYC, which regulate PcG expression. Interplays of PcG and miRNA deregulations often establish a vicious signal-amplification loop in lymphoma associated with adverse clinical outcomes. Importantly, aberrant enzymatic activities associated with polycomb deregulation, notably those caused by EZH2 gain-of-function mutations, have provided a rationale for developing small-molecule inhibitors as novel therapies. In this review, we summarize our current understanding of PcG-mediated gene silencing, interplays of PcG with other epigenetic regulators such as miRNAs during B-cell differentiation and lymphomagenesis, and recent advancements in targeted strategies against PcG as promising therapeutics for B-cell malignancies. (*Blood*. 2015;125(8):1217-1225)

Introduction

Histone posttranslational modifications represent a fundamental mechanism for regulating DNA accessibility in various DNA-templated processes such as gene transcription.[1] Dysregulation of chromatin-modifying mechanisms is one of the central oncogenic pathways in human cancer,[1-3] including B-cell malignancies.[4-6]

Among various chromatin-modifying factors, polycomb group (PcG) proteins are critical for controlling gene expression, maintaining repressive chromatin states, and defining cellular identities during development.[7,8] PcG proteins act in multimeric complexes known as polycomb repressive complexes (PRCs). Two major PcG complexes exist in mammalian cells: PRC1 and PRC2. Biochemically, PRC1 employs an E3 ligase, RING1A or RING1B, to induce monoubiquitination of histone H2A, lysine 119 (H2AK119ub1) (Figure 1), a reaction that requires essential cofactors such as BMI1.[8] PRC2 utilizes an enzymatic subunit, enhancer of zeste homolog 2 (EZH2) or related EZH1, to methylate histone H3, lysine 27 (H3K27; Figure 1)[7]; other PRC2 subunits (EED and SUZ12) and accessory cofactors such as JARID2 and polycomb-like harbor either DNA- or histone-binding activities to modulate PRC2 activity and mediate its targeting or spreading on chromatin.[7-9] H2AK119ub1 and H3K27 trimethylation (H3K27me3) are prominent histone markers associated with gene silencing, indicating a causal role of PcG-mediated enzymatic activity in transcriptional regulation.[7,8] H3K27me3 also coexists with the gene-activation–associated trimethylation of histone H3, lysine 4 (H3K4me3) at "bivalent domain genes" to maintain genes in a repressed but poised conformation, which can be subsequently activated or stably repressed according to lineage-specific differentiation programs.[1]

In a simplistic hierarchical model, PRC2 acts upstream of PRC1 as H3K27me3 serves as a "docking" site for CBX, a chromodomain-containing protein (Figure 1A), which then recruits PRC1 to induce H2AK119ub1[7,8] (Figure 1B). However, more recently, data have demonstrated that PRC1 recruitment is both PRC2 dependent and PRC2 independent.[10,11] Furthermore, recent studies show that PRC1 can act upstream of PRC2. In this case, a PRC1 variant utilizes KDM2B, a CxxC-domain protein, to bind to the nonmethylated cytosine guanine dinucleotide sequence where PRC1-induced H2AK119ub1 recruits PRC2 via an unknown mechanism[12-14] (Figure 1C). EED, a PRC2 subunit, also physically interacts with PRC1, thus linking PRC2 to PRC1.[15] Overall, PRC2 and PRC1 cooperate and enforce gene silencing via positive-feedback loops.

Increasing evidence has revealed crucial roles of PcG proteins in myriad biological processes, including self-renewal, differentiation, cell-cycle control, senescence, and gene expression and imprinting,[7,8,16,17] all of which have been linked to oncogenesis when deregulated. Notably, *PcG* genes were found mutated in B-cell malignancies. B lymphoma Mo-MLV insertion region 1 homolog (*BMI1*, also known as polycomb group ring finger 4 or PCGF4 [Figure 1]) was originally isolated as a gene upregulated in murine B-cell lymphomas[18]; recurrent gain-of-function mutations of *EZH2* were identified in germinal center (GC) B-cell lymphomas.[4,19,20] Here, we focus on deregulations of PcG and cofactors during the initiation and development of B-cell malignancies. We also discuss the interplays between PcG and other epigenetic regulators such as microRNAs (miRNAs), histone deacetylases (HDACs), and DNA methytransferases (DNMTs). Finally, we summarize recent progress in development of PcG-specific inhibitors as novel therapies of B-cell malignancies.

Submitted October 16, 2014; accepted December 26, 2014. Prepublished online as *Blood* First Edition paper, January 7, 2015; DOI 10.1182/blood-2014-10-606822.

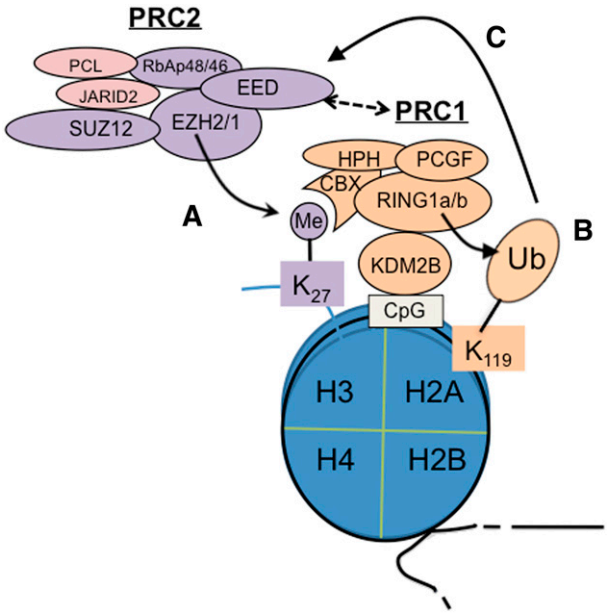

Figure 1. Cooperation of PRC2 and PRC1 in epigenetic silencing of genes. PRC2 catalyzes trimethylation of histone H3 at lysine 27 (H3K27me3) (A), which is recognized and bound by CBX proteins such as CBX7, a PRC1 subunit, to subsequently recruit PRC1 for induction of monoubiquitination of histone H2A at lysine 119 (H2AK119ub1)[7,8] (B).Conversely, recent studies show that a variant form of PRC1 can act upstream of PRC2 to initiate formation of the polycomb domain; in this case, H2AK119ub1 serves as a PRC2 recruitment mechanism (C).[12-14] In addition, EED is also shown to interact to PRC1 physically.[15] CpG, cytosine guanine dinucleotide; Me, trimethylation; Ub, ubiquitination.

Biological function of PcG proteins in B-cell development and lymphomagenesis

The development and differentiation of B-cell lineages initially occur with progenitor B-cell expansion and V(D)J gene rearrangement, a DNA recombination process that produces clonally unique, immunoglobulin variable regions for antigen recognition.[21] Upon antigen stimulation, B cells undergo activation through proliferation, somatic hypermutation, and antibody class switching, which occur in the GCs of secondary lymphoid tissues. A proliferative feature of GC B lymphocytes, with concomitant attenuation of their DNA damage repair function and ongoing somatic hypermutation, increases the likelihood of oncogenic mutation, genomic instability, and subsequent lymphomas. B-cell development is tightly controlled by genetic and epigenetic mechanisms, including DNA methylation, histone modification, chromatin remodeling,[22] and noncoding RNAs.[23] During normal B-lymphocyte differentiation, expression of PRC1 and PRC2 genes shows a restricted, stage-specific pattern. BMI1 and its PRC1 partners are primarily detected among resting B cells in the GC mantle zone and in nondividing centrocytes of the GC follicles; these PRC1 genes are silenced in proliferating follicular centroblasts, which then express the PRC2 genes instead.[24-26] In contrast, lymphomas generally lose such a mutually exclusive expression pattern, and altered expression of PRC1 and PRC2 genes is a general theme in lymphomas, including diffuse large B-cell lymphomas (DLBCL),[27] follicular lymphomas (FLs), and mantle cell lymphomas (MCLs).[28] These findings suggest essential regulatory roles of PRC1 and PRC2 in both normal B-lymphocyte development and lymphoma pathogenesis.

PRC1 in B-cell development and lymphomagenesis

BMI1

Bmi1 (also known as PCGF4 [Figure 1]) was initially discovered from a locus activated by viral integration in murine lymphomas.[18] BMI1 controls a range of B-cell developmental genes, including lineage master regulators *Ebf1* and *Pax5*.[29] *Bmi1* deficiency causes conversion of the "bivalent domain" states associated with *Ebf1* and *Pax5* to a monovalent active state, resulting in their premature expression and accelerated lymphoid differentiation.[29] BMI1 also directly represses expression of the tumor suppressors p16Ink4a/p19Arf and p15Ink4b; therefore, BMI1 overexpression prevents c-MYC–mediated apoptosis and was sufficient to induce lymphoma, a process further accelerated by *c-MYC*.[18,30] Furthermore, BMI1 represses the proapoptotic genes *Noxa* and *Bim*, supporting its pro-survival role in B-cell development and lymphomas.[31,32] In human B-cell lymphomas, BMI1 overexpression is common in almost all subtypes.[33] Expression of BMI1 alone or in combination with EZH2 characterizes aggressive B-cell lymphomas with unfavorable prognosis.[27,33,34] Recently, a novel t(10;14)(p12;q32) translocation was identified in chronic lymphocytic leukemia and MCLs leading to *IgH-BMI1* rearrangement and *BMI1* overexpression[35]; *IgH-BMI1* rearrangement was acquired during tumor high-grade transformation and correlated with chemoresistance.[35] Transcriptome analyses of multiple cancers found that BMI1-driven gene signatures define a phenotype of cancer stem cells,[36] suggesting that BMI1 confers malignant cells with features of cancer stem cells, the rare cancerous subpopulations that confer drug resistance and regeneration abilities.[16,37] Indeed, BMI1-mediated repression of p16Ink4a/p19Arf was shown to be essential for self-renewal of hematopoietic stem cells.[38] Overall, these studies support critical roles of BMI1 in promoting lymphoma progression and conferring therapy resistance.

Other PRC1 factors

Evidence exists showing direct involvement of other PRC1 components in B-cell lymphomas. CBX7 (Figure 1) was found highly expressed in GC lymphocytes and GC-derived FLs, where its elevated expression was correlated with *c-MYC* expression and an aggressive feature.[39] Lymphoid-specific overexpression of Cbx7 in mice initiated lymphomagenesis and cooperated with c-MYC to produce aggressive B-cell lymphomas.[39] Similar to BMI1, Cbx7 overexpression was linked to repression of p16Ink4a/p19Arf.[39] RING1A is associated with the risk of non-Hodgkin lymphomas[40] and high expression of RING1B detected in lymphomas such as DLBCLs and Burkitt lymphoma.[41] However, in the absence of p16Ink4a, RING1B deficiency accelerated lymphomagenesis through upregulation of cyclin D2 and Cdc6.[42] Thus, PRC1 harbors both oncogenic and tumor-suppressive roles in different contexts, which is reminiscent of PRC2's dual functions described among different hematopoietic malignancies.[43-45]

PRC2 in B-cell development and lymphomagenesis

EZH2 is highly expressed in lymphoid progenitors and required for efficient V(D)J recombination in pro–B cells.[46] *EZH2* is silenced

in resting GC B cells but massively upregulated when GC B cells get activated and undergo rapid proliferation and immunoglobulin affinity maturation[26,47]; EZH2 blocks the DNA damage response pathways, allowing cells to survive the somatic hypermutation during antibody maturation.[26] Expression of *EZH2* strongly associates with B-cell malignancies, with its high levels correlated with the Ki67 labeling index, lymphoma aggressiveness, and unfavorable prognosis.[33,34] The highest percentage of EZH2 positivity was found in 100% of Burkitt lymphomas, 87.5% of grade-3 FLs, and 85.7% of DLBCLs. Multivariate survival analysis identified EZH2 as the strongest prognostic predictor of inferior outcomes of MCLs.[27] *SUZ12* expression was also found to be restricted to proliferating lymphoid cells during development and at high levels in MCLs, in comparison with its general absence in nontumorous mantle zone cells.[48]

The importance of PRC2 in lymphomagenesis is further strengthened by recent identification of recurrent missense mutations in EZH2, with the most prevalent ones altering a single residue in the catalytic domain, Y641 (the numeration of EZH2 amino acids based on a short isoform of EZH2 [National Center for Biotechnology Information accession Q15910.2]), among ~10% to 20% of GC-derived B-cell lymphomas such as DLBCLs and FLs.[4,5,49] These EZH2 mutations are likely to be early lesions during lymphomagenesis.[6,49] Biochemically, EZH2^{Y641} mutations alter substrate specificity of EZH2.[19,20,50] Being a catalytic subunit of PRC2, EZH2 induces sequential mono-, di-, and trimethylation of H3K27, with the highest methylation status most strongly associated with gene silencing.[51] Wild-type EZH2 has a greater catalytic efficiency for conducting monomethylation of H3K27 (H3K27me1) and a diminished efficiency for subsequent reactions (mono- to di- and di- to trimethylations).[19,20,50] In contrast, lymphoma-associated EZH2^{Y641X} mutations (X means Asn/Phe/Ser/His/Cys) show the exactly opposite substrate specificity, displaying limited ability to induce H3K27 monomethylation yet extremely high efficiency catalyzing the H3K27 di- to trimethylation reaction.[19,20,50] Such enzymatic differences between wild-type and EZH2^{Y641X} mutant protein suggest that EZH2^{Y641X} mutations must occur heterozygously in lymphomas, which is indeed the case in human patients,[4,5,49] allowing for EZH2^{Y641X} to cooperate with wild-type EZH2 to induce a global increase in H3K27me3[19,20,50] and aberrant transcriptional alteration. Later on, 2 additional somatic mutations, EZH2^{A677G} and EZH2^{A687V}, were identified at a lower frequency (~1% to 3%) among GC B-cell lymphomas,[5,49,52,53] and they demonstrate enzymatic properties distinct from EZH2^{Y641X} mutants.[50,52-54] EZH2^{A677G} and EZH2^{A687V} possess the almost equally enhanced catalytic activity towards all the H3K27 substrates with different methylation status.[50,52-54] Thus, EZH2^{A677G} and EZH2^{A687V} mutants are able to induce a global increase in H3K27me3 without the need for wild-type EZH2.[50] Besides kinetics, EZH2^{Y641X} also affects protein stability.[55] Phosphorylation of *Y641*, a known phosphorylation site of JAK2 kinases, leads to interaction of EZH2 with β-TrCP, a SCF E3 ubiquitin ligase, and promotes EZH2 degradation. Loss of this phosphorylation site due to somatic *Y641* mutations reduces EZH2 turnover, which has been postulated to contribute to the hyper-H3K27me3 phenotype.[55] Taken together, different gain-of-function mutations induce EZH2 hyperactivity through distinct molecular mechanisms, and despite the fact that lymphomas carrying different EZH2 mutations may possess different levels of the lowly methylated H3K27, they all have a consistently higher level of H3K27me3.[50,52-54]

Recent studies have provided a better understanding of the in vivo function of *EZH2* and mutation in normal B-cell development and lymphomagenesis.[47,56-58] Using *Ezh2* knockout mice, Beguelin et al[56] and Caganova et al[47] have independently shown that EZH2 is crucial for the formation of GCs and GC B-cell development. Mechanistically, EZH2 represses myriad downstream genes including the negative cell-cycle regulators *Cdkn2a* (p16Ink4a/p19Arf) and *Cdkn1a/p21* and crucial transcription factor genes IRF4 and BLIMP1/PRDM1, which are known to be essential for post GC B-cell development[47,56,57] (Figure 2). Indeed, depletion of EZH2 from lymphomas suppressed their proliferation and attenuated tumor formation.[57] These studies support the notion that EZH2 hyperactivation promotes malignant transformation by repressing both antiproliferative and differentiation-inducing programs. Furthermore, *Ezh2*-deficient GC B cells had profound impairments in GC responses and memory B-cell formation and failed to protect themselves from the genotoxic damages induced by activation-induced cytidinedeaminase,[47] an enzyme critical for somatic hypermutation and antibody affinity maturation,[21] demonstrating an essential role of EZH2 in the GC B-cell development (Figure 2). B-cell–specific expression of the EZH2^{Y641N} or EZH2^{Y641F} mutant in transgenic mice elevated the global H3K27me3, promoted a high proliferation of GC B cells, and resulted in follicular hyperplasia.[56,58] However, additional oncogenic events are required for neoplastic transformation, although GC-derived lymphomas remain addicted to EZH2 mutations. It has been shown that EZH2$^{Y641N/F}$ mutants cooperate with BCL2 to generate malignant GC B-cell lymphomas[56]; similarly, genetic interaction of EZH2^{Y641F} and MYC in transgenic mice gave rise to high-grade lymphomas with a mature B-cell phenotype.[58] Collectively, these findings have shown that dynamic expression of *EZH2* allows expansion and development of GC B cells, which undergo terminal differentiation and develop into antibody-secreting cells and plasma cells as *EZH2* expression declines (Figure 2). EZH2 hyperactivity perturbs the fine balance of GC B-cell proliferation and differentiation, permanently locking GC B cells in an immature and proliferative state, a prelude to full-blown lymphoma. Although not sufficient on its own to cause lymphoma, EZH2 gain-of-function mutations serve as a driver of lymphomagenesis and collaborate with additional lesions to generate and/or accelerate GC B-cell lymphomas (Figure 2).

In contrast to the oncogenic role of EZH2 in B-cell lineages, the tumor-suppressive roles of PRC2 in T-cell acute lymphoblastic leukemia[44,45] and myeloid malignancies[43] were identified due to a range of missense, nonsense, and frameshift mutations in EZH2, SUZ12, or EED (Figure 1). These lesions can be homozygous, are found throughout the gene, and are generally predicted to disable PRC2 activity, implying its disease-dependent functions. These observations emulate those obtained in Eμ-Myc lymphoma models showing that PRC2 can be a tumor suppressor in Eμ-Myc–induced lymphomagenesis, wherein the lymphoma onset was accelerated by knockdown of Suz12 or Ezh2.[59] Such an effect is likely due to the enhanced self-renewal of B-lymphoid progenitors upon PRC2 loss,[59] which is in contrast to cooperation between EZH2^{Y641F} and Eμ-Myc reported by Berg et al in GC B-cell compartments.[58] These studies emphasize the complicated, context-dependent role of PRC2 in oncogenesis, which might be due to a tightly controlled expression pattern of EZH2 throughout B-cell lineage differentiation. As a result, PRC2 activity at various developmental stages may either suppress or facilitate lymphomagenesis. Indeed, EZH2 expression is high in pro–B cells and decreased in pre–B cells and becomes nearly undetectable in immature naive cells[46,57]; EZH2 is then upregulated again during affinity maturation in GC B cells.[26,47] Therefore, it could be the case that whereas PRC2 restricts the proliferative and self-renewal potential of immature B-lymphoid progenitors, its gain-of-function mutations stimulate proliferation specifically in maturing

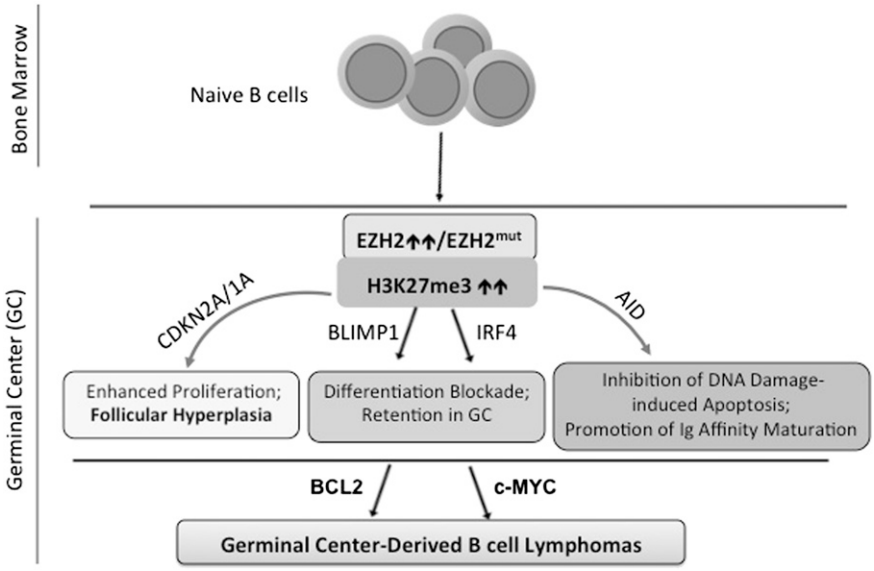

Figure 2. Biological functions of EZH2 in normal B-cell development and lymphomagenesis. During B-cell differentiation, naive B cells enter the GC and EZH2 is transcriptionally upregulated during GC B-cell maturation.[26,47] Via induction of H3K27me3, EZH2 then transcriptionally represses a myriad of downstream effector genes, which at least include the negative cell-cycle regulators (CDKN2A and CDKN1A) and B-cell differentiation-promoting transcription factors (IRF4 and BLIMP1/PRDM1), hence allowing for rapid expansion of immature B cells[47,56,57]; in addition, EZH2 protects GC B cells from the genotoxic damages induced by activation-induced cytidinedeaminase (AID),[47] an enzyme critical for immunoglobulin affinity maturation via a mechanism of somatic hypermutation that modifies the immunoglobulin variable region of the rearranged antibody genes in GC B cells.[21] EZH2 levels decrease as B cells exit the GC, enabling derepression of EZH2-targeted genes and hence terminal differentiation.[47,56,57] However, EZH2 hyperactivity (either somatic mutation or overexpression) disrupts such fine equilibrium, continuously enhances H3K27me3, and results in exaggerated silencing of EZH2 targeted genes, which then block GC B-cell differentiation and promote their proliferation and survival. EZH2 mutations alone lead to follicular hyperplasia, and, with acquisition of additional oncogenic events such as upregulation of BCL2 or c-MYC, EZH2 mutations cooperatively enable or accelerate malignant transformation of GC B cells.[56,58]

GC B cells. Further work with mouse models engineered to overexpress or delete EZH2 at each specific stage of B-cell differentiation shall provide insight into the role of PRC2 in various B-cell malignancies.

Interplay of PcG with other epigenetic enzymes

In addition to intrinsic enzymatic functions, PcG complexes also recruit other chromatin-modifying factors such as HDACs and DNMTs to re-enforce transcriptional repression. PRC2 recruits HDAC1-3, linking 2 distinctive repressive machineries together.[60] Several broad-spectrum HDAC inhibitors, including sodium butyrate, decrease the messenger RNA and protein levels of *BMI1* and *EZH2* in cancer cells.[61] These findings implicate that HDACs positively regulate cellular PcG levels and that epigenetic control of gene expression is governed by cooperation of PRC2 and HDACs. In addition, histone methylation influences DNA methylation and, in turn, DNA methylation serves as an instructive template for histone modification. In cancer, PcG-suppressed genes are likely to be associated with DNA hypermethylation, and hypermethylated promoters more frequently premarked with PcG.[8,62,63] Indeed, EZH2 directly associates with DNMTs.[64] This mechanism also appears to be operative in B-cell lymphoma because DNA methylation profiling of lymphomas revealed a significant enrichment of PcG targets at the de novo methylated genes,[65] indicating that crosstalk between histone and DNA methylation may form a double "locking" mechanism of an undifferentiated cell state during malignant transformation. Perturbation of cellular factors that antagonize PcG, such as trithorax group (TrxG) proteins,[17] may equally influence the regulatory roles and biological outputs of PcG complexes. Indeed, direct sequencing of patients with B-cell malignancies has recently led to identification of recurrent damaging mutations of several TrxG genes such as *MLL2*, *p300*, and *CBP*.[5,6,66] Loss-of-function mutations of TrxG and gain-of-function mutations of PcG genes may equally perturb a fine equilibrium of histone methylation dynamics during B-cell lymphomagenesis.

Interplay of PcG with miRNAs

miRNAs are 22-nucleotide, noncoding single-stranded RNAs that can repress gene expression at a posttranscriptional level. miRNAs are increasingly recognized as one of the major players in numerous biological processes, and their downderegulation is often seen in tumors, suggesting their tumor-suppressive roles. It can be anticipated that miRNA deregulation can contribute to PcG deregulation. Indeed, *EZH2* was the first PcG gene shown to be regulated by miRNA.[67,68] By targeting the 3′ untranslated region of *EZH2* messenger RNA, *miR-101* and *miR-26* repress cellular *EZH2* levels.[67,68] miRNAs that repress PRC1 genes were also identified.[69-71] Downregulation and deletion of these miRNAs are frequent in various tumors, including prostate cancer and lymphomas.[67,68] Conversely, PcG proteins also contribute to miRNA expression and deregulation during malignant development, given their frequent alterations found in tumors. Indeed, many miRNA genes are repressed by PRC2 and demarcated with H3K27me3.[72] PRC2 represses *miR-31* in adult T-cell lymphoma, leading to activation of nuclear factor κB oncogenic signaling.[73] Thus, these findings have shown an intriguing interplay between miRNAs and PcG. Below, we summarize recent advances in understanding their interactions in cancers, especially

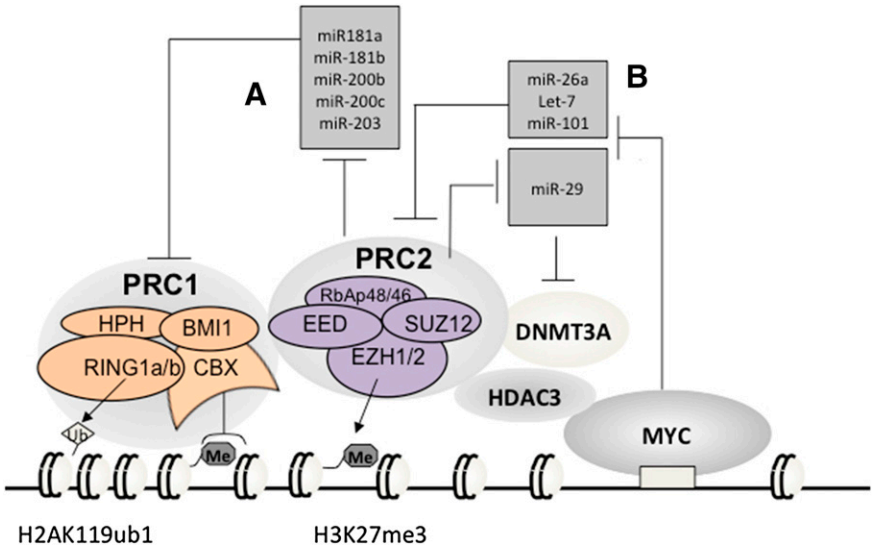

Figure 3. Vicious amplification loops involving a myriad of PcG proteins and miRNAs. Repression of PRC1-repressing miRNAs by PRC2 (A) establishes a positive-feedback loop ensuring coexpression and cooperation of 2 main PcG repressor complexes in stem and cancer cells; c-MYC, which is frequently translocated or overexpressed in Burkitt lymphoma and other B-cell lymphoma types, assembles a gene-silencing complex with PRC2 and HDACs to downregulate a list of tumor-suppressive miRNAs that can repress EZH2 and DNMT3A (B), hence establishing positive-feedback loops to enforce expression and functionality of PRC2 in B-cell lymphomas. Me3, trimethylation. Ub1, monoubiquitination.

B-cell malignancies, which reveal the hitherto-unappreciated regulatory circuits involving miRNA and epigenetic factors.

PRC2–miRNA–PRC1 circuitry

A subset of miRNAs, including miR-181a, miR-181b, miR-200b, miR-200c, and miR-203 (Figure 3A), are transcriptionally silenced by PRC2 in cancer.[69] Interestingly, these miRNAs repress PRC1 genes such as *BMI1* and RING1B[69-71] (Figure 3A). It has been shown that downregulation of these miRNAs such as miR-200c ensures the cellular level and functionality of PRC1 in stem cells[70,71] and cancers including lymphoma,[69-71,74] promoting cell "stemness" properties. These data demonstrate that expression of PRC1 and PRC2 is integrated through a network of regulatory miRNAs wherein epigenetic repression of PRC1-targeting miRNAs by PRC2 establishes a positive feedback loop, ensuring coexpression and cooperation of 2 major PcG complexes.

EZH2/c-MYC–miRNA–EZH2 circuitry

Recent studies of B-cell malignancies also unveiled a second circuitry involving EZH2, miRNAs, and c-MYC, an oncogenic transcription factor almost invariably translocated in Burkitt lymphoma. *c-MYC* assembles a repressive complex with PRC2 and HDACs to downregulate a broad spectrum of tumor-suppressive miRNAs, including miR-15a/16-1, miR-26, miR-27, miR-29, let-7, miR-494, and miR-548m[67,75-79] (Figure 3B). A similar c-MYC–PRC2 complex also represses miR-101 in hepatocellular carcinoma.[80] Among these repressed miRNAs, miR-101 and miR-26 were recurrently deleted in tumors including lymphoma[67,68]; miR-15a/16-1 targets BCL2 and acts as tumor suppressor in chronic lymphocytic leukemia.[81] Interestingly, several of these c-MYC–repressed miRNAs, including miR-26a, miR-101, and let-7, actually repress EZH2 directly[67,75,78] (Figure 3B); miR-29, a family of miRNAs known to be involved in B-cell lymphomagenesis,[75,82] was shown to downregulate DNMT3A, a PRC2-interacting factor, in chronic lymphocytic leukemia[83] (Figure 3B). Thus, via recruitment of PRC2 and HDACs, c-MYC, a prominent lymphoma-promoting factor, represses miRNAs that negatively regulate EZH2 and its cofactors, establishing a positive-feedback loop for enforcing polycomb genes expression and functionality in B-cell lymphomas. As knocking down EZH2 and HDACs led to re-expression of the MYC-repressed miRNAs,[75,78,84,85] the existing pharmacologic agents for inhibition of these c-MYC–associated corepressors shall represent a promising way to disrupt such a vicious amplification loop associated with lymphomagenesis.

Epigenetic therapy and perspective

Epigenetic deregulation of chromatin structure and function leads to aberrant gene expression and oncogenesis. Consequently, epigenetic therapies aim to restore normal chromatin-modification patterns through inhibition of the deregulated epigenetic machinery. HDAC and DNMT inhibitors are among the first promising agents for epigenetic therapies,[2] and, more recently, specific inhibitors for PcG proteins have been developed.

Targeting PRC1

A recent high-throughput screen discovered a small-molecule compound PTC-209 as an inhibitor of BMI1.[86] PTC-209 inhibited expression of *BMI1* and induced a dose-dependent reduction of global H2AK119ub1.[86] *BMI1* knockdown conferred PTC-209 insensitivity, indicating its specificity.[86] Similar to *BMI1* knockdown, PTC-209 treatment inhibited self-renewal of cancer-initiating stem cells.[86] This study implicates that BMI1 has the potential to be developed as a drug target for treating B-cell lymphomas with *BMI1* overexpression.

Targeting PRC2

Several highly selective small-molecule inhibitors of PRC2 (with K_i values within the low-nanomolar range) have recently been discovered,[87-93] many of which possess a common pyridone-containing motif that confers EZH2 or EZH1 inhibition (Figure 4A). Among them, EPZ005687[88] and GSK126[87] show high selectivity for EZH2 vs other methyltransferases, with >50- to 150-fold selectivity for EZH2 over EZH1 (Figure 4A). Early success was seen in treating B-cell lymphomas bearing EZH2 gain-of-function mutation with these inhibitors in DLBCL xenografts in mice.[56,87-93] GSK126,[87] EPZ005687, and EPZ-6438[88,94] (Figure 4A-B) show their particular effectiveness in suppressing growth of the EZH2-mutant lymphomas

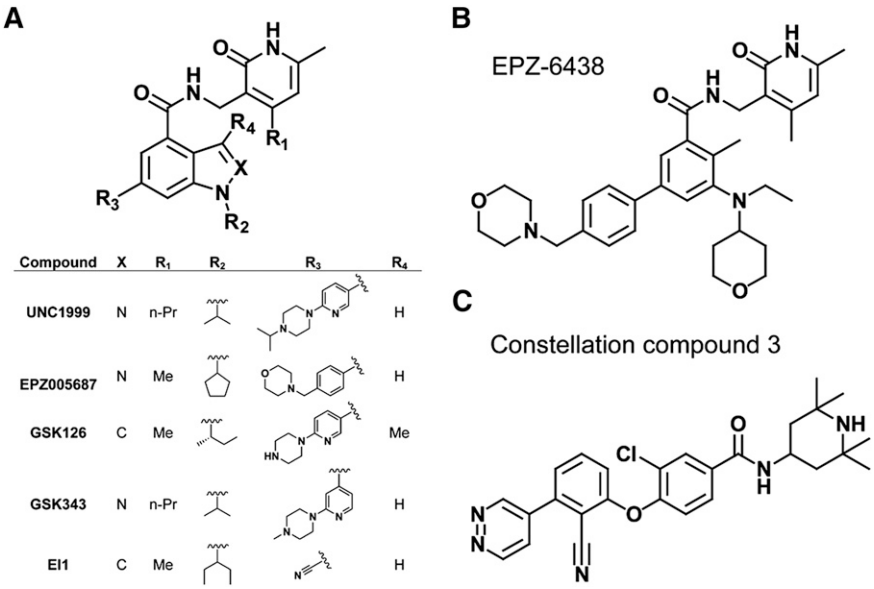

Figure 4. Highly selective, small-molecule inhibitors of PRC2. (A) Scaffold demonstrating that several of the recently developed EZH2 or EZH2/1 inhibitors all possess a pyridone motif as well as an indole or indazole core. The inserted table details the identity of each designated substituent of the described inhibitors. (B) Chemical structure of EPZ-6438. (C) Chemical structure of Constellation Pharmaceuticals compound 3, the first non–pyridone-containing EZH2 inhibitor.

vs those with wild-type EZH2. At the transcriptome level, and in contrast to minimal transcriptional responses in wild-type EZH2, drug-insensitive lines, reactivation of the formerly H3K27me3-demarcated genes was generally seen in drug-sensitive GC B-cell (GCB) type of DLBCL lines.[87,93] However, only a limited number of upregulated genes were found common across different inhibitor-sensitive lines, although upregulated genes in each individual line are enriched in those related to cell-cycle and apoptotic regulation,[87] thus highlighting a challenge to define relevant targets presumably due to variations of genetic backgrounds. The biological responses such as growth suppression after treatment with EZH2 inhibitors show a delayed pattern in comparison with the biochemical responses; the diminution of H3K27me3 was apparent within 24 to 48 hours post-treatment, and yet the cellular response is usually not fully presented until days 4 to 7 posttreatment and beyond.[87] Such a delayed effect with the PRC2 inhibitors was seen in acute myeloid leukemia[95] and for inhibitors of the histone methyltransferase DOT1L,[96] which is in contrast to quick responses associated with HDAC inhibitors. It has been speculated that additional time and/or chromatin factors may be required to reverse the histone methylation-regulated events, and, alternatively, catalytic inhibition induces compensatory recruitment of more enzymatic complexes at crucial gene targets, thus delaying demethylation. It is worth noting that PRC2 possesses noncanonical functions such as methylation of nonhistone substrates[97] or acting as transcriptional activator,[98] but it remains unclear if these mechanisms exist in lymphomas. Treatment of EZH2-mutant, GCB-DLBCL xenograft models with GSK126 or GSK343 (Figure 4A) resulted in tumor regression,[56,87] and the inhibitor was well tolerated. [87] Currently, various PRC2 inhibitors are under clinical evaluation and it would be exciting to see whether PRC2 inhibition provides clinical benefits for lymphoma patients.

EZH2 mutation ($EZH2^{Y641X}$, $EZH2^{A677G}$, or $EZH2^{A687V}$) is a known predictor of EZH2 inhibitor sensitivity; however, later studies showed that GCB-DLBCL is addicted to EZH2 and shows general sensitivity to the EZH2 inhibitor independent of its mutational state,[56] and such an EZH2 addiction was not seen in the activated B-cell type of DLBCLs, a more differentiated lymphoma subtype with EZH2 repressed.[56] These findings are consistent with the clinical observation that EZH2 mutations exclusively occur in GCB-DLBCLs and not activated B-cell DLBCL,[4] providing a rationale for a personalized medicine for lymphoma therapy. Furthermore, the efficacy of EZH2 inhibitors has been established in various B-cell lymphomas with wild-type EZH2, including MCLs and Burkitt lymphoma.[75,93] Therefore, other molecular determinants for EZH2 inhibitor sensitivity remain to be defined for B-cell lymphomas in order to improve personalized therapy. Such genetic determinants were defined in other cancers, including SNF inactivation in malignant rhabdoidtumors,[91] MMSET/NSD2 translocation in multiple myeloma,[99] and MLL rearrangement in acute leukemia,[95,100] and all of these affected pathways have been connected to PRC2 genetically. Thus, it is likely that lymphomas carrying TrxG gene mutations,[5,6,66] such as MLL2 mutations, may render sensitivity to PRC2 inhibition.

Furthermore, it remains to be examined if EZH1, a less-studied EZH2-related enzyme, is overexpressed in B-cell malignancies and if EZH1 inhibition improves the therapeutic potential. Given that EZH1 compensates the function of EZH2, inhibitors that target both EZH2 and EZH1 such as UNC1999[90] (Figure 4A) and Constellation Pharmaceuticals compound 3[92] (Figure 4C), are expected to have benefits for treating a broader spectrum of B-cell malignancies with overexpression of EZH2 or EZH1. Indeed, we have recently shown that UNC1999 offers advantages over EZH2-selective inhibitors and represents a novel efficient therapeutic for MLL-rearranged leukemias that coexpress EZH2 and EZH1.[95]

In line with therapeutic advances, combination therapy shall be explored, because EZH2 inhibitors can be used together with inhibitors against other oncogenic pathways that act in parallel. Indeed, our recent studies demonstrated synergy of EZH2 and HDAC inhibitors to inhibit lymphoma clonogenic cell growth, induce apoptosis, and suppress growth of MCLs or aggressive c-MYC–associated lymphomas.[75,77] The effects are at least partially due to disruption of c-MYC/EZH2-mediated miRNA silencing and vicious amplification loops (Figure 3B). In addition, combination treatment with EZH2 and BCL2 inhibitors outperformed the single-drug therapies in lymphoma models.[56] Lastly, given cooperation between DNA methylation and histone modification in transcriptional regulation, it would be of great interest to test if lymphoma cases with a higher degree of epigenetic silencing and hence reduced reversibility are less sensitive to PRC2 inhibitor single treatment but more responsive to a combined treatment with DNA demethylating agents.

Conclusion

Gene regulation by PcG complexes is critical for regulation of various biological programs related to normal development and oncogenesis. PcG aberration, caused by its deregulated expression, somatic mutation, and chromosomal translocation, is common in various B-cell malignancies, demonstrating PcG as a central mechanism in lymphoma initiation and development. PcG complexes interact with other epigenetic machineries such as HDACs, DNMTs, and miRNAs in a context-dependent manner to control gene expression and promote lymphomagenesis. Recent advances in developing targeted strategies against PcG have demonstrated early success and display great potential in treating incurable B-cell malignancies.

Acknowledgments

G.G.W. is supported by a National Institutes of Health National Cancer Institute "Pathway to Independence" Award in Cancer Research (CA151683), a Department of Defense Career Development Award (CA130247), and grants from Gabrielle's Angel Foundation and Concern Foundation. G.G.W. is a Kimmel Scholar of Sidney Kimmel Foundation for Cancer Research and an American Society of Hematology Scholar in Basic Science. K.D.K. is supported by an American Chemical Society Medicinal Chemistry Predoctoral Fellowship. J.T. is supported by grants from the National Institutes of Health National Cancer Institute (R01 CA137123), Maher Fund, Lymphoma Research Foundation, National Functional Genomics Center Programmatic Research grant, and an American Society of Hematology Bridge Grant.

Authorship

Contribution: All authors participated in the preparation of the manuscript and illustrations and approved the final version of the manuscript.

Conflict-of-interest disclosure: The authors declare no competing financial interests.

Correspondence: Jianguo Tao, Departments of Hematopathology and Laboratory Medicine, H. Lee Moffitt Cancer Center and Research Institute, Tampa, FL 33612; e-mail: jianguo.tao@moffitt.org; and G. Greg Wang, Lineberger Comprehensive Cancer Center, University of North Carolina at Chapel Hill, 450 West Dr, CB 7295, Chapel Hill, NC 27599; e-mail: greg_wang@med.unc.edu.

References

1. Chi P, Allis CD, Wang GG. Covalent histone modifications—miswritten, misinterpreted and mis-erased in human cancers. *Nat Rev Cancer.* 2010;10(7):457-469.
2. Arrowsmith CH, Bountra C, Fish PV, Lee K, Schapira M. Epigenetic protein families: a new frontier for drug discovery. *Nat Rev Drug Discov.* 2012;11(5):384-400.
3. Wang GG, Allis CD, Chi P. Chromatin remodeling and cancer, Part I: Covalent histone modifications. *Trends Mol Med.* 2007;13(9): 363-372.
4. Morin RD, Johnson NA, Severson TM, et al. Somatic mutations altering EZH2 (Tyr641) in follicular and diffuse large B-cell lymphomas of germinal-center origin. *Nat Genet.* 2010;42(2): 181-185.
5. Morin RD, Mendez-Lago M, Mungall AJ, et al. Frequent mutation of histone-modifying genes in non-Hodgkin lymphoma. *Nature.* 2011; 476(7360):298-303.
6. Okosun J, Bödör C, Wang J, et al. Integrated genomic analysis identifies recurrent mutations and evolution patterns driving the initiation and progression of follicular lymphoma. *Nat Genet.* 2014;46(2):176-181.
7. Margueron R, Reinberg D. The Polycomb complex PRC2 and its mark in life. *Nature.* 2011; 469(7330):343-349.
8. Di Croce L, Helin K. Transcriptional regulation by Polycomb group proteins. *Nat Struct Mol Biol.* 2013;20(10):1147-1155.
9. Cai L, Rothbart SB, Lu R, et al. An H3K36 methylation-engaging Tudor motif of polycomb-like proteins mediates PRC2 complex targeting. *Mol Cell.* 2013;49(3):571-582.
10. Tavares L, Dimitrova E, Oxley D, et al. RYBP-PRC1 complexes mediate H2A ubiquitylation at polycomb target sites independently of PRC2 and H3K27me3. *Cell.* 2012;148(4):664-678.
11. Leeb M, Pasini D, Novatchkova M, Jaritz M, Helin K, Wutz A. Polycomb complexes act redundantly to repress genomic repeats and genes. *Genes Dev.* 2010;24(3):265-276.
12. Cooper S, Dienstbier M, Hassan R, et al. Targeting polycomb to pericentric heterochromatin in embryonic stem cells reveals a role for H2AK119u1 in PRC2 recruitment. *Cell Reports.* 2014;7(5):1456-1470.
13. Blackledge NP, Farcas AM, Kondo T, et al. Variant PRC1 complex-dependent H2A ubiquitylation drives PRC2 recruitment and polycomb domain formation. *Cell.* 2014;157(6): 1445-1459.
14. Kalb R, Latwiel S, Baymaz HI, et al. Histone H2A monoubiquitination promotes histone H3 methylation in Polycomb repression. *Nat Struct Mol Biol.* 2014;21(6):569-571.
15. Cao Q, Wang X, Zhao M, et al. The central role of EED in the orchestration of polycomb group complexes. *Nat Commun.* 2014;5:3127.
16. Bracken AP, Helin K. Polycomb group proteins: navigators of lineage pathways led astray in cancer. *Nat Rev Cancer.* 2009;9(11):773-784.
17. Schuettengruber B, Chourrout D, Vervoort M, Leblanc B, Cavalli G. Genome regulation by polycomb and trithorax proteins. *Cell.* 2007; 128(4):735-745.
18. van Lohuizen M, Verbeek S, Scheijen B, Wientjens E, van der Gulden H, Berns A. Identification of cooperating oncogenes in E mu-myc transgenic mice by provirus tagging. *Cell.* 1991;65(5):737-752.
19. Sneeringer CJ, Scott MP, Kuntz KW, et al. Coordinated activities of wild-type plus mutant EZH2 drive tumor-associated hypertrimethylation of lysine 27 on histone H3 (H3K27) in human B-cell lymphomas. *Proc Natl Acad Sci USA.* 2010;107(49):20980-20985.
20. Yap DB, Chu J, Berg T, et al. Somatic mutations at EZH2 Y641 act dominantly through a mechanism of selectively altered PRC2 catalytic activity, to increase H3K27 trimethylation. *Blood.* 2011;117(8):2451-2459.
21. Klein U, Dalla-Favera R. Germinal centres: role in B-cell physiology and malignancy. *Nat Rev Immunol.* 2008;8(1):22-33.
22. Wang GG, Allis CD, Chi P. Chromatin remodeling and cancer, Part II: ATP-dependent chromatin remodeling. *Trends Mol Med.* 2007; 13(9):373-380.
23. Schmidt A, Küppers R. Role of microRNAs in B cell leukemias and lymphomas. *Curr Mol Med.* 2014;14(5):580-597.
24. Raaphorst FM, van Kemenade FJ, Fieret E, et al. Cutting edge: polycomb gene expression patterns reflect distinct B cell differentiation stages in human germinal centers. *J Immunol.* 2000;164(1):1-4.
25. Raaphorst FM, Otte AP, van Kemenade FJ, et al. Distinct BMI-1 and EZH2 expression patterns in thymocytes and mature T cells suggest a role for Polycomb genes in human T cell differentiation. *J Immunol.* 2001;166(10): 5925-5934.
26. van Galen JC, Dukers DF, Giroth C, et al. Distinct expression patterns of polycomb oncoproteins and their binding partners during the germinal center reaction. *Eur J Immunol.* 2004;34(7):1870-1881.
27. van Kemenade FJ, Raaphorst FM, Blokzijl T, et al. Coexpression of BMI-1 and EZH2 polycomb-group proteins is associated with cycling cells and degree of malignancy in B-cell non-Hodgkin lymphoma. *Blood.* 2001;97(12): 3896-3901.
28. Visser HP, Gunster MJ, Kluin-Nelemans HC, et al. The Polycomb group protein EZH2 is upregulated in proliferating, cultured human mantle cell lymphoma. *Br J Haematol.* 2001; 112(4):950-958.
29. Oguro H, Yuan J, Ichikawa H, et al. Poised lineage specification in multipotential hematopoietic stem and progenitor cells by the polycomb protein Bmi1. *Cell Stem Cell.* 2010; 6(3):279-286.
30. Jacobs JJ, Scheijen B, Voncken JW, Kieboom K, Berns A, van Lohuizen M. Bmi-1 collaborates with c-Myc in tumorigenesis by inhibiting c-Myc-induced apoptosis via INK4a/ARF. *Genes Dev.* 1999;13(20):2678-2690.

31. Yamashita M, Kuwahara M, Suzuki A, et al. Bmi1 regulates memory CD4 T cell survival via repression of the Noxa gene. *J Exp Med.* 2008; 205(5):1109-1120.
32. Jagani Z, Wiederschain D, Loo A, et al. The Polycomb group protein Bmi-1 is essential for the growth of multiple myeloma cells. *Cancer Res.* 2010;70(13):5528-5538.
33. Abd Al Kader L, Oka T, Takata K, et al. In aggressive variants of non-Hodgkin lymphomas, Ezh2 is strongly expressed and polycomb repressive complex PRC1.4 dominates over PRC1.2. *Virchows Arch.* 2013;463(5):697-711.
34. van Galen JC, Muris JJ, Oudejans JJ, et al. Expression of the polycomb-group gene BMI1 is related to an unfavourable prognosis in primary nodal DLBCL. *J Clin Pathol.* 2007;60(2): 167-172.
35. Rouhigharabaei L, Ferreiro JF, Put N, et al. BMI1, the polycomb-group gene, is recurrently targeted by genomic rearrangements in progressive B-cell leukemia/lymphoma. *Genes Chromosomes Cancer.* 2013;52(10):928-944.
36. Glinsky GV, Berezovska O, Glinskii AB. Microarray analysis identifies a death-from-cancer signature predicting therapy failure in patients with multiple types of cancer. *J Clin Invest.* 2005;115(6):1503-1521.
37. Lessard J, Sauvageau G. Bmi-1 determines the proliferative capacity of normal and leukaemic stem cells. *Nature.* 2003;423(6937):255-260.
38. Park IK, Qian D, Kiel M, et al. Bmi-1 is required for maintenance of adult self-renewing haematopoietic stem cells. *Nature.* 2003; 423(6937):302-305.
39. Scott CL, Gil J, Hernando E, et al. Role of the chromobox protein CBX7 in lymphomagenesis. *Proc Natl Acad Sci USA.* 2007;104(13): 5389-5394.
40. Wang SS, Menashe I, Cerhan JR, et al. Variations in chromosomes 9 and 6p21.3 with risk of non-Hodgkin lymphoma. *Cancer Epidemiol Biomarkers Prev.* 2011;20(1):42-49.
41. Sánchez-Beato M, Sánchez E, González-Carreró J, et al. Variability in the expression of polycomb proteins in different normal and tumoral tissues. A pilot study using tissue microarrays. *Mod Pathol.* 2006;19(5):684-694.
42. Calés C, Román-Trufero M, Pavón L, et al. Inactivation of the polycomb group protein Ring1B unveils an antiproliferative role in hematopoietic cell expansion and cooperation with tumorigenesis associated with Ink4a deletion. *Mol Cell Biol.* 2008;28(3):1018-1028.
43. Shih AH, Abdel-Wahab O, Patel JP, Levine RL. The role of mutations in epigenetic regulators in myeloid malignancies. *Nat Rev Cancer.* 2012; 12(9):599-612.
44. Simon C, Chagraoui J, Krosl J, et al. A key role for EZH2 and associated genes in mouse and human adult T-cell acute leukemia. *Genes Dev.* 2012;26(7):651-656.
45. Ntziachristos P, Tsirigos A, Van Vlierberghe P, et al. Genetic inactivation of the polycomb repressive complex 2 in T cell acute lymphoblastic leukemia. *Nat Med.* 2012;18(2): 298-301.
46. Su IH, Basavaraj A, Krutchinsky AN, et al. Ezh2 controls B cell development through histone H3 methylation and Igh rearrangement. *Nat Immunol.* 2003;4(2):124-131.
47. Caganova M, Carrisi C, Varano G, et al. Germinal center dysregulation by histone methyltransferase EZH2 promotes lymphomagenesis. *J Clin Invest.* 2013;123(12): 5009-5022.
48. Martín-Pérez D, Sánchez E, Maestre L, et al. Deregulated expression of the polycomb-group protein SUZ12 target genes characterizes mantle cell lymphoma. *Am J Pathol.* 2010; 177(2):930-942.
49. Bödör C, Grossmann V, Popov N, et al. EZH2 mutations are frequent and represent an early event in follicular lymphoma. *Blood.* 2013; 122(18):3165-3168.
50. Swalm BM, Knutson SK, Warholic NM, et al. Reaction coupling between wild-type and disease-associated mutant EZH2. *ACS Chem Biol.* 2014;9(11):2459-2464.
51. Barski A, Cuddapah S, Cui K, et al. High-resolution profiling of histone methylations in the human genome. *Cell.* 2007;129(4):823-837.
52. Majer CR, Jin L, Scott MP, et al. A687V EZH2 is a gain-of-function mutation found in lymphoma patients. *FEBS Lett.* 2012;586(19):3448-3451.
53. McCabe MT, Graves AP, Ganji G, et al. Mutation of A677 in histone methyltransferase EZH2 in human B-cell lymphoma promotes hypertrimethylation of histone H3 on lysine 27 (H3K27). *Proc Natl Acad Sci USA.* 2012;109(8): 2989-2994.
54. Ott HM, Graves AP, Pappalardi MB, et al. A687V EZH2 Is a Driver of Histone H3 Lysine 27 (H3K27) Hypertrimethylation. *Mol Cancer Ther.* 2014;13(12):3062-3073.
55. Sahasrabuddhe AA, Chen X, Chung F, Velusamy T, Lim MS, Elenitoba-Johnson KS. Oncogenic Y641 mutations in EZH2 prevent Jak2/β-TrCP-mediated degradation [published online ahead of print January 27, 2014]. *Oncogene.*
56. Béguelin W, Popovic R, Teater M, et al. EZH2 is required for germinal center formation and somatic EZH2 mutations promote lymphoid transformation. *Cancer Cell.* 2013;23(5): 677-692.
57. Velichutina I, Shaknovich R, Geng H, et al. EZH2-mediated epigenetic silencing in germinal center B cells contributes to proliferation and lymphomagenesis. *Blood.* 2010;116(24): 5247-5255.
58. Berg T, Thoene S, Yap D, et al. A transgenic mouse model demonstrating the oncogenic role of mutations in the polycomb-group gene EZH2 in lymphomagenesis. *Blood.* 2014;123(25): 3914-3924.
59. Lee SC, Phipson B, Hyland CD, et al. Polycomb repressive complex 2 (PRC2) suppresses Eμ-myc lymphoma. *Blood.* 2013;122(15): 2654-2663.
60. van der Vlag J, Otte AP. Transcriptional repression mediated by the human polycomb-group protein EED involves histone deacetylation. *Nat Genet.* 1999;23(4):474-478.
61. Fiskus W, Wang Y, Sreekumar A, et al. Combined epigenetic therapy with the histone methyltransferase EZH2 inhibitor 3-deazaneplanocin A and the histone deacetylase inhibitor panobinostat against human AML cells. *Blood.* 2009;114(13):2733-2743.
62. Ohm JE, McGarvey KM, Yu X, et al. A stem cell-like chromatin pattern may predispose tumor suppressor genes to DNA hypermethylation and heritable silencing. *Nat Genet.* 2007;39(2): 237-242.
63. Schlesinger Y, Straussman R, Keshet I, et al. Polycomb-mediated methylation on Lys27 of histone H3 pre-marks genes for de novo methylation in cancer. *Nat Genet.* 2007;39(2): 232-236.
64. Viré E, Brenner C, Deplus R, et al. The Polycomb group protein EZH2 directly controls DNA methylation. *Nature.* 2006;439(7078): 871-874.
65. Martín-Subero JI, Kreuz M, Bibikova M, et al; Molecular Mechanisms in Malignant Lymphomas Network Project of the Deutsche Krebshilfe. New insights into the biology and origin of mature aggressive B-cell lymphomas by combined epigenomic, genomic, and transcriptional profiling. *Blood.* 2009;113(11):2488-2497.
66. Mullighan CG, Zhang J, Kasper LH, et al. CREBBP mutations in relapsed acute lymphoblastic leukaemia. *Nature.* 2011; 471(7337):235-239.
67. Sander S, Bullinger L, Klapproth K, et al. MYC stimulates EZH2 expression by repression of its negative regulator miR-26a. *Blood.* 2008; 112(10):4202-4212.
68. Varambally S, Cao Q, Mani RS, et al. Genomic loss of microRNA-101 leads to overexpression of histone methyltransferase EZH2 in cancer. *Science.* 2008;322(5908):1695-1699.
69. Cao Q, Mani RS, Ateeq B, et al. Coordinated regulation of polycomb group complexes through microRNAs in cancer. *Cancer Cell.* 2011;20(2): 187-199.
70. Shimono Y, Zabala M, Cho RW, et al. Downregulation of miRNA-200c links breast cancer stem cells with normal stem cells. *Cell.* 2009;138(3):592-603.
71. Wellner U, Schubert J, Burk UC, et al. The EMT-activator ZEB1 promotes tumorigenicity by repressing stemness-inhibiting microRNAs. *Nat Cell Biol.* 2009;11(12):1487-1495.
72. Marson A, Levine SS, Cole MF, et al. Connecting microRNA genes to the core transcriptional regulatory circuitry of embryonic stem cells. *Cell.* 2008;134(3):521-533.
73. Yamagishi M, Nakano K, Miyake A, et al. Polycomb-mediated loss of miR-31 activates NIK-dependent NF-κB pathway in adult T cell leukemia and other cancers. *Cancer Cell.* 2012; 21(1):121-135.
74. Cui J, Cheng Y, Zhang P, et al. Down regulation of miR200c promotes radiation-induced thymic lymphoma by targeting BMI1. *J Cell Biochem.* 2014;115(6):1033-1042.
75. Zhang X, Zhao X, Fiskus W, et al. Coordinated silencing of MYC-mediated miR-29 by HDAC3 and EZH2 as a therapeutic target of histone modification in aggressive B-Cell lymphomas. *Cancer Cell.* 2012;22(4):506-523.
76. Zhang X, Chen X, Lin J, et al. Myc represses miR-15a/miR-16-1 expression through recruitment of HDAC3 in mantle cell and other non-Hodgkin B-cell lymphomas. *Oncogene.* 2012;31(24):3002-3008.
77. Zhao X, Lwin T, Zhang X, et al. Disruption of the MYC-miRNA-EZH2 loop to suppress aggressive B-cell lymphoma survival and clonogenicity. *Leukemia.* 2013;27(12):2341-2350.
78. Tao J, Zhao X, Tao J. c-MYC-miRNA circuitry: a central regulator of aggressive B-cell malignancies. *Cell Cycle.* 2014;13(2):191-198.
79. Chang TC, Yu D, Lee YS, et al. Widespread microRNA repression by Myc contributes to tumorigenesis. *Nat Genet.* 2008;40(1):43-50.
80. Wang L, Zhang X, Jia LT, et al. c-Myc-mediated epigenetic silencing of MicroRNA-101 contributes to dysregulation of multiple pathways in hepatocellular carcinoma. *Hepatology.* 2014; 59(5):1850-1863.
81. Cimmino A, Calin GA, Fabbri M, et al. miR-15 and miR-16 induce apoptosis by targeting BCL2. *Proc Natl Acad Sci USA.* 2005;102(39): 13944-13949.
82. Zhao JJ, Lin J, Lwin T, et al. microRNA expression profile and identification of miR-29 as a prognostic marker and pathogenetic factor by targeting CDK6 in mantle cell lymphoma. *Blood.* 2010;115(13):2630-2639.
83. Santanam U, Zanesi N, Efanov A, et al. Chronic lymphocytic leukemia modeled in mouse by

targeted miR-29 expression. *Proc Natl Acad Sci USA.* 2010;107(27):12210-12215.

84. Lwin T, Zhao X, Cheng F, et al. A microenvironment-mediated c-Myc/miR-548m/HDAC6 amplification loop in non-Hodgkin B cell lymphomas. *J Clin Invest.* 2013;123(11):4612-4626.
85. Ferreira AC, Robaina MC, Rezende LM, Severino P, Klumb CE. Histone deacetylase inhibitor prevents cell growth in Burkitt's lymphoma by regulating PI3K/Akt pathways and leads to upregulation of miR-143, miR-145, and miR-101. *Ann Hematol.* 2014;93(6):983-993.
86. Kreso A, van Galen P, Pedley NM, et al. Self-renewal as a therapeutic target in human colorectal cancer. *Nat Med.* 2014;20(1):29-36.
87. McCabe MT, Ott HM, Ganji G, et al. EZH2 inhibition as a therapeutic strategy for lymphoma with EZH2-activating mutations. *Nature.* 2012;492(7427):108-112.
88. Knutson SK, Wigle TJ, Warholic NM, et al. A selective inhibitor of EZH2 blocks H3K27 methylation and kills mutant lymphoma cells. *Nat Chem Biol.* 2012;8(11):890-896.
89. Qi W, Chan H, Teng L, et al. Selective inhibition of Ezh2 by a small molecule inhibitor blocks tumor cells proliferation. *Proc Natl Acad Sci USA.* 2012;109(52):21360-21365.
90. Konze KD, Ma A, Li F, et al. An orally bioavailable chemical probe of the Lysine Methyltransferases EZH2 and EZH1. *ACS Chem Biol.* 2013;8(6):1324-1334.
91. Knutson SK, Warholic NM, Wigle TJ, et al. Durable tumor regression in genetically altered malignant rhabdoid tumors by inhibition of methyltransferase EZH2. *Proc Natl Acad Sci USA.* 2013;110(19):7922-7927.
92. Garapaty-Rao S, Nasveschuk C, Gagnon A, et al. Identification of EZH2 and EZH1 small molecule inhibitors with selective impact on diffuse large B cell lymphoma cell growth. *Chem Biol.* 2013;20(11):1329-1339.
93. Bradley WD, Arora S, Busby J, et al. EZH2 Inhibitor Efficacy in Non-Hodgkin's Lymphoma Does Not Require Suppression of H3K27 Monomethylation. *Chem Biol.* 2014;21(11):1463-1475.
94. Knutson SK, Kawano S, Minoshima Y, et al. Selective inhibition of EZH2 by EPZ-6438 leads to potent antitumor activity in EZH2-mutant non-Hodgkin lymphoma. *Mol Cancer Ther.* 2014;13(4):842-854.
95. Xu B, On DM, Ma A, et al. Selective inhibition of EZH2 and EZH1 enzymatic activity by a small molecule suppresses MLL-rearranged leukemia [published online ahead of print November 13, 2014]. *Blood.* 2015;125(2):346-357.
96. Daigle SR, Olhava EJ, Therkelsen CA, et al. Selective killing of mixed lineage leukemia cells by a potent small-molecule DOT1L inhibitor. *Cancer Cell.* 2011;20(1):53-65.
97. Kim E, Kim M, Woo DH, et al. Phosphorylation of EZH2 activates STAT3 signaling via STAT3 methylation and promotes tumorigenicity of glioblastoma stem-like cells. *Cancer Cell.* 2013;23(6):839-852.
98. Xu K, Wu ZJ, Groner AC, et al. EZH2 oncogenic activity in castration-resistant prostate cancer cells is Polycomb-independent. *Science.* 2012;338(6113):1465-1469.
99. Popovic R, Martinez-Garcia E, Giannopoulou EG, et al. Histone methyltransferase MMSET/NSD2 alters EZH2 binding and reprograms the myeloma epigenome through global and focal changes in H3K36 and H3K27 methylation. *PLoS Genet.* 2014;10(9):e1004566.
100. Neff T, Sinha AU, Kluk MJ, et al. Polycomb repressive complex 2 is required for MLL-AF9 leukemia. *Proc Natl Acad Sci USA.* 2012;109(13):5028-5033.

2015 125: 1217-1225
doi:10.1182/blood-2014-10-606822 originally published online January 7, 2015

Polycomb genes, miRNA, and their deregulation in B-cell malignancies

Gang Greg Wang, Kyle D. Konze and Jianguo Tao

Blood (print ISSN 0006-4971, online ISSN 1528-0020), is published weekly by the American Society of Hematology, 2021 L St, NW, Suite 900, Washington DC 20036.

Report

Cell Reports

An Allosteric Interaction Links USP7 to Deubiquitination and Chromatin Targeting of UHRF1

Graphical Abstract

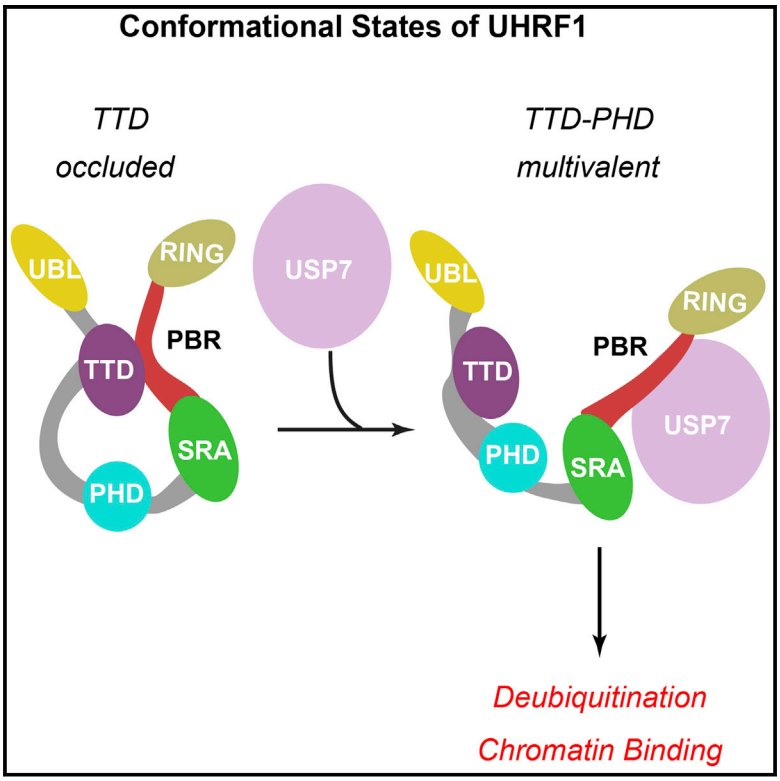

Authors

Zhi-Min Zhang, Scott B. Rothbart, David F. Allison, ..., Brian D. Strahl, Gang Greg Wang, Jikui Song

Correspondence

jikui.song@ucr.edu

In Brief

Zhang et al. report the crystal structure of USP7 ubiquitin-like domains in complex with the UHRF1 polybasic region. Structural analysis, combined with biochemical and cellular analysis, reveals that the USP7 interaction influences both ubiquitination and chromatin association of UHRF1.

Highlights

- USP7 ubiquitin-like domains bind to the UHRF1 polybasic region
- USP7 interaction promotes USP7-mediated deubiquitination of UHRF1
- USP7 allosterically regulates the conformational states of UHRF1
- USP7 interaction affects the chromatin association of UHRF1

Accession Numbers

5C6D

Zhang et al., 2015, Cell Reports *12*, 1400–1406
September 1, 2015
http://dx.doi.org/10.1016/j.celrep.2015.07.046

OPEN ACCESS
CellPress

Cell Reports
Report

An Allosteric Interaction Links USP7 to Deubiquitination and Chromatin Targeting of UHRF1

Zhi-Min Zhang,[1] Scott B. Rothbart,[2] David F. Allison,[3] Qian Cai,[4] Joseph S. Harrison,[3,5] Lin Li,[4] Yinsheng Wang,[4] Brian D. Strahl,[3,5] Gang Greg Wang,[3,5] and Jikui Song[1,*]
[1]Department of Biochemistry, University of California, Riverside, Riverside, CA 92521, USA
[2]Center for Epigenetics, Van Andel Research Institute, Grand Rapids, MI 49503, USA
[3]The Lineberger Comprehensive Cancer Center, University of North Carolina at Chapel Hill School of Medicine, Chapel Hill, NC 27599, USA
[4]Department of Chemistry, University of California, Riverside, Riverside, CA 92521, USA
[5]Department of Biochemistry and Biophysics, University of North Carolina at Chapel Hill School of Medicine, Chapel Hill, NC 27599, USA
*Correspondence: jikui.song@ucr.edu
http://dx.doi.org/10.1016/j.celrep.2015.07.046

SUMMARY

The protein stability and chromatin functions of UHRF1 (ubiquitin-like, containing PHD and RING finger domains, 1) are regulated in a cell-cycle-dependent manner. We report a structural characterization of the complex between UHRF1 and the deubiquitinase USP7. The first two UBL domains of USP7 bind to the polybasic region (PBR) of UHRF1, and this interaction is required for the USP7-mediated deubiquitination of UHRF1. Importantly, we find that the USP7-binding site of the UHRF1 PBR overlaps with the region engaging in an intramolecular interaction with the N-terminal tandem Tudor domain (TTD). We show that the USP7-UHRF1 interaction perturbs the TTD-PBR interaction of UHRF1, thereby shifting the conformation of UHRF1 from a TTD-"occluded" state to a state open for multivalent histone binding. Consistently, introduction of a USP7-interaction-defective mutation to UHRF1 significantly reduces its chromatin association. Together, these results link USP7 interaction to the dynamic deubiquitination and chromatin association of UHRF1.

INTRODUCTION

One of the fundamental principles in epigenetic regulation involves temporal and spatial control of macromolecular machineries that govern epigenetic events. Epigenetic modifications, including DNA methylation and histone modifications, are recognized by a diverse family of effector proteins (Bogdanović and Veenstra, 2009; Musselman et al., 2012) whose functions are often subject to dynamic regulation in response to environmental cues. However, how these chromatin effector proteins are regulated remains incompletely understood.

UHRF1 (ubiquitin-like, containing PHD and RING finger domains, 1), also known as ICBP90 and NP95 in mouse, is a multidomain protein that plays critical roles in regulating various processes, such as DNMT1 (DNA methyltransferase 1)-mediated DNA methylation maintenance (Bostick et al., 2007; Sharif et al., 2007). UHRF1 contains a ubiquitin-like (UBL) domain at the N terminus, followed by a tandem Tudor domain (TTD), a plant homeodomain (PHD), a SET- and RING-associated (SRA) domain, and a RING domain (Figure 1A). Among these protein modules, the PHD and TTD recognize the N-terminal tail of histone H3 unmethylated at arginine 2 (Hu et al., 2011; Lallous et al., 2011; Rajakumara et al., 2011) and dimethylated/trimethylated at lysine 9 (H3K9me2/3) (Arita et al., 2012; Cheng et al., 2013; Karagianni et al., 2008; Rothbart et al., 2012, 2013; Xie et al., 2012), respectively, whereas the SRA domain specifically binds to hemimethylated CpG sites (Arita et al., 2008; Avvakumov et al., 2008; Bostick et al., 2007; Hashimoto et al., 2008; Sharif et al., 2007). The RING domain of UHRF1 has been shown to serve as an E3 ubiquitin ligase to promote monoubiquitination of H3 at lysine 18 and/or 23 (Nishiyama et al., 2013; Qin et al., 2015), which in turn recruits DNMT1 to replicating chromatin.

Despite these advances, the mechanism underlying the regulation of UHRF1 remains to be elucidated. Indeed, emerging evidence has shown that UHRF1 is subject to temporal and spatial control (Gelato et al., 2014; Ma et al., 2012). First, the stability of UHRF1 is regulated by ubiquitination in a cell-cycle-dependent manner (Ma et al., 2012). During S phase, deubiquitinase USP7 (ubiquitin-specific-processing protease 7) associates with UHRF1, keeping it from being ubiquitinated (Ma et al., 2012). When cells enter mitosis, USP7 dissociates from UHRF1, exposing it for ubiquitination and consequent proteasomal degradation (Ma et al., 2012). Second, the chromatin association of UHRF1 peaks in mid S phase to accompany pericentromeric heterochromatin replication (Miura et al., 2001; Papait et al., 2007; Taylor et al., 2013), which is likely mediated by a conformational transition between two alternative functional states of UHRF1 (Gelato et al., 2014). In one state, the H3K9me3-binding site of the UHRF1 TTD is occluded due to its intramolecular interaction with a C-terminal polybasic region (PBR). In the second state, the TTD is relieved from the PBR interaction and thus forms a multivalent histone-binding cassette with the PHD (Gelato et al.,

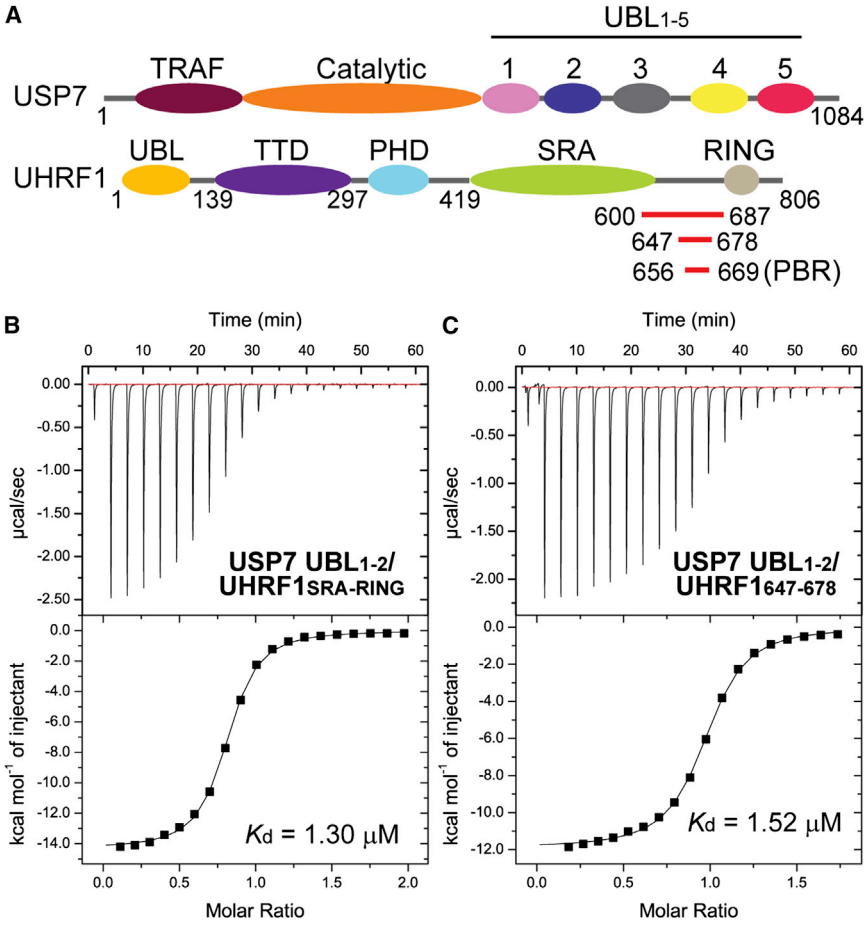

Figure 1. Identification of the UHRF1 and USP7 Interaction Domains

(A) Domain architectures of UHRF1 and USP7. The UHRF1 fragments used for biochemical analysis are labeled with residue numbers. TRAF, tumor necrosis factor receptor-associated factor.

(B and C) ITC binding curves for USP7 UBL_{1-2} over $UHRF1_{SRA-RING}$ (B) and $UHRF1_{647–678}$ (C).

See also Figure S1.

2014). Binding of the signaling molecule phosphatidylinositol 5-phosphate (PI5P) to the UHRF1 PBR switches the UHRF1 conformation from the TTD-"occluded" state to the TTD-PHD multivalent state, which leads to its increased heterochromatin association (Gelato et al., 2014). However, how networks of interactions functionally regulate UHRF1 in cells remains unresolved.

In this study, we characterized the interaction between UHRF1 and USP7 by structure determination of the UHRF1-USP7 complex. Our structural analyses reveal that the UHRF1-USP7 interaction is mediated by the first two UBL domains of USP7 and the PBR of UHRF1. Through functional assays, we show that the interaction of UHRF1 with USP7 is not only critical for its deubiquitination but also for disrupting the intramolecular TTD-PBR interaction, thereby shifting the conformation of UHRF1 to promote multivalent histone engagement of the TTD-PHD cassette. Indeed, point mutations that disrupt the USP7 interaction greatly reduce the chromatin association of UHRF1. Our study thus uncovers a novel mechanism by which USP7 promotes both the stability and chromatin association of UHRF1.

RESULTS

Characterization of the UHRF1-USP7 Interaction

A recent study suggests that the interaction between USP7 and UHRF1 is mediated by the UBL domains of USP7 and a linker region between the SRA and RING finger domains of UHRF1 (residues 600–687; $UHRF1_{600–687}$) (Figure 1A) (Ma et al., 2012). To further map the USP7 and UHRF1 interaction interface, we performed isothermal titration calorimetry (ITC) to measure the binding between truncated USP7 and UHRF1 fragments. The first two UBL domains (UBL_{1-2}) of USP7 interact directly with a fragment of UHRF1 encompassing its SRA and RING domains (residues 419–806; $UHRF1_{SRA-RING}$), with a dissociation constant (K_d) of 1.30 µM (Figure 1B). To narrow this interaction surface further, we showed that the UBL_{1-2} dual domain of USP7 binds to $UHRF1_{600–687}$ with a K_d of 1.42 µM (Figure S1A), and comparable binding activity is observed (K_d 1.52 µM) when we truncated UHRF1 further to a 32-amino acid sequence, $UHRF1_{647–678}$ (Figure 1B). By contrast, we did not observe appreciable interaction between the first UBL domain (UBL_1) of USP7 and $UHRF1_{SRA-RING}$ (Figure S1B), indicating that UBL_1 alone is insufficient for mediating the UHRF1-USP7 interaction. Collectively, these data show that the $UHRF1_{647–678}$ fragment and the USP7 UBL_{1-2} domains mediate the UHRF1-USP7 interaction.

Structure of the $UHRF1_{647–678}$-USP7 $UBL_{1–3}$ Complex

Next, to provide the molecular basis for the UHRF1-USP7 interaction, we determined the crystal structure of $UHRF1_{647–678}$ in complex with the first three UBL domains ($UBL_{1–3}$) of USP7 at 2.3-Å resolution (Table S1). It is notable that there are two UHRF1-USP7 complexes in each asymmetric unit (Figure S1C), and in both complexes the UHRF1 fragments superimpose well, except for one region (residues S652–T655) that is only observable in one of the complexes due to crystal packing (Figure S1D). The UHRF1 segment containing residues G656–R662 is anchored to an acidic surface formed by the closely packed UBL_1 and UBL_2 domains of USP7, whereas no intermolecular interaction involves the USP7 UBL_3 domain (Figures 2A and 2B). The interactions between the USP7 UBL_{1-2} domains and the $UHRF1_{647–678}$ peptide are mediated by hydrogen bonds and electrostatic attractions (Figure 2C). Of particular note, the side chain of UHRF1 K659 is inserted into an acidic pocket of USP7, formed by residues R628, E736, D764, E759, and

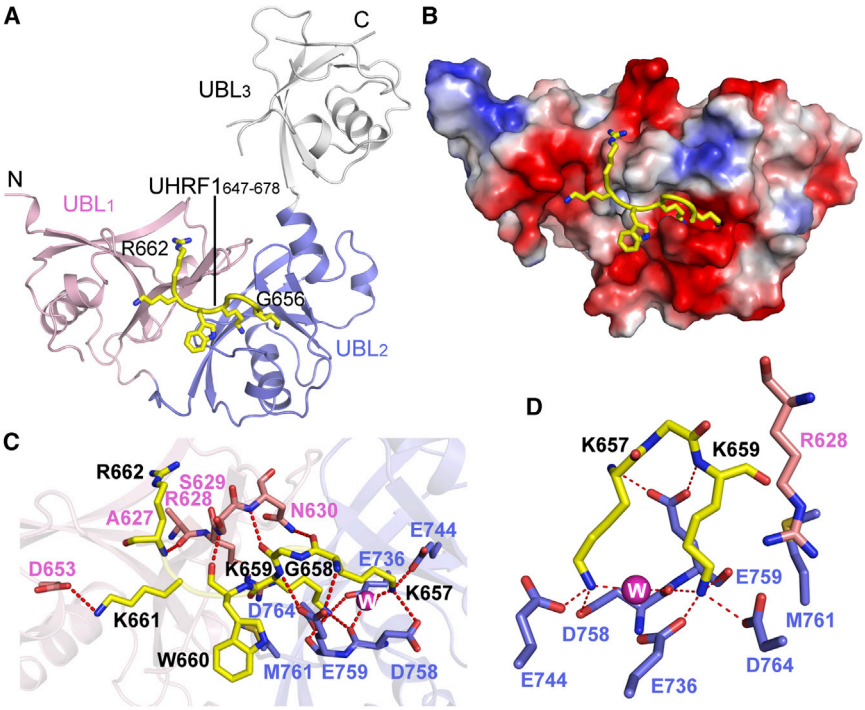

Figure 2. Structural Basis of the UHRF1$_{647–678}$-USP7 UBL$_{1–3}$ Complex

(A) Ribbon representation of the UHRF1$_{647–678}$-USP7 UBL$_{1–3}$ complex, with USP7 UBL$_1$, UBL$_2$, and UBL$_3$ colored pink, light blue, and silver, respectively. The UHRF1$_{647–678}$ fragment is shown in stick representation.

(B) Electrostatic surface representation of the UHRF1$_{647–678}$-UHRF1 UBL$_{1–3}$ complex. For clarity, the USP7 UBL$_3$ domain is not shown.

(C) Hydrogen-bonding interactions (dashed lines) between USP7 and UHRF1. The water molecule is shown as a sphere labeled "W."

(D) Close-up view of the UHRF1 K657- and K659-associated intermolecular interactions.

See also Table S1.

M761, with the K659 ε-amino group hydrogen bonded to the side-chain carboxylates of USP7 E736 and D764 and to the backbone carbonyl oxygen atoms of USP7 D758 and E759 (Figures 2C and 2D). In a parallel configuration, the ε-amino group of UHRF1 K657 forms direct hydrogen bonds with the side-chain carboxylates of USP7 E744 and D758 and a water-mediated hydrogen bond with the backbone carbonyl oxygen of USP7 D758 (Figures 2C and 2D). Meanwhile, the backbone amide groups of UHRF1 K657 and K659 each form a hydrogen bond with the side-chain carboxylate of USP7 E759 (Figures 2C and 2D). The backbone carbonyl oxygen of UHRF1 K657 forms a hydrogen bond with the side-chain amide of USP7 N630 (Figure 2C). C-terminal to UHRF1 K657 and K659, the ε-amino group of UHRF1 K661 forms a hydrogen bond with the side-chain carboxylate of USP7 D653 (Figure 2C). In addition, three main-chain hydrogen bonds, formed between UHRF1 G658, W660, and R662 and USP7 N630, S629, and A627, respectively, further support the UHRF1-USP7 interaction (Figure 2C).

Mutational Analysis of the UHRF1-USP7 Interaction

To test our structural observations, we mutated a number of key interacting residues for ITC (Table S2). In comparison with the wild-type (WT) UHRF1$_{647–687}$-USP7 UBL$_{1-2}$ interaction, UHRF1 K659E and USP7 E736A mutations reduced the binding affinity by 38- and 4-fold, respectively (Figure 3A). Furthermore, the UHRF1 K657Q/K659Q and K657E/K659E double mutations both reduced the binding affinity by over 200-fold (Figure 3A). Together, these data support our structural observations. Consistently, sequence alignment of UHRF1 protein orthologs revealed that except for K657, which is not present in NP95, the USP7-interacting residues, including UHRF1 G658, K659, and K661, are highly conserved across species (Figure 3B), suggesting an important role for these residues in UHRF1 regulation.

To test whether UHRF1 K657 and K659 are important for association of full-length UHRF1 with USP7, we ectopically expressed hemagglutinin (HA)-tagged USP7 in HEK293 cells in the presence or absence of Flag-tagged UHRF1 (WT or K657Q/K659Q mutant), followed by coimmunoprecipitation with an anti-Flag antibody (Figure 3C). We found that USP7 coprecipitates with WT UHRF1, confirming that these proteins form a complex in cells (Figure 3C). As predicted from the structural data, the UHRF1 K657Q/K659Q double mutant reduced the association of UHRF1 with USP7, further supporting a critical role for these residues in mediating the UHRF1-USP7 interaction.

Effect of the UHRF1-USP7 Interaction on USP7-Mediated Deubiquitination of UHRF1

To investigate the functional consequence of the UHRF1-USP7 interaction, we next performed in vitro ubiquitination assays, monitoring autoubiquitination of wild-type UHRF1 or the K659E mutant in the presence of full-length USP7. Consistent with previous observations (Felle et al., 2011; Ma et al., 2012), our results showed that USP7 reduced autoubiquitination activity of wild-type UHRF1 (Figure 3D). In contrast, USP7 cannot reduce the autoubiquitination of the UHRF1 K659E mutant. These data confirm previous observations that the USP7-UHRF1 interaction is required for USP7-mediated deubiquitination of UHRF1 (Felle et al., 2011; Ma et al., 2012).

Effect of the UHRF1-USP7 Interaction on the Allosteric Regulation of UHRF1

A recent study (Gelato et al., 2014) showed that an intramolecular TTD-PBR interaction of UHRF1 occludes its TTD from binding to H3K9me3. Given the fact that the USP7-binding site of UHRF1 from this study is located within the UHRF1 PBR sequence (Figure 4A) (Gelato et al., 2014), we postulated that the UHRF1-USP7 interaction might interfere with the UHRF1 TTD-PBR interaction. To test this hypothesis, we performed NMR

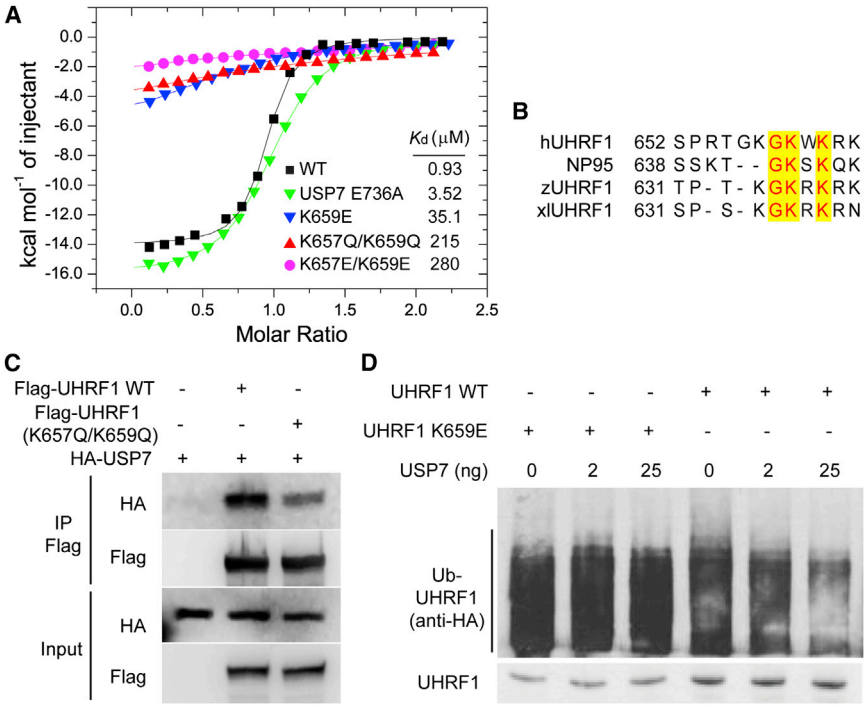

Figure 3. Biochemical Analysis of the UHRF1-USP7 Interaction

(A) ITC and mutational analysis of the $UHRF1_{647–687}$-USP7 UBL_{1-2} interaction. The mutations include USP7 E736A, UHRF1 K659E, K657Q/K659Q, and K657E/K659E.

(B) Sequence alignment of the USP7-binding motif of human UHRF1 with its mouse (NP95), zebrafish (zUHRF1), and *Xenopus laevis* (xlUHRF1) orthologs. Identical residues are colored red and highlighted in yellow.

(C) Immunoprecipitation (IP) analysis of the interaction between full-length Flag-tagged UHRF1 and HA-tagged USP7.

(D) In vitro ubiquitination assay of wild-type and K659E UHRF1 in the presence of HA-tagged ubiquitin and USP7. The ubiquitination level (upper panel) and total amount of UHRF1 (lower panel) were analyzed by anti-HA western blot and SYPRO staining, respectively.

See also Figure S4 and Table S2.

titrations to investigate whether the UHRF1 TTD-PBR interaction is affected by the USP7 UBL_{1-2} dual domain. A number of $^{1}H,^{15}N$-HSQC spectra were collected for the ^{15}N-labeled UHRF1 TTD, alone or in the presence of the UHRF1 PBR ($UHRF1_{647–687}$) and/or the USP7 UBL_{1-2} domains (Figures 4B–4D; Figure S2A). Consistent with a previous study (Gelato et al., 2014), we observed that a number of NMR peaks of the UHRF1 TTD were significantly shifted upon addition of $UHRF1_{647–687}$ with 20% molar excess (Figures 4B–4D; Figure S2A). Based on the reported chemical shift assignment of the TTD (Nady et al., 2011), we were able to assign a number of NMR peaks with large chemical shift changes to UHRF1 residues, including I224, G275, and V287. It is notable that the chemical shift perturbations of these residues by the UHRF1 PBR were also observed in a previous study (Gelato et al., 2014), and that residues I224 and V287 were conceived as part of the putative PBR-binding pocket of the TTD (Gelato et al., 2014). However, when we further mixed the NMR sample with the USP7 UBL_{1-2} dual domain (40% molar excess over the UHRF1 TTD), the majority of PBR-perturbed TTD peaks shifted back toward the peak positions corresponding to the free state (Figures 4B–4D; Figure S2A). These data suggest that the USP7 UBL_{1-2} dual domain affects the intramolecular TTD-PBR interaction of UHRF1 through direct interaction with the UHRF1 PBR. Consistently, we found that the presence of USP7 $UBL_{1–5}$ (residues 560–1084) modestly increased the binding of full-length UHRF1 to the $H3_{(1–20)}$K9me3 peptide by a pull-down assay, confirming that the USP7 interaction enhances TTD-H3K9me3 binding in the context of full-length UHRF1 (Figure S2B).

We then performed ITC for the USP7 UBL_{1-2} dual domain over a UHRF1 fragment spanning from the TTD toward the C-terminal RING domain (residues 138–806; $UHRF1_{TTD-RING}$) to further examine whether an intramolecular UHRF1 TTD-PBR interaction affects the UHRF1-USP7 interaction. Our results showed that the USP7 UBL_{1-2} dual domain binds to $UHRF1_{TTD-RING}$ with a K_d of 27.2 μM (Figure 4E), a binding affinity that is ~20-fold weaker in comparison with the binding of the USP7 UBL_{1-2} to $UHRF1_{SRA-RING}$ (Figure 4E). This result suggests that the presence of the UHRF1 TTD conversely disfavors the UHRF1-USP7 interaction.

Taken together, these findings establish that the UHRF1-USP7 interaction disrupts the intramolecular TTD-PBR interaction of UHRF1, thereby shifting the conformation of the UHRF1 TTD from the occluded state to an open state that allows multivalent histone binding by the TTD-PHD.

Effect of the USP7-UHRF1 Interaction on the Chromatin Association of UHRF1

The observation that the USP7 interaction modulates the conformational states and H3K9me3 binding of UHRF1 prompted us to investigate whether the UHRF1-USP7 interaction affects chromatin association of UHRF1. Toward this end, we tested recombinant full-length UHRF1 and a USP7-binding mutant (K657E/K659E) in histone peptide-binding assays by fluorescence polarization (Figure S3A). Consistent with our previous findings (Rothbart et al., 2013), both full-length wild-type and K657E/K659E UHRF1 were found to bind to $H3_{(1–20)}$K9me3 peptides conjugated with 5-carboxyfluorescein (5-FAM) at the C terminus similarly. By contrast, neither protein had measurable interaction with $H3_{(1–20)}$K9me3 peptides conjugated with 5-FAM at the N terminus, the peptides that were previously shown to block UHRF1 PHD-histone binding (Rothbart et al., 2013). These data, in line with a recent study (Gelato et al., 2014) that the K657E/K659E mutant alone does not affect the UHRF1 TTD-PBR interaction appreciably, suggest that the previously described multivalent histone engagement of the TTD-PHD (Rothbart et al.,

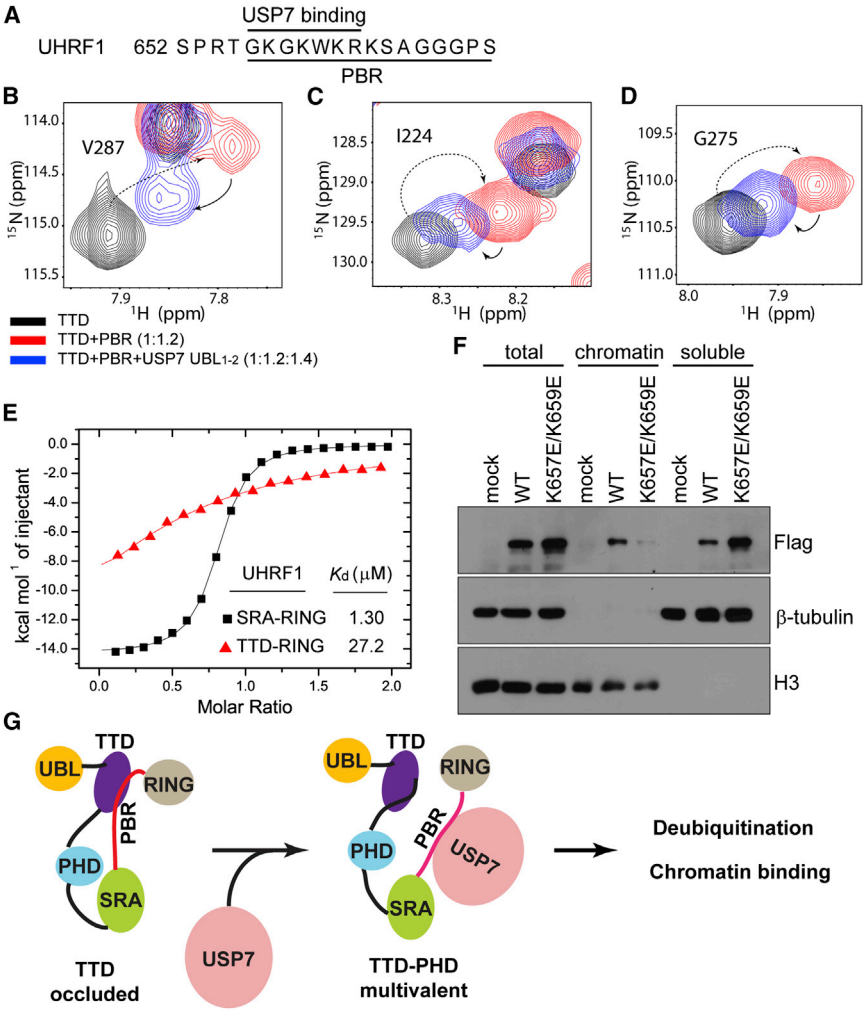

Figure 4. UHRF1-USP7 Interaction Affects UHRF1 Intramolecular Regulation and Chromatin Association

(A) Sequence of a selected UHRF1 fragment, with the USP7-binding site and PBR sequence labeled.

(B–D) Overlaid 2D $^{1}H,^{15}N$-HSQC spectra highlight the chemical shift changes of selected residues in the UHRF1 TTD. The spectra were collected for the UHRF1 TTD free (black) and in the presence of the UHRF1 PBR (red) or UHRF1 PBR and USP7 UBL_{1-2} (blue). The arrows with dashed and solid lines mark the chemical shift changes of selected residues under different conditions.

(E) ITC binding curves for USP7 UBL_{1-2} over $UHRF1_{SRA-RING}$ (black) or $UHRF1_{TTD-RING}$ (red).

(F) Chromatin association assay of Flag-tagged WT and K657E/K659E UHRF1 from asynchronously growing HeLa cells. Mock indicates no DNA control.

(G) Model for USP7 regulation. The USP7 interaction allosterically regulates the conformational states of UHRF1 and affects its ubiquitination and chromatin binding.

See also Figures S2 and S3 and Table S2.

2013) remains for full-length UHRF1 and its K657E/K659E mutant. Furthermore, we showed that unlike wild-type UHRF1, the UHRF1 K657E/K659E mutant dramatically decreases its association with chromatin isolated from HeLa cells (Figure 4F; Figure S3B). Collectively, these observations suggest that the USP7 interaction facilitates the association of UHRF1 with chromatin.

DISCUSSION

Cell-Cycle-Dependent USP7 Regulation of UHRF1

UHRF1 has emerged as an important epigenetic regulator in the maintenance of DNA methylation through regulating the recruitment and stability of DNMT1 (Bostick et al., 2007; Du et al., 2010; Sharif et al., 2007). This regulation is achieved, in part, through dynamic regulation of UHRF1—both at the level of its chromatin association and ubiquitination—throughout the cell cycle (Gelato et al., 2014; Ma et al., 2012; Taylor et al., 2013). In this study, we have confirmed the requirement of USP7 interaction for UHRF1 deubiquitination through an in vitro ubiquitination assay. More importantly, we uncovered the UHRF1 PBR, a region known to be crucial for modulating an interconversion between the two alternative functional states of UHRF1 (Gelato et al., 2014), as the region responsible for mediating its interaction with USP7. The interaction between USP7 and the UHRF1 PBR therefore may help release the TTD from the PBR-bound state, entering into a state that allows TTD-PHD multivalent histone engagement, as characterized previously (Rothbart et al., 2013). Indeed, with a series of structural, biochemical, and mutagenesis assays, we demonstrated that the USP7 interaction with the UHRF1 PBR sequence promotes H3K9me3 binding by UHRF1 through interfering with its intramolecular TTD-PBR interaction; consistently, disruption of the UHRF1-USP7 interactions leads to a significantly decreased chromatin association of UHRF1 in vivo. Taken together, this study reveals that the USP7 interaction plays a dual regulatory role in both deubiquitination and chromatin association of UHRF1 (Figure 4G).

Effects of Posttranslational Modifications on UHRF1-USP7 Association

A previous study suggested that phosphorylation of UHRF1 S652 regulates the dissociation of the UHRF1-USP7 complex in M phase (Ma et al., 2012). Interestingly, our study indicates that this residue is indeed adjacent to the USP7 interaction site. However, we did not observe any direct interaction between UHRF1 S652 and USP7. Moreover, our ITC analysis revealed that phosphorylation of UHRF1 S652 only leads to a modest (2-fold) reduction of the binding affinity of $UHRF1_{651-664}$ for USP7 (Figure S4A). Meanwhile, the serine-to-glutamate mutation of UHRF1 S664 (S664E), which is located immediately downstream of the USP7 interaction site (Figure 4A) and manifests M phase-specific

phosphorylation as well (Rigbolt et al., 2011), leads to a reduction of the UHRF1$_{647–687}$ binding affinity for USP7 by 4-fold (Figure S4B). Together, these observations suggest that multistep posttranslational modification events may be required to dissociate the UHRF1-USP7 complex during M phase.

Recent evidence has indicated that USP7 also deubiquitinates DNMT1 during S phase; in late S phase, acetylation of DNMT1 by Tip60 leads to disruption of the DNMT1-USP7 complex (Du et al., 2010). This previous work also prompted us to query whether UHRF1 can be acetylated by Tip60 at the PBR, which falls into the Tip60-preferred acetylation sequences (Kimura and Horikoshi, 1998). Indeed, following in vitro acetylation by recombinant Tip60, we detected acetylation of UHRF1 at K659 (Figure S4C) and found that this modification greatly decreased the UHRF1-USP7 interaction (Figure S4A), indicating a mechanism for UHRF1-USP7 dissociation. However, further studies are needed to define such a potential regulation of UHRF1 in vivo.

USP7 Interaction and Chromatin Targeting of UHRF1

One of the major findings in this study is that the USP7 interaction regulates the chromatin association of UHRF1. Consistent with this, a recent study showed that the UHRF1 S664E mutation, with a 4-fold reduction in USP7 binding based on our ITC analysis (Figure S4B), significantly reduced the chromatin binding of UHRF1 (Chu et al., 2012). Whereas the underlying mechanism of this regulation has yet to be elucidated, we show that the UHRF1-USP7 interaction interferes with the intramolecular TTD-PBR interaction of UHRF1, which therefore shifts the conformation of UHRF1 from the TTD-occluded state to a state that allows multivalent histone binding by the TTD-PHD. Such a change in the conformational dynamics of UHRF1 may synergize with the allosteric effect of PI5P (Gelato et al., 2014) in stabilizing the chromatin association of UHRF1. Indeed, a previous study showed that the nuclear level of PI5P is cell-cycle dependent, with ~20-fold enrichment in G1 phase (Clarke et al., 2001). However, the relationship between PI5P and the USP7-UHRF1 interaction remains to be determined. In addition, complex formation between UHRF1 and USP7 may also boost their respective interactions with the methyl-CpG-binding protein MBD4 (Meng et al., 2015), which has recently been shown to mediate the recruitment of USP7 to heterochromatin (Meng et al., 2015).

EXPERIMENTAL PROCEDURES

USP7 and UHRF1 proteins, except for the UHRF1$_{651–664}$ peptides, were expressed in BL21 (DE3) recombinant inbred line cells and purified through nickel affinity, size exclusion, and/or anion exchange chromatography. The crystal structure of the UHRF1$_{647–678}$-USP7 UBL$_{1–3}$ complex was determined by molecular replacement using the structure of the corresponding sequence of free USP7 (PDB: 2YLM) as the search model. ITC assays for USP7 and UHRF1 proteins were performed at 25°C. The resultant binding curves were processed with Origin 7.0 software (MicroCal). Chromatin association assays were performed in HeLa cells stably transfected with 3×Flag UHRF1 (wild-type and K657E/K659E) as previously described (Rothbart et al., 2013). Full details of experimental procedures are provided in Supplemental Experimental Procedures.

ACCESSION NUMBERS

The accession number for the structure of UHRF1-USP7 reported in this paper is PDB: 5C6D.

SUPPLEMENTAL INFORMATION

Supplemental Information includes four figures, two tables, and Supplemental Experimental Procedures and can be found with this article online at http://dx.doi.org/10.1016/j.celrep.2015.07.046.

AUTHOR CONTRIBUTIONS

Z.-M.Z., S.B.R., D.F.A., J.S.H., Q.C., L.L., and J.S. performed the experiments. J.S., G.G.W., B.D.S., and Y.W. conceived the project. J.S. wrote the manuscript with the input of all the authors.

ACKNOWLEDGMENTS

J.S. is a Kimmel Scholar of the Sidney Kimmel Foundation for Cancer Research and is also supported by the March of Dimes Foundation, a Hellman fellowship, and University of California Cancer Research Coordination Committee funds (CRC-15-380558). D.F.A. is supported by a postdoctoral fellowship from AACR-Debbie's Dream Foundation. G.G.W. is a Kimmel Scholar of the Sidney Kimmel Foundation for Cancer Research and is also supported by grants from an NCI K99/R00 "Pathway to Independence" award (CA151683) and the Concern Foundation of Cancer Research. S.B.R., B.D.S., and Y.W. acknowledge grant support from the NIH (CA181343, GM110058, and ES019873, respectively). We would like to thank Dr. Yang Shi for providing the USP7 plasmid.

Received: May 11, 2015
Revised: June 30, 2015
Accepted: July 23, 2015
Published: August 20, 2015

REFERENCES

Arita, K., Ariyoshi, M., Tochio, H., Nakamura, Y., and Shirakawa, M. (2008). Recognition of hemi-methylated DNA by the SRA protein UHRF1 by a base-flipping mechanism. Nature *455*, 818–821.

Arita, K., Isogai, S., Oda, T., Unoki, M., Sugita, K., Sekiyama, N., Kuwata, K., Hamamoto, R., Tochio, H., Sato, M., et al. (2012). Recognition of modification status on a histone H3 tail by linked histone reader modules of the epigenetic regulator UHRF1. Proc. Natl. Acad. Sci. USA *109*, 12950–12955.

Avvakumov, G.V., Walker, J.R., Xue, S., Li, Y., Duan, S., Bronner, C., Arrowsmith, C.H., and Dhe-Paganon, S. (2008). Structural basis for recognition of hemi-methylated DNA by the SRA domain of human UHRF1. Nature *455*, 822–825.

Bogdanović, O., and Veenstra, G.J.C. (2009). DNA methylation and methyl-CpG binding proteins: developmental requirements and function. Chromosoma *118*, 549–565.

Bostick, M., Kim, J.K., Estève, P.O., Clark, A., Pradhan, S., and Jacobsen, S.E. (2007). UHRF1 plays a role in maintaining DNA methylation in mammalian cells. Science *317*, 1760–1764.

Cheng, J., Yang, Y., Fang, J., Xiao, J., Zhu, T., Chen, F., Wang, P., Li, Z., Yang, H., and Xu, Y. (2013). Structural insight into coordinated recognition of trimethylated histone H3 lysine 9 (H3K9me3) by the plant homeodomain (PHD) and tandem tudor domain (TTD) of UHRF1 (ubiquitin-like, containing PHD and RING finger domains, 1) protein. J. Biol. Chem. *288*, 1329–1339.

Chu, J., Loughlin, E.A., Gaur, N.A., SenBanerjee, S., Jacob, V., Monson, C., Kent, B., Oranu, A., Ding, Y., Ukomadu, C., and Sadler, K.C. (2012). UHRF1 phosphorylation by cyclin A2/cyclin-dependent kinase 2 is required for zebrafish embryogenesis. Mol. Biol. Cell *23*, 59–70.

Clarke, J.H., Letcher, A.J., D'Santos, C.S., Halstead, J.R., Irvine, R.F., and Divecha, N. (2001). Inositol lipids are regulated during cell cycle progression in the nuclei of murine erythroleukaemia cells. Biochem. J. *357*, 905–910.

Du, Z., Song, J., Wang, Y., Zhao, Y., Guda, K., Yang, S., Kao, H.Y., Xu, Y., Willis, J., Markowitz, S.D., et al. (2010). DNMT1 stability is regulated by proteins

coordinating deubiquitination and acetylation-driven ubiquitination. Sci. Signal. *3*, ra80.

Felle, M., Joppien, S., Németh, A., Diermeier, S., Thalhammer, V., Dobner, T., Kremmer, E., Kappler, R., and Längst, G. (2011). The USP7/Dnmt1 complex stimulates the DNA methylation activity of Dnmt1 and regulates the stability of UHRF1. Nucleic Acids Res. *39*, 8355–8365.

Gelato, K.A., Tauber, M., Ong, M.S., Winter, S., Hiragami-Hamada, K., Sindlinger, J., Lemak, A., Bultsma, Y., Houliston, S., Schwarzer, D., et al. (2014). Accessibility of different histone H3-binding domains of UHRF1 is allosterically regulated by phosphatidylinositol 5-phosphate. Mol. Cell *54*, 905–919.

Hashimoto, H., Horton, J.R., Zhang, X., Bostick, M., Jacobsen, S.E., and Cheng, X. (2008). The SRA domain of UHRF1 flips 5-methylcytosine out of the DNA helix. Nature *455*, 826–829.

Hu, L., Li, Z., Wang, P., Lin, Y., and Xu, Y. (2011). Crystal structure of PHD domain of UHRF1 and insights into recognition of unmodified histone H3 arginine residue 2. Cell Res. *21*, 1374–1378.

Karagianni, P., Amazit, L., Qin, J., and Wong, J. (2008). ICBP90, a novel methyl K9 H3 binding protein linking protein ubiquitination with heterochromatin formation. Mol. Cell. Biol. *28*, 705–717.

Kimura, A., and Horikoshi, M. (1998). Tip60 acetylates six lysines of a specific class in core histones in vitro. Genes Cells *3*, 789–800.

Lallous, N., Legrand, P., McEwen, A.G., Ramón-Maiques, S., Samama, J.P., and Birck, C. (2011). The PHD finger of human UHRF1 reveals a new subgroup of unmethylated histone H3 tail readers. PLoS ONE *6*, e27599.

Ma, H., Chen, H., Guo, X., Wang, Z., Sowa, M.E., Zheng, L., Hu, S., Zeng, P., Guo, R., Diao, J., et al. (2012). M phase phosphorylation of the epigenetic regulator UHRF1 regulates its physical association with the deubiquitylase USP7 and stability. Proc. Natl. Acad. Sci. USA *109*, 4828–4833.

Meng, H., Harrison, D.J., and Meehan, R.R. (2015). MBD4 interacts with and recruits USP7 to heterochromatic foci. J. Cell. Biochem. *116*, 476–485.

Miura, M., Watanabe, H., Sasaki, T., Tatsumi, K., and Muto, M. (2001). Dynamic changes in subnuclear NP95 location during the cell cycle and its spatial relationship with DNA replication foci. Exp. Cell Res. *263*, 202–208.

Musselman, C.A., Lalonde, M.E., Côté, J., and Kutateladze, T.G. (2012). Perceiving the epigenetic landscape through histone readers. Nat. Struct. Mol. Biol. *19*, 1218–1227.

Nady, N., Lemak, A., Walker, J.R., Avvakumov, G.V., Kareta, M.S., Achour, M., Xue, S., Duan, S., Allali-Hassani, A., Zuo, X., et al. (2011). Recognition of multivalent histone states associated with heterochromatin by UHRF1 protein. J. Biol. Chem. *286*, 24300–24311.

Nishiyama, A., Yamaguchi, L., Sharif, J., Johmura, Y., Kawamura, T., Nakanishi, K., Shimamura, S., Arita, K., Kodama, T., Ishikawa, F., et al. (2013). Uhrf1-dependent H3K23 ubiquitylation couples maintenance DNA methylation and replication. Nature *502*, 249–253.

Papait, R., Pistore, C., Negri, D., Pecoraro, D., Cantarini, L., and Bonapace, I.M. (2007). Np95 is implicated in pericentromeric heterochromatin replication and in major satellite silencing. Mol. Biol. Cell *18*, 1098–1106.

Qin, W., Wolf, P., Liu, N., Link, S., Smets, M., La Mastra, F., Forné, I., Pichler, G., Hörl, D., Fellinger, K., et al. (2015). DNA methylation requires a DNMT1 ubiquitin interacting motif (UIM) and histone ubiquitination. Cell Res., Published online June 12, 2015 http://dx.doi.org/10.1038/cr.2015.72.

Rajakumara, E., Wang, Z., Ma, H., Hu, L., Chen, H., Lin, Y., Guo, R., Wu, F., Li, H., Lan, F., et al. (2011). PHD finger recognition of unmodified histone H3R2 links UHRF1 to regulation of euchromatic gene expression. Mol. Cell *43*, 275–284.

Rigbolt, K.T., Prokhorova, T.A., Akimov, V., Henningsen, J., Johansen, P.T., Kratchmarova, I., Kassem, M., Mann, M., Olsen, J.V., and Blagoev, B. (2011). System-wide temporal characterization of the proteome and phosphoproteome of human embryonic stem cell differentiation. Sci. Signal. *4*, rs3.

Rothbart, S.B., Krajewski, K., Nady, N., Tempel, W., Xue, S., Badeaux, A.I., Barsyte-Lovejoy, D., Martinez, J.Y., Bedford, M.T., Fuchs, S.M., et al. (2012). Association of UHRF1 with methylated H3K9 directs the maintenance of DNA methylation. Nat. Struct. Mol. Biol. *19*, 1155–1160.

Rothbart, S.B., Dickson, B.M., Ong, M.S., Krajewski, K., Houliston, S., Kireev, D.B., Arrowsmith, C.H., and Strahl, B.D. (2013). Multivalent histone engagement by the linked tandem Tudor and PHD domains of UHRF1 is required for the epigenetic inheritance of DNA methylation. Genes Dev. *27*, 1288–1298.

Sharif, J., Muto, M., Takebayashi, S., Suetake, I., Iwamatsu, A., Endo, T.A., Shinga, J., Mizutani-Koseki, Y., Toyoda, T., Okamura, K., et al. (2007). The SRA protein Np95 mediates epigenetic inheritance by recruiting Dnmt1 to methylated DNA. Nature *450*, 908–912.

Taylor, E.M., Bonsu, N.M., Price, R.J., and Lindsay, H.D. (2013). Depletion of Uhrf1 inhibits chromosomal DNA replication in *Xenopus* egg extracts. Nucleic Acids Res. *41*, 7725–7737.

Xie, S., Jakoncic, J., and Qian, C. (2012). UHRF1 double Tudor domain and the adjacent PHD finger act together to recognize K9me3-containing histone H3 tail. J. Mol. Biol. *415*, 318–328.